8-2016

Synthesis and Application of Polymer Brush-Grafted Nanoparticles as Hydrogel Gelators and Lubricant Additives

Roger Anthony Emory Wright
University of Tennessee, Knoxville, rwrigh23@vols.utk.edu

To the Graduate Council:

I am submitting herewith a dissertation written by Roger Anthony Emory Wright entitled "Synthesis and Application of Polymer Brush-Grafted Nanoparticles as Hydrogel Gelators and Lubricant Additives." I have examined the final electronic copy of this dissertation for form and content and recommend that it be accepted in partial fulfillment of the requirements for the degree of Doctor of Philosophy, with a major in Chemistry.

Bin Zhao, Major Professor

We have read this dissertation and recommend its acceptance:

Brian Long, John Bartmess, Hong Guo

Accepted for the Council:

Carolyn R. Hodges

Vice Provost and Dean of the Graduate School

(Original signatures are on file with official student records.)

Synthesis and Application of Polymer Brush-Grafted Nanoparticles as Hydrogel Gelators and Lubricant Additives

A Dissertation Presented for the

Doctor of Philosophy

Degree

The University of Tennessee, Knoxville

Roger Anthony Emory Wright

August 2016

Acknowledgements

I would first like to thank my advisor, Professor Bin Zhao, who has set the standard for critical thought and attention to detail I still aspire to meet. Prof. Zhao has taught me the importance of walking the line between skepticism and open-mindedness, and I am certain the lessons I have learned under his stewardship will serve me well throughout my career.

I would also like to acknowledge my graduate committee: Prof. Brian Long, Prof. John Bartmess, and Prof. Hong Guo as well as Prof. Wei He. They have very graciously given time and effort to further my scientific growth, and I sincerely appreciate their contributions.

I also greatly appreciate the support provided by the NSF and DOE. Their funding was crucial in the completion of this work.

Many thanks to our collaborator, Dr. Jun Qu, as well as Dr. Austin Shaw, and Bo Barnhill in the Material Science and Technology Division at Oak Ridge National Laboratory for their help with tribological characterization and analysis. I would also like to thank Dr. John Dunlap for his training and aid in electron microscopy, and Dr. Ed Wright for his help with ultracentrifugation.

My thanks go also to Dr. Carlos Steren, who has taught me much about NMR, solving problems, and working with people. Working with him has constantly been a high point for the past several years.

To the members of Prof. Zhao's research group, both past and current, I will always be grateful for their friendship and advice. My thanks to Dr. Xueguang Jiang, Dr. Xiaoming Jiang, Dr. Thomas G. O'Lenick, Dr. Jeremiah W. Woodcock, Dr. Naixiong Jin, Dr. Chunhui Bao, Daniel Henn, Bin Hu, Sisi Jiang, Bryan Seymour, Jessica Holmes, Ethan Kent, Dr. Kewei Wang, Dr. Wenxin Fu, and Prof. Chunhui Luo.

My family has always been there for me, and I have always been able to rely on their support. To my parents Roger and Penny who have always had my best interests at heart, I owe a

debt of gratitude I can never repay. I would also like to thank my aunts, uncles and cousins, who have helped me to feel that there is always someone in my corner.

Finally, to my wife Laura, I feel like we have done this together, and I couldn’t imagine it any other way.

Abstract

This dissertation describes the synthesis of polymer brush-grafted nanoparticles (hairy NPs) and an analysis of their behavior or utility in multiple areas. The hairy NPs were synthesized from silica NPs functionalized with initiating moieties by surface-initiated atom transfer radical polymerization. A brief introduction to hairy NPs, with a focus on the synthesis and behavior of stimuli-responsive polymer brush-grafted particles, is given in Chapter 1 to provide context for this work.

Chapters 2 and 3 present the synthesis of thermosensitive diblock copolymer brush-grafted nanoparticles designed as hairy NP analogues in place of thermosensitive block copolymers micelles for the construction of hybrid, physical hydrogels. Chapter 2 details a series of hairy NPs with a thermosensitive poly(methoxydi(ethylene glycol) methacrylate) (PDEGMMA) inner block and a charge-bearing, poly(DEGMMA-*co*-2-(methacryloyloxy)ethyltrimethylammonium iodide) (PDEGMMA-*co*-TMAEMA-I) outer block. These hairy particles underwent a reversible, cooling-induced gelation at moderate concentrations in water, based on the packing of hairy NPs due to the LCST-driven increase in brush volume fraction upon cooling. Another series of thermosensitive hairy NPs was made with brushes composed of P(TMAEMA-I)-*b*-PDEGMMA, which exhibited a heating-induced reversible gelation at concentrations as low as 3 wt % in water, due to the association of PDEGMMA outer blocks at temperatures above their LCST. The inner hydrophilic polyelectrolyte block served to bridge these domains and NPs to form a three-dimensional gel network.

Chapter 4 details the use of NPs grafted with oil-soluble poly(lauryl mathacrylate) as lubricant additives. These hairy NPs showed superior stability in a poly(alphaolefin) (PAO) base lubricating oil, and the addition of 1.0 wt % hairy NPs to PAO yielded significant reductions in

both friction and material wear. These gains were attributed to the formation of a load-bearing tribofilm at the rubbing interface. Chapter 5 explores the brush microphase separation of poly(*n*-butyl acrylate)-*b*-polystyrene (P*n*BA-*b*-PS) brush-grafted particles with P*n*BA as inner block. From TEM analysis, there appeared an evolution of phase morphology from a stripe-like nanostructure to a more uniform layered structure with increasing PS molecular weight, in qualitative agreement with simulation studies. Chapter 6 includes a look back on this dissertation work in its entirety and possible future work.

Table of Contents

Chapter 1. Introduction 1

1.1 Introduction 2

1.1.1 Introduction to Polymer Brush-Grafted Particles 2

1.1.2 Stimuli-Responsive Hairy Particles 6

1.1.2.1 Thermosensitive Polymer 6

1.1.2.2. Synthesis and Behavior of Stimuli-Responsive Hairy Particles 14

1.1.3. Multicomponent Polymer Brush-Grafted Particles 17

1.2. Dissertation Overview 21

References 24

Chapter 2. Reversible Sol-Gel Transitions of Aqueous Dispersions of Silica Nanoparticles Grafted with Diblock Copolymer Brushes Composed of a Thermosensitive Inner Block and a Charged Outer Block 29

Abstract 30

2.1. Introduction 31

2.2. Experimental Section 33

2.2.1. Materials 33

2.2.2. Characterization 35

2.2.3. Synthesis of ATRP Initiator-Functionalized, 17 nm Silica NPs 36

2.2.4. Synthesis of PDEGMMA-*b*-P(DEGMMA-*co*-DMAEMA) Brushes on 17 nm Silica NPs 37

2.2.5. Quaternization of PDEGMMA-*b*-P(DEGMMA-*co*-DMAEMA) Brush-Grafted Silica NPs Using CH_3I 38

2.2.6. Preparation of Aqueous Dispersions of PDEGMMA-*b*-P(DEGMMA-*co*-TMAEMA-I) Brush-Grafted Silica NPs 39
2.2.7. Rheology Studies 39
2.2.8. Dynamic Light Scattering (DLS) Studies of Thermoresponsive Properties of PDEGMMA-*b*-P(DEGMMA-*co*-TMAEMA-I) Brush-Grafted Silica NPs 40
2.3. Results and Discussion 40
2.3.1. Synthesis of PDEGMMA-*b*-P(DEGMMA-*co*-DMAEMA) Brushes on 17 nm Silica NPs 40
2.3.2. Quaternization of DMAEMA Units in PDEGMMA-*b*-P(DEGMMA-*co*-DMAEMA) Brush-Grafted Silica NPs 46
2.3.3 Thermally-Induced, Reversible Sol-Gel Transitions of Aqueous Dispersions of BHP-1-Q. 49
2.3.4. Solution Behavior of Aqueous Dispersions of BHP-2-Q and BHP-3-Q at Low-to-Moderate Concentrations 59
2.3.5. Dynamic Light Scattering (DLS) Study of PDEGMMA-*b*-P(DEGMMA-*co*-TMAEMA-I) Brush-Grafted Silica Nanoparticles in Milli-Q Water 63
2.4. Conclusion 66
References 68
Appendix A 71
A.1. Cleavage of Polymer Brushes from Hairy Silica NPs Using HF. 72
A.2. Calculation of Degree of Polymerization (DP) of PDEGMMA Formed in Synthesis of PDEGMMA Brush-Grafted, 17 nm Silica Nanoparticles (HHP) 72

A.3. Calculation of Grafting Density of PDEGMMA Brushes Grafted on 17 nm Silica Nanoparticles (HHP) 73
A.4. Calculation of the DP of PDEGMMA-*b*-P(DEGMMA-*co*-DMAEMA) 73
A.5. Calculation of Grafting Density of Diblock Copolymer Brushes 74
A.6. Quaternization of PDEGMMA-*b*-P(DEGMMA-*co*-DMAEMA) (BCP-3) Using CH_3I 75
Chapter 3. Physically Crosslinked Hydrogels Formed Solely by Thermosensitive Hairy Silica Nanoparticles 82
Abstract 83
3.1. Introduction 84
3.2. Experimental Section 86
3.2.1. Materials 86
3.2.2. Characterization 89
3.2.3. Synthesis of ATRP Initiator-Functionalized Silica Nanoparticles 89
3.2.4. Synthesis of PDMAEMA Brushes from Initiator NPs 90
3.2.5. Synthesis of PDMAEMA-*b*-PDEGMMA Brush-Grafted Silica NPs……..91
3.2.6. HF Cleavage of Polymer Brushes from Silica NPs 92
3.2.7. Quaternization of PDMAEMA-*b*-PDEGMMA Brush-Grafted NPs with CH_3I 93
3.2.8. Rheological Study of Gelation of Aqueous Dispersions of P(TMAEMA-I)-*b*-PDEGMMA Brush-Grafted Silica NPs 93
3.3. Results and Discussion 94
3.3.1. Synthesis of PDMAEMA-*b*-PDEGMMA Brush-Grafted Silica NPs 94

3.3.2. Quaternization of Tertiary Amine Moieties in PDMAEMA-*b*-PDEGMMA Brush-Grafted Silica NPs by CH_3I 100
3.3.3. Reversible Sol-Gel Transitions of a 6.0 wt% Dispersion of Q-100 in Water 103
3.3.4. Reversible Sol-Gel Transitions of Dispersions of Q-195 in Water 108
3.3.5. Effect of Concentration on Gelation of Aqueous Dispersions of P(TMAEMA-I)-*b*-PDEGMMA Brush-Grafted Silica NPs 111
3.3.6. Recovery Test of Physically Crosslinked Hydrogels of Hairy NPs 114
3.4. Conclusions 114
References 117
Appendix B 120
Chapter 4. Oil-Soluble Polymer Brush-Grafted Silica Nanoparticles as Effective Lubricant Additives 125
Abstract 126
4.1. Introduction 127
4.2. Experimental Section 131
4.2.1. Materials 131
4.2.2. General Characterization 132
4.2.3. Synthesis of ATRP Initiator-Functionalized Silica Nanoparticles 133
4.2.4. Synthesis of Poly(lauryl methacrylate) (PLMA) Brush-Grafted Silica Nanoparticles 134
4.2.5. Preparation of Dispersions of Hairy Silica NPs in PAO and Stability Studies. 135
4.2.6. Tribological Testing 135

4.3. Results and Discussion……..…….…….……136

4.3.1. Synthesis and Characterization of ATRP Initiator-Functionalized Silica Nanoparticles 136

4.3.2. Synthesis of PLMA Brush-Grafted Silica NPs 137

4.3.3. Dispersibility and Stability Study of PLMA Hairy Silica Nanoparticles in PAO 139

4.3.4. Tribological Properties of PLMA Hairy Silica Nanoparticles as Additives for PAO 139

4.3.5. Characterization of the Tribofilm Formed from Tribological Testing 139

4.4. Conclusions 155

References 159

Appendix C 162

Chapter 5. Synthesis, Characterization, and Microphase Separation of Poly(*n*-butyl acrylate)-*b*-Polystyrene Diblock Copolymer Brushes Grafted on Silica Particles 174

Abstract 175

5.1 Introduction 176

5.2 Experimental 179

5.2.1 Materials 179

5.2.2 Characterization 181

5.2.3 Synthesis of Bare Silica Particles 181

5.2.4 Synthesis of ATRP Initiator-Functionalized Silica Particles (IP) 182

5.2.5 Synthesis of P*n*BA Brush-Grafted Silica Particles 182

5.2.6 Synthesis of P*n*BA-*b*-PS Brush-Grafted Silica Particles 183

5.2.7 Cleavage of P*n*BA-*b*-PS Brushes from Silica Particles 184
5.2.8 Differential Scanning Calorimetry of Free P*n*BA-*b*-PS 184
5.2.9 Transmission Electron Microscopy Study of P*n*BA-*b*-PS Brush-Grafted Particles 184
5.3 Results and Discussion 185
5.3.1 Synthesis of P*n*BA Brush-Grafted Silica Particles 185
5.3.2 Synthesis of P*n*BA-*b*-PS Diblock Copolymer Brush-Grafted Silica Particles 188
5.3.3 TEM Study of Microphase Separation of P*n*BA-*b*-PS Brushes Grafted on Particles 193
5.4 Conclusion 198
References 199
Appendix D 201
Chapter 6. Conclusions and Future Work 206
References 211
Vita 213

List of Tables

2.1. Characterization Data for PDEGMMA Brush-Grafted Silica NPs, PDEGMMA-*b*-P(DEGMMA-*co*-DMAEMA) Brush-Grafted Silica NPs, and the Corresponding Free Polymers……48

3.1. Characterization Data for PDMAEMA and PDMAEMA-*b*-PDEGMMA Brush-Grafted Silica NPs and Their Corresponding Free Polymers……101

4.1. Characterization Data for PLMA Brush-Grafted Silica Nanoparticles and Corresponding Free PLMA Polymers……..141

4.2. Wear Volumes for Balls and Flats from Tribological Tests…….……148

4.3. Wear Volumes for Balls and Flats from Tribological Testing…….153

5.1. Characterization Data for P*n*BA and P*n*BA-*b*-PS Brush-Grafted Silica Particles and Their Corresponding Free Polymers ……....……190

List of Figures

1.1. Reversible clouding transition of an aqueous solution of a thermosensitive polymer and a schematic of an LCST transition illustrating the melting of ordered water surrounding hydrophobic domains upon heating and the aggregation of polymer chains……..…….…..…..……...…….8

1.2. Digital optical images of an aqueous, 20 wt % solution of a doubly thermosensitive diblock copolymer at various temperatures (top) and a schematic illustration of the transition from a clear molecular sol to a clear micellar sol, clear micellar gel, clear micellar sol, and cloudy mixture upon increasing temperature…….11

1.3. Digital optical pictures of a 10.0 wt% aqueous solution of an ABA triblock copolymer with thermosensitive A blocks and a hydrophilic B block at three temperatures (top) and a schematic illustration of the reversible formation of a three-dimensional network above the LCST of the A blocks……..13

1.4. Optical images of aqueous and ethyl acetate layers after seventh cooling in an ice/water bath (a); seventh heating in an 60 °C oil bath (b); eighth cooling (c); eighth heating (d); ninth cooling (e); and ninth heating (f). The PTEGMMA brush-grafted nanoparticles were originally dispersed in water-saturated ethyl acetate at 63 °C (concentration: 1.0 mg/mL)……..……..16

1.6. Top-view TEM micrographs of Mixed P*t*BA/PS brush-grafted silica particles with $M_{n,PS} < M_{n,PtBA}$ (A and B), $M_{n,PS} \approx M_{n,PtBA}$ (C) and $M_{n,PS} > M_{n,PtBA}$ (D), with schematic illustrations of the observed morphologies. The hairy particles were cast from CHCl3, a nonselective good solvent for both P*t*BA and PS, and thermally annealed and stained with RuO4 vapor……..20

2.1. (A) Size exclusion chromatography (SEC) traces of free homopolymer PDEGMMA and PDEGMMA-*b*-P(DEGMMA-*co*-DMAEMA) diblock copolymers (BCP-1, BCP-2, and BCP-3). (B) Thermogravimetric analysis of (i) ATRP initiator-functionalized silica nanoparticles (NPs), (ii) PDEGMMA brush-grafted silica NPs (HHP), and (iii)-(v) PDEGMMA-*b*-P(DEGMMA-*co*-DMAEMA) brush-grafted silica NPs (BHP-1, BHP-2, and BHP-3, respectively)……...43

2.2. Size exclusion chromatography (SEC) traces of (A) the free PDEGMMA formed in the synthesis of PDEGMMA brush-grafted silica nanoparticles (HHP), (B) the PDEGMMA brush cleaved from HHP, (C) the free diblock copolymer PDEGMMA-*b*-P(DEGMMA-*co*-DMAEMA) (BCP-3) formed in the synthesis of diblock copolymer brush-grafted silica NPs (BHP-3), and (D) the polymer cleaved from hairy NPs BHP-3. The SEC analysis was performed using a PL-GPC 50 Plus with DMF as the carrier solvent…….44

2.3. Bright field TEM micrographs of (A) PDEGMMA-*b*-P(DEGMMA-*co*-DMAEMA) diblock copolymer brush-grafted silica NPs (BHP-1), (B) BHP-2, and (C) BHP-3. The hairy NPs were cast onto carbon-coated, copper TEM grids from the $CHCl_3$ dispersions with a hairy NP concentration of ~ 4 mg/mL…….47

2.4. ^{1}H NMR spectra of (A) PDEGMMA-*b*-P(DEGMMA-*co*-DMAEMA) brush-grafted silica nanoparticles (BHP-3) in $CDCl_3$ and (B) PDEGMMA-*b*-P(DEGMMA-*co*-TMAEMA-I) (BHP-3-Q) in D_2O……..50

2.5. Digital optical pictures of a 6.5 wt % aqueous dispersion of PDEGMMA-*b*-P(DEGMMA-*co*-TMAEMA-I) brush-grafted silica NPs (BHP-1-Q) at 35 and 15 °C……52

2.6. Plots of dynamic storage modulus G' and loss modulus G'' of a 6.5 wt % aqueous dispersion of PDEGMMA-*b*-P(DEGMMA-*co*-TMAEMA-I) brush-grafted silica nanoparticles (BHP-

1-Q) versus temperature obtained from an oscillatory shear experiment performed (A) in a cooling ramp using a frequency of 1 Hz, a strain amplitude of 1.0 %, and a cooling rate of 3 °C/min and (B) in a heating ramp using a frequency of 1 Hz, a strain amplitude of 1.0 %, and a heating rate of 3 °C/min; (C) A strain sweep performed at 5 °C on the 6.5 wt % aqueous dispersion of BHP-1-Q using a frequency of 1 Hz……53

2.7. Plots of dynamic storage modulus G' and loss modulus G'' of a 6.5 wt % aqueous dispersion of PDEGMMA-*b*-P(DEGMMA-*co*-TMAEMA-I) brush-grafted silica NPs (BHP-1-Q) versus frequency at (A) 30 °C, (B) 23 °C, and (C) 5 °C using a strain amplitude of 1.0 %.....55

2.8. $T_{gel\text{-}sol}$ of aqueous dispersion of BHP-1-Q (black square) and BHP-2-Q (red circle), obtained from rheological measurements, as a function of concentration of hairy nanoparticles. For BHP-2-Q, the $T_{gel\text{-}sol}$ at 7.0 wt % was determined by visual examination……58

2.9. Digital optical pictures of a 6.0 % aqueous dispersion of BHP-2-Q at 50 and 25 °C (top), and temperature ramps (bottom) from oscillatory shear experiments using a fixed frequency of 1 Hz, a strain amplitude of 1.0 %, and a heating/cooling rate of 3 °C/min.....60

2.10. Digital optical pictures of aqueous dispersions of BHP-3-Q with concentrations of 4.0 (left) and 3.0 wt % (right) at ambient conditions. **……**62

2.11. Average apparent hydrodynamic size D_h, obtained from DLS study of 0.2 mg/g aqueous dispersion of PDEGMMA-*b*-P(DEGMMA-*co*-TMAEMA-I) brush-grafted silica NPs in Milli-Q water using CONTIN analysis, along with the standard deviation as a function of temperature for BHP-1-Q (black square), BHP-2-Q (red circle), and BHP-3-Q (blue triangle). ……64

A1. ^{1}H NMR spectra of free diblock copolymer BCP-3 PDEGMMA-*b*-P(DEGMMA-*co*-DMAEMA) before (A) and after (B) quaternization with iodomethane for 90 min……..76

A2. Plots of dynamic storage modulus G' (black square) and loss modulus G'' (red circle) of aqueous dispersions of BHP-1-Q at various concentrations versus temperature. The data were collected from oscillatory shear experiments performed in heating ramps by using a frequency of 1 Hz, a strain amplitude of 1.0 %, and a heating rate of 3 °C/min……77

A3. A strain sweep performed on the 6.0 wt % aqueous dispersion of BHP-2-Q at 5 °C using a frequency of 1 Hz. ……..78

A4. Plots of dynamic storage modulus G' and loss modulus G'' of a 6.0 wt % aqueous dispersion of BHP-2-Q versus frequency at (A) 40 °C, (B) 35 °C, and (C) 5 °C with a constant strain amplitude of 1.0 %.……79

A5. Plots of dynamic storage modulus G' (black square) and loss modulus G'' (red circle) of aqueous dispersions of BHP-2-Q at various concentrations versus temperature. The data were collected from oscillatory shear experiments performed in heating ramps by using a frequency of 1 Hz, a strain amplitude of 1.0 %, and a heating rate of 3 °C/min……...80

A6. Plot of dynamic storage modulus G' (black square) and loss modulus G''' (red circle) of a 4.0 wt% aqueous dispersion of BHP-3-Q. The data were collected from an oscillatory shear experiment performed in a heating ramp by using a frequency of 1 Hz, a strain amplitude of 1.0 %, and a heating rate of 3 °C/min. ……81

3.1. Size exclusion chromatography (SEC) analysis of (i) free PDMAEMA formed in the synthesis of PDMAEMA brush-grafted silica NPs, (ii) free PDMAEMA-*b*-PDEGMMA with the PDEGMMA block DP of 100 (FDB-100) formed in the synthesis of DB-100 hairy

NPs, and (iii) free PDMAEMA-*b*-PDEGMMA with the PDEGMMA block DP of 195 (FDB-195) formed in the synthesis of DB-195 hairy NPs. ……96

3.2. Thermogravimetric analysis (TGA) of (i) initiator-functionalized silica NPs, (ii) PDMAEMA brush-grafted silica NPs, (iii) PDMAEMA-*b*-PDEGMMA brush-grafted silica NPs with PDEGMMA block DP of 100 (DB-100), and (iv) PDMAEMA-*b*-PDEGMMA brush-grafted silica NPs with PDEGMMA block DP of 195 (DB-195)……97

3.3. Bright field TEM micrographs of (A) PDMAEMA brush-grafted silica NPs, (B) PDMAEMA-*b*-PDEGMMA brush-grafted silica NPs with PDEGMMA block DP of 100 (DB-100), and (C) PDMAEMA-*b*-PDEGMMA brush-grafted silica NPs with PDEGMMA block DP of 195 (DB-195). The scale bars are the same for the three TEM micrographs. The TEM samples were prepared by drop casting of the dispersions of hairy NPs in chloroform with a concentration of 2 mg/mL onto carbon-coated, copper TEM grid…….99

3.4. SEC analysis of the cleaved polymer (red) and the free polymer (black) corresponding to PDMAEMA brush-grafted NPs (A) and DB-100 (B). ……102

3.5. ^{1}H NMR spectrum of (A) PDMAEMA-*b*-DEGMMA brush-grafted silica NPs (DB-100) in $CDCl_3$ and (B) P(TMAEMA-I)-*b*-PDEGMMA brush-grafted NPs (Q-100) in D_2O after quaternization with CH_3I. ……104

3.6. Digital optical pictures of a 6.0 wt % aqueous dispersion of P(TMAEMA-I)-*b*-PDEGMMA brush-grafted silica NPs (Q-100) at 20 °C and 50 °C. ……..105

3.7. Plots of dynamic storage modulus G′ and loss modulus G″ of a 6.0 wt % aqueous dispersion of P(TMAEMA-I)-*b*-PDEGMMA brush-grafted silica nanoparticles (Q-100) obtained from oscillatory shear experiments performed in a temperature ramp at a frequency of 1

Hz, a strain amplitude of 0.2 %, and (A) a heating rate of 3 °C/min or (B) a cooling rate of -3 °C/min. (C) Strain sweep at a frequency of 1 Hz and 55 °C. ……106

3.8. Digital optical pictures of a 6.0 wt% aqueous dispersion of P(TMAEMA-I)-*b*-PDEGMMA brush-grafted silica NPs (Q-195) at 20 °C and 40 °C. ……..109

3.9. Plots of dynamic storage modulus G′ and loss modulus G″ of a 6.0 wt % aqueous dispersion of P(TMAEMA-I)-*b*-PDEGMMA brush-grafted silica nanoparticles (Q-195) obtained from oscillatory shear experiment performed (A) in a heating ramp at a frequency of 1 Hz, a strain amplitude of 0.2 %, and a heating rate of 3 °C/min, and (B) in a cooling ramp using a frequency of 1 Hz, a strain amplitude of 0.2 %, and a cooling rate of -3 °C/min (B). (C) Strain sweep at a frequency of 1 Hz and 55 °C. ……110

3.10. Plots of dynamic storage modulus G′ and loss modulus G″ versus frequency for a 6.0 wt% aqueous dispersion of P(TMAEMA-I)-*b*-PDEGMMA brush-grafted silica nanoparticles (Q-195) obtained from oscillatory shear experiments performed at 10 °C (A), 27 °C (B), and 55 °C (C)) at 0.2 % strain amplitude. ……112

3.11. Plot of $T_{sol\text{-}gel}$ versus concentration for aqueous dispersions of Q-100 (red solid circle) and Q-195 (black solid square), obtained from rheological measurements.…….....……...113

3.12. Plots of dynamic storage modulus G′ and loss modulus G″ (left axis) of a 6.0 wt % aqueous dispersion of Q-100 (A) and Q-195 (B) obtained from oscillatory shear experiments performed at 55 °C using a frequency of 1 Hz. The strain amplitude was oscillated between 0.2 % and 100 % amplitude (right axis) at given intervals. ……115

B1. ^{1}H NMR Spectra of free PDMAEMA-*b*-PDEGMMA corresponding to DB-100 (left) and free DB-195 (right). The DP of PDEGMMA was found by comparing the integrations of

ethylene glycol protons (3.50 - 3.75 ppm, -$OCH_2CH_2OCH_2CH_2OCH_3$) to the pendant methyl groups of PDMAEMA (2.20 - 2.35 ppm, -$N(CH_3)_2$). ……...……121

B2. Plots of dynamic storage modulus G′ and loss modulus G″ of a 8.0 wt % aqueous dispersion of P(TMAEMA-I)-*b*-PDEGMMA brush-grafted silica nanoparticles (Q-100) obtained from oscillatory shear experiments performed across a temperature ramp at a frequency of 1 Hz, a strain amplitude of 0.2 %, and a heating rate of 3 °C/min (A). Frequency sweep experiments were performed at 5, 35, and 55 °C (B-D) using a 0.2 % strain amplitude. (E) Strain sweeps performed at 55 °C using a fixed frequency of 1 Hz. ……122

B3. Plots of dynamic storage modulus G′ and loss modulus G″ of aqueous dispersions of P(TMAEMA-I)-*b*-PDEGMMA brush-grafted silica nanoparticles (Q-100) with a concentration of 5.0 wt% (A), 4.0 wt% (B), and 3.0 wt% (C) obtained from oscillatory shear experiments performed across a temperature ramp at a frequency of 1 Hz, a strain amplitude of 0.2 %, and a heating rate of 3 °C/min. ……123

B4. Plots of dynamic storage modulus G′ and loss modulus G″ of an aqueous dispersion of P(TMAEMA-I)-*b*-PDEGMMA brush-grafted silica nanoparticles (Q-195) with a concentration of 10.0 (A), 8.0 (B), 5.0 (C), 4.0 (D), and 3.0 wt % E) obtained from oscillatory shear experiments performed across a temperature ramp at a frequency of 1 Hz, a strain amplitude of 0.2 %, and a heating rate of 3 °C/min. ……124

4.1. Example of an additized lubricant in which the additive is no longer stable in the lubricating oil, as evidenced by the dark vial wall and the clarity of the oil. This lack of stability has likely compromised lubrication performance.....129

4.2. Size exclusion chromatography (SEC) traces of free PLMA polymers formed in the synthesis of (i) HNP-SiO_2-38.0k ($M_{n\ SEC}$ = 38.0 kDa, PDI = 1.09), (ii) HNP-SiO_2-21.7k (M_n

$_{SEC}$ = 21.7 kDa, PDI = 1.10), (iii) HNP-SiO_2-11.8k ($M_{n\ SEC}$ = 11.8 kDa, PDI = 1.13), (iv) HNP-SiO_2-9.0k ($M_{n\ SEC}$ = 9.0 kDa, PDI = 1.12 and (v) HNP-SiO_2-4.1k ($M_{n\ SEC}$ = 4.1 kDa, PDI = 1.14) 138

4.3. Thermogravimetric analysis (TGA) of ATRP initiator-functionalized silica NPs, INP-SiO_2-I (i) INP-SiO_2-II (ii), with an average size of 23.8 nm and 23.5 nm, respectively, HNP-SiO_2-4.1k (iii), HNP-SiO_2-9.0k (iv), HNP-SiO_2-11.8k (v), HNP-SiO_2-21.7k (vi), and HNP-SiO_2-38.0k (vii). HNP-SiO_2-9.0k was synthesized from INP-SiO_2-II; all other PLMA brush-grafted NP samples were synthesized using INP-SiO_2-I. TGA was performed in air at a heating rate of 20 °C/min. ……140

4.4. Bright field TEM micrographs of PLMA brush-grafted silica NPs with $M_{n,SEC}$ of 38.0 kDa (A), 21.7 kDa (B), 11.8 kDa (C), 9.0 kDa (D), and 4.1 kDa (E). The hairy NPs were cast onto carbon-coated, copper TEM grids from dispersions in $CHCl_3$, a good solvent, with a concentration of 4 mg/mL. ……...142

4.5. Intensity-weighted size distributions obtained by DLS. The average sizes were 102.6 nm for HNP-SiO_2-38k (i), 95.1 nm for HNP-SiO_2-21.7k (ii), 59.2 nm for HNP-SiO_2-11.8k (iii), 56.9 nm for HNP-SiO_2-9.0k (iv), and 44.1 nm for HNP-SiO_2-4.1k (v). ……...143

4.6. ^{1}H NMR spectrum of HNP-SiO_2-21.7k in $CDCl_3$ exhibits all characteristic peaks of PLMA, indicating that the HNPs are well dispersed. ……...144

4.7. Photos of 1 wt% dispersions of HNP-SiO_2-4.1k in PAO in the initial state (A) and after being kept at -20, 22, 100 °C for 55 days (B). ……146

4.8. Friction curves for PAO SpectraSyn^{TM} 4 (A), PAO containing 1 wt% of free PLMA with a $M_{n,SEC}$ of 38.0 kDa (B), HNP-SiO_2-38.0k (C), HNP-SiO_2-21.7k (D), HNP-SiO_2-11.8k (E), HNP-SiO_2-9.0k (F), and HNP-SiO_2-4.1k (G). The tribological tests were performed

using a Plint TE-77 tribo-tester at 100 °C under a point contact load of 100 N for a sliding distance of 1000 m. ……..147

4.9. Optical micrographs of wear scars on the iron flats following tribological testing of neat PAO (A), and 1 wt% dispersion of HNP-SiO_2-38.0k (B), HNP-SiO_2-21.7 (C), HNP-SiO_2-11.8k (D), HNP-SiO_2-9.0k (E), and HNP-SiO_2-4.1k (F) in PAO. Note the entire width of the wear scar obtained from neat PAO testing was too large to be fully shown in the viewing area, a result of the scuffing observed in the corresponding COF curve……150

4.10. Friction curves for PAO dispersion containing (A) 0.25 wt%, (B) 1.0 wt%, (C) 2.0 wt%, and (D) 4.0 wt% of HNP-SiO_2-21.7k performed using a Plint TE-77 tribo-tester at 100 °C under a point contact load of 100 N for a sliding distance of 1000 m……....151

4.11. Friction curves for PAO additized with (A) 1 wt% HNP-SiO_2-4.1k, (B) 1.67 wt % amine phosphate,[39] (C), 1 wt% HNP-TiO_2-8.1k,[40] and (D) 1 wt% ZDDP. Measurements were performed using a Plint TE-77 tribo-tester at 100 °C under a point contact load of 100 N for a sliding distance of 1000 m. ……..154

4.12. (A) Transmission electron micropscopy (TEM) micrograph of the cross-section of the wear scar on the cast iron flat tested with 1 wt% HNP-SiO_2-4.1k-additized PAO. The element mapping data of Si, C, Fe, and O of the selected area are shown on the left. The cross-section TEM sample was prepared using the focused ion beam (FIB) technique. (B) Higher magnification TEM micrograph of the area of the tribofilm pointed to by the arrow……156

4.13. Transmission electron micropscopy (TEM) micrographs of the cross-section of the wear scar on the cast iron flat tested with 1 wt% HNP-SiO_2-4.1k-additized PAO. The element mapping data of Fe, O, Si, C, and a combined overlay of the selected area are shown on

the bottom row. The cross-section TEM sample was prepared using the focused ion beam (FIB) technique. ……...157

C1. Individual friction curves for neat PAO obtained using a Plint TE-77 tribo-tester at 100 °C under a point contact load of 100 N for a sliding distance of 1000 m. ……163

C2. Individual friction curves for 1 wt% free PLMA-38.0k PAO solution obtained using a Plint TE-77 tribo-tester at 100 °C under a point contact load of 100 N for a sliding distance of 1000 m. ……164

C3. Individual friction curves for 1 wt% HNP-SiO_2-38.0k PAO dispersion obtained using a Plint TE-77 tribo-tester at 100 °C under a point contact load of 100 N for a sliding distance of 1000 m. ……165

C4. Individual friction curves for 1 wt% HNP-SiO_2-22.7k PAO dispersion obtained using a Plint TE-77 tribo-tester at 100 °C under a point contact load of 100 N for a sliding distance of 1000 m. ……166

C5. Individual friction curves for 1 wt% HNP-SiO_2-11.8k PAO dispersion obtained using a Plint TE-77 tribo-tester at 100 °C under a point contact load of 100 N for a sliding distance of 1000 m. . …….167

C6. Individual friction curves for 1 wt% HNP-SiO_2-9.0k PAO dispersion obtained using a Plint TE-77 tribo-tester at 100 °C under a point contact load of 100 N for a sliding distance of 1000 m. . ……..168

C7. Individual friction curves for 1 wt% HNP-SiO_2-4.1k PAO dispersion obtained using a Plint TE-77 tribo-tester at 100 °C under a point contact load of 100 N for a sliding distance of 1000 m. . ……..169

C8. Individual friction curves for 0.25 wt% HNP-SiO_2-21.7k PAO dispersion obtained using a Plint TE-77 tribo-tester at 100 °C under a point contact load of 100 N for a sliding distance of 1000 m. . ……170

C9. Individual friction curves for 2 wt% HNP-SiO_2-21.7k PAO dispersion obtained using a Plint TE-77 tribo-tester at 100 °C under a point contact load of 100 N for a sliding distance of 1000 m. . ……171

C10. Individual Friction curves for 4 wt% HNP-SiO_2-21.7k PAO dispersion obtained using a Plint TE-77 tribo-tester at 100 °C under a point contact load of 100 N for a sliding distance of 1000 m. . ……172

C11. Individual friction curves for 1 wt% ZDDP PAO solution obtained using a Plint TE-77 tribo-tester at 100 °C under a point contact load of 100 N for a sliding distance of 1000 m……...……...173

5.1. Evolution of phase morphologies of diblock copolymer brushes grafted by the B block to a spherical substrate. B-rich domains are transparent, while A-rich domains are red.…… ……..……..……....…….……..……..178

5.2. SEC traces of free P*n*BA (i), P*n*BA-*b*-PS diblock copolymer withdrawn from the polymerization mixture at 120 min (ii, BC-120), 155 min (iii, BC-155), 180 min (iv, BC-180), and 215 min (v, BC-215). . ……..186

5.3. Thermogravimetric analysis of initiator particles, P*n*BA brush-grafted particles (i), DBP-120 (ii), DBP-155 (iii), DBP-180 (iv), and DBP-215 (v).....187

5.4. SEC traces of the diblock copolymer cleaved from DBP-155 and free BC-155 P*n*BA-*b*-PS (red). . ……..191

5.5. DSC trace of P*n*BA-*b*-PS with $M_{n,SEC}$ = 50.1 kDa and PDI = 1.16, showing two distinct glass transition temperatures: one at -44 °C corresponding to P*n*BA and another one at 84 °C corresponding to PS. . ……192

5.6. Bright field TEM micrographs of P*n*BA-*b*-PS brush-grafted silica particles with DP_{PnBA} of 193 and DP_{PS} of 153 (DBP-120). The hairy NPs were cast onto carbon-coated, copper TEM grids from $CHCl_3$, a nonselective good solvent, at a concentration of 1 mg mL^{-1}…….194

5.7. Bright field TEM micrographs of P*n*BA-*b*-PS brush-grafted silica particles with DP_{PnBA} of 193 and DP_{PS} of 207 (DBP-155). The hairy NPs were cast onto carbon-coated, copper TEM grids from $CHCl_3$, a nonselective good solvent, at a concentration of 1 mg mL^{-1}…….195

5.8. Bright field TEM micrographs of P*n*BA-*b*-PS brush-grafted silica particles with DP_{PnBA} of 193 and DP_{PS} of 247 (DBP-180). The hairy NPs were cast onto carbon-coated, copper TEM grids from $CHCl_3$, a nonselective good solvent, at a concentration of 1 mg mL^{-1}…….196

5.9. Bright field TEM micrographs of P*n*BA-*b*-PS brush-grafted silica particles with DP_{PnBA} of 193 and DP_{PS} of 261 (DBP-215). The hairy NPs were cast onto carbon-coated, copper TEM grids from $CHCl_3$, a nonselective good solvent, at a concentration of 1 mg mL^{-1}. ……197

D1. Bright field TEM micrographs of P*n*BA-*b*-PS brush-grafted silica particles with DP_{PnBA} of 193 and DP_{PS} of 153 (DBP-120). The hairy NPs were cast onto carbon-coated, copper TEM grids from $CHCl_3$, a nonselective good solvent, at a concentration of 1 mg mL^{-1}. ……202

D2. Bright field TEM micrographs of P*n*BA-*b*-PS brush-grafted silica particles with DP_{PnBA} of 193 and DP_{PS} of 207 (DBP-155). The hairy NPs were cast onto carbon-coated, copper TEM grids from $CHCl_3$, a nonselective good solvent, at a concentration of 1 mg mL^{-1}. ……203

D3. Bright field TEM micrographs of P*n*BA-*b*-PS brush-grafted silica particles with DP_{PnBA} of 193 and DP_{PS} of 247 (DBP-180). The hairy NPs were cast onto carbon-coated, copper TEM grids from $CHCl_3$, a nonselective good solvent, at a concentration of 1 mg mL^{-1}. ……204

D4. Bright field TEM micrographs of P*n*BA-*b*-PS brush-grafted silica particles with DP_{PnBA} of 193 and DP_{PS} of 261 (DBP-215). The hairy NPs were cast onto carbon-coated, copper TEM grids from $CHCl_3$, a nonselective good solvent, at a concentration of 1 mg mL^{-1}. ……205

List of Schemes

1.1. Three general strategies for the synthesis of polymer brush-grafted particles: "grafting to" (A), "*in situ*" (B), and "grafting from" (C)……4

1.2. A schematic illustration of the self-assembly of mixed homopolymer brushes under equilibrium melt conditions and in neutral or selective solvents.....……..……18

2.1. Synthesis of PDEGMMA-*b*-P(DEGMMA-*co*-TMAEMA-I) Brush-Grafted Silica Nanoparticles (NPs) by a Surface-Initiated, One-Pot Atom Transfer Radical Polymerization and Subsequent Quaternization of Tertiary Amine Units with Iodomethane……...……34

2.2. Proposed Mechanism for Hydrogel Formation from Aqueous Dispersion of Thermosensitive Diblock Copolymer Brush-Grafted Silica NPs by Packing (for Simplicity, Counteranions are Omitted)…….....57

3.1. Synthesis of P(TMAEMA-I)-*b*-PDEGMMA brush-grafted silica NPs by sequential surface-initiated atom transfer radical polymerizations (SI-ATRP) of DMAEMA (M_1) and DEGMMA (M_2) followed by quaternization with methyl iodide, and molecular structures of DMAEMA and DEGMMA……87

3.2. Thermally reversible physically crosslinked 3-dimensional network hydrogels formed solely by thermosensitive diblock copolymer brush-grafted silica nanoparticles composed of a hydrophilic inner block and thermosensitive outer block……88

4.1. Schematic Illustration for Synthesis of Oil-Miscible Poly(lauryl methacrylate) (PLMA) Brush-Grafted Silica Nanoparticles (NPs) by Surface-Initiated Atom Transfer Radical Polymerization (SI-ATRP)……...130

5.1. Synthesis of P*n*BA-*b*-PS brush-grafted silica particles from ATRP initiator-functionalized silica particles through sequential SI-ATRP of *n*BA and styrene……180

Chapter 1. Introduction

1.1 Introduction

This dissertation work is focused on the synthesis, behavior, and applications of polymer brush-grafted nanoparticles (hairy NPs). These hybrid particles are composed of a particle core and a layer of surface-tethered polymer. Section 1.1.1 presents a general introduction to hairy NPs, including the scope and the synthesis of these hybrid materials. A significant portion of this dissertation work is concerned with thermosensitive polymer-brush grafted nanoparticles. Thermosensitive water-soluble polymers have been widely studied for the drastic physical changes in water upon heating or cooling to a given temperature. A brief introduction to stimuli-responsive polymers and thermosensitive hairy NPs is given in Section 1.1.2. Section 1.1.3 then describes the self-assembly of multicomponent polymer brushes tethered to a substrate and the nanostructures that they form on the particle surface. An overview of the dissertation is given at the end of Chapter 1 (Section 1.2).

1.1.1 Introduction to Polymer Brush-Grafted Particles

Polymer brush-grafted particles are hybrid materials composed of distinct core and outer layer. The core can be formed from a wide variety of materials including inorganic substances such as silica or iron oxide, metals such as gold and copper, organic latexes or microgels, and others. On the surface of these substrates is a covalently end-tethered layer of polymer, which, at sufficiently high grafting densities, extends outward from the substrate surface to relieve crowding at the grafting site. This extended polymer layer has led to brush-grafted particles commonly being referred to as “hairy” particles. The particle substrates are often spherical, but can include other regular or irregular shapes and feature mesoporous or hollow structures as well. Likewise, the grafted polymers can be of various architectures including homopolymer brushes, mixed brushes,

block copolymer brushes, cyclic brushes, and others. In this way, hairy particles are a highly versatile class of materials, exhibiting desired functionalities of both core substrates, e.g. mechanical, optical, or magnetic properties, and grafted polymer. Among the benefits imparted to hairy particles by their outer brush layer is environmental compatibility. As a result of their extended conformation, dispersion behavior of hairy particles is dominated by the grafted polymer; if the polymer is compatible with a given medium, this favorable enthalpic interaction is usually sufficiently strong so as to overcome any incompatibility between medium and substrate. In the case of nanoparticles, the ever-present danger of irreversible aggregation is minimized if not completely eliminated through a combination of this solubilizing and steric stabilization.

Three methods are generally available for the synthesis of polymer brush-grafted particles: "grafting to," *in situ* formation of core particles, and "grafting from," as described in Scheme 1.1. "Grafting to" refers to the linkage of pre-formed polymers to the surface of the core substrate. This linkage is typically accomplished with polymers and substrates having, or being made to have, complementary functionalities, such as a thiol terminated polymer for grafting to gold nanoparticles[1] or the use of "click" chemistry to attach azide-terminated polymers to an alkyne-functionalized metal-oxide.[2] This method is perhaps the most straightforward route to hairy particles, with well characterized polymers, but steric interactions between grafted and incoming polymer chains typically result in relatively low grafting densities. This effect can be abated somewhat by forming the particle substrates in situ. This method also makes use of preformed polymers, which, in this case, are typically block copolymers. These block copolymers can be made to assemble, e.g. into micelles or networks, which can serve as a directed locus for the

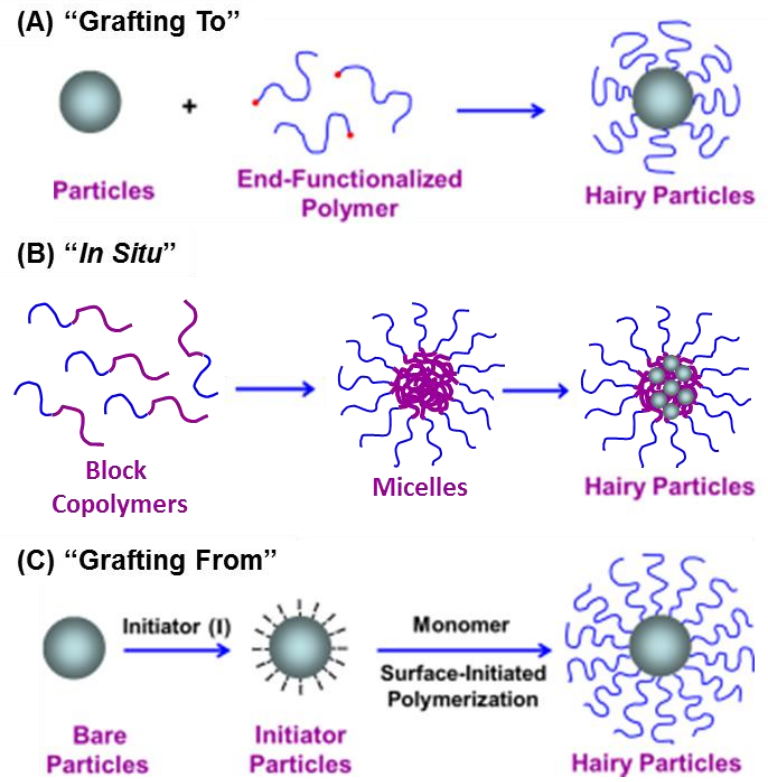

Scheme 1.1. Three general strategies for the synthesis of polymer brush-grafted particles: "grafting to" (A), "*in situ*" (B), and "grafting from" (C).[3] (Adapted from Ref. 3 with permission from John Wiley and Sons)

synthesis of core particles through the reduction of metal salts, chemical crosslinking, or other means. This route avoids much of the steric repulsion that hinders "grafting to," but grafting density is still limited by the number of chains present in the formative polymer assemblies, and multiple particles can sometimes form in these assemblies. Also, the range of hairy particles available for synthesis by this method is somewhat limited by the relatively stringent reaction conditions.

The third method, "grafting from," is named in reference to the use of initiator-functionalized particles, from which polymer chains are grown. One of the earliest examples of this method is the immobilization of azo-initiators onto silica gels by Pruker and Rühe, who used these functionalized particles to grow surface-bound polystyrene *via* conventional radical polymerization.[4] Also referred to as surface-initiated polymerization, the "grafting from" method has the potential for high grafting density, as reaction rates are governed by diffusion of monomer, as opposed to preformed polymer, to the surface-bound reaction sites. The disadvantage of not having preformed polymers, in terms of ease of synthesis and characterization, has been lessened significantly by the progress of controlled radical polymerization techniques, namely nitroxide mediated radical polymerization (NMRP), reversible addition-fragmentation chain transfer (RAFT), and atom transfer radical polymerization (ATRP). These so-called "living" radical polymerizations have been used to synthesize brushes of well-defined architectures and molecular weights from a variety of substrates. Initiator-functionalized particles are typically made using silane chemistries , similar to those used in the fabrication of self-assembled monolayers (SAMs),[5] thiol groups for functionalization of coinage metals, and catechol groups.[6] Surface-initiated controlled radical polymerizations are typically carried out in the presence of a small molecule "sacrificial" initiator, which results in free polymers that can be used to indirectly monitor and characterize their surface-

bound counterparts; bound and free polymers made in this way have been found on many occasions to be essentially identical in terms of molecular weights and molecular weight distributions.[7]

1.1.2 Stimuli-Responsive Hairy Particles

The designation of stimuli responsive brush-grafted particles is given typically in reference to functionality of the grafted polymer. Although there is certainly potential for stimuli responsiveness in core substrates, with examples including magnetic nanoparticles, light responsive titania, quantum dots, and, of course, polymeric substrates designed using stimuli-responsive polymers. Nevertheless, as it is perhaps more germane to this dissertation work, the following discussion will focus on responsiveness imparted by grafted polymers or their constituent monomer units.

1.1.2.1 Thermosensitive Polymer

Stimuli-responsive polymers exhibit sudden, significant physical changes in response to alteration in some facet of their environment.[8] Generally, the stimuli to which these polymers respond are considered to be chemical or physical in nature. Perhaps the most commonly explored chemical stimulus is pH, but other chemical stimuli include reducing/oxidizing agents, ionic strength, charge interactions, and other complementary chemical species. On the other hand, physical stimuli include temperature, magnetic fields, mechanical force, light, and others. Responsiveness to physical stimuli are particularly attractive as they are often more easily tuned *in situ*, and, of these, temperature is by far the most studied.

Polymers exhibiting thermosensitivity in water can be divided into two categories: those with an upper critical solution temperature (UCST) and those with a lower critical solution temperature (LCST). The former are polymers that are insoluble at lower temperatures, but, upon heating above

a transition temperature, become soluble. This transition is based on the weakening of interchain attractive forces, usually due to coulombic or hydrogen bonding interactions.[9] Indeed, the two major types of polymers with UCST transitions in water are zwitterionic polymers, such as the heavily studied poly(3-dimethyl(methacryloyloxyethyl) ammonium propane sulfonate), or polymers with a large degree of hydrogen bonding, with the preeminent example being poly(*N*-acryloylglycinamide) (PNAGA).[9]

Unlike UCST polymers, which undergo enthalpy-driven transitions upon heating in solution, LCST type polymers become insoluble upon heating above a transition temperature due to entropic effects, as shown in Figure 1.1. The most intensively studied LCST-type polymer is poly(*N*-isopropyl acrylamide) (PNIPAAm). As with all water-soluble polymers, PNIPAAm is able to interact with water through its polar moieties, particularly the hydrogen bonding acrylamide group. PNIPAAm, however, has significant nonpolar regions which cannot interact with water in an energetically favorable fashion, forcing water molecules around these groups to form ordered domains, referred to as clathrate or ice-like structures.[10] This hydrophobic effect acts to reduce mixing entropy; at higher temperatures, when this entropic penalty is no longer energetically tenable, these ice-like structures are said to "melt," as evidenced by an endotherm upon analysis by differential scanning calorimetry, causing a dehydration driven collapse and subsequent phase separation. This phase transition is often referred to as the cloud point due to the increase in turbidity observed in solutions of PNIPAAm at or above this temperature. The terms cloud point and LCST are often used interchangeably, but a distinction should be made as the former refers to a transition temperature at a given concentration whereas the latter refers to the lowest temperature at which this transition occurs, *i.e.* the "bottom" of the phase boundary. Perhaps the reason these terms are sometimes conflated is that, while some dependence of cloud point on concentration can

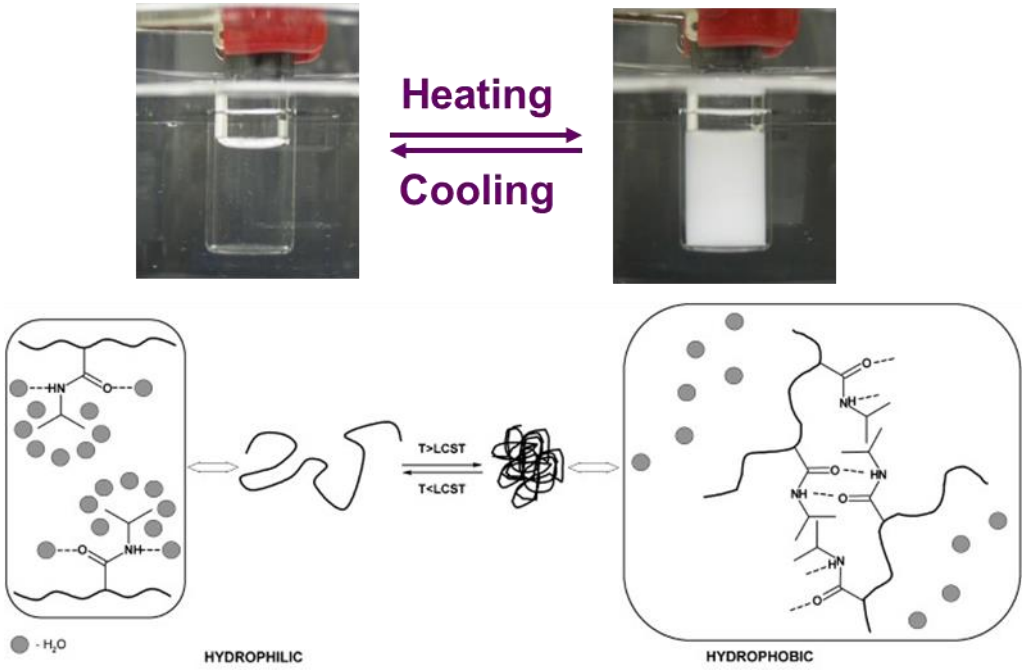

Figure 1.1. Reversible clouding transition of an aqueous solution of a thermosensitive polymer and a schematic of an LCST transition illustrating the melting of ordered water surrounding hydrophobic domains upon heating and the aggregation of polymer chains.[11] (Adapted from Ref. 11 with permission from Elsevier)

be observed, it is often small for LCST type polymers compared to UCST polymers and is very small for PNIPAAm in particular.[12]

The transition from hydrophilic to hydrophobic chains is key to the application of thermosensitive polymers, but a significant portion of their utility is not found in the application of free homopolymers, but as block copolymers in the formation of micelles. Thermosensitive micelles can be formed by pairing a thermosensitive block with a hydrophilic block or a hydrophobic block. By using thermosensitive-hydrophobic block copolymers, micelles comprised of a thermosensitive outer shell and hydrophobic core can be engineered. These micelles are formed at lower temperature, *i.e.* below the LCST of the thermoresponsive block, and undergo reversible aggregation/dispersion around the LCST of the micellar corona. Thermosensitive-hydrophilic block copolymers, on the other hand, yield reversible micelles with a thermosensitive core which disassociates into unimers at temperatures around the LCST of the thermosensitive block.[8] Thermoresponsive properties, including the temperature of micellization, can be tuned by modifying the LCST of the thermosensitive polymer; one method to this is the selection of a polymer with a more desirable LCST, but a more flexible approach is the incorporation of a second stimulus-responsive moiety into the responsive block.[13] For example, Yin and coworkers synthesized a P(NIPAAm-*co*-propylacrylic acid) random copolymer, the LCST of which could be increased by deprotonating the weak acid groups by increasing solution pH.[13d] It has also been observed that end-groups, particularly those of a specifically hydrophilic or hydrophobic nature, can significantly alter the effective transition temperature of thermosensitive polymers.[14]

A particularly useful feature of this reversible transition from unimers to micelles is the potential for reversible hydrogels; above the critical gelation concentration, which is typically ~20 wt % for star-like block copolymer micelles, the increase in volume fraction associated with

micellization is sufficient to form packing-based hydrogels.[8, 10-11] An example of this type of thermosensitive block copolymer-based gel, also referred to as injectable hydrogels as they can be injected *via* syringe below the LCST of the core-forming block before gelling at higher temperature, can be found in aqueous solutions of block copolymers of poly(ethylene oxide) (PEO) and the thermosensitive poly(propylene oxide) (PPO), such as PEO-*b*-PPO-*b*-PEO.[15] Above the LCST of PPO, the block copolymers self-associates to form micelles with collapsed, PPO cores. As temperature is further increased, the PEO corona also undergoes a decrease in length. As this shrinkage will eventually reduce the micellar volume fraction below that required for gelation, these packing-based micellar hydrogels often have a C-shaped phase diagram at moderate concentrations, referring to the lower temperature sol-gel transition occurring upon micellization and the gel-sol transition observed at higher temperatures, as shown in Figure 1.2.[16]

Our group has done much work investigating the unimer-micelle and sol-gel transitions of doubly thermosensitive diblock copolymer micelles, which can be said to be an amalgam of the two types of thermosensitive micelles described above; the block with the lower transition temperature ($LCST_1$) acts as the core-forming block in the reversible formation of micelles, and the block with the higher transition temperature ($LCST_2$) acts as a thermosensitive corona, shrinking due to dehydration upon sufficient heating and, at temperatures sufficiently above their LCST cause reversible aggregation and precipitation of micelles.[17] Visually, these gels are transparent in the low temperature sol and gel state, but become cloudy when heated to temperatures above $LCST_2$. Both the sol-gel and gel-sol transitions were able to be modified by incorporating a small amount of weak acid, *e.g.* acrylic acid, into the first and second block, respectively.

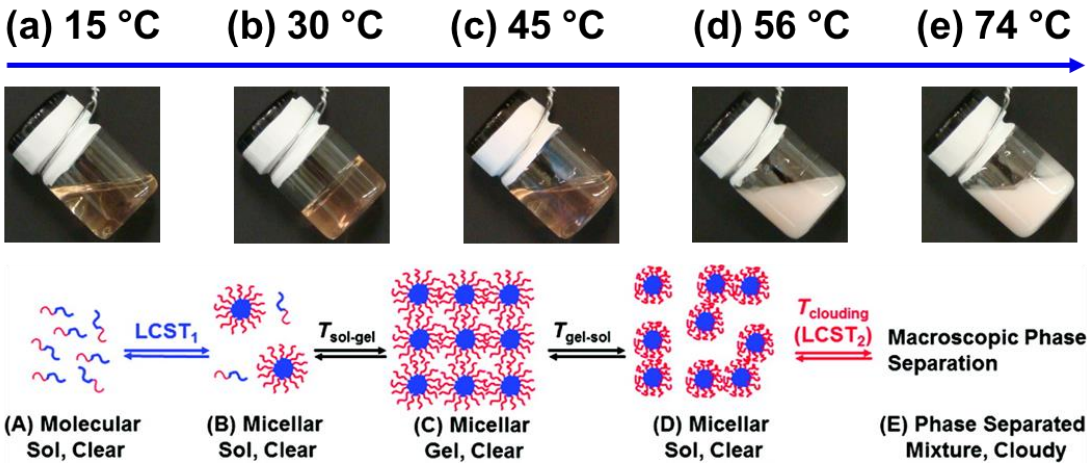

Figure 1.2. Digital optical images of an aqueous, 20 wt % solution of a doubly thermosensitive diblock copolymer at various temperatures[17a] (top) and a schematic illustration of the transition from a clear molecular sol to a clear micellar sol, clear micellar gel, clear micellar sol, and cloudy mixture upon increasing temperature.[17b] (Adapted from Refs. 17a and 17b with permission from the American Chemical Society)

Another type of these so-called injectable hydrogels is based on the formation of a three-dimensional physically crosslinked network in water. These network-based gels are typically composed of ABA or ABC triblock copolymers in which the center block is a relatively long, hydrophilic block, and the outer blocks are thermosensitive.[16a, 18] As before, these thermosensitive blocks will associate into micellar cores at temperatures above their LCSTs; gelation, however, is brought about through the bridging of the cores by the hydrophilic block, as shown in Figure 1.3. These gels exhibit a sol-gel transition based on the LCST of the thermosensitive block similar to the packing-based micellar hydrogels described above, but the interconnected nature of this gelation system requires significantly less polymer, often ~5 wt % or less.[19] The strategy of incorporating small quantities of responsive groups into thermosensitive polymers is still viable for network-based gels, and thermosensitive micellar gels have been synthesized with sensitivity toward pH,[20] light,[19b] enzyme,[19a] and other stimuli for the tuning of sol-gel transition temperature to good effect.

Micellar hydrogels based on thermosensitive diblock copolymers are an intriguing class of materials with potential applications in drug delivery, tissue engineering and the design of other "smart" materials. However, in aqueous systems, towards which a large portion of research is focused due to biocompatibility and environmental considerations, these reversible micellar gels are limited to polymeric, hydrophobic cores. Chapters 2 and 3 of this dissertation describe unique, hybrid injectable gels which may lead to more versatile gelation systems with a wider array of potential payloads and functionalities.

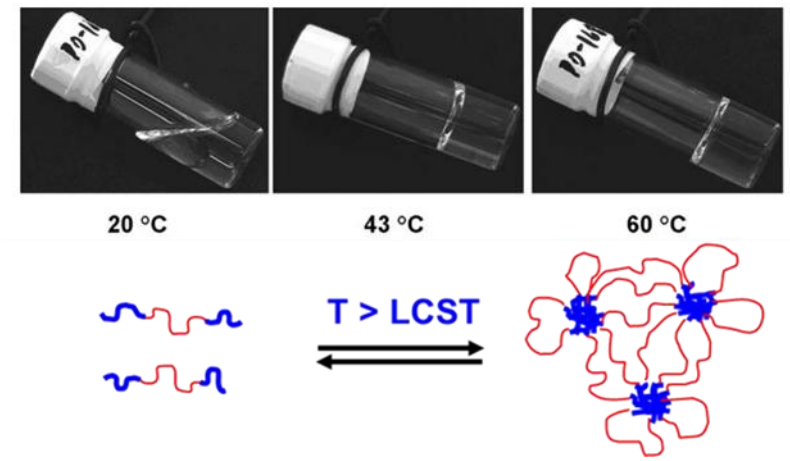

Figure 1.3. Digital optical pictures of a 10.0 wt% aqueous solution of an ABA triblock copolymer with thermosensitive A blocks and a hydrophilic B block at three temperatures (top) and a schematic illustration of the reversible formation of a three-dimensional network above the LCSt of the A blocks.[19b] (Adapted from Reference 19b with permission from the Royal Society of Chemistry)

1.1.2.2. Synthesis and Behavior of Stimuli-Responsive Hairy Particles

Stimuli-responsive polymers can be utilized to impart environmental sensitivity to brush-grafted particles as well. Particles grafted with thermosensitive polymer brushes undergo an overall decrease in hydrodynamic volume at temperatures above the LCST of the tethered polymer. The nature of this transition is not unlike that observed in micelles with a thermosensitive corona, and the dehydration of grafted polymers at higher temperatures will eventually lead to aggregation similar to what is observed in those systems. The transition behavior of thermosensitive hairy particles, however, is often more complex than that of individual chains or micelles, as it is influenced by substrate size, curvature, and grafting density. One example of this substrate effect can be seen in the work performed by the Tenhu research group, who prepared 3.2 nm gold nanoparticles (NPs) with PNIPAAm tethered by thiol-gold linkages. These brush grafted NPs exhibited two phase transitions according to microcalorimetry: a narrow transition at 30.2 °C and a broader transition at 39.0 °C. These brushes were synthesized *via* RAFT using a cumyl-dithiobenzoate chain transfer agent (CTA), and the polymer prior to grafting exhibited a single transition at 34.3 °C.[21] As mentioned previously, grafted polymers assume an extended conformation to relieve chain crowding. The fixation of the end group results in a gradient decrease in segmental density as distance from the substrate surface is increased, particularly for NPs of a few nanometers. This inhomogeneity leads to broad or even step-wise transitions because the higher segmental density near the surface impedes hydration and results in a lower LCST, while the segments further from the grafting sites are subjected to this effect to a lesser, or even nonexistent, degree.[22] Using a "grafting from" method, our group synthesized thermosensitive brush-grafted silica particles using oligo(ethylene glycol) methacrylates, which are another class

of monomers for use in the synthesis of LCST type polymers.[23] These hairy particles exhibited a relatively broad LCST transition at temperatures consistently lower than those of free polymer.[24]

An interesting feature of thermosensitive brush-grafted particles is their ability for spontaneous transfer between two phases, namely from water to an immiscible liquid phase and *vice versa*.[3] At temperatures above the LCST transition, the brushes become hydrophobic and will drive the transfer to another appropriate liquid phase. This transport of particles can be reversible; cooling below the brush LCST will trigger the migration back to the aqueous layer. The extent of this transfer is dependent on the relative affinities of the brushes for either phase below and above their LCST. For example, using poly(methoxytri(ethylene glycol) methacrylate) (PTEGMMA) brush-grafted particles, our group observed a quantitative transfer from water to ethyl acetate upon heating to 60 °C, as shown in Figure 1.4; the LCST of unbound PTEGMMA is 48 °C.[25] When partitioned between water and 1-butanol, only a 60 % transfer from water was observed, and no transfer was observed when using toluene as the organic phase. Interestingly, Wang and coworkers were able to facilitate the transfer of poly(methoxydi(ethylene glycol) methacrylate)-*co*-poly(ethylene glycol) methacrylate (P(DEGMMA-*co*-PEGMMA)) brush-grafted gold NPs, from water into toluene by adding sodium chloride to the aqueous layer.[26] The addition of salt typically lowers the effective LCST of thermosensitive polymers,[10] and, in this case, decreased their affinity toward water such that transfer to toluene became thermodynamically favored; this transfer was reversed when cooled below 5 °C. In another example of modulating the driving force of phase transfer, our group observed the reversible transfer of PTEGMMA-grafted particles between water and an ionic liquid, 1-ethyl-3-methylimidazolium bis(trifluoromethylsulfonyl)imide ([EMIM][TFSI]), but particles grafted with brushes of PDEGMMA, which has the lower LCST of 26 °C and, therefore, less hydrophilicity, did not return to water after transfer to the ionic liquid,

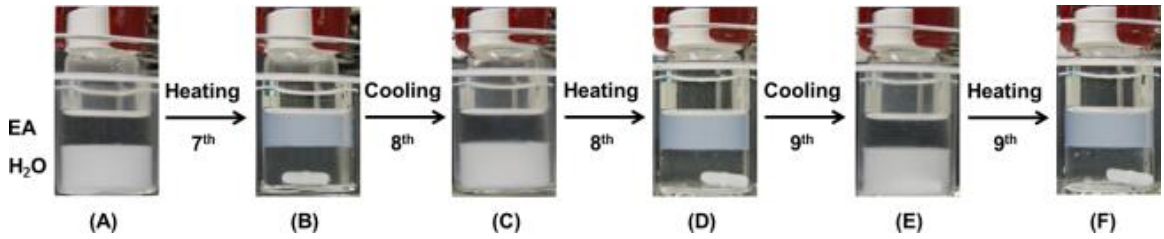

Figure 1.4. Optical images of aqueous and ethyl acetate layers after seventh cooling in an ice/water bath (a); seventh heating in an 60 °C oil bath (b); eighth cooling (c); eighth heating (d); ninth cooling (e); and ninth heating (f). The PTEGMMA brush-grafted nanoparticles were originally dispersed in water-saturated ethyl acetate at 63 °C (concentration: 1.0 mg/mL).[25] (Reprinted from Ref. 25 with permission from the American Chemical Society)

despite being kept at 0 °C for a prolonged period.[27] The ability to transfer substances across a liquid-liquid interface, especially in a reversible manner using thermoresponsive brush-grafted particles, has potential applications in purification and payload delivery and is particularly useful in the engineering of recyclable catalysts. [28]

1.1.3 Multicomponent Polymer Brush-Grafted Particles

Another type of environmental responsiveness available to hairy particles is that of multicomponent brushes, specifically substrates to which two or more immiscible polymers are tethered. Perhaps the most studied case of this class of hairy particles is mixed polymer brush-grafted particles, which consist of two different polymers grafted randomly or alternately to a substrate. These grafted polymers undergo microphase separation in an attempt to minimize contacts between unlike segments while also minimizing the entropically unfavorable stretching of individual chains. In this way, they are much like the analogous AB diblock copolymers, which have long been known to exhibit microphase separation into A or B-rich domains. The phase behavior of diblock copolymers are governed primarily by the Flory-Huggins interaction parameter (χ), degree of polymerization (DP), and volume fraction of each block (f_A and f_B);[29] additional parameters for mixed brushes include distribution of grafting sites, grafting density, and substrate curvature. As both polymers are covalently tethered to the substrate and limited in the extent they can rearrange, the responsive properties of mixed brushes are dictated by the interaction between each polymer and the environment.[30] Marko and Witten first theorized that melt state mixed brushes would undergo phase separation into a laterally segregated "ripple" state, as opposed to a layered structure. In selective solvents, mixed brushes assume the layered structure with the swollen, solvophilic block encompassing the solvophobic block, forming what is essentially tethered micelles, as shown in Scheme 1.2.[30-31] For example, poly(acrylic acid)/PS

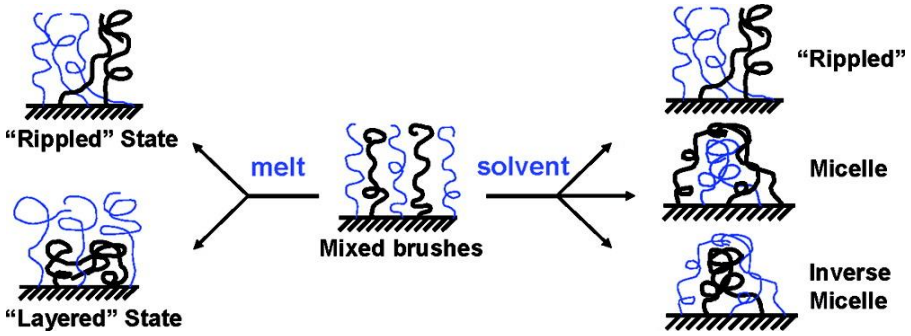

Scheme 1.2. A schematic illustration of the self-assembly of mixed homopolymer brushes under equilibrium melt conditions and in neutral or selective solvents.[30] (Reprinted from Ref. 30, with permission from the American Chemical Society).

mixed brush-grafted silica particles were found to form stable dispersions in both chloroform, a poor solvent for PAA, and methanol, a poor solvent for PS.[7b]

Our group has extensively studied mixed brush-grafted particles to elucidate the effect of various parameters on phase morphology, primarily through the use of silica particles functionalized with an asymmetric "Y-initiator" which allowed for the synthesis of well-defined mixed brushes by sequential controlled radical polymerizations, *e.g.* ATRP and NMRP. Poly(*tert*-butyl acrylate)(P*t*BA)/PS mixed brushes were made in this way, and the nanodomains formed were studied by TEM using RuO_4 as a selective staining agent for PS. By keeping the P*t*BA molecular weight constant and increasing the length of PS, an evolution was observed from isolated, spherical PS domains to short cylindrical domains to an essentially bicontinuous morphology at similar values of $M_{n,PS}$ and $M_{n,PtBA}$ to isolated P*t*BA nanodomains at larger $M_{n,PS}$ (Figure 1.6).[32] Similar studies were carried out to observe the effects of grafting density and overall molecular weight.[33]

Another type of multicomponent brush system is that of diblock copolymer brush-grafted particles. End-tethered diblock copolymers and their phase behavior have recently garnered interest and have been studied *via* simulation.[34] These morphologies differ from their analogues observed in mixed brushes in multiple ways, primarily in the vertical nature of this microphase separation and in the existence of substantial uniform phases at both low and high volume fractions of the outer (A) block. As this block is increased in length, the uniform phase is expected to give way to A-rich dots, stripes, holes, and full coverage as f_A approaches 0.5. This prediction has not yet been observed experimentally, and an initial exploration of this phase behavior is presented in Chapter 5.

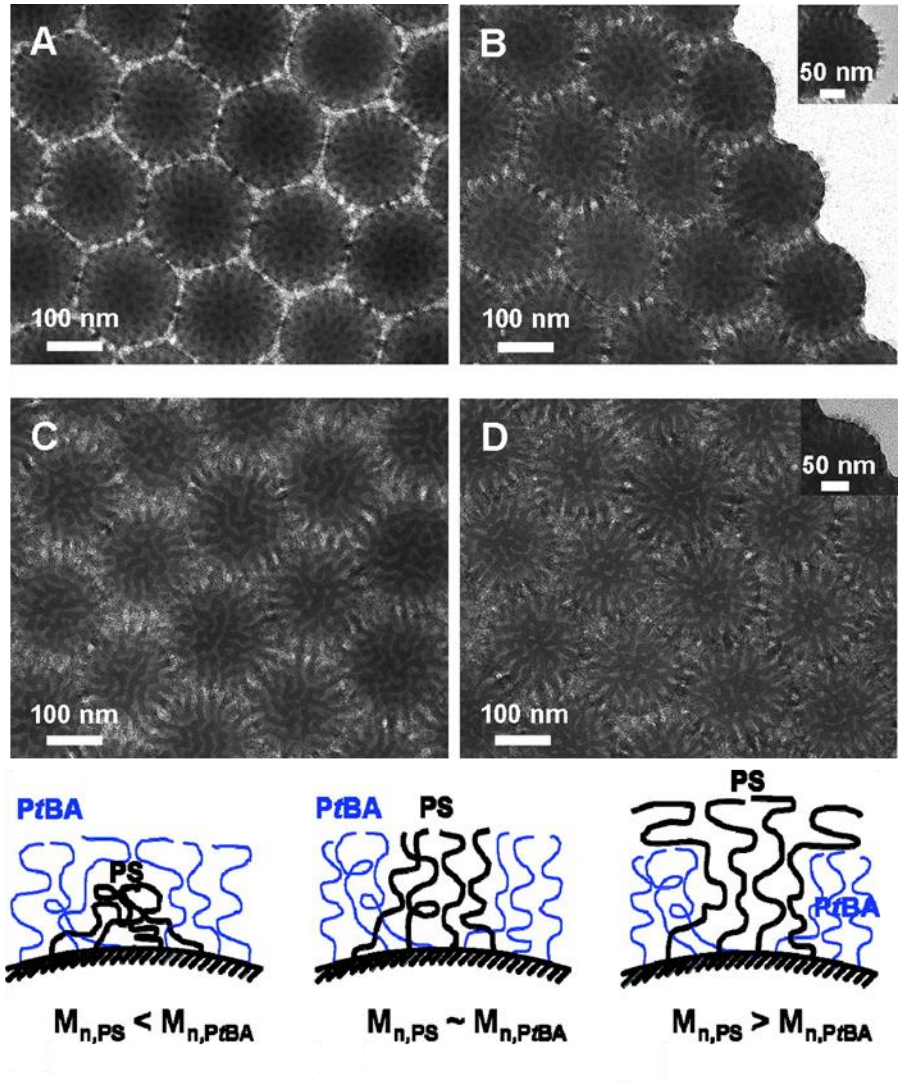

Figure 1.6. Top-view TEM micrographs of Mixed P*t*BA/PS brush-grafted silica particles with $M_{n,PS} < M_{n,PtBA}$ (A and B), $M_{n,PS} \approx M_{n,PtBA}$ (C) and $M_{n,PS} > M_{n,PtBA}$ (D), with schematic illustrations of the observed morphologies. The hairy particles were cast from CHCl3, a nonselective good solvent for both P*t*BA and PS, and thermally annealed and stained with RuO4 vapor.[32] (Adapted from Ref. 32 with permission from the American Chemical Society)

1.2. Dissertation Overview

This dissertation work is focused on the synthesis of polymer brush-grafted NPs and their applications in dispersed systems. The first portion presents the use of diblock copolymer brush-grafted particles in lieu of micelles in the formation of reversible, physical hydrogels. The second part explores the use of hydrophobic brush-grafted NPs as additives for lubricating oil, and the final part presents a preliminary analysis of the microphase separation of poly(*n*-butyl acrylate)-*b*-PS brushes grafted on silica particles.

As mentioned previously, micellar gels composed of thermosensitive block copolymers are a useful system for many applications, especially targeted delivery and release of drugs or other payloads. These hydrogels, however, are typically limited to hydrophobic, polymeric cores, limiting their versatility in terms of potential cargo. Thermosensitive brush-grafted NPs, on the other hand, can be made with mesoporous or hollow cores, which can be functionalized as desired, making them intriguing candidates for the engineering of uniquely adaptable hydrogel systems. Inspired by the collapse of thermosensitive brushes above their LCST and their similarity to the gel-sol transition observed in micellar gels of doubly thermosensitive diblock copolymers, we synthesized a series of thermosensitive hairy NPs for use in packing-based hydrogels. Sufficiently concentrated dispersions of these brush-grafted NPs were expected to form gels upon cooling due to the hydration-induced stretching of brushes and the subsequent increase in volume fraction. Upon heating, the gel would reversibly transition into a sol. A problem with both thermosensitive brush-grafted NPs and micelles with thermosensitive coronas is the clouding out and eventual precipitation at higher temperatures. To avoid this issue and maintain a homogenous system at higher temperatures, diblock copolymer brushes were grown from 17 nm silica NPs using a one pot SI-ATRP of DEGMMA, during which a second monomer, *N*,*N*-dimethylaminoethyl

methacrylate (DMAEMA), was added to produce brushes of PDEGMMA-*b*-P(DEGMMA-*co*-DMAEMA). The tertiary amine moieties were quaternized to yield P(DEGMMA-*co*-TMAEMA-I), a permanently charged outer block, which served to prevent heat-induced irreversible aggregation. This block was also found to modulate the gel-sol transition temperature and the LCST transition itself, as revealed by DLS experiments.

Encouraged by the success of these particles in packing-based hydrogels, we pursued the use of thermosensitive diblock copolymer brush grafted NPs to form three-dimensional network-based gels. In Chapter 3, the synthesis of hairy NPs composed of a hydrophilic, charged inner block and a thermosensitive outer block though sequential SI-ATRPs of DMAEMA and DEGMMA is described. The outer PDMAEMA block was converted to a permanently hydrophilic, charged polymer. These hairy NPs were easily dispersed in water, and these dispersions underwent a sol-gel transition at sufficiently high temperatures. The mechanism of this gelation is the association of the collapsed PDEGMMA blocks into micellar cores, which were linked to the NP substrates by the long, bridging hydrophilic polyelectrolyte block. We envision these hairy NP-based hydrogels as a step towards the synthesis of injectable hydrogels with truly designer properties and applications not available to conventional micellar hydrogels.

Chapter 4 marks somewhat of a departure from Chapters 2 and 3. Nanoparticles of various materials have great potential as lubricant additives.[35] Indispersibility of NPs in oils and the propensity of NPs to aggregate have led to some difficulties fully realizing this potential. Brush-grafted NPs, however, are known both for dispersibility and stability in dispersion due to the strongly favorable interaction between brushes and good solvents. We synthesized a series of oil-soluble hairy NPs through SI-ATRP of lauryl methacrylate. The brush-grafted NPs were easily dispersed in poly(alpha olefin) (PAO) lubricating base oil to yield homogenously additized

lubricants that exhibited excellent stability across a range of temperatures. Significant gains in friction reduction and wear prevention were observed upon the addition of 1.0 wt % of these hairy NP additives into PAO, relative to neat PAO, as confirmed through tribological analysis. Both molecular weight and concentration of NPs were found to affect tribological performance.

Chapter 5 details the initial steps in the elucidation of phase behavior of diblock copolymer brushes tethered on particles. P*n*BA-*b*-PS brushes were grown from 171 nm silica particles, and their microphase separation was observed *via* TEM, having selectively stained the PS domains using RuO_4. In qualitative agreement with the simulation work performed by Matsen and coworkers,[34c] we observed what appeared to be a progression from stripes to full coverage as PS block length was increased. While this study is preliminary in nature, we expect that these results will prove useful in the exploration of this system.

References

1. (a) Lowe, A. B.; Sumerlin, B. S.; Donovan, M. S.; McCormick, C. L., *J. Am. Chem. Soc.* **2002,** *124* (39), 11562-11563; (b) Shen, Y.; Kuang, M.; Shen, Z.; Nieberle, J.; Duan, H.; Frey, H., *Angew. Chem. Int. Ed.* **2008,** *47* (12), 2227-2230; (c) Zhang, T.; Zheng, Z.; Ding, X.; Peng, Y., *Macromol. Rapid Commun.* **2008,** *29* (21), 1716-1720.
2. Ranjan, R.; Brittain, W. J., *Macromolecules* **2007,** *40* (17), 6217-6223.
3. Bao, C.; Horton, J. M.; Bai, Z.; Li, D.; Lodge, T. P.; Zhao, B., *J. Polym. Sci., Part B: Polym. Phys.* **2014,** *52* (24), 1600-1619.
4. (a) Prucker, O.; Rühe, J., *Macromolecules* **1998,** *31* (3), 592-601; (b) Prucker, O.; Rühe, J., *Macromolecules* **1998,** *31* (3), 602-613.
5. Sagiv, J., *J. Am. Chem. Soc.* **1980,** *102* (1), 92-98.
6. Li, B.; Yu, B.; Ye, Q.; Zhou, F., *Acc. Chem. Res.* **2015,** *48* (2), 229-237.
7. (a) Husseman, M.; Malmström, E. E.; McNamara, M.; Mate, M.; Mecerreyes, D.; Benoit, D. G.; Hedrick, J. L.; Mansky, P.; Huang, E.; Russell, T. P.; Hawker, C. J., *Macromolecules* **1999,** *32* (5), 1424-1431; (b) Li, D.; Sheng, X.; Zhao, B., *J. Am. Chem. Soc.* **2005,** *127* (17), 6248-6256; (c) Ohno, K.; Morinaga, T.; Koh, K.; Tsujii, Y.; Fukuda, T., *Macromolecules* **2005,** *38* (6), 2137-2142.
8. Gil, E. S.; Hudson, S. M., *Prog. Polym. Sci.* **2004,** *29* (12), 1173-1222.
9. Seuring, J.; Agarwal, S., *Macromol. Rapid Commun.* **2012,** *33* (22), 1898-1920.
10. Schild, H. G., *Prog. Polym. Sci.* **1992,** *17* (2), 163-249.
11. Dimitrov, I.; Trzebicka, B.; Müller, A. H. E.; Dworak, A.; Tsvetanov, C. B., *Prog. Polym. Sci.* **2007,** *32* (11), 1275-1343.

12. Taylor, L. D.; Cerankowski, L. D., *J. Polym. Sci.: Polm. Chem. Ed.* **1975,** *13* (11), 2551-2570.

13. (a) Bütün, V.; Billingham, N. C.; Armes, S. P., *J. Am. Chem. Soc.* **1998,** *120* (45), 11818-11819; (b) Liu, S.; Armes, S. P., *Angew. Chem. Int. Ed.* **2002,** *41* (8), 1413-1416; (c) Lokitz, B. S.; York, A. W.; Stempka, J. E.; Treat, N. D.; Li, Y.; Jarrett, W. L.; McCormick, C. L., *Macromolecules* **2007,** *40* (18), 6473-6480; (d) Yin, X.; Hoffman, A. S.; Stayton, P. S., *Biomacromolecules* **2006,** *7* (5), 1381-1385; (e) Jiang, X.; Zhao, B., *Macromolecules* **2008,** *41* (23), 9366-9375; (f) Jiang, X.; Lavender, C. A.; Woodcock, J. W.; Zhao, B., *Macromolecules* **2008,** *41* (7), 2632-2643.

14. (a) Jiang, X.; Zhao, B., *J. Polym. Sci., Part A: Polym. Chem.* **2007,** *45* (16), 3707-3721; (b) Luo, C.; Zhao, B.; Li, Z., *Polymer* **2012,** *53* (8), 1725-1732.

15. (a) Mortensen, K.; Brown, W.; Nordén, B., *Phys. Rev. Lett.* **1992,** *68* (15), 2340-2343; (b) Pozzo, D. C.; Walker, L. M., *Macromolecules* **2007,** *40* (16), 5801-5811.

16. (a) Hamley, I., Block Copolymers in Solution: Fundamentals and Applications. John Wiley & Sons, Ltd: 2005; (b) Hamley, I. W.; Pople, J. A.; Fairclough, J. P. A.; Ryan, A. J.; Booth, C.; Yang, Y. W., *Macromolecules* **1998,** *31* (12), 3906-3911.

17. (a) Jin, N.; Woodcock, J. W.; Xue, C.; O'Lenick, T. G.; Jiang, X.; Jin, S.; Dadmun, M. D.; Zhao, B., *Macromolecules* **2011,** *44* (9), 3556-3566; (b) Jin, N.; Zhang, H.; Jin, S.; Dadmun, M. D.; Zhao, B., *Macromolecules* **2012,** *45* (11), 4790-4800; (c) Jin, N.; Zhang, H.; Jin, S.; Dadmun, M. D.; Zhao, B., *J. Phys. Chem. B* **2012,** *116* (10), 3125-3137.

18. (a) Kirkland, S. E.; Hensarling, R. M.; McConaughy, S. D.; Guo, Y.; Jarrett, W. L.; McCormick, C. L., *Biomacromolecules* **2008,** *9* (2), 481-486; (b) Madsen, J.; Armes, S. P.;

Lewis, A. L., *Macromolecules* **2006,** *39* (22), 7455-7457; (c) Mortensen, K.; Brown, W.; Joergensen, E., *Macromolecules* **1994,** *27* (20), 5654-5666; (d) Zhou, C.; Hillmyer, M. A.; Lodge, T. P., *J. Am. Chem. Soc.* **2012,** *134* (25), 10365-10368.

19. (a) Woodcock, J. W.; Jiang, X.; Wright, R. A. E.; Zhao, B., *Macromolecules* **2011,** *44* (14), 5764-5775; (b) Woodcock, J. W.; Wright, R. A. E.; Jiang, X.; O'Lenick, T. G.; Zhao, B., *Soft Matter* **2010,** *6* (14), 3325-3336.

20. (a) Henn, D. M.; Wright, R. A. E.; Woodcock, J. W.; Hu, B.; Zhao, B., *Langmuir* **2014,** *30* (9), 2541-2550; (b) O'Lenick, T. G.; Jin, N.; Woodcock, J. W.; Zhao, B., *J. Phys. Chem. B* **2011,** *115* (12), 2870-2881.

21. Shan, J.; Chen, J.; Nuopponen, M.; Tenhu, H., *Langmuir* **2004,** *20* (11), 4671-4676.

22. Zhulina, E. B.; Borisov, O. V.; Pryamitsyn, V. A.; Birshtein, T. M., *Macromolecules* **1991,** *24* (1), 140-149.

23. Lutz, J.-F., *Adv. Mater.* **2011,** *23* (19), 2237-2243.

24. Li, D.; Jones, G. L.; Dunlap, J. R.; Hua, F.; Zhao, B., *Langmuir* **2006,** *22* (7), 3344-3351.

25. Li, D.; Zhao, B., *Langmuir* **2007,** *23* (4), 2208-2217.

26. (a) Edwards, E. W.; Chanana, M.; Wang, D.; Möhwald, H., *Angew. Chem. Int. Ed.* **2008,** *47* (2), 320-323; (b) Stocco, A.; Chanana, M.; Su, G.; Cernoch, P.; Binks, B. P.; Wang, D., *Angew. Chem. Int. Ed.* **2012,** *51* (38), 9647-9651.

27. Horton, J. M.; Bai, Z.; Jiang, X.; Li, D.; Lodge, T. P.; Zhao, B., *Langmuir* **2011,** *27* (5), 2019-2027.

28. (a) Hao, Y.; Jiang, J.; Wang, Y.; Jin, Z., *Catal. Commun.* **2015,** *71*, 106-110; (b) Li, K.; Wang, Y.; Jiang, J.; Jin, Z., *Catal. Commun.* **2010,** *11* (6), 542-546; (c) Li, W.; Wang, Y.;

Zeng, M.; Jiang, J.; Jin, Z., *RSC Advances* **2016,** *6* (8), 6329-6335; (d) Marcilla, R.; Curri, M. L.; Cozzoli, P. D.; Martínez, M. T.; Loinaz, I.; Grande, H.; Pomposo, J. A.; Mecerreyes, D., *Small* **2006,** *2* (4), 507-512.

29. (a) Bates, F. S.; Fredrickson, G. H., *Annu. Rev. Phys. Chem.* **1990,** *41* (1), 525-557; (b) Bates, F. S.; Fredrickson, G. H., *Physics Today* **1999,** *52* (2), 32-38; (c) Leibler, L., *Macromolecules* **1980,** *13* (6), 1602-1617.

30. Zhao, B.; Zhu, L., *Macromolecules* **2009,** *42* (24), 9369-9383.

31. Zhu, L.; Zhao, B., *J. Phys. Chem. B* **2008,** *112* (37), 11529-11536.

32. Jiang, X.; Zhong, G.; Horton, J. M.; Jin, N.; Zhu, L.; Zhao, B., *Macromolecules* **2010,** *43* (12), 5387-5395.

33. (a) Bao, C.; Tang, S.; Horton, J. M.; Jiang, X.; Tang, P.; Qiu, F.; Zhu, L.; Zhao, B., *Macromolecules* **2012,** *45* (19), 8027-8036; (b) Bao, C.; Tang, S.; Wright, R. A. E.; Tang, P.; Qiu, F.; Zhu, L.; Zhao, B., *Macromolecules* **2014,** *47* (19), 6824-6835; (c) Jiang, X.; Zhao, B.; Zhong, G.; Jin, N.; Horton, J. M.; Zhu, L.; Hafner, R. S.; Lodge, T. P., *Macromolecules* **2010,** *43* (19), 8209-8217.

34. (a) Chantawansri, T. L.; Bosse, A. W.; Hexemer, A.; Ceniceros, H. D.; García-Cervera, C. J.; Kramer, E. J.; Fredrickson, G. H., *Physical Review E* **2007,** *75* (3), 031802; (b) Griffiths, G. H.; Vorselaars, B.; Matsen, M. W., *Macromolecules* **2011,** *44* (9), 3649-3655; (c) Vorselaars, B.; Kim, J. U.; Chantawansri, T. L.; Fredrickson, G. H.; Matsen, M. W., *Soft Matter* **2011,** *7* (11), 5128-5137.

35. (a) Bakunin, V. N.; Suslov, A. Y.; Kuzmina, G. N.; Parenago, O. P.; Topchiev, A. V., *Journal of Nanoparticle Research 6* (2), 273-284; (b) Kim, D.; Archer, L. A.,

Langmuir **2011,** *27* (6), 3083-3094; (c) Wu, Y. Y.; Tsui, W. C.; Liu, T. C., *Wear* **2007,** *262* (7–8), 819-825.

Chapter 2. Reversible Sol-Gel Transitions of Aqueous Dispersions of Silica Nanoparticles Grafted with Diblock Copolymer Brushes Composed of a Thermosensitive Inner Block and a Charged Outer Block

Abstract

This chapter presents the synthesis of thermosensitive diblock copolymer brush-grafted silica nanoparticles (hairy NPs) and the study of thermally induced, reversible sol-gel transitions of their aqueous dispersions. The brushes consisted of a thermosensitive poly(methoxydi(ethylene glycol) methacrylate) (PDEGMMA) inner block and a charge-carrying, poly(DEGMMA-*co*-2-(methacryloyloxy)ethyltrimethylammonium iodide) outer block, which were prepared by a one-pot, surface-initiated atom transfer radical polymerization and subsequent quaternization of tertiary amine moieties in the second block with iodomethane. Above a critical concentration, the aqueous dispersion of hairy NPs with an appropriate block copolymer composition exhibited a reversible transition from a free flowing liquid to a free standing hydrogel upon cooling from elevated temperatures, which was driven by the lower critical solution temperature transition of the thermosensitive inner block of hairy NPs as confirmed by dynamic light scattering study. At the same concentration of hairy NPs, the sol-gel transition temperature was higher when the highly hydrated, charged outer block was longer. The transition temperature decreased with decreasing the concentration of hairy NPs in the dispersion; reversible gelation was achieved with a concentration of hairy NPs in water as low as 5.5 wt %. Interestingly, the LCST transition of the inner thermosensitive PDEGMMA block disappeared and no sol-gel transition was observed in the studied temperature range when the charged outer block was sufficiently long.

2.1. Introduction

Micellar hydrogels of thermosensitive hydrophilic block copolymers have received substantial attention due to their ability to exhibit *in situ* sol–gel transitions in response to temperature changes.[1] These hydrogels, often referred to as injectable hydrogels, can offer utility in a wide range of applications, particularly in the controlled release of substances.[1,2] Unlike their chemically crosslinked counterparts, aqueous solutions of thermosensitive block copolymers can be injected as free-flowing liquids via syringe and needle and turn into hydrogels upon exposure to temperature variations. There are generally two types of thermosensitive injectable block copolymer micellar hydrogels: (i) 3-dimensional network hydrogels formed by the bridging of a soluble middle block, typically, of an ABA triblock copolymer among micellar cores,[1,3] and (ii) packing-based hydrogels made up of discrete micelles.[1,4,5] Our lab recently showed that the incorporation of a small amount of pH- or light-responsive moieties into the thermosensitive outer blocks of ABA triblock copolymers led to 3-D micellar network hydrogels with tunable sol–gel transition temperatures.[6] Examples of the second type of micellar gels include those of thermosensitive diblock copolymers and PEO-*b*-PPO-*b*-PEO.[4,5] While the critical gelation concentration (CGC) for 3-D network gels can be as low as 5 wt %,[3c,6a] the CGC for packing-based polymer micellar hydrogels is typically ~ 20 wt %.[1,5]

Polymer brush-grafted nanoparticles (NPs), also known as hairy NPs, are composed of a core, typically inorganic or metallic, and a dense layer of polymer chains with one end bound covalently on the core surface.[7-9] These NPs, with a distinct core and a shell, are structurally similar to block copolymer micelles in some sense. Our lab has been interested in the synthesis and behavior of well-defined stimuli-responsive, particularly thermosensitive, hairy NPs.[10] The brushes grafted on the NPs can undergo swelling-collapse transitions in response to external

stimuli, which alter the solvophilicity of hairy NPs and can be exploited to control the accessibility of functional groups or substances within the brushes or core NPs.[11]

Given that thermosensitive hairy NPs are structurally and conceptually similar to block copolymer micelles, it should be possible to use them to fashion injectable hydrogels by utilizing the lower critical solution temperature (LCST) transitions induced by temperature changes. Similar to block copolymer micellar hydrogels, it is possible to achieve the gelation of aqueous dispersions of hairy NPs through the two mechanisms mentioned earlier. These hybrid hydrogels, if realized, would add additional functions to the traditional block copolymer micellar hydrogels and thus expand the area of injectable hydrogels. Unlike thermosensitive block copolymer micelles where the core of the micelles is typically organic and hydrophobic, hairy NPs can be fabricated using a wide variety of inorganic and metallic NPs with various material functionalities,[7-11] such as magnetic and optical properties.[12] The rigid nature of the core also lends itself to various shapes, such as disk-like or cubic,[13] which are not easily accessible by polymer micelles. In addition, the core NPs can be porous or hollow,[13,14] and the interior surface can be made hydrophobic or hydrophilic, charged or neutral, allowing for loading of a variety of substances and effectively overcoming the limitations of block copolymer micelle systems.

Motivated by these prospects, we initiated an effort to develop hybrid hydrogels solely based on stimuli-responsive hairy NPs. In the present work, we synthesized thermosensitive diblock copolymer brush-grafted, 17 nm silica NPs. The brushes were poly(methoxydi(ethylene glycol) methacrylate)-*b*-poly(methoxydi(ethylene glycol) methacrylate-*co*-2-(methacryloyloxy)ethyltrimethylammonium iodide) (PDEGMMA-*b*-P(DEGMMA-*co*-TMAEMA-I)), which were prepared by one-pot surface-initiated atom transfer radical polymerization (ATRP) using monomers DEGMMA and *N*,*N*-dimethylaminoethyl methacrylate

(DMAEMA) and subsequent quaternization of DMAEMA units in the second block with iodomethane (Scheme 2.1). The second monomer, DMAEMA, was added into the polymerization mixture after a desired conversion of DEGMMA was achieved. PDEGMMA is a thermosensitive polymer with a lower critical solution temperature (LCST) of 26 °C in water.[15] The outer block contains quaternized DMAEMA units; these permanently charged moieties are introduced to facilitate the dispersion of hairy NPs in water and to grant stability against aggregation at elevated temperatures. We show that at a sufficient concentration, aqueous dispersions of these hairy NPs can undergo *in situ*, reversible transitions from free-flowing liquids to free standing hydrogels upon cooling from elevated temperatures. The sol-gel transition can be achieved with a concentration of hairy NPs in water as low as 5.5 wt %, far less than the typical CGC of thermosensitive diblock copolymers (~ 20 wt%). This is the first example of temperature-induced sol-gel transitions of aqueous dispersions of thermoresponsive polymer brush-grafted inorganic NPs, demonstrating the potential of hairy NPs in the area of hybrid polymer hydrogels.

2.2. Experimental Section

2.2.1. Materials

MIBK-ST, a dispersion of silica nanoparticles (NPs) with a size of 10–15 nm (according to the manufacturer) in methyl isobutyl ketone (MIBK) (30-31 wt % SiO_2), was from Nissan Chemical. Chlorodimethylsilane (98%) was obtained from Alfa Aesar and stored in a refrigerator. Karstedt's catalyst (Platinum-divinyltetramethyldisiloxane complex in xylene, 2.1~2.4% Pt concentration in xylene) was purchased from Gelest, Inc. Tetrahydrofuran (THF) and toluene were each distilled from sodium and benzophenone and used immediately. CuBr (98%, Aldrich) was

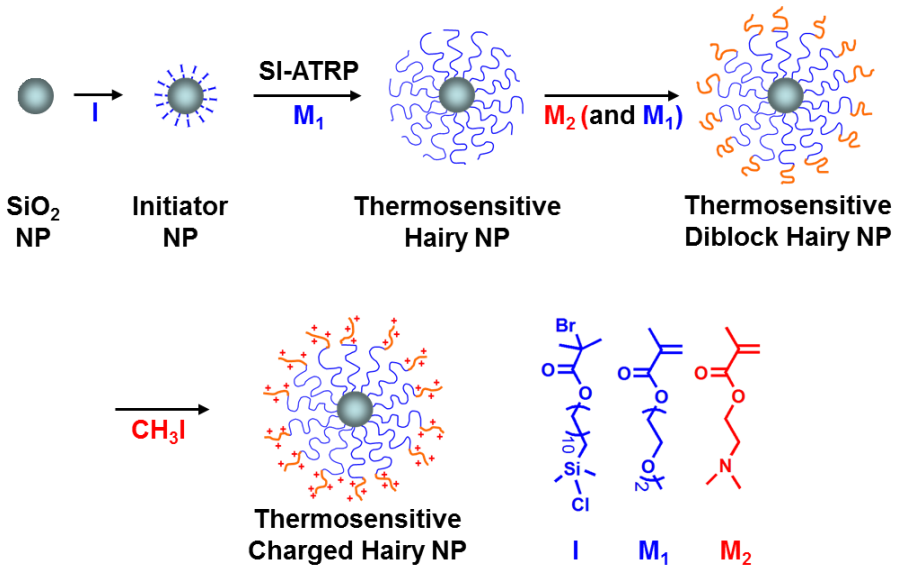

Scheme 2.1. Synthesis of PDEGMMA-*b*-P(DEGMMA-*co*-TMAEMA-I) Brush-Grafted Silica Nanoparticles (NPs) by a Surface-Initiated, One-Pot Atom Transfer Radical Polymerization and Subsequent Quaternization of Tertiary Amine Units with Iodomethane

stirred in glacial acetic acid overnight, filtered, and washed with absolute ethanol and diethyl ether. The purified CuBr powder was dried under high vacuum and stored in a desiccator. $CuBr_2$ (anhydrous, 99%) and iodomethane (99%, stabilized) were purchased from Acros and used as received. *N*, *N*, *N′*, *N′*, *N″*-Pentamethyldiethylenetriamine (PMDETA, 99%, Aldrich) and ethyl 2-bromoisobutyrate (EBiB, 98%, Aldrich) were dried with calcium hydride, distilled under reduced pressure, and stored in a desiccator. Methoxydi(ethylene glycol) methacrylate (or di(ethylene glycol) methyl ether methacrylate, DEGMMA, 95%, Aldrich) was stirred in the presence of CaH_2, distilled under vacuum, and stored in a refrigerator. *N, N*-Dimethylaminoethyl methacrylate (DMAEMA, 99%, Acros) was passed through a short column of silica gel (bottom)/activated basic aluminum oxide (top) (2/1, v/v) to remove the initiator and stored in a refrigerator. 10-Undecenyl 2-bromoisobutyrate was synthesized according to a literature procedure.[10b] All other chemical reagents were purchased from either Aldrich or Fisher and used without further purification.

2.2.2. Characterization

Size exclusion chromatography (SEC) was carried out at ambient temperature using an SEC system composed of a Waters 510 pump, a Knauer Smartline 2300 RI detector, and three PSS GRAM linear columns in series (each 8 × 300 mm, 3000 Å, 1000 Å, 100 Å, Polymer Standards Service-USA, Inc.). HPLC grade *N*,*N*-dimethylformamide (DMF) with 0.1 *M* LiBr was used as the mobile phase with a flow rate of 1.0 mL/min. The system was calibrated by using polystyrene standards, and the data were processed using Cirrus^{TM} GPC/SEC software. ^{1}H NMR spectra were recorded on a Varian VNMRS 500 MHz spectrometer, and the residual solvent proton signal was used as the internal standard. Thermogravimetric analysis (TGA) was carried out in air at a heating rate of 20 °C/min from room temperature to 800 ºC using a TA Discovery TGA-MS. Transmission electron microscopy (TEM) was performed using a Zeiss Libra 200 HT FE MC microscope with

an accelerating voltage of 200 kV, and bright field images were taken with a bottom-mounted Gatan UltraScan US1000XP CCD camera. Samples were drop-cast from dispersions in chloroform with a concentration of ~ 4 mg/mL onto a carbon-coated, copper TEM grid using a glass pipet and were allowed to dry at ambient conditions.

2.2.3. Synthesis of ATRP Initiator-Functionalized, 17 nm Silica NPs

10-Undecenyl 2-bromoisobutyrate (2.002 g, 6.27 mmol) was added to a 50 mL two-necked flask and dried under high vacuum. Chlorodimethylsilane (3.0 mL, 27 mmol) was added to the flask under an N_2 atmosphere, followed by the injection of a solution of Karstedt's catalyst in xylene (75 µL). After the reaction was complete, as demonstrated by the disappearance of the double bond peaks in the ^{1}H NMR spectrum of the reaction mixture, the unreacted excess chlorodimethylsilane was removed *in vacuo* and the obtained 11-(chlorodimethylsilyl)undecyl 2-bromoisobutyrate was dissolved in THF (5 mL).

MIBK-ST (6.663 g, corresponding to 1.999 g bare silica NPs) was added to a 100 mL three-necked flask and diluted with 15 mL anhydrous toluene. A portion of the solvents (~10 mL) was then distilled off under vacuum to azeotropically remove the trace amount of water. Dry toluene (15 mL) was then injected into the flask, and the azeotropic distillation was carried out again. This process was repeated for a total of three times, followed by the addition of dry THF (20 mL). The dispersion was concentrated and diluted again with THF (20 mL). The resultant dispersion of silica NPs in the mixture of MIBK, toluene, and THF, totaling 30 mL, was transferred into the flask containing the chlorodimethylsilane–terminated ATRP initiator described in the preceding paragraph. The mixture was heated to 70 °C, and the reaction was carried out at this temperature under N_2 for 42 h. The initiator-functionalized silica NPs (initiator NPs) were then diluted in DMF and collected via centrifugation (Beckman Optima L-90K Ultracentrifuge with type 60 Ti rotor,

35,000 rpm, 30 min). The initiator NPs were then dispersed in DMF and centrifuged again. This dispersion-centrifugation cycle was repeated for a total of 4 times. The purified initiator NPs were dried under a stream of air, affording a slightly brown powder (1.901 g).

2.2.4. Synthesis of PDEGMMA-*b*-P(DEGMMA-*co*-DMAEMA) Brushes on 17 nm Silica NPs

The initiator NPs (1.057 g) were placed into a 100 mL three-necked flask, followed by the addition of anisole (44.046 g). The mixture was ultrasonicated until a homogeneous dispersion was obtained. DEGMMA (20.074 g, 0.107 mol), copper(I) bromide (30.9 mg, 2.15×10^{-4} mol), copper(II) bromide (7.7 mg, 3.5×10^{-5} mol), and ethyl 2-bromoisobutyrate (29.7 mg, 1.52×10^{-4} mol) were added to the dispersion. After PMDETA (30.2 mg, 1.74×10^{-4} mol) was injected, the mixture was immediately degassed by three freeze–pump–thaw cycles. The flask was then placed in a thermostated oil bath at 60 °C. The polymerization was monitored by ^{1}H NMR spectroscopy, using the peaks located at 4.34 and 4.16 ppm, which were from the -C*H*$_2$OOC- of monomer DEGMMA and polymer PDEGMMA, respectively. After the reaction proceeded for 4.5 h, a monomer conversion of 29.8% was reached, at which a large sample (17.785 g, 27.25 wt %) was removed from the polymerization mixture for the characterization of free polymer PDEGMMA and PDEGMMA brush-grafted NPs (HHP). The degree of polymerization (DP) of the polymer was calculated to be 101, taking into consideration both the free initiator and the surface-immobilized initiator.[16]

Immediately after the large sample was taken from the polymerization mixture at the monomer conversion of 29.8%, DMAEMA (9.312 g, 59.23 mmol), having been degassed *via* freeze-pump-thaw, was injected by syringe. A small aliquot was withdrawn for use as the $t = 0$ min sample in the ^{1}H NMR characterization of the synthesis of the second block, using the integral of the vinyl peak at 6.15 ppm along with the summed integrals of all -COOC*H*$_2$- peaks from 4.35

to 4.00 ppm. Portions of the reaction mixture were removed at t = 90 min (the free diblock copolymer was designated as BCP-1 and the hairy NPs was designated as BHP-1), 195 min (the free copolymer designated as BCP-2 and the hairy NPs designated as BHP-2), and 400 min (the free copolymer designated as BCP-3 and the hairy NPs designated as BHP-3) after the injection of DMAEMA, corresponding to the monomer conversions of 8.6, 15.2, and 30.3 %, respectively, on the basis of the new t = 0 min sample. (i.e., the monomer conversion of DEGMMA for the first block was excluded in the calculation of these monomer conversions.) The DPs were found to be 42, 75, 149 for the second block of three samples, respectively. Each withdrawn portion was opened to air, and diluted with DMF. The hairy NPs were isolated *via* ultracentrifugation (Beckman Optima L-90K Ultracentrifuge with type 60 Ti rotor, 35,000 rpm, 45 min), and washed five times with DMF through a cycle of re-dispersion, ultracentrifugation, and decanting of the supernatant solution. A portion of the supernatant liquid from the first cycle was passed through a column of silica gel (bottom)/activated basic aluminum oxide (top) (2:1, v/v). The free polymers were analyzed by SEC and ^{1}H NMR spectroscopy after precipitation in hexane and drying under vacuum.

2.2.5. Quaternization of PDEGMMA-*b*-P(DEGMMA-*co*-DMAEMA) Brush-Grafted Silica NPs Using CH_3I

Below is a representative procedure for the quaternization of DMAEMA units of BHP-3 using CH_3I, producing charged PDEGMMA-*b*-P(DEGMMA-*co*-TMAEMA-I brush-grafted silica NPs (BHP-3-Q). BHP-3 (215.1 mg, 0.237 mmol DMAEMA units) was added into a 25 mL two-necked flask and dispersed in dry THF (10 mL) under N_2. The flask was then completely wrapped with aluminum foil to protect the reaction mixture from exposure to light. Iodomethane (2.103 g, 14.82 mmol) was added into the NP dispersion, which was then stirred at ambient temperature

overnight. After water (10 mL) was added into the mixture, the volatile components were removed under high vacuum, yielding a pale yellow NP dispersion. The obtained hairy NPs, designated as BHP-3-Q, were purified by three cycles of ultracentrifugation (Beckman Optima L-90K Ultracentrifuge with type 60 Ti rotor, 35,000 rpm, 45 min) and re-dispersion using water. The NPs were collected as a transparent yellow gelatinous solid, re-dispersed in water, and freeze-dried overnight using a LABCONCO FreeZone 1 Liter Benchtop Freeze Dry System, yielding a light, fibrous solid (187.6 mg).

2.2.6. Preparation of Aqueous Dispersions of PDEGMMA-*b*-P(DEGMMA-*co*-TMAEMA-I) Brush-Grafted Silica NPs

The freeze-dried quaternized hairy NPs were added into a pre-weighed vial, to which Milli-Q water was added to achieve the desired concentration. The mixture was sonicated in an ice/water ultrasonic bath (Fisher Scientific Model B200 Ultrasonic Cleaner) to disperse the NPs, followed by sonication in warm water to facilitate dispersal. For rheological samples, the vials were stored in a refrigerator (~ 4 °C) overnight and further sonicated at room temperature to obtain a transparent, homogeneous dispersion.

2.2.7. Rheology Studies

Rheological experiments were conducted on a TA Instruments rheometer (Model TA AR2000ex). A cone-plate geometry with a cone diameter of 20 mm and an angle of 2° (truncation 52 μm) was used; the temperature was controlled *via* a Peltier plate. In each rheological measurement, an aqueous dispersion of quaternized hairy NPs (90 μL), which was warmed at an elevated temperature to facilitate the transfer, was added onto the bottom plate by a micropipet. To minimize water evaporation during the rheological measurement, the solvent trap was filled with water and covered. Dynamic storage modulus G' and loss modulus G'' were recorded from

oscillatory shear experiments performed at a fixed frequency of 1 Hz in a temperature ramp with a heating or cooling rate of 3 °C/min. The frequency dependences of G' and G'' at certain temperatures were obtained by frequency sweep tests from 0.1 to 100 Hz. A strain amplitude of γ = 1.0 % was used in all dynamic tests.

2.2.8. Dynamic Light Scattering (DLS) Studies of Thermoresponsive Properties of PDEGMMA-*b*-P(DEGMMA-*co*-TMAEMA-I) Brush-Grafted Silica NPs

The DLS studies of thermoresponsive properties of quaternized hairy silica NPs in water at a concentration of 0.2 mg/g were carried out on a Brookhaven Instruments BI-200SM goniometer equipped with a PCI BI-9000AT digital correlator, a temperature controller, and a solid-state laser (model 25-LHP-928-249, λ = 633 nm). The scattering angle was set at 90°. The aqueous dispersions of quaternized hairy NPs were filtered, using Millipore hydrophilic PTFE filters, into borosilicate glass tubes with an inner diameter of 7.5 mm, and the tubes were sealed with PE stoppers. The sample was placed in the sample holder of the DLS system, and the temperature was gradually varied. At each temperature, the DLS sample was equilibrated for 20 min before the data were recorded. A Laplace inversion program (CONTIN) was used to analyze the DLS data. For each temperature, multiple measurements (15 – 30 measurements) were taken, and the average apparent hydrodynamic size was calculated along with the standard deviation.

2.3. Results and Discussion

2.3.1. Synthesis of PDEGMMA-*b*-P(DEGMMA-*co*-DMAEMA) Brushes on 17 nm Silica NPs

Three PDEGMMA-*b*-P(DEGMMA-*co*-DMAEMA) brush-grafted silica NP samples with the same molecular weight for the first (inner) PDEGMMA block but different block lengths for the second (outer) P(DEGMMA-*co*-DMAEMA) block were synthesized through a one-pot, surface-initiated ATRP from initiator-functionalized silica NPs.

The silica NPs used in this work had an average size of 17 nm, determined from transmission electron microscopy (TEM) micrographs, and were surface-functionalized with a chlorodimethylsilane-terminated ATRP initiator, 11-(chlorodimethylsilyl)undecyl 2-bromoisobutyrate. To ensure the anhydrous conditions required for the immobilization of the chlorosilane-terminated initiator, the original dispersion of silica NPs in methyl isobutyl ketone was azeotropically distilled with toluene under vacuum three times to remove the trace amount of water in the dispersion. The remaining dispersion of silica NPs was subjected to a stepwise solvent exchange with anhydrous THF, which was freshly distilled from sodium/benzophenone, before a solution of 11-(chlorodimethylsilyl)undecyl 2-bromoisobutyrate in THF was added. The mass ratio of the chlorodimethylsilane-terminated initiator to silica NPs was 1.30 : 1.00. The immobilization reaction was carried out at 70 °C under a N_2 atmosphere for 42 h. The initiator-functionalized NPs were purified by multiple rounds of ultracentrifugation/re-dispersion in THF. After drying with a stream of air, the initiator NPs were collected as a slightly brown powder that can be readily dispersed in common organic solvents such as THF, $CHCl_3$, and DMF.

PDEGMMA-*b*-P(DEGMMA-*co*-DMAEMA) brushes were then grown from the initiator NPs by a one-pot, surface-initiated ATRP polymerization (Scheme 2.1). The initiator NPs were fully dispersed in anisole by ultrasonication before the addition of the first monomer, DEGMMA, and the catalyst. A free initiator, ethyl 2-bromoisobutyrate, was added into the reaction mixture to achieve a finer control of the surface polymerization and to produce a more easily characterized free polymer for ^{1}H NMR spectroscopy and size exclusion chromatography (SEC) analysis. The surface-initiated ATRP of DEGMMA was conducted at 60 °C using CuBr/$CuBr_2$/PMDETA as the catalyst system. After the DEGMMA conversion reached 29.8%, determined by ^{1}H NMR spectroscopy, a portion of the polymerization mixture was removed using a degassed syringe for

the characterization of free polymer PDEGMMA and the PDEGMMA brush-grafted silica NPs (HHP). From SEC analysis of the free homopolymer (Figure 2.1A), a unimodal peak was observed with $M_{n,SEC}$ of 22.8 kDa and a polydispersity index (PDI) of 1.24, indicating that the polymerization was controlled. TGA showed that the weight retentions of the initiator NPs and the purified HHP at ~ 800 °C were 89.4 and 22.8%, respectively (Figure 2.1B, curve i and ii), which confirmed that PDEGMMA brushes were successfully grown on the initiator NPs.

To study the molecular weight and molecular weight distribution of the grafted PDEGMMA brushes in HHP, we used HF to etch the silica core,[7c,17] collected and analyzed the cleaved polymer by SEC.[16] The SEC traces of the free PDEGMMA and the PDEGMMA cleaved from HHP were superimposed, indicating that the molecular weights and PDIs were essentially identical (Figure 2.2). By using the monomer conversion and the molar ratio of DEGMMA to the sum of free and surface-bound initiators, the degree of polymerization (DP) of PDEGMMA was calculated to be 101. Note that the amount of the surface initiator that successfully initiated polymerization was calculated from the ratio of the weight of grafted PDEGMMA brushes to the total weight of both free and grafted PDEGMMA by using the free initiator as reference. The mass of the PDEGMMA brushes grafted on silica NPs was determined from the TGA data and the amount of initiator NPs; the total weight of PDEGMMA was found from the monomer conversion and the amount of monomer DEGMMA used in the polymerization.[16]

Immediately after the removal of the first portion from the polymerization mixture, the second monomer, DMAEMA, which had already been degassed, was injected into the reaction system for the synthesis of the second block, P(DEGMMA-*co*-DMAEMA). Excluding both the

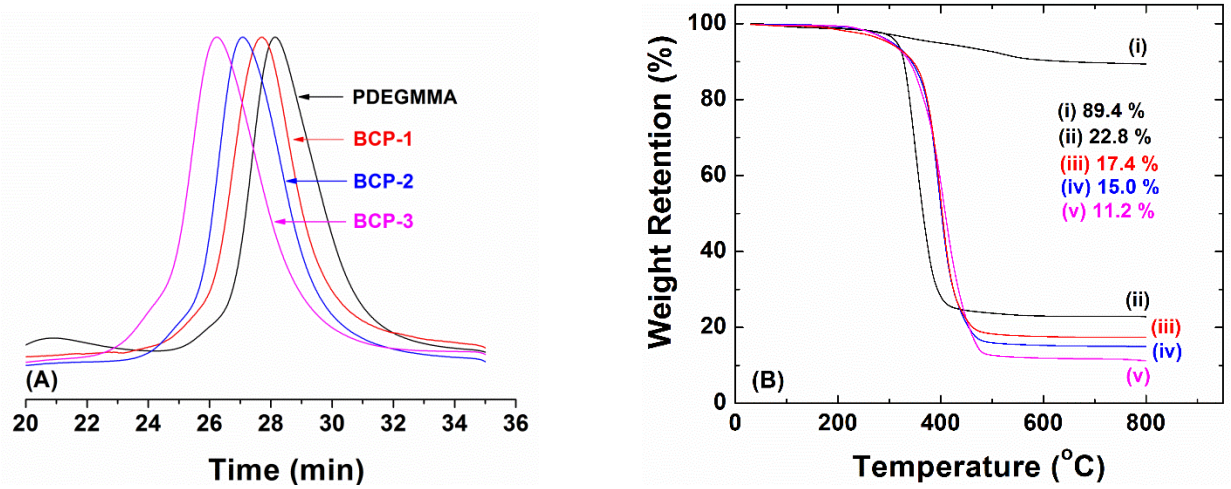

Figure 2.1. (A) Size exclusion chromatography (SEC) traces of free homopolymer PDEGMMA and PDEGMMA-*b*-P(DEGMMA-*co*-DMAEMA) diblock copolymers (BCP-1, BCP-2, and BCP-3). (B) Thermogravimetric analysis of (i) ATRP initiator-functionalized silica nanoparticles (NPs), (ii) PDEGMMA brush-grafted silica NPs (HHP), and (iii)-(v) PDEGMMA-*b*-P(DEGMMA-*co*-DMAEMA) brush-grafted silica NPs (BHP-1, BHP-2, and BHP-3, respectively).

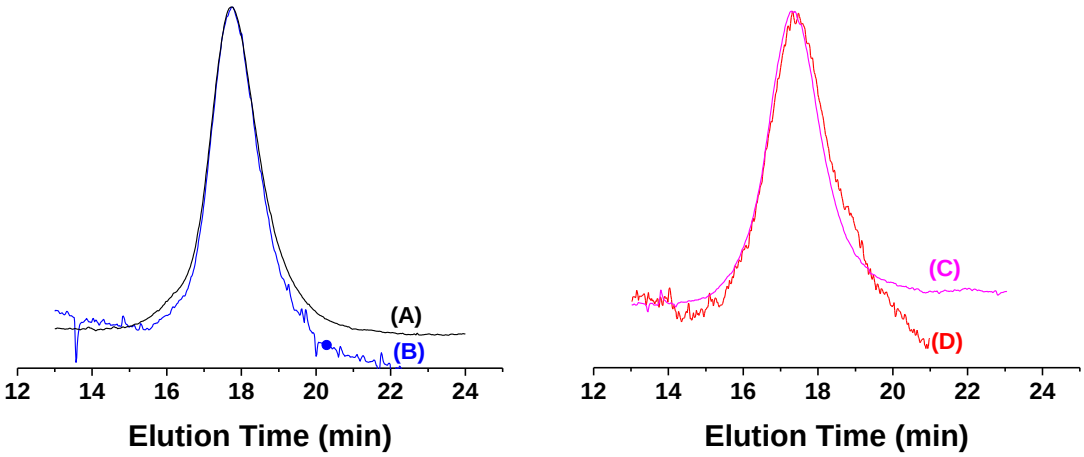

Figure 2.2. Size exclusion chromatography (SEC) traces of (A) the free PDEGMMA formed in the synthesis of PDEGMMA brush-grafted silica nanoparticles (HHP), (B) the PDEGMMA brush cleaved from HHP, (C) the free diblock copolymer PDEGMMA-*b*-P(DEGMMA-*co*-DMAEMA) (BCP-3) formed in the synthesis of diblock copolymer brush-grafted silica NPs (BHP-3), and (D) the polymer cleaved from hairy NPs BHP-3. The SEC analysis was performed using a PL-GPC 50 Plus with DMF as the carrier solvent.

reacted and the removed DEGMMA, the second phase of the polymerization had a feed DMAEMA-to-DEGMMA ratio of 1.09 : 1.00. The reaction was allowed to continue at 60 °C; two large samples were removed when the monomer conversion reached 8.6 % and 15.2 %, based on the amount of the two monomers immediately after the addition of DMAEMA. The corresponding free block copolymers were designated as BCP-1 and BCP-2, and the hairy NPs were designated as BHP-1 and BHP-2, respectively. The polymerization was stopped at the monomer conversion of 30.3 % (the free diblock copolymer: BCP-3 and the hairy NPs: BHP-3). These three sets of hairy NPs had the same PDEGMMA block with a DP of 101 but different block lengths for the second block. From the SEC analysis of the three free diblock copolymers (Figure 2.1A), the peak gradually shifted to the high molecular weight side with the increase of the monomer conversion and remained narrow, indicating that the polymerization was controlled and that the removal of large portions of the reaction mixture did not adversely impact the "living" nature of the polymerization. The $M_{n,SEC}$ values for BCP-1, BCP-2, and BCP-3 were 30.0, 36.1, and 50.4 kDa, respectively, and the corresponding PDIs were 1.24, 1.25, and 1.30. TGA analysis showed that the weight retention at 800 °C decreased progressively from 22.80 % for HHP to 17.36 % for BHP-1, 14.97 % for BHP-2, and 11.23 % for BHP-3 (Figure 2.1B).

Similar to the study of the molecular weight of PDEGMMA brushes, we found that the SEC traces of BCP-3 and the diblock copolymer cleaved from BHP-3 using HF were basically the same (Figure 2.2C and D). Using the same method for the determination of the DP of PDEGMMA, the block lengths of the second block in the three block copolymer samples were calculated to be 42, 75, 149, respectively, on the basis of the monomer conversions and the monomer-to-initiator ratio, which were re-defined after the addition of the second monomer.[16] The molar percentage of DMAEMA units in each sample was determined from the ^{1}H NMR spectrum of the free diblock

copolymer using the peak at 2.56 ppm, which was from –CH_2N- of DMAEMA units, and the peak at 3.38 ppm, which was from –OCH_3 of DEGMMA. Given that the DPs of both blocks were known, the composition of the second block was obtained, and the numbers of DMAEMA units in BCP-1, -2, and -3 were found to be 17, 32, and 57, respectively. Figure 2.3 shows representative TEM micrographs of hairy NPs BHP-1, -2, and -3 cast from chloroform dispersions. Although we are not certain if hairy NPs in each sample achieved perfect close-packing via self-assembly during the solvent evaporation, it is clear that qualitatively, the interparticle distance increased from BHP-1, to BHP-2, and to BHP-3, consistent with the increased block lengths for the second block of three samples in the same order.

Using the average size of silica NPs (17 nm), TGA data, DPs of the polymers, and assuming that the density of silica NPs was 2.07 g/cm^3, the grafting densities of PDEGMMA brushes in HHP and diblock copolymer brushes in BHP-1, -2, and -3 were calculated, and were found to be 0.60 – 0.61 chains/nm^2. This further confirmed the "living" characteristic of the one-pot ATRP for the synthesis of homopolymer and diblock copolymer brushes. The characterization data for all hairy NPs and the corresponding free polymers are summarized in Table 2.1.

2.3.2. Quaternization of DMAEMA Units in PDEGMMA-*b*-P(DEGMMA-*co*-DMAEMA) Brush-Grafted Silica NPs

To enhance the dispersibility and stability of thermosensitive hairy silica NPs in water, we converted the DMAEMA units in the PDEGMMA-*b*-P(DEGMMA-*co*-DMAEMA) brushes to quaternized ammonium iodide units using CH_3I,[17] affording PDEGMMA-*b*-P(DEGMMA-*co*-TMAEMA-I) brush-grafted silica NPs. The reaction was carried out at room temperature in anhydrous THF under an N_2 atmosphere. The flask was wrapped in aluminum foil to prevent exposure to light, as strong discoloration would occur otherwise. After the reaction proceeded

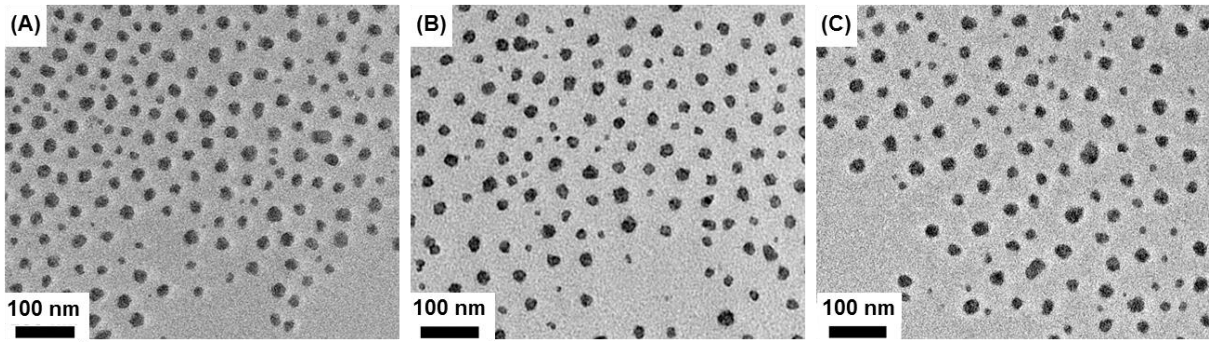

Figure 2.3. Bright field TEM micrographs of (A) PDEGMMA-*b*-P(DEGMMA-*co*-DMAEMA) diblock copolymer brush-grafted silica NPs (BHP-1), (B) BHP-2, and (C) BHP-3. The hairy NPs were cast onto carbon-coated, copper TEM grids from the $CHCl_3$ dispersions with a hairy NP concentration of ~ 4 mg/mL.

Table 2.1. Characterization Data for PDEGMMA Brush-Grafted Silica NPs, PDEGMMA-*b*-P(DEGMMA-*co*-DMAEMA) Brush-Grafted Silica NPs, and the Corresponding Free Polymers.

Polymer Brush-Grafted Nanoparticle Sample	$M_{n,SEC}$ (kDa) and PDI of Free Polymer [a]	DPs of 1st and 2nd Block [b]	n_{DMAEMA} [c]	σ (chains/nm^2) [d]
HHP [e]	22.8, 1.24	101, 0	0	0.61
BHP-1 [e]	30.0, 1.24	101, 42	17	0.61
BHP-2 [e]	36.1, 1.25	101, 75	32	0.61
BHP-3 [e]	50.0, 1.30	101, 149	57	0.60

[a] The values of $M_{n,SEC}$ and polydispersity indices (PDI) were obtained by size exclusion chromatography (SEC) calibrated with polystyrene standards. [b] The degree of polymerization (DP) was calculated using the monomer conversion and the molar ratio of monomer(s) to both free and surface-bound initiators. [c] The number of DMAEMA monomer units in each sample was calculated using the ^{1}H NMR spectrum of the free copolymer along with the DPs of the 1st and 2nd block. [d] The grafting densities of polymer brushes were calculated by using TGA data, DPs of polymers, and the core silica nanoparticle size of 17 nm. [e] HHP and BHP stand for homopolymer brush-grafted NPs and diblock copolymer brush-grafted silica NPs. Their corresponding free polymers are PDEGMMA and BCP-1, -2, and -3, respectively.

overnight, the NPs were washed with water *via* repeated ultracentrifugation. Figure 2.4 shows the ^{1}H NMR spectra of BHP-3 before and after the reaction. The complete alkylation was evidenced by the disappearance of the -N(C*H*$_3$)$_2$ peak at 2.4 ppm and the appearance of -N^{+}(C*H*$_3$)$_3$ peak at 3.2 ppm. Note that we also conducted a control quaternization experiment using BCP-3 under the similar conditions and found that the reaction was complete after 90 min.[16]

2.3.3 Thermally-Induced, Reversible Sol-Gel Transitions of Aqueous Dispersions of BHP-1-Q.

The purified, quaternized hairy NPs collected after ultracentrifugation were re-dispersed in Milli-Q water and freeze-dried, which allowed for easier storage and dispersal. For study of thermally induced sol-gel transitions, the quaternized hairy NPs were dispersed in Milli-Q water through several cycles of ultrasonication in cold and warm water baths before storing in a refrigerator overnight to ensure homogeneity. The resultant dispersions were transparent and either pale yellow (BHP-1-Q and -2-Q) or colorless (BHP-3-Q). To obtain desired concentrations, water was either added or evaporated under a gentle nitrogen stream. The dispersions of hairy NPs were then heated and ultrasonicated until homogeneity was achieved. We note here that it is extremely difficult, if not impossible, to disperse freeze-dried HHP, the PDEGMMA brush-grafted silica NPs, in water at sufficiently high concentrations, despite the presence of a layer of PDEGMMA brushes.

Aqueous dispersions of BHP-1-Q were found to exhibit a reversible, cooling-induced gelation at low-to-moderate concentrations. To visually examine the sol-gel transition of a 6.5 wt % aqueous dispersion of BHP-1-Q, the sample, which was a free-flowing, slightly viscous liquid at and above room temperature**,** was gradually cooled from elevated temperatures; the dispersion was allowed to equilibrate at a given temperature for 20 min before the vial was tilted to check if

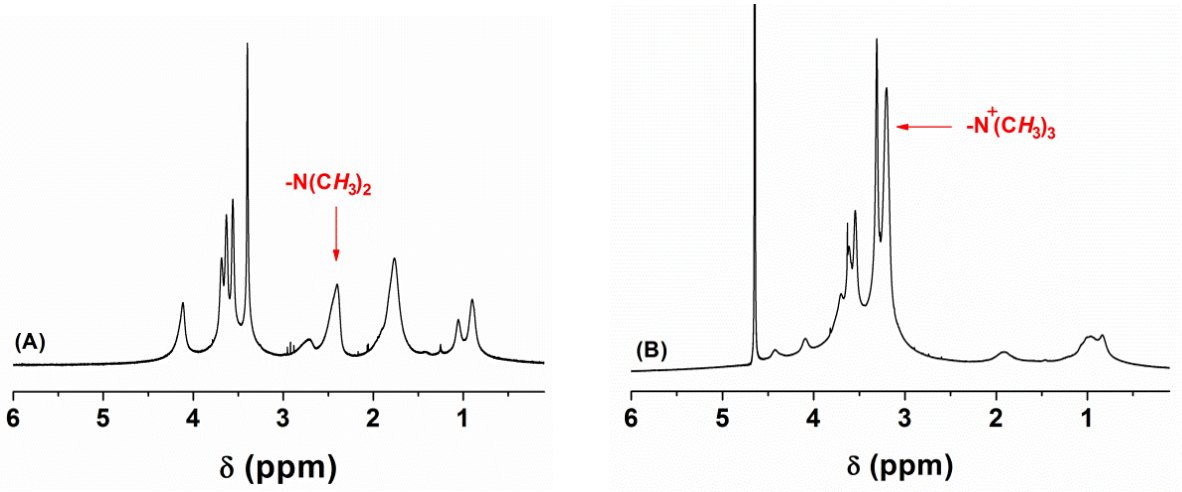

Figure 2.4. ^{1}H NMR spectra of (A) PDEGMMA-*b*-P(DEGMMA-*co*-DMAEMA) brush-grafted silica nanoparticles (BHP-3) in $CDCl_3$ and (B) PDEGMMA-*b*-P(DEGMMA-*co*-TMAEMA-I) (BHP-3-Q) in D_2O.

the sample was a liquid or a gel. As shown in Figure 2.5, the dispersion was a free-flowing liquid at 35 °C, but was found to be a stationary gel at 15 °C. The sol-gel transition temperature ($T_{sol\text{-}gel}$) obtained in this way was $T_{sol\text{-}gel}$ = 17 °C. The sol-gel transition was reversible; increasing temperature converted the gel into a sol. The gelation did not noticeably alter the appearance of the dispersion, nor did any visual change or loss in transparency occur at temperatures well above or well below $T_{sol\text{-}gel}$ or the cloud point of PDEGMMA (26 °C). This consistency suggests that the charged outer block indeed stabilized the hairy NPs in the aqueous dispersion and prevented the irreversible aggregation of hairy NPs against temperature variations. We previously observed that clear micellar hydrogels of doubly thermosensitive diblock copolymers turned into clear and then opaque liquids upon heating from below to above the cloud point of the thermosensitive corona polymer.[5c]

To quantitatively characterize the thermally-induced reversible sol-gel transition of the 6.5 wt % aqueous dispersion of BHP-1-Q, we carried out oscillatory shear experiments at a fixed frequency of 1 Hz in a temperature ramp with a cooling rate of 3 °C/min (Figure 2.6A). A strain amplitude of γ = 1.0 % was used, which was in the linear viscoelastic regime, as demonstrated by a strain sweep experiment performed at 5 °C (Figure 2.6C). The values of dynamic storage modulus G' were lower than those of dynamic loss modulus G'' at higher temperatures, indicative of a liquid state. As the temperature decreased, G' slowly increased, eventually surpassing G'' after a crossover point of 18.1 °C, suggesting that the aqueous dispersion of hairy NPs had changed from a viscous liquid into a gel. The crossover point in the temperature ramp is often taken as the $T_{sol\text{-}gel}$.[19] The NP dispersion was also subjected to a heating ramp at the same rate, from which the gel-to-sol transition temperature ($T_{gel\text{-}sol}$) was obtained as 20.0 °C (Figure 2.6B); the small difference between $T_{sol\text{-}gel}$ (18.1 °C) and $T_{gel\text{-}sol}$ (20.0 °C) demonstrated a minimal hysteresis

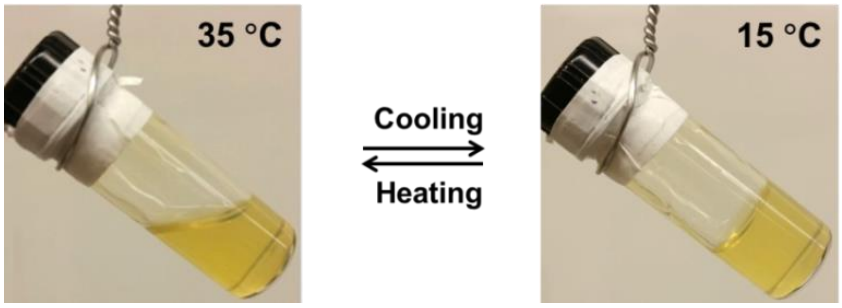

Figure 2.5. Digital optical pictures of a 6.5 wt % aqueous dispersion of PDEGMMA-*b*-P(DEGMMA-*co*-TMAEMA-I) brush-grafted silica NPs (BHP-1-Q) at 35 and 15 °C.

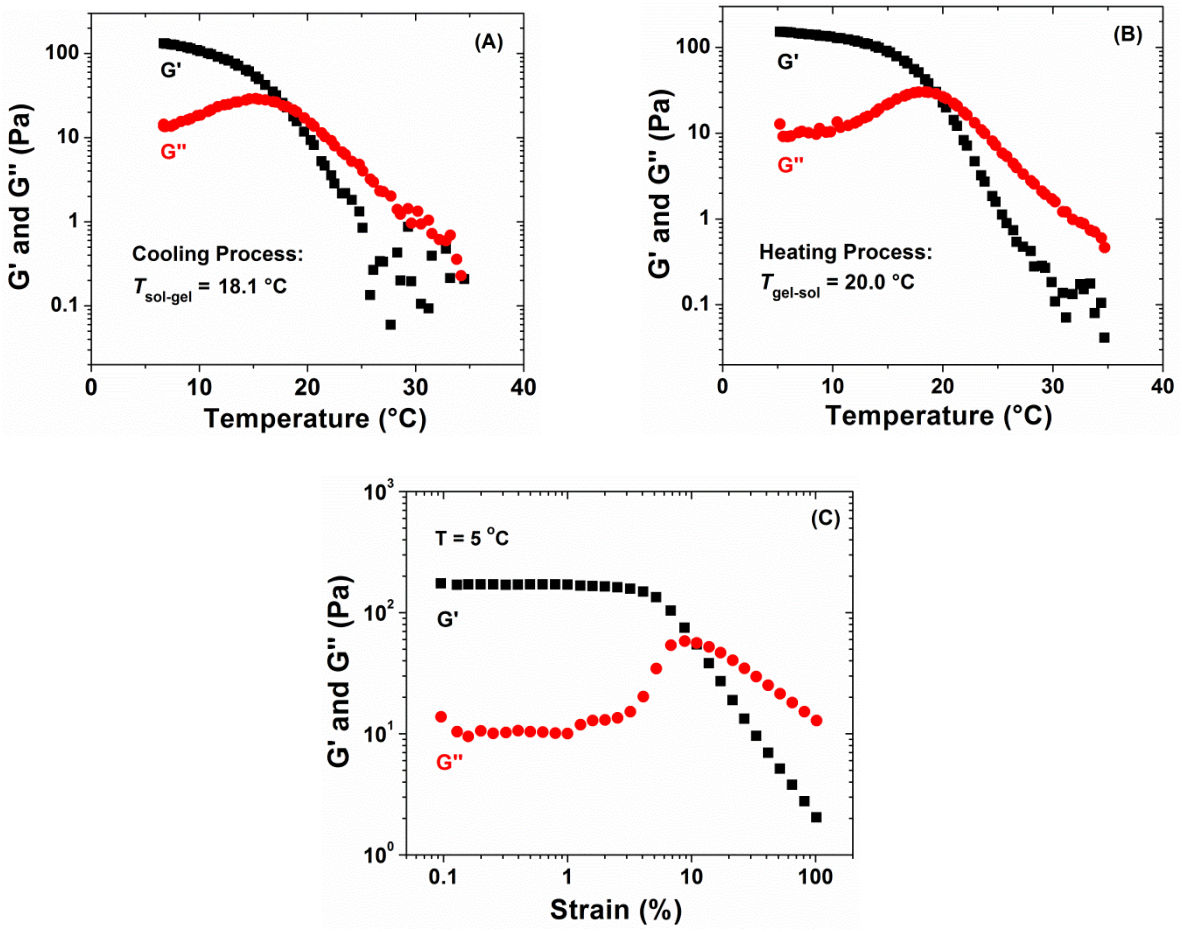

Figure 2.6. Plots of dynamic storage modulus *G′* and loss modulus *G″* of a 6.5 wt % aqueous dispersion of PDEGMMA-*b*-P(DEGMMA-*co*-TMAEMA-I) brush-grafted silica nanoparticles (BHP-1-Q) versus temperature obtained from an oscillatory shear experiment performed (A) in a cooling ramp using a frequency of 1 Hz, a strain amplitude of 1.0 %, and a cooling rate of 3 °C/min and (B) in a heating ramp using a frequency of 1 Hz, a strain amplitude of 1.0 %, and a heating rate of 3 °C/min; (C) A strain sweep performed at 5 °C on the 6.5 wt % aqueous dispersion of BHP-1-Q using a frequency of 1 Hz.

between cooling and heating processes. Compared with moderately concentrated aqueous solutions of doubly thermosensitive diblock copolymers (e.g., 20 wt %),[5] where G' and G'' usually changed rather rapidly with temperature, the sol-gel/gel-sol transitions of the current system were quite broad, spanning a temperature range of ~ 15 °C, which might be related to the less drastic change in the volume fraction of hairy NPs with temperature than that of thermosensitive diblock copolymers transitioning from unimers to micelles as well as the relatively small volume fraction of the thermosensitive block in the hairy NPs. As will be discussed later, one source of the slow change of the volume fraction of hairy NPs with temperature is the broad LCST transition of the inner PDEGMMA block.

The effect of temperature on the rheological properties of the 6.5 wt % aqueous dispersion of BHP-1-Q was further studied by means of frequency (f) sweep experiments in the range of 0.1 to 100 Hz at selected temperatures using a strain amplitude of 1.0 % (Figure 2.7). At 30 °C, well above the $T_{sol\text{-}gel}$, the G'' scaled with f in a linear fashion, while G', in addition to being lower in magnitude at lower frequencies, scaled approximately with the square of f. These are the characteristic of a viscoelastic fluid. At 23 °C, G' and G'' were effectively congruent, scaling with $f^{0.5}$ as is typical for a system transitioning between liquid and elastic solid states. Finally, at 5 °C, as expected for a gelled system, G' was essentially independent of f from 0.1 Hz to ~ 50 Hz, and G'' varied only slightly with a minimum around 4 Hz. These frequency sweeps at different temperatures also demonstrated the sol-gel transition with decreasing temperature.

The observed thermally induced reversible sol-gel/gel-sol transitions of the 6.5 wt % aqueous dispersion of BHP-1-Q are believed to originate from the LCST transition of the inner PDEGMMA block. At lower temperatures, the inner block is more hydrated and assumes more extended conformations, increasing the volume fraction of hairy NPs in the dispersion. When the volume

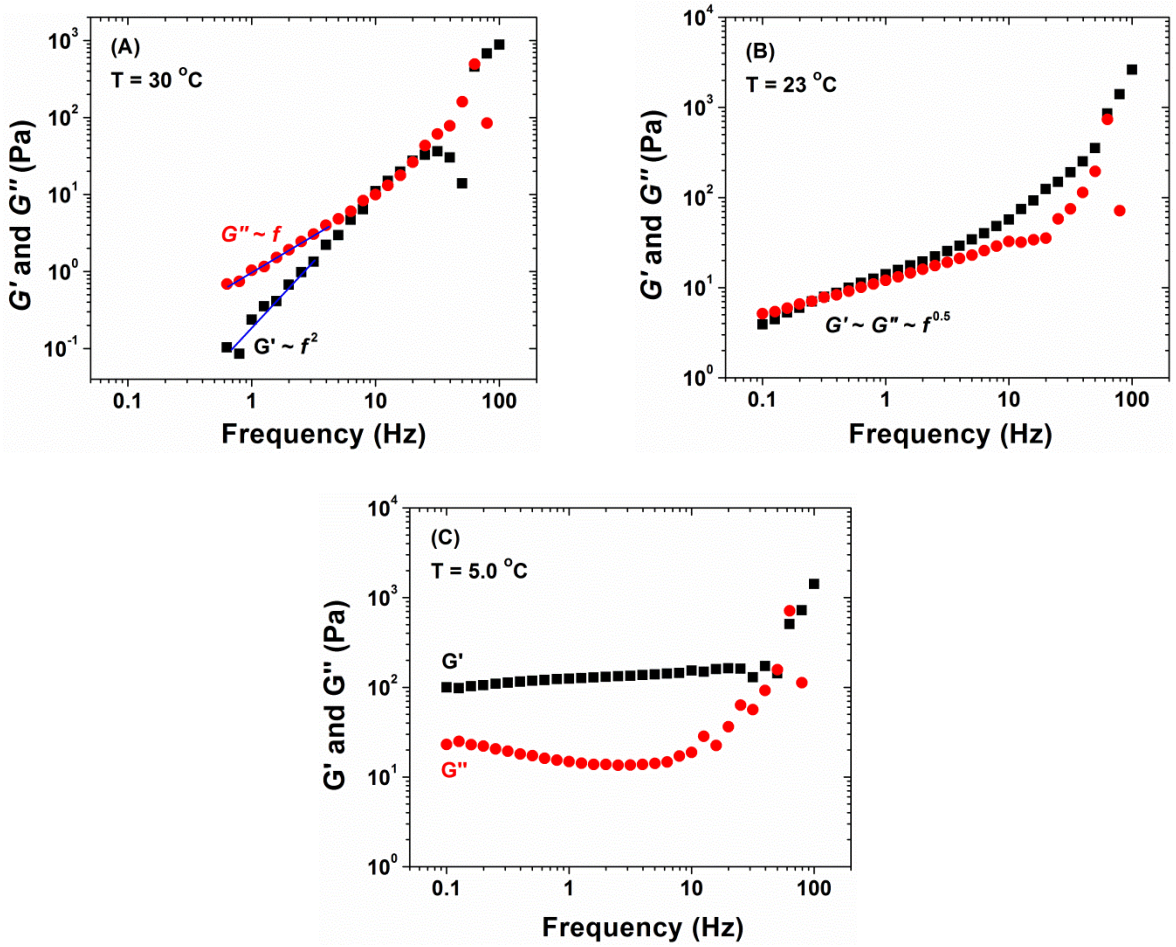

Figure 2.7. Plots of dynamic storage modulus *G′* and loss modulus *G″* of a 6.5 wt % aqueous dispersion of PDEGMMA-*b*-P(DEGMMA-*co*-TMAEMA-I) brush-grafted silica NPs (BHP-1-Q) versus frequency at (A) 30 °C, (B) 23 °C, and (C) 5 °C using a strain amplitude of 1.0 %.

fraction is at or above the critical value for packing,[1] the hairy NPs cannot pass one another, resulting in the formation of a hydrogel (Scheme 2.2). Above the LCST transition, the PDEGMMA block collapsed, driving the transition from a gel to a sol. This mechanism is similar to those for thermally induced sol-gel transitions of aqueous solutions of thermosensitive hydrophilic diblock copolymers and aqueous dispersions of chemically crosslinked, spherical poly(*N*-isopropylacrylamide) microgels.[5,20]

To investigate the effect of hairy NP concentration on $T_{gel\text{-}sol}$, heating ramp experiments were performed on aqueous dispersions of BHP-1-Q with various NP concentrations using the same conditions as for the determination of $T_{gel\text{-}sol}$ of the 6.5 wt % aqueous dispersion (that is, a frequency of 1 Hz, a strain amplitude of 1.0 %, and a heating rate of 3 °C/min).[16] As summarized in Figure 2.8, with the increase of BHP-1-Q concentration, $T_{gel\text{-}sol}$ increased, from 13.3 °C at 6.0 wt % to 45.9 °C at 8.0 wt %. No sol-gel or gel-sol transition was observed visually or rheologically for the 5.0 wt % aqueous dispersion of BHP-1-Q in the temperature range of 5 to 65 °C, indicating that the critical gelation concentration for BHP-1-Q is between 5 – 6 wt %.

Apparently, the greater volume fraction of hairy NPs in the dispersion afforded by the increase in the number of hairy NPs reduces the need for a higher degree of swelling of the thermosensitive inner block to achieve gelation. (i.e., the brushes do not need to stretch to such an extent to prevent the dispersion from flowing.) While it may seem unusual for the sol-gel/gel-sol transitions to occur at temperatures above the commonly reported cloud point of free PDEGMMA in water (26 °C) for aqueous dispersions with concentrations higher than 7.0 wt %, there are three possible reasons. (i) The $T_{gel\text{-}sol}$ and $T_{sol\text{-}gel}$ are related to the mechanical properties of the hydrogels; they are related to but not directly determined by the LCST transition of the PDEGMMA block.[5c] (ii) The LCST

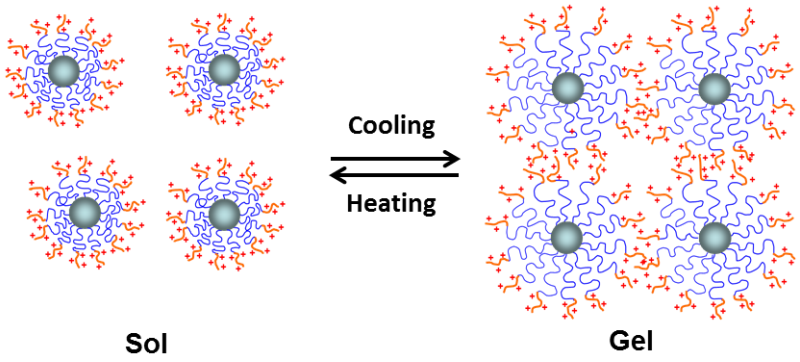

Scheme 2.2. Proposed Mechanism for Hydrogel Formation from Aqueous Dispersion of Thermosensitive Diblock Copolymer Brush-Grafted Silica NPs by Packing (for Simplicity, Counteranions are Omitted).

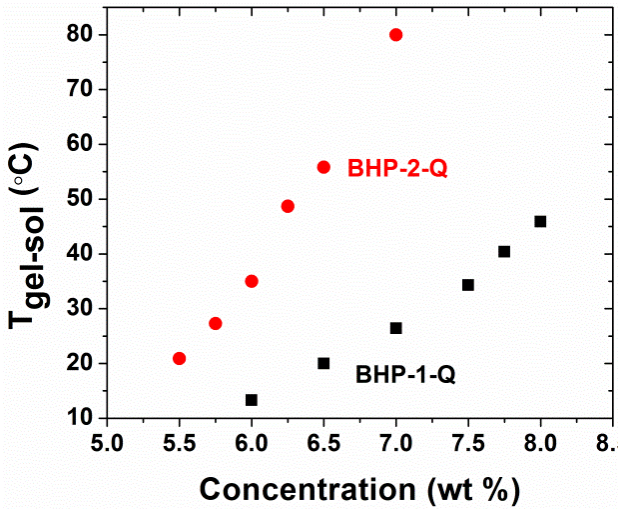

Figure 2.8. $T_{gel\text{-}sol}$ of aqueous dispersion of BHP-1-Q (black square) and BHP-2-Q (red circle), obtained from rheological measurements, as a function of concentration of hairy nanoparticles. For BHP-2-Q, the $T_{gel\text{-}sol}$ at 7.0 wt % was determined by visual examination.

transition of the inner PDEGMMA block is very likely different from that of the free PDEGMMA because one end is grafted to the surface of silica NPs and the other end is covalently bonded to the charged outer block. (iii) It has been commonly observed and generally accepted that with the increase of temperature, the solvent quality of water becomes increasingly poor for the PEO-type thermosensitive water-soluble polymers.[1,5,21]

2.3.4. Solution Behavior of Aqueous Dispersions of BHP-2-Q and BHP-3-Q at Low-to-Moderate Concentrations

We also examined the solution behavior of aqueous dispersions of BHP-2-Q and BHP-3-Q in response to temperature changes. At a sufficiently high concentration, the aqueous dispersion of BHP-2-Q, which had a longer charged outer block than that of BHP-1-Q, also underwent thermally-induced, reversible sol-gel transitions. Figure 2.9 shows the optical pictures of a 6.0 % aqueous dispersion of BHP-2-Q at 50 and 25 °C as well as the cooling and heating ramps of the same sample from rheological measurements. The $T_{sol\text{-}gel}$ and $T_{gel\text{-}sol}$, determined from temperature ramps, were found to be essentially the same (35.2 and 35.0 °C, respectively). Although the concentration of BHP-2-Q in Figure 2.9 was lower than that of BHP-1-Q in Figures 2.5 and 2.6, the $T_{sol\text{-}gel}$ and $T_{gel\text{-}sol}$ were higher. The concentration effect on $T_{gel\text{-}sol}$ of aqueous dispersion of BHP-2-Q was also investigated, and the results are summarized in Figure 2.8. Similar to BHP-1-Q, the $T_{gel\text{-}sol}$ increased with the increase of hairy NP concentration, from 20.9 °C at 5.5 wt % to 80 °C at 7.0 %. The latter was determined by visual examination using a temperature-controlled oil bath due to instrumental limitation. At a given concentration, the $T_{gel\text{-}sol}$ of BHP-2-Q was significantly higher, by > 20 °C**,** than that of BHP-1-Q, which should be the result of a longer charged outer block of BHP-2-Q, making the volume of single hairy nanoparticle larger and thus the $T_{gel\text{-}sol}$ greater. Furthermore, the increase in $T_{sol\text{-}gel}$ with concentration was found to be steeper than that

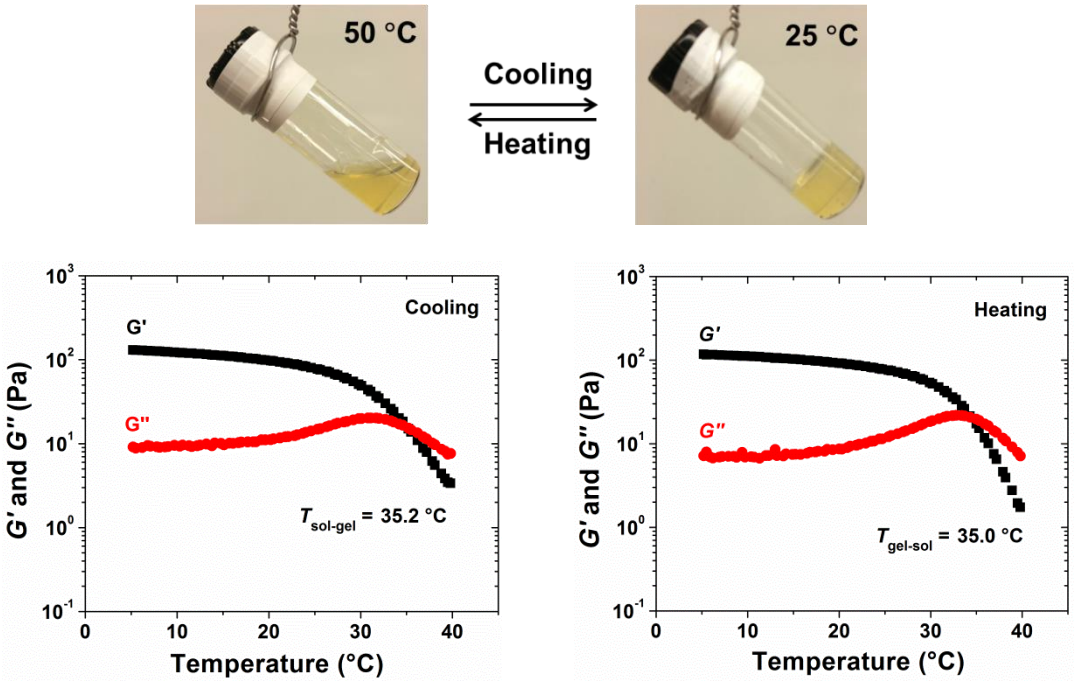

Figure 2.9. Digital optical pictures of a 6.0 % aqueous dispersion of BHP-2-Q at 50 and 25 °C (top), and temperature ramps (bottom) from oscillatory shear experiments using a fixed frequency of 1 Hz, a strain amplitude of 1.0 %, and a heating/cooling rate of 3 °C/min.

of BHP-1-Q. For instance, the $T_{gel\text{-}sol}$ was 35.0 °C at 6.0 wt % and 80 °C at 7.0 wt % for BHP-2-Q, compared to 13 °C and 26.4 °C at the same concentrations, respectively, for BHP-1-Q. This is likely due to the increased hydrophilicity granted by the more substantial charged block of BHP-2-Q; a greater temperature is required to decrease the volume fraction of hairy NPs to below a critical value. As a result, the $T_{gel\text{-}sol}$ of BHP-2-Q spanned over an even larger temperature range than that of BHP-1-Q.

To investigate the lower limit of $T_{gel\text{-}sol}$, a sample with 5.0 wt % BHP-2-Q was prepared and was found to be a free flowing fluid in the temperature range of 0 to 65 °C by visual inspection. Since the 5.5 wt % aqueous dispersion of BHP-2-Q exhibited a thermally induced sol-gel transition, the CGC for BHP-2-Q should be between 5.0 and 5.5 wt %, and is likely lower than that of BHP-1-Q. This is reasonable because the outer charged block in BHP-2-Q was longer, making the hydrodynamic volume of individual hairy NPs larger.

Among the three sets of hairy NPs, BHP-3-Q had the longest charged outer block with a DP of 149 in comparison to 75 for BHP-2-Q and 42 for BHP-1-Q (Table 2.1). For this set of hairy NPs, we found by visual examination that the aqueous dispersion with a concentration of 4.0 wt % or higher remained a gel in the temperature range of 0 to ~ 100 °C, while the 3.0 wt % dispersion appeared to be a liquid and no sol-gel transition was observed from 0 °C to 65 °C (Figure 2.10). There was also no change in the appearance of these two aqueous dispersions of BHP-Q-3 with temperature, though the sample was markedly less yellow than either BHP-1-Q or BHP-2-Q. Rheology study also showed that the 4.0 wt % aqueous dispersion of BHP-3-Q was a gel in the temperature range of 5 – 70 °C.[16] Likely, this is because the charged outer block of BHP-3-Q was too long, making the LCST transition of the inner PDEGMMA block either too weak to drive a sol-gel transition or simply disappear in the studied temperature range.

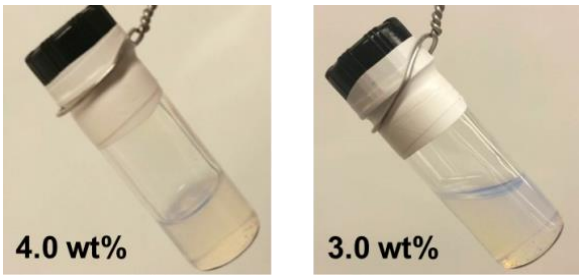

Figure 2.10. Digital optical pictures of aqueous dispersions of BHP-3-Q with concentrations of 4.0 (left) and 3.0 wt % (right) at ambient conditions.

2.3.5. Dynamic Light Scattering (DLS) Study of PDEGMMA-*b*-P(DEGMMA-*co*-TMAEMA-I) Brush-Grafted Silica Nanoparticles in Milli-Q Water

The observed thermally induced, reversible sol-gel transitions of aqueous dispersions of BHP-1-Q and BHP-2-Q were believed to be driven by the LCST transition of the inner thermosensitive PDEGMMA block, and the fact that no sol-gel transitions were observed for aqueous dispersions of BHP-3-Q was likely a result of the very weak or no LCST transition of the PDEGMMA block due to the long charged outer block, as mentioned earlier. To confirm the origin of the solution behavior of BHP-1-Q, -2-Q, and -3-Q in water at low-to-moderate concentrations, we conducted DLS studies of thermoresponsive properties of these hairy NPs in Milli-Q water. The concentration of hairy NPs in the aqueous dispersion was 0.2 mg/g for all three samples. The temperature was gradually increased, and at each selected temperature the DLS sample was equilibrated for 20 min before the measurements were taken. Figure 2.11 shows the plots of average apparent hydrodynamic size (D_h) versus temperature along with standard deviations for the three sets of hairy NPs. For BHP-1-Q, D_h remained essentially the same in the temperature range of 5 – 15 °C, and began to decrease when the temperature was above 15 °C, from ~ 117 nm to ~ 89 nm in the range of 15 °C to 55 °C. The onset temperature of the LCST transition appeared to be at ~ 20 °C. Above 55 °C, the D_h leveled off.

Our lab previously reported that the LCST transition of thermosensitive polymer brushes grafted on silica (nano)particles began at a lower temperature and continued over a broader temperature range (4 – 10 °C) than those of the free polymers in water (< 2 °C).[10c] Interestingly, the LCST transition of the PDEGMMA block in BHP-1-Q was even more broadened, over a range of nearly 40 °C. This is presumably because one end of the PDEGMMA block was fixed to the surface of silica NPs and another end was covalently bonded to the P(DEGMMA-*co*-TMAEMA-

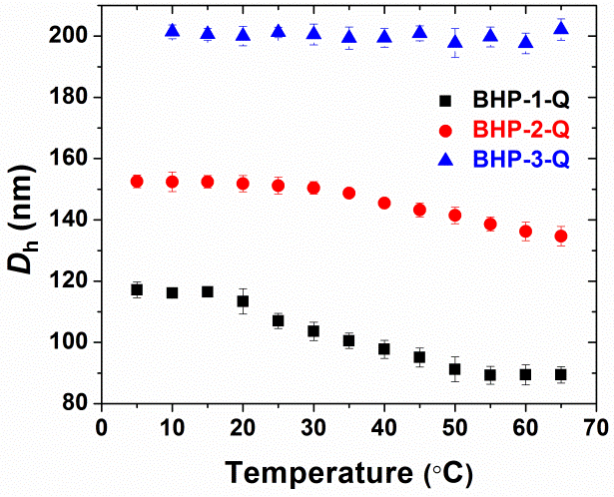

Figure 2.11. Average apparent hydrodynamic size D_h, obtained from DLS study of 0.2 mg/g aqueous dispersion of PDEGMMA-*b*-P(DEGMMA-*co*-TMAEMA-I) brush-grafted silica NPs in Milli-Q water using CONTIN analysis, along with the standard deviation as a function of temperature for BHP-1-Q (black square), BHP-2-Q (red circle), and BHP-3-Q (blue triangle).

I) block. The outer block is charged and highly solvated (hydrated), which opposes the contraction force arising from the LCST transition and thus weakens the LCST transition. In addition, both blocks of the brushes are not monodisperse but polydisperse in nature, despite the relatively low PDI (1.24 for the free BCP-1). Moreover, the relatively high grafting density of polymer brushes resulted in increased intersegmental and interchain interactions, which decreased as the distance from the grafting site increased due to substrate curvature. The segment-segment interactions reduce water-monomer interactions, which is the source of LCST type behavior, making the LCST transition occur at a lower temperature and over a wider temperature range. Combining all these factors, it is understandable that the inner PDEGMMA block collapses in a significantly non-uniform manner and the LCST transition of the PDEGMMA block in BHP-1-Q is much broader than that of the corresponding free polymer. The broader LCST transition should be at least one source of the broader sol-gel transitions observed in Figure 2.6.

A similar behavior was observed for BHP-2-Q. The LCST transition began at ~ 30 °C, which was ~ 10 – 15 °C higher than that of BHP-1-Q, and continued over the temperature range of 30 – 65 °C. The size change in the studied temperature range, from ~ 152 nm at 5 – 30 °C to ~ 135 nm at 65 °C, was smaller than that of BHP-1-Q, and did not appear to level off even when the temperature reached 65 °C. All these observations indicate that the LCST transition of BHP-2-Q was even weaker than that of BHP-1-Q. Apparently, the higher onset temperature for the LCST transition of BHP-2-Q is caused by the longer charged outer block of BHP-2-Q (DP = 75) compared with that of BHP-1-Q (DP = 42). It is known that the LCST of a thermosensitive polymer is higher when linked to a more hydrophilic polymer.[1,22] The charged P(DEGMMA-*co*-TMAEMA-I) block was highly solvated, imposing a stronger resistance to the LCST transition-induced shrinking of the PDEGMMA block.

Different from BHP-1-Q and -2-Q, the variation of the D_h of BHP-3-Q was very small, and no obvious LCST transition was observed. This suggests that the resistance to collapse of the inner PDEGMMA block from the long, highly solvated polyelectrolyte block was so large that the PDEGMMA block was unable to undergo the LCST transition, with an essentially constant D_h of ~ 200 nm across the studied temperature range. Consequently, there were no sol-gel transitions for aqueous dispersions of BHP-3-Q, simply because the volume fraction of hairy NPs in the dispersion did not change to any significant extent with temperature.

2.4. Conclusion

A series of thermosensitive PDEGMMA-*b*-P(DEGMMA-*co*-TMAEMA-I) diblock copolymer brush-grafted silica NPs with an identical PDEGMMA inner block but different block lengths for the charged outer block was synthesized by a one-pot surface-initiated ATRP from initiator-functionalized, 17 nm silica NPs and subsequent quaternization of tertiary amine groups using iodomethane.[23] At a sufficient concentration, aqueous dispersions of hairy NPs with an appropriate composition for the diblock copolymer brushes underwent *in situ*, reversible transitions between a free-flowing, slight viscous liquid and a free-standing hydrogel in response to temperature changes. The sol-gel transition temperature increased with increasing the NP concentration. Dynamic light scattering studies confirmed that the thermally-induced sol-gel transitions of hairy NPs in water were driven by the LCST transition of the thermosensitive PDEGMMA inner block. When the charged outer block was too long, no obvious LCST transition was observed, and the aqueous dispersions did not exhibit sol-gel transitions in response to temperature changes. Currently, we are working on stimuli-responsive polymer brush-grafted mesoporous silica NPs and hollow silica NPs with mesoporous walls to demonstrate the formation

of both physically crosslinked 3-D network hydrogels and packing-based hybrid hydrogels. The utility of these hairy NPs in specific applications will be shown in due course.

References

1. Hamley, I. W. *Block Copolymers in Solution: Fundamentals and Applications*; John Wiley & Sons: Chichester, 2005.
2. (a) Jeong, B.; Kim, S.W.; Bae, Y. H. *Adv. Drug Delivery Rev*. **2002**, *54*, 37–51; (b) Yu, L.; Ding, J. *Chem. Soc. Rev*. **2008**, *37*, 1473-1481; (c) He, C.; Kim, S. W.; Lee, D. S. *J. Controlled Release* **2008**, *127*, 189-207; (d) Moon, H. J.; Ko, D. Y.; Park, M. H.; Joo, M. K. Jeong, B. *Chem. Soc. Rev.* **2012**, *41*, 4860-4883.
3. (a) Li, C.; Buurma, N. J.; Haq, I.; Turner, C.; Armes, S. P.; Castelletto, V.; Hamley, I. W.; Lewis, A. L. *Langmuir* **2005**, *21*, 11026-11033; (b) Li, C.; Tang, Y.; Armes, S. P.; Morris, C. J.; Rose, S. F.; Lloyd, A. W.; Lewis, A. L. *Biomacromolecules* **2005**, *6*, 994-999; (c) Kirkland, S. E.; Hensarling, R. M.; McConaughy, S. D.; Guo, Y.; Jarrett, W. L.; McCormick, C. L. *Biomacromolecules* **2007**, *9*, 481-486; (d) Vogt, A. P.; Sumerlin, B. S. *Soft Mater* **2009**, *5*, 2347–2351; (e) Iatridi, Z.; Mattheolabakis, G.; Avgoustakis, K.; Tsitsilianis, C. *Soft Matter* **2011**, *7*, 11160-11168; (f) Han, D. H.; Boissiere, O.; Kumar, S.; Tong, X.; Tremblay, L.; Zhao, Y. *Macromolecules* **2012**, *45*, 7440-7445.
4. (a) Hamley, I. W.; Pople, J. A.; Fairclough, J. P. A.; Ryan, A. J.; Booth, C.; Yang, Y. W. *Macromolecules* **1998**, *31*, 3906-3911; (b) Mortensen, K.; Brown, W.; Nordén, B. *Phys. Rev. Lett.* **1992**, *68*, 2340-2343; (c) Wanka, G.; Hoffmann, H.; Ulbricht, W. *Macromolecules* **1994**, *27*, 4145-4159; (d) Pozzo, D. C.; Walker, L. M. *Macromolecules* **2007**, *40*, 5801-5811.
5. (a) Sugihara, S.; Kanaoka, S.; Aoshima, S. *Macromolecules* **2005**, *38*, 1919– 1927; (b) Aoshima, S.; Kanaoka, S. *Adv. Polym. Sci.* **2008**, *210*, 169– 208; (c) Jin, N. X.; Zhang, H.; Jin, S.; Dadmun, M. D.; Zhao, B. *J. Phys. Chem. B.* **2012**, *116*, 3125-3137.

6. (a) Woodcock, J. W.; Wright, R. A. E.; Jiang, X.; O'Lenick, T. G.; Zhao, B. *Soft Matter* **2010**, *6*, 3325-3336; (b) O'Lenick, T. G.; Jin, N. X.; Woodcock, J. W.; Zhao, B. *J. Phys. Chem. B.* **2011**, *115*, 2870-2881; (c) Henn, D. M.; Wright, R. A. E.; Woodcock, J. W.; Hu, B.; Zhao, B. *Langmuir* **2014**, *30*, 2541-2550.

7. (a) O. Prucker, J. Rühe, *Macromolecules*, 1998, **31**, 592-601; (b) T. von Werne, T. E. Patten, *J. Am. Chem. Soc.* 1999, **121**, 7409-7410; (c) M. Husseman, E. E. Malmström, M. McNamara, M. Mate, D. Mecerreyes, D. G. Benoit, J. L. Hedrick, P. Mansky, E. Huang, T. P. Russell, C. J. Hawker, *Macromolecules*, 1999, **32**, 1424-1431; (d) K. Ohno, K. Koh, Y. Tsujii, T. Fukuda, *Angew. Chem. Int. Ed.*, 2003, **42**, 2751-2754. (e) L. Wang, B. C. Benicewicz, *ACS Macro Lett.*, 2013, **2**, 173-176.

8. (a) Pyun, J.; Matyjaszewski, K. *Chem. Mater.* **2001**, *13*, 3436–3448; (b) Chen, L.; Klok, H.-A. *Soft Matter* **2013**, *9*, 10678–10688; (c) Hui, C. M.; Pietrasik, J.; Schmitt, M.; Mahoney, C.; Choi, J.; Bockstaller, M. R.; Matyjaszewski, K. *Chem. Mater.* **2014**, *26*, 745– 762.

9. Zhao, B.; Zhu, L. *Macromolecules* **2009**, *42*, 9369-9383.

10. (a) Bao, C.; Horton, J. M.; Bai, Z.; Li, D. J.; Lodge, T. P.; Zhao, B. *J. Polym. Sci. Part B: Polym. Phys.* **2014**, *52*, 1600-1619; (b) Horton, J. M.; Bai, Z.; Jiang, X.; Li, D.; Lodge, T. P.; Zhao, B. *Langmuir* **2011**, *27*, 2019-2027; (c) Hu, B.; Henn, D. M.; Wright, R. A. E.; Zhao, B. *Langmuir* **2014**, *30*, 11212-11224; (d) Aqil, A.; Qiu, H.; Greisch, J.-F.; Jérôme, R.; De Pauw, E.; Jérôme, C. *Polymer* **2008**, *49*, 1145-1153.

11. (a) Sun, J.-T.; Hong, C.-Y.; Pan, C.-Y. *J. Phys. Chem. C* **2010**, *114*, 12481-12486; (b) Jiang, X. M.; Wang, B. B.; Li, C. Y.; Zhao, B. *J. Polym. Sci. Part A: Polym. Chem.* **2009**, *46*, 2853-2870.

12. (a) Zhu, M.-Q.; Wang, L.-Q.; Exarhos, G. J.; Li, A. D. Q. *J. Am. Chem. Soc.* **2004**, *126*, 2656-2657; (b) Farrukh, A.; Akram, A.; Ghaffar, A.; Hanif, S.; Hamid, A.; Duran, H.; Yameen, B. *ACS Appl. Mater. Interfaces* **2013**, *5*, 3784-3793; (c) Liu, G.; Cai, M.; Wang, X.; Zhou, F.; Liu, W. *ACS Appl. Mater. Inter.* **2014**, *6*, 11625-11632.
13. Yavuz, M. S.; Cheng, Y. Y.; Chen, J. Y.; Cobley, C. M.; Zhang, Q.; Rycenga, M.; Xie, J. W.; Kim, C.; Song, K. H.; Schwartz, A. G.; Wang, L. H. V.; Xia, Y. N. *Nat. Mater.* **2009**, *8*, 935-939.
14. Argyo, C.; Weiss, V.; Bräuchle, C.; Bein, T. *Chem. Mater.* **2014**, *26*, 435-451.
15. (a) Han, S.; Hagiwara, M.; Ishizone, T. *Macromolecules* **2003**, *36*, 8312-8319; (b) Lutz, J.-F.; Hoth, A. *Macromolecules* **2006**, *39*, 893-896.
16. The information can be found in Appendix A.
17. Li, D. J.; Sheng, X.; Zhao, B. *J. Am. Chem. Soc.* **2005**, *127*, 6248-6256.
18. Yancheva, E.; Paneva, D.; Danchev, D.; Mespouille, L.; Dubois, P.; Manolova, N.; Rashkov, I. *Macromol. Biosci.* **2007**, *7*, 940-954.
19. Noro, A.; Matshushita, Y.; Lodge, T. P. *Macromolecules* **2009**, *42*, 5802−5810.
20. (a) Zhao, Y.; Zhang, G.; Wu, C. *Macromolecules* **2001**, *34*, 7804-7808; (b) Zhao, Y.; Cao, Y.; Yang, Y.; Wu, C. *Macromolecules* **2003**, *36*, 855-859.
21. Bai, Z. F.; Lodge, T. P. *J. Phys. Chem. B* **2009**, *113*, 14151–14157.
22. Gil, E. S.; Hudson, S. M. *Prog. Polym. Sci.* **2004**, *29*, 1173–1222.
23. The work presented in this chapter has been published as an article:

    Wright, R. A. E.; Henn, D. M.; Zhao, B. *Soft Matter* **2015,** *11* (34), 6808-6820.

Appendix A

for

Chapter 2: Reversible Sol-Gel Transitions of Aqueous Dispersions of Silica Nanoparticles Grafted with Diblock Copolymer Brushes Composed of a Thermosensitive Inner Block and a Charged Outer Block

A.1. Cleavage of Polymer Brushes from Hairy Silica NPs Using HF.

The following is the procedure for the cleavage of PDEGMMA-*b*-P(DEGMMA-*co*-DMAEMA) diblock copolymer brushes from BHP-3 hairy NPs. A similar procedure was used to cleave PDEGMMA brushes from HHP. PDEGMMA-*b*-P(DEGMMA-*co*-DMAEMA) brush-grafted silica NPs (BHP-3, 10.1 mg) were dispersed in THF (5 mL) in a Teflon tube. Hydrofluoric acid (HF, 48 ~ 51 % aqueous solution, 0.5 mL) was then added to the dispersion, and the mixture was stirred overnight. After the excess HF was neutralized using a saturated aqueous solution of $Ca(OH)_2$, the cleaved polymer from hairy NPs was extracted with methylene chloride at 35 °C. The free polymer and the cleaved polymer were analyzed back-to-back using a PL-GPC 50 Plus, an integrated GPC/SEC system from Polymer Laboratories, Inc. with a differential refractive index detector, one PSS GRAL guard column (50 × 8 mm, Polymer Standards Service-USA, Inc.), and two PSS GRAL linear columns (each 300 × 8 mm, molecular weight range from 500 to 1,000,000 according to Polymer Standards Service-USA, Inc.) at ambient conditions. DMF was the carrier solvent with a flow rate of 1.0 mL/min. Narrow-disperse polystyrene standards (Polymer Laboratories, Inc.) were used for calibration.

A.2. Calculation of Degree of Polymerization (DP) of PDEGMMA Formed in Synthesis of PDEGMMA Brush-Grafted, 17 nm Silica Nanoparticles (HHP).

The DP of PDEGMMA formed in the synthesis of HHP was calculated using monomer conversion, determined by ^{1}H NMR spectroscopy, and TGA data of hairy NPs and initiator NPs.

The TGA curve of the initiator NPs was shifted vertically so that the weight retentions of initiator NPs and HHP at 100 °C were identical. (The difference in weight retentions of initiator NPs and HHP at 100 °C is believed to come from the absorbed moisture despite drying under high vacuum.) The corrected weight retention of the initiator NPs at 800 °C is 89.90 %. The ratio of the

silica residue to the volatile portion at 800 °C is 100 : 11.23 for initiator NPs and 100 : 338.60 for HHP. As the mass of the initiator NPs used in the polymerization was 1.057 g, the total mass of the grafted polymer is [(338.60 – 11.23)/(100 + 11.23)] × 1.057 g = 3.111 g. Because the mass of DEGMMA used in the polymerization was 20.074 g and the monomer conversion was 29.84 %, the total mass of polymer, both free and grafted polymer, is 5.990 g. Thus, the mass of free polymer is 2.879 g. Using the ratio of free to bound polymer and the amount of free initiator used (29.7 mg, 152.3 μmol), the surface initiator that successfully initiated polymerization was found to be 164.6 μmol. Therefore, as the sum of the free initiator and the surface initiator is 316.9 μmol and the amount of monomer added was 106.7 mmol, the monomer-to-initiator ratio was calculated to be 337 : 1. Thus, the DP of PDEGMMA is 101.

A.3. Calculation of Grafting Density of PDEGMMA Brushes Grafted on 17 nm Silica Nanoparticles (HHP)

For the calculation of grafting density of PDEGMMA brushes, assuming that the silica NPs are spherical and the density is 2.07 g/cm^3, the mass of a single NP with a diameter of 17 nm is 5.32×10^{-18} g. Therefore, the amount of the grafted PDEGMMA on one silica NP is 1.74×10^{-17} g. The molecular weight of PDEGMMA calculated from DP is 19010 g/mol. Thus, the number of the grafted PDEGMMA chains on one silica NP is (1.74×10^{-17} g/19010 g/mol) × 6.022×10^{23} = 551 chains. The surface area of one bare silica NP is πD^2 = 908 nm^2. Therefore, the grafting density of PDEGMMA brushes on silica NPs is 0.61 chains/nm^2.

A.4. Calculation of the DP of PDEGMMA-*b*-P(DEGMMA-*co*-DMAEMA)

To determine the total monomer conversion in the synthesis of the second block, the small sample removed for ^{1}H NMR spectroscopy analysis immediately after the addition of DMAEMA was designated as t = 0 min for this phase of the polymerization. The sum of the integrals of the

two vinyl peaks at 6.15 and 6.13 ppm was compared against the t = 0 sample, using the summed integrals of all -COO CH_2- peaks (from 4.35 to 4.00 ppm), which was a constant through the polymerization, as internal reference. In this way, a conversion was obtained regarding only the polymerization of the second block. To calculate the new monomer-to-initiator ratio, it must be recalled that a significant portion of the polymerization mixture (27.25 wt %) had been removed, and the amounts of DEGMMA and both free and bound initiator must be recalculated accordingly: mmol DEGMMA = 106.7 mmol × (1 – 0.2725) × (1 – 0.2984) = 54.46 mmol, where 0.2984 corresponds to the fraction of monomer having already been polymerized (monomer conversion), and mmol initiator = (free initiator + bound initiator) = 316.9 µmol × (1 – 0.2725) = 230.5 µmol. Therefore, the ratio of monomer-to-initiator is (54.46 mmol DEGMMA + 59.23 mmol DMAEMA)/230.5 µmol initiator = 493 : 1. In the case of BCP-1, the monomer conversion for the second block was 8.6 %, making the DP of the second block 0.086 × 493 = 42 units and the total DP = 101 + 42 = 143. To calculate the number of DMAEMA units (n_{DMAEMA}), the molar percentage of DMAEMA units was obtained from the ^{1}H NMR analysis of the free polymer by comparing the integral of the peak at 2.56 ppm (-CH_2N(CH_3)$_2$ from DMAEMA units) to the integral of the peak at 3.38 ppm (-OCH_3 from DEGMMA units). The molar content of DMAEMA units in BCP-1 was found to be 12.1 %. Therefore, n_{DMAEMA} = 143 × 0.121 = 17, making the composition of the second block 17 DMAEMA units and 25 DEGMMA units. The DPs and the values of n_{DMAEMA} and n_{DEGMMA} units in the second block of BCP-2 and BCP-3 were calculated using the same method.

A.5. Calculation of Grafting Density of Diblock Copolymer Brushes

The grafting densities of PDEGMMA-*b*-P(DEGMMA-*co*-DMAEMA) brushes in BHP-1, -2, and -3 were calculated using the same method as for that of PDEGMMA brushes.

A.6. Quaternization of PDEGMMA-*b*-P(DEGMMA-*co*-DMAEMA) (BCP-3) Using CH_3I

A control quaternization experiment using free diblock copolymer BCP-3 was performed under the similar conditions as for BHP-3 to further confirm that the quaternization of DMAEMA units with iodomethane went to completion. BCP-3 (190.3 mg, 0.2394 mmol DMAEMA units) were added to a 25 mL two-necked flask and dissolved in dry THF (10 mL) under an N_2 atmosphere. The flask was then completely wrapped in aluminum foil, preventing any exposure to light. Iodomethane (1.953 g, 13.76 mmol) was added to the solution, which was then stirred at ambient temperature for 90 min. All volatile portions were removed under vacuum and the polymer residue was characterized using ^{1}H NMR spectroscopy. As shown in Figure A1, the reaction was complete after 90 min.

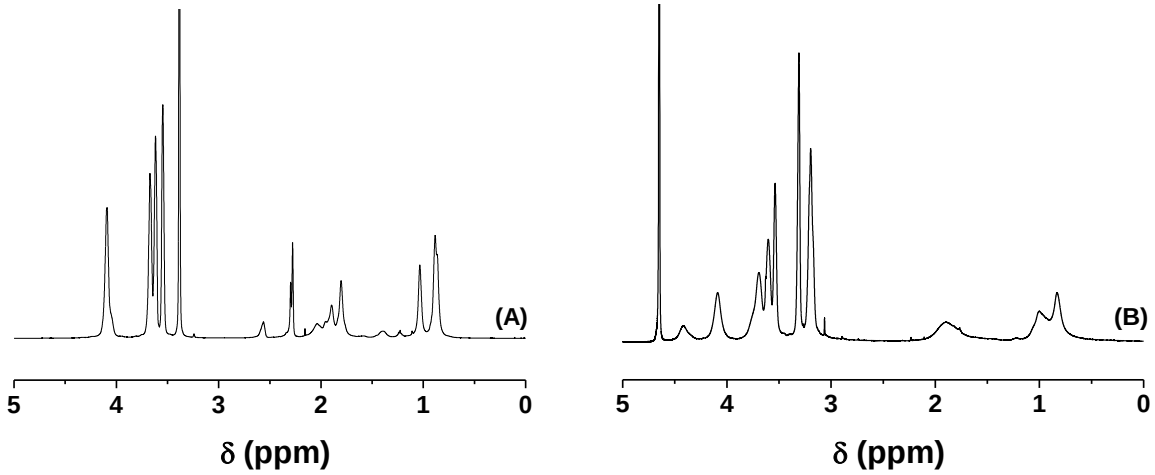

Figure A1. ^{1}H NMR spectra of free diblock copolymer BCP-3 PDEGMMA-*b*-P(DEGMMA-*co*-DMAEMA) before (A) and after (B) quaternization with iodomethane for 90 min.

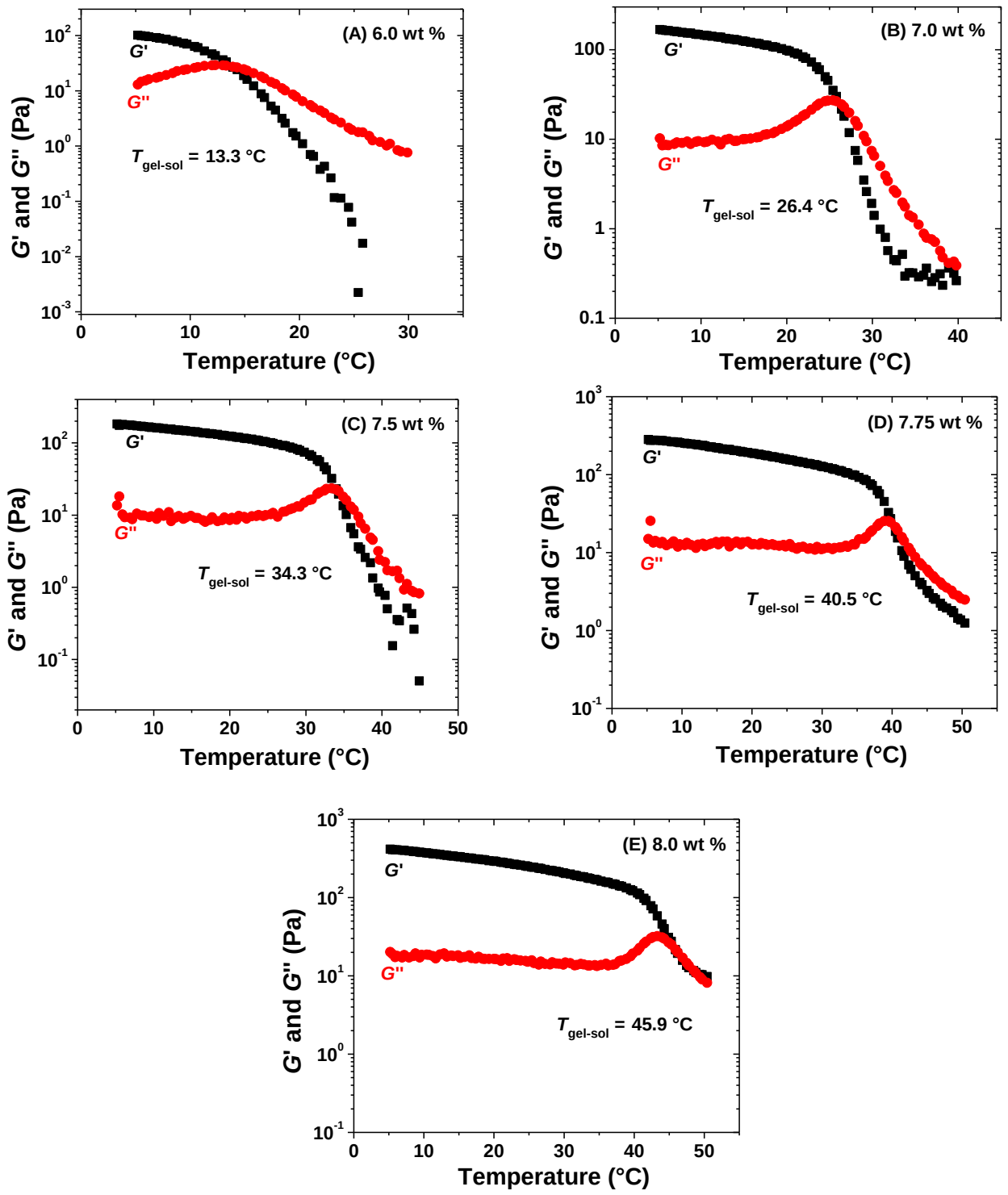

Figure A2. Plots of dynamic storage modulus G' (black square) and loss modulus G'' (red circle) of aqueous dispersions of BHP-1-Q at various concentrations versus temperature. The data were collected from oscillatory shear experiments performed in heating ramps by using a frequency of 1 Hz, a strain amplitude of 1.0 %, and a heating rate of 3 °C/min.

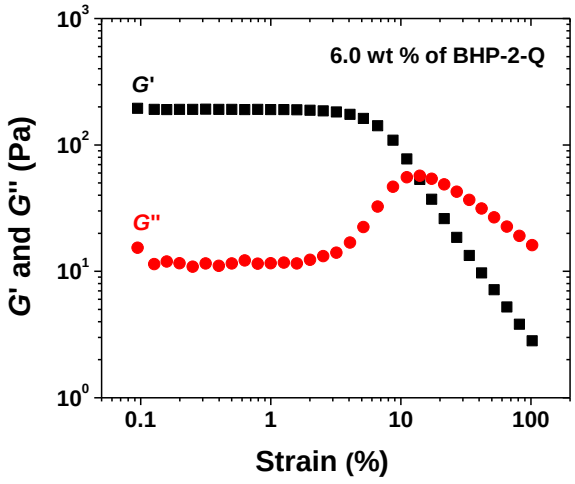

Figure A3. A strain sweep performed on the 6.0 wt % aqueous dispersion of BHP-2-Q at 5 °C using a frequency of 1 Hz.

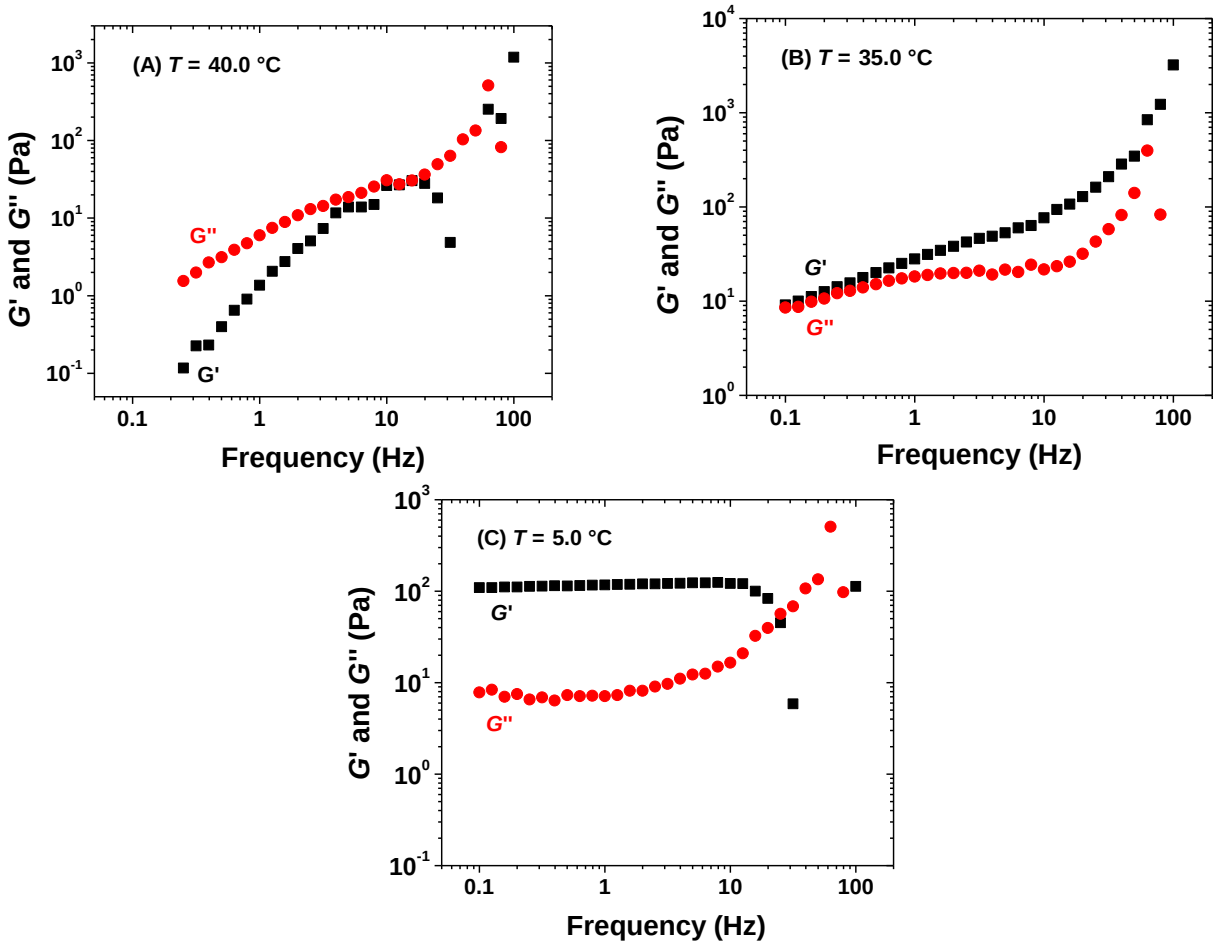

Figure A4. Plots of dynamic storage modulus *G′* and loss modulus *G″* of a 6.0 wt % aqueous dispersion of BHP-2-Q versus frequency at (A) 40 °C, (B) 35 °C, and (C) 5 °C with a constant strain amplitude of 1.0 %.

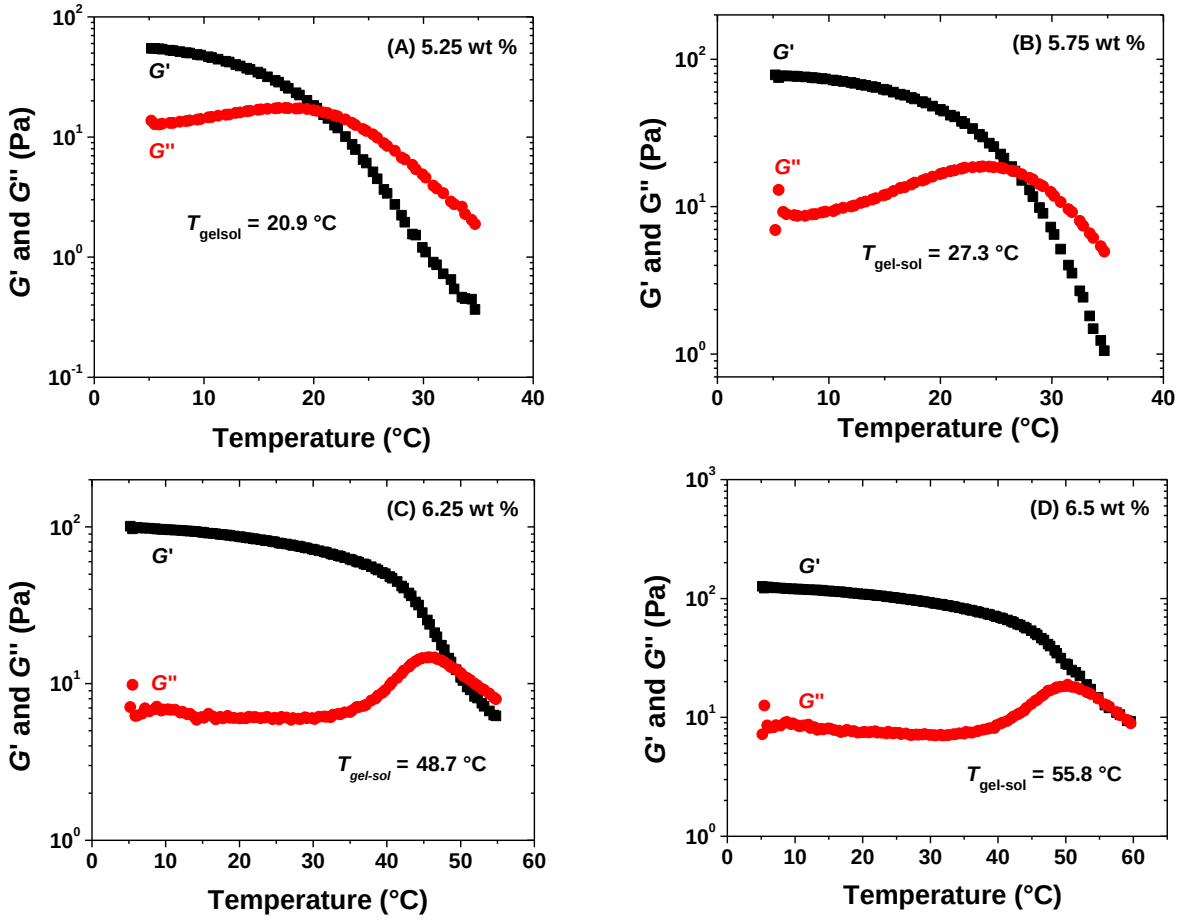

Figure A5. Plots of dynamic storage modulus *G′* (black square) and loss modulus *G″* (red circle) of aqueous dispersions of BHP-2-Q at various concentrations versus temperature. The data were collected from oscillatory shear experiments performed in heating ramps by using a frequency of 1 Hz, a strain amplitude of 1.0 %, and a heating rate of 3 °C/min.

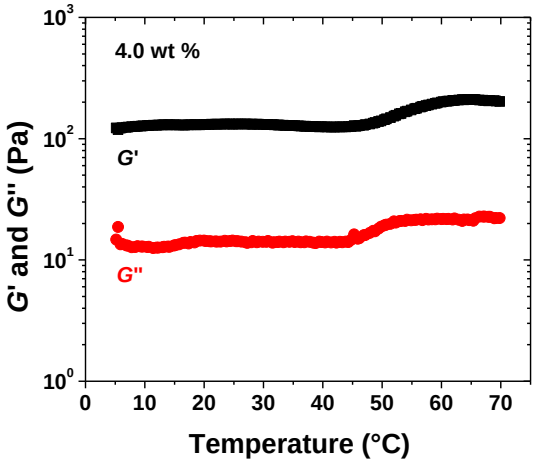

Figure A6. Plot of dynamic storage modulus *G′* (black square) and loss modulus *G″*’ (red circle) of a 4.0 wt% aqueous dispersion of BHP-3-Q. The data were collected from an oscillatory shear experiment performed in a heating ramp by using a frequency of 1 Hz, a strain amplitude of 1.0 %, and a heating rate of 3 °C/min.

Chapter 3. Physically Crosslinked Hydrogels Formed Solely by Thermosensitive Hairy Silica Nanoparticles

Abstract

This Chapter describes thermally-induced reversible formation of three-dimensional network-based hydrogels from aqueous dispersions of thermosensitive diblock copolymer brush-grafted silica nanoparticles (hairy NPs). These hairy NPs consisted of a silica core, a water-soluble polyelectrolyte inner block of poly(2-(methacryloyloxy)ethyltrimethylammonium iodide), and a thermosensitive poly(methoxydi(ethylene glycol) methacrylate) (PDEGMMA) outer block synthesized by sequential surface-initiated atom transfer radical polymerizations and post-polymerization modification. Moderately concentrated dispersions of these hairy particles in water underwent an *in situ* transition from free flowing liquid to self-supporting gel upon heating to sufficiently high temperatures; the transition was fully reversible upon cooling. The gelation was driven by the lower critical solution temperature (LCST) transition of the outer PDEGMMA block, which self-associated into hydrophobic domains upon heating acting as physical crosslinking points for the gel networks. Rheological studies showed that the sol-gel transition temperature decreased with increasing hairy NP concentration, and gelation was achieved at concentrations as low as 3 wt %.

3.1. Introduction

Polymer brush-grafted nanoparticles (hairy NPs) are unique hybrid materials consisting of polymer chains end-tethered to the surface of core NPs.[1,2] They have shown great promise in a wide range of applications such as advanced polymer nanocomposites, chemical sensing, catalysis, and lubrication.[1-3] The NP cores are typically inorganic[1-2,4-5] or metallic[6] in nature with a variety of possible shapes and functionalities.[7,8] Hairy NPs with high grafting densities are often synthesized by growing the brushes from the NP surface, i.e., "grafting from". By coupling this approach with "living"/controlled radical polymerization techniques such as atom transfer radical polymerization (ATRP), nitroxide-mediated radical polymerization, or reversible addition fragmentation chain transfer polymerization, well-defined polymer brushes with controlled molecular weights have been synthesized from a variety of NPs.[1-2,4,9-11] Hairy particles allow for a combination of desired properties from both the polymer, such as stimuli-responsiveness[12] or environmental compatibility,[2,13] and the NPs, including optical,[14] magnetic,[15] or other physical properties.[16-18]

We have been particularly interested in environmentally responsive polymer brush-grafted NPs, e.g., thermosensitive hairy NPs, and their behavior in response to external stimuli.[12,19-23] Thermoresponsive hairy NPs, typically made with polymers displaying a lower critical solution temperature (LCST) in water, exhibit a decrease in hydrodynamic volume when the temperature is raised from below to above the LCST. Polymer brushes also determine the interactions between hairy NPs and their environments. For example, our group discovered that thermosensitive hairy NPs can be reversibly and quantitatively transferred between water and an immiscible liquid phase, either organic solvents or hydrophobic ionic liquids upon heating/cooling.[12,19-20,23]

Thermosensitive hairy NPs are structurally similar to block copolymer micelles with a thermosensitive corona. Thermosensitive block copolymers have received considerable attention for their utility in the formation of physical hydrogels, which exhibit reversible, in situ sol-gel transitions in response to temperature changes.[24-27] These hydrogels have advantages over their chemically cross-linked analogues for some applications, e.g., site-specific drug delivery where their unique sol-gel transition behavior can allow them to be injected as a free-flowing solution which turns into a gel immediately due to the temperature change. There are generally two types of injectable block copolymer hydrogels: gels based on the packing of discrete micelles[24,28-29] and gels based on the bridging of micellar cores by a water-soluble block, usually the center block of ABA or ABC triblock copolymers.[24,30-32] The similarity between thermosensitive block copolymer micelles and hairy NPs presents the opportunity to fashion injectable hydrogels with NP properties not typically available to block copolymer micellar hydrogels. For example, one can use mesoporous or hollow NP[8,33] to make thermoresponsive hairy NPs; the mesopores or hollow interiors can be functionalized to allow for loading of substances incompatible with the hydrophobic polymer-based cores. In a recent work, we took advantage of the structural similarity of hairy NPs to thermosensitive block copolymer micelles to achieve hydrogels based on the cooling-induced jamming of diblock copolymer brush-grafted silica NPs.[34] These NPs were composed of a silica core with a thermosensitive inner block, which underwent a dehydration-hydration transition at lower temperatures, and a hydrophilic polyelectrolyte outer block, which served to prevent aggregation at higher temperatures.

In the present work, the formation of 3-D network hydrogels using thermosensitive diblock copolymer brush-grafted silica NPs is achieved. The hairy NPs were synthesized by sequential surface-initiated ATRPs of *N*,*N*-dimethylaminoethyl methacrylate (DMAEMA) and

methoxydi(ethylene glycol) methacrylate (DEGMMA) (Scheme 3.1). PDEGMMA is a thermosensitive water-soluble polymer with a LCST of 26 °C. The tertiary amines of PDMAEMA were converted to permanently charged trimethylammonium iodide moieties by alkylation with methyl iodide, yielding brushes with a hydrophilic inner block and a thermosensitive outer block. At sufficiently high concentrations and above the LCST of the outer block, the PDEGMMA blocks self-assembled into hydrophobic domains (micellar cores), which were linked to core silica NPs by the bridging polyelectrolyte chains in a manner similar to thermosensitive ABA or ABC micellar gels (Scheme 3.2). The gel properties were studied by rheological measurements.

3.2. Experimental Section

3.2.1. Materials

A dispersion of silica NPs with a size of 10–15 nm, according to the manufacturer, in methyl isobutyl ketone (30 -31 wt%) was obtained from Nissan Chemical. Karstedt's catalyst (2,1-2.4 % Pt in xylene) was purchased from Gelest. Chlorodimethylsilane (98%, Alfa Aesar) was stored in a refrigerator prior to use. 10-Undecenyl 2-bromoisobutyrate was synthesized according to a literature procedure.[19] CuCl (98%, Aldrich), $CuCl_2$ (98%, Aldrich) were used as received. *N*, *N*, *N′*, *N′*, *N″*-Pentamethyldiethylenetriamine (PMDETA, 99%, Aldrich), ethyl 2-bromoisobutyrate (EBiB, 98%, Aldrich), and methoxydi(ethylene glycol) methacrylate (DEGMMA, 95%, Aldrich) were dried over calcium hydride, distilled under vacuum, and kept in a desiccator. *N*, *N*-Dimethylaminoethyl methacrylate (DMAEMA, 99%, Acros) was passed through a column of silica gel and basic alumina (2/1, v/v) to remove the inhibitor. All monomers were stored in a refrigerator prior to use. Methyl iodide (99%, stabilized) was purchased from Acros and used as

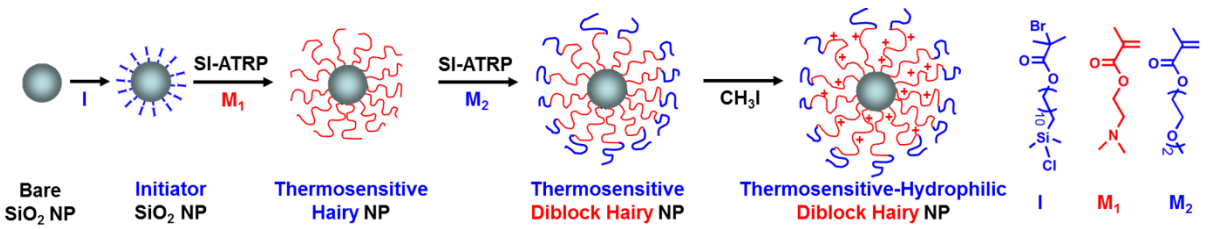

Scheme 3.1. Synthesis of P(TMAEMA-I)-*b*-PDEGMMA brush-grafted silica NPs by sequential surface-initiated atom transfer radical polymerizations (SI-ATRP) of DMAEMA (M_1) and DEGMMA (M_2) followed by quaternization with methyl iodide, and molecular structures of DMAEMA and DEGMMA.

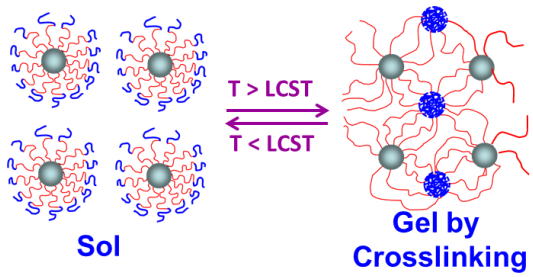

Scheme 3.2. Thermally reversible physically crosslinked 3-dimensional network hydrogels formed solely by thermosensitive diblock copolymer brush-grafted silica nanoparticles composed of a hydrophilic inner block and thermosensitive outer block.

received. All other chemical reagents were purchased from either Aldrich or Fisher and used without further purification.

3.2.2. Characterization

In order to characterize the polymers cleaved off the nanoparticles as well as the untethered polymers produced from the free initiators during the synthesis of hairy nanoparticles, size exclusion chromatography (SEC) was carried out at ambient temperature using a PL-GPC-50 from Polymer Laboratories, Inc. with a differential refractive index detector, a guard column (PLgel 10 μm, 50 × 7.5 mm, Agilent Technologies), and three PLgel 10 μm Mixed-B columns (300 × 7.5 mm, Agilent Technologies) with a linear range from 500 to 10,000,000 Da according to the manufacturer. *N*,*N*-Dimethylformamide (DMF) with 0.1 *M* LiBr was used as the mobile phase with a flow rate of 1.0 mL/min. The data were processed using Cirrus^{TM} GPC/SEC software, according to a calibration with PS standards. ^{1}H NMR spectra were obtained using a Varian VNMRS 500 MHz spectrometer; the residual solvent proton signal (either D_2O or $CDCl_3$) was used as reference peak. Thermogravimetric analysis (TGA) was carried out in air using a Seiko 6300 TG/DTA at a heating rate of 20 °C/min. Transmission electron microscopy (TEM) was performed on a Zeiss Libra 200 HT FE MC microscope at an accelerating voltage of 200 kV. Bright field images were recorded using a bottom-mounted Gatan UltraScan US1000XP CCD camera. Hairy silica NPs were cast from chloroform (~2 mg/mL) onto a carbon-coated, copper TEM grid and allowed to dry at ambient conditions.

3.2.3. Synthesis of ATRP Initiator-Functionalized Silica Nanoparticles

10-Undecenyl 2-bromoisobutyrate (6.020 g, 18.85 mmol) was added into a 50 mL two-necked flask and dried under high vacuum, followed by the injection of chlorodimethylsilane (3.1 mL, 27.9 mmol) under an N_2 atmosphere and a solution of Karstedt's catalyst in xylene (75 μL).

After the ^{1}H NMR spectroscopy analysis showed that the reaction was complete, the remaining chlorodimethylsilane was evaporated in vacuum, and the obtained 11-(chlorodimethylsilyl)undecyl 2-bromoisobutyrate was dissolved in toluene (5 mL).

MIBK-ST (26.700 g dispersion, corresponding to 8.010 g bare silica NPs) was added into a 250 mL three-necked flask and diluted with 20 mL anhydrous toluene. A portion of the mixture (~15 mL) was then distilled off under vacuum to azeotropically remove any trace amount of water. Dry toluene (20 mL) was then injected into the flask, and the azeotropic distillation was carried out again. This process was repeated for a total of three times. The resultant dispersion of silica NPs had a volume ~ 60 mL. The solution of the freshly synthesized 11-(chlorodimethylsilyl)undecyl 2-bromoisobutyrate in toluene was added into the dispersion, and the mixture was heated to 90 °C and stirred under a N_2 atmosphere for 64 h. The initiator-functionalized silica NPs were then diluted in DMF and isolated via centrifugation (Beckman Optima L-90K Ultracentrifuge with type 60 Ti rotor, 35,000 rpm, 30 min). The initiator NPs were re-dispersed in DMF and centrifuged again. This dispersion-centrifugation cycle was repeated for a total of three times. Fractionation of the initiator NPs was carried out to achieve a more uniform size distribution. The obtained initiator NPs were dispersed in DMF and the dispersion was centrifuged at 20,000 rpm. The NPs deposited at the bottom of the tube were removed, and the supernatant dispersion was then centrifuged at 30,000 rpm. The NPs collected in this fraction were dried under a stream of air, affording a slightly brown powder (2.401 g).

3.2.4. Synthesis of PDMAEMA Brushes from Initiator NPs

ATRP initiator-functionalized NPs (0.291 g) were ultrasonicated in anisole (7.301 g) in a 25 mL two-necked flask to yield a homogeneous dispersion. *N*,*N*-Dimethylaminoethyl methacrylate (DMAEMA, 2.907 g, 18.49 mmol), copper(I) chloride (12.8 mg, 1.29×10^{-4} mol), copper(II)

chloride (4.7 mg, 3.5×10^{-5} mol), and ethyl 2-bromoisobutyrate (EBiB, 3.9 mg, 1.99×10^{-5} mol) were added into the dispersion. The flask was then sealed under nitrogen, and *N*, *N*, *N'*, *N'*, *N''*-pentamethyldiethylenetriamine (PMDETA, 41.2 mg, 2.38×10^{-5} mol) was injected into the reaction mixture immediately before degassing by three freeze–pump–thaw cycles. The polymerization was carried out at 85 °C and monitored by ^{1}H NMR spectroscopy. After 8.5 h, the monomer conversion reached 65.8 %, and the reaction was halted. The degree of polymerization (DP) of the polymer was calculated to be 271 accounting for both the free and surface-bound initiator, as described in a previous work.[34]

The PDMAEMA brush-grafted silica NPs were collected and purified through five cycles of re-dispersion in THF and ultracentrifugation. The PDMAEMA homopolymer brush-grafted NPs were designated as HP. A portion of the supernatant liquid from the first cycle was passed through a column of silica gel (bottom)/activated neutral aluminum oxide (top) (2:1, v/v) to obtain the free polymer. The PDMAEMA free polymer was purified by precipitation in a mixture of hexane and diethyl ether (v/v, 10 : 1), dried under high vacuum, and stored in a stock solution in anisole for use as a free macroinitiator in the synthesis of diblock copolymer brush-grafted NPs.

3.2.5. Synthesis of PDMAEMA-*b*-PDEGMMA Brush-Grafted Silica NPs

Two samples of PDMAEMA-*b*-PDEGMMA brush-grafted silica NPs were synthesized with differing PDEGMMA block lengths using the same PDMAEMA brush-grafted NPs. Below is the synthesis of PDMAEMA-*b*-PDEGMMA brushes on silica NPs with the PDEGMMA outer block DP of 100 (DB-100); another sample with the PDEGMMA outer block DP of 195 (DB-195) was made in a similar fashion.

PDMAEMA brush-grafted silica NPs (206.3 mg) were dispersed in anisole (3.555 g) and added into a 25 mL, two-necked flask. Free PDMAEMA (89.1 mg, 2.10×10^{-6} mol) and

DEGMMA (0.873 g, 4.63 mmol) was then added, followed by copper(I) chloride (3.1 mg, 3.4×10^{-5} mol), and copper(II) chloride (2.3 mg, 1.7×10^{-5} mol). PMDETA (5.7 mg, 3.3×10^{-5} mol) was injected into the mixture immediately before freezing for degassing. The mixture was subjected to three freeze-pump-thaw cycles and heated to 65 °C. After 80 min, the reaction was halted by exposure to air and dilution with THF. The hairy NPs were collected and purified by repeated ultracentrifugation as done for PDMAEMA brush-grafted NPs. The free diblock copolymer PDMAEMA-*b*-PDEGMMA (FDB-100) was purified by precipitation in a mixture of hexane and diethyl ether (v/v, 10:1), dried under vacuum and analyzed by ^{1}H NMR spectroscopy to determine the DP of PDEGMMA using the DP of the PDMAEMA block as the basis.

3.2.6. HF Cleavage of Polymer Brushes from Silica NPs

The following procedure was used for the cleavage of P(DMAEMA-*b*-DEGMMA) brushes from silica NPs (DB-100) by HF for direct characterization; a similar process was employed for the cleavage of PDMAEMA brushes from HP. Please note that HF is particularly hazardous and should not be used when alone or without proper safety precautions, including ready access to calcium gluconate gel.

DB-100 hairy NPs (10.1 mg) and THF (10 mL) were added into a Teflon tube and sonicated to achieve a homogeneous dispersion. Hydrofluoric acid (HF, 48 ~ 51 % in water, 0.5 mL) was added slowly. The mixture was stirred at room temperature for 24 h and then neutralized with a saturated aqueous solution of calcium hydroxide. The mixture was then partitioned between methylene chloride and water at 35 °C; the aqueous phase was then extracted with methylene chloride (5 mL × 4). The extracts were combined and dried over anhydrous sodium sulfate. The cleaved polymer was then analyzed using SEC.

3.2.7. Quaternization of PDMAEMA-*b*-PDEGMMA Brush-Grafted NPs with CH_3I

Described below is the quaternization of tertiary amine moieties in DB-100, producing hairy NPs denoted as Q-100. A similar procedure was used for the quaternization of DB-195, yielding Q-195. A dispersion of DB-100 (203.1 mg, 0.764 mmol DMAEMA units) in THF (10 mL) was prepared in a 25 mL two-necked flask by ultrasonication and sealed under a N_2 atmosphere. The flask was covered with aluminum foil to prevent exposure to light prior to the addition of methyl iodide (2.816 g, 19.84 mmol). The reaction mixture was stirred overnight. The mixture was then diluted with water and placed under vacuum to remove THF and excess methyl iodide. The quaternized polymer brush-grafted silica NPs, denoted as Q-100, were isolated from the resultant aqueous dispersion by ultracentrifugation (35000 rpm, 45 min) and washed by three subsequent rounds of ultracentrifugation/re-dispersion in water.

3.2.8. Rheological Study of Gelation of Aqueous Dispersions of P(TMAEMA-I)-*b*-PDEGMMA Brush-Grafted Silica NPs

Aqueous dispersions of P(TMAEMA-I)-*b*-PDEGMMA brush-grafted silica NPs were prepared by ultrasonication in an ice water bath (Fisher Scientific Model B200 Ultrasonic Cleaner), and stored in a refrigerator. The aqueous dispersions obtained were both transparent and homogeneous.

Rheological analysis was carried out using a rheometer from TA Instruments (Model TA AR 2000ex) to elucidate the gelation behavior and gel properties of aqueous dispersions of both Q-100 and Q-195. A cone–plate geometry with a cone diameter of 20 mm and an angle of 2° (truncation 52 μm) was employed; the temperature was controlled by the bottom Peltier Plate. For each rheological experiment, an aqueous dispersion of quaternized hairy NPs (90 μL), which was cooled in an ice water bath to aid in sample loading, was added directly onto the plate by a

micropipette. The solvent trap was filled with water and a solvent trap cover was used to minimize water evaporation during rheological measurements. Dynamic storage modulus G′ and loss modulus G″ were recorded from oscillatory shear experiments performed by using a fixed frequency of 1 Hz and strain amplitude (γ) of 0.2 % in a temperature ramp with a heating or cooling rate of 3 °C/min. The frequency and strain amplitude dependences of G′ and G″ at the desired concentrations and temperatures were obtained by frequency sweep tests from 0.1 to 100 Hz using a strain amplitude of 0.2 % and strain amplitude sweeps from 0.1 to 100 % strain using a frequency of 1 Hz, respectively.

3.3. Results and Discussion

3.3.1. Synthesis of PDMAEMA-*b*-PDEGMMA Brush-Grafted Silica NPs

PDMAEMA-*b*-PDEGMMA diblock copolymer brush-grafted silica NPs were synthesized by sequential SI-ATRPs of DMAEMA and DEGMMA. The NPs with a size of 23.5 nm measured by TEM were surface-functionalized with an ATRP initiator-terminated chlorosilane, 11-(chlorodimethylsilyl)undecyl 2-bromoisobutyrate, according to a procedure similar to that used in a previous work.[34] Briefly, anhydrous toluene was added into the dispersion of silica NPs in methyl isobutyl ketone and was distilled off under vacuum to azeotropically remove any water present, which was repeated additional two times. A solution of freshly prepared 11-(chlorodimethylsilyl)undecyl 2-bromoisobutyrate in toluene was then added to the dispersion; the mass ratio of initiator silane to NPs was 97 : 100. The reaction mixture was then heated to 90 °C and stirred for 64 h before the immobilization reaction was stopped. The initiator-functionalized silica nanoparticles were isolated and purified by repeated ultracentrifugation and re-dispersion in DMF.

PDMAEMA brushes were then grown from the initiator-functionalized silica NPs; the initiator NPs were dispersed in anisole and the SI-ATRP of DMAEMA was carried out at 85 °C using a catalyst system of CuCl/$CuCl_2$/PMDETA. Additionally, a free initiator, ethyl 2-bromoisobutyrate, was added into the polymerization mixture to facilitate the characterization of PDMAEMA brushes through the formation of analogous free polymer, which is known to closely mirror the molecular weight and dispersity of their surface-tethered counterparts.[35,36] These free polymer analogues allow for more convenient and faster characterization of brush molecular weights by SEC than the cleavage and analysis of polymer brushes. However, we note here that given the amount of the surface initiator on silica nanoparticles, it is certainly possible to achieve living radical polymerization without the addition of a free initiator. The polymerization was monitored by SEC and ^{1}H NMR spectroscopy and was stopped after 8.5 h, at which the monomer conversion reached 65.8 %. The PDMAEMA brush-grafted silica NPs, denoted as HP, were isolated and purified through multiple cycles of ultracentrifugation and dispersal. SEC analysis of the free PDMAEMA (Figure 3.1) yielded an $M_{n,SEC}$ of 54.6 kDa and a PDI of 1.17 relative to polystyrene standards, suggesting that control was maintained throughout the polymerization. TGA revealed a decrease in weight retention at 800 °C from 89.9 % for initiator-functionalized NPs to 18.3% for HP, verifying the presence of tethered PDMAEMA on the surface of silica NPs (Figure 3.2). The DP of PDMAEMA was calculated using the TGA data alongside the monomer conversion to calculate the mass of grafted polymer and total polymer. The proportion of the surface-bound polymer was then used to back-calculate the amount of the "effective" surface initiator, the portion of the surface initiator that successfully initiated polymerization, and to define the molar ratio of monomer DMAEMA to the total initiating species. The molar ratio of DMAEMA to total initiator was then multiplied by the monomer conversion determined by

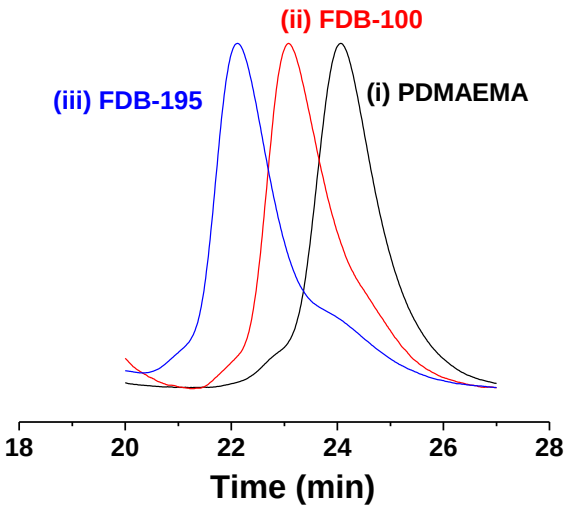

Figure 3.1. Size exclusion chromatography (SEC) analysis of (i) free PDMAEMA formed in the synthesis of PDMAEMA brush-grafted silica NPs, (ii) free PDMAEMA-*b*-PDEGMMA with the PDEGMMA block DP of 100 (FDB-100) formed in the synthesis of DB-100 hairy NPs, and (iii) free PDMAEMA-*b*-PDEGMMA with the PDEGMMA block DP of 195 (FDB-195) formed in the synthesis of DB-195 hairy NPs.

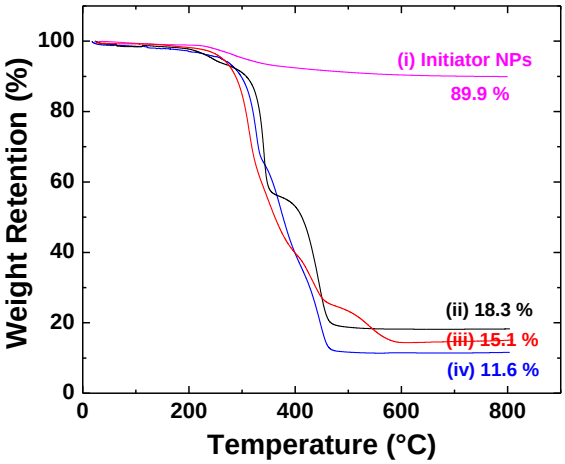

Figure 3.2. Thermogravimetric analysis (TGA) of (i) initiator-functionalized silica NPs, (ii) PDMAEMA brush-grafted silica NPs, (iii) PDMAEMA-*b*-PDEGMMA brush-grafted silica NPs with PDEGMMA block DP of 100 (DB-100), and (iv) PDMAEMA-*b*-PDEGMMA brush-grafted silica NPs with PDEGMMA block DP of 195 (DB-195).

^{1}H NMR spectroscopy analysis to yield a DP of 271 for PDMAEMA.

Following the purification of HP and the free PDMAEMA by centrifugation and precipitation, respectively, a subsequent SI-ATRP was performed to grow a thermosensitive PDEGMMA block from the Cl-capped chain ends of surface-bound PDMAEMA chains. As such, HP was used in the presence of the free PDMAEMA which acted as a "sacrificial" macroinitiator in the same vein as ethyl 2-bromoisobutyrate in the SI-ATRP of DMAEMA described above. The ATRP of DEGMMA was carried out at 65 °C using a catalyst system of CuCl/$CuCl_2$/PMDETA. The polymerization was monitored by SEC. After 80 min, the reaction was stopped, and the diblock copolymer brush-grafted NPs (DB) and free copolymer (FDB) were purified in the same manner as HP and PDMAEMA through centrifugation and precipitation, respectively. Two hairy NP samples were made. From SEC analysis, the peak shifted to the high molecular weight side (Figure 3.1); one had an $M_{n,SEC}$ of 83.9 kDa with a PDI of 1.20, and another one had an $M_{n\ SEC}$ of 151.7 kDa with a PDI of 1.27. The DP_{DEGMMA} for the two diblock copolymers was found to be 100 and 195, respectively, calculated from the ^{1}H NMR spectra of PDMAEMA-*b*-PDEGMMA free polymers by comparing the integrals of the peaks at 3.50 - 3.75 ppm from -$OCH_2CH_2OCH_2CH_2OCH_3$ of DEGMMA monomer units to the peak at 2.20 - 2.35 ppm from -$N(CH_3)_2$ of DMAEMA units.

TGA analysis showed a further reduction in weight retention at 800 °C after the growth of the second block, with the shorter diblock copolymer brush-grafted silica NPs (DB-100) at 15.1 % and the longer (DB-195) at 11.6% (Figure 3.2). Figure 3.3 shows the representative TEM micrographs of HP, DB-100, and DB-195 cast from chloroform dispersions with the same concentration. The interparticle distance for DB-100 in Figure 3.3B appears to be larger than that for DB-195 in Figure 3.3C, through it is uncertain that these hairy NPs achieved close-packing

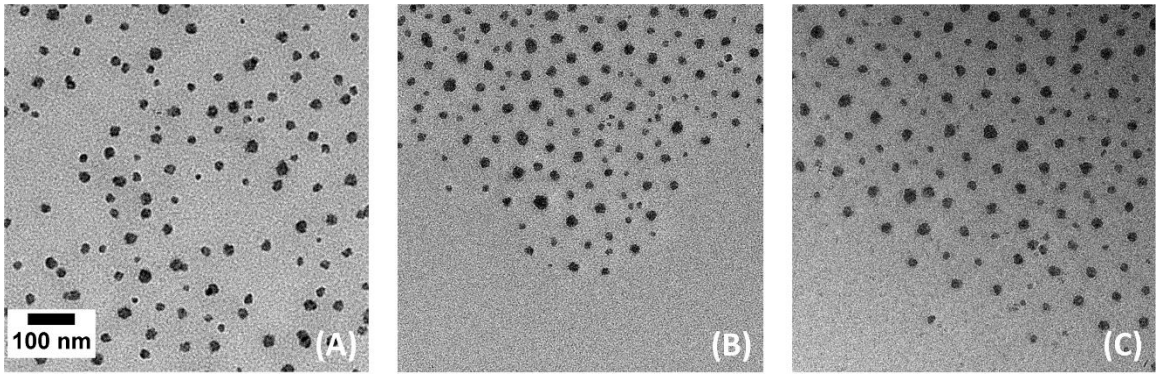

Figure 3.3. Bright field TEM micrographs of (A) PDMAEMA brush-grafted silica NPs, (B) PDMAEMA-*b*-PDEGMMA brush-grafted silica NPs with PDEGMMA block DP of 100 (DB-100), and (C) PDMAEMA-*b*-PDEGMMA brush-grafted silica NPs with PDEGMMA block DP of 195 (DB-195). The scale bars are the same for the three TEM micrographs. The TEM samples were prepared by drop casting of the dispersions of hairy NPs in chloroform with a concentration of 2 mg/mL onto carbon-coated, copper TEM grid.

during the evaporation of the solvent. Finally, the numbers of the grafted PDMAEMA chains on HP and the PDMAEMA-*b*-PDEGMMA brush chains on DB-100 and -195 were obtained using a core NP size of 23.5 nm, silica density of 2.07 g cm^{-3}, and TGA data. The grafting density was found to be between 0.43 and 0.47 chains/nm^2. The characterization data for hairy NPs and the corresponding free polymers are summarized in Table 3.1.

To confirm that the brush molecular weight and molecular weight distribution can be represented by those of the free polymer formed from the free initiator, the core silica NPs of HB were etched away using HF and the cleaved polymer was evaluated by SEC. The analysis revealeda molecular weight distribution essentially identical to that of PDMAEMA free polymer (Figure 3.4A). A similar cleavage was performed using DB-100, and the SEC analysis showed that the SEC curves of the cleaved polymer brushes and the free diblock copolymer almost overlapped (Figure 3.4B), confirming the validity of using the free polymer to estimate the molecular characteristics of the grafted polymer chains.

3.3.2. Quaternization of Tertiary Amine Moieties in PDMAEMA-*b*-PDEGMMA Brush-Grafted Silica NPs by CH_3I

To enhance the hydrophilicity of the inner block, making it more capable of serving as a bridging chain between particles and domains of associated PDEGMMA chains, we subjected the tertiary amine groups to exhaustive alkylation using methyl iodide. The converted monomer unit (TMAEMA-I) possess a permanently positive charge, greatly increasing solubility in water. The resultant P(TMAEMA-I)-*b*-PDEGMMA brush-grafted silica NPs were designated as Q-100 (from DB-100) and Q-195 (from DB-195). The quaternization reaction was carried out at ambient temperature in THF under a nitrogen atmosphere. Exposure to light was minimized by covering the reaction flask in aluminum foil to decrease light-induced discoloration. After the reaction

Table 3.1. Characterization Data for PDMAEMA and PDMAEMA-*b*-PDEGMMA Brush-Grafted Silica NPs and Their Corresponding Free Polymers

Polymer Brush-Grafted Silica NP Sample	$M_{n,SEC}$ [a] (kDa)	PDI [a]	DP_{DMAEMA} [b]	DP_{DEGMMA} [c]	Grafting density [d]
HP [e]	54.6	1.17	271		0.47 chains/nm^2
DB-100 [e]	83.9	1.24	271	100	0.44 chains/nm^2
DB-195 [e]	151.7	1.27	271	195	0.43 chains/nm^2

[a] determined by size exclusion chromatography (SEC) calibrated with polystyrene standards. [b] The degree of polymerization (DP) of the inner PDMAEMA block was calculated using monomer conversion and the ratio of monomer to initiating moieties (both free and surface-bound). [c] The DP of the outer PDEGMMA block was calculated using the ^{1}H NMR spectrum of the free block copolymer. [d] The grafting densities of polymer brushes were calculated using TGA data, the DPs of both blocks, and the core silica nanoparticle size of 23.5 nm. [e] HP and DB are designations for homopolymer brush-grafted NPs and diblock copolymer brush-grafted silica NPs. Their corresponding free polymers are PDMAMEA, FDB-100, and FDB-195, respectively.

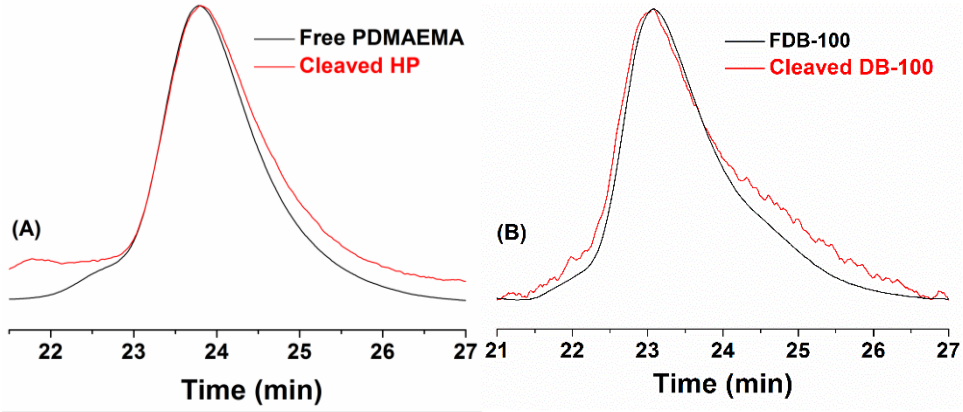

Figure 3.4. SEC analysis of the cleaved polymer (red) and the free polymer (black) corresponding to PDMAEMA brush-grafted NPs (A) and DB-100 (B).

proceeded overnight, the hairy NPs were isolated and purified by repeated ultracentrifugation in water. The ^{1}H NMR spectra of DB-100 and Q-100 show nearly complete alkylation of tertiary amine moieties, evidenced by the almost disappearance of the -N(CH_3)$_2$ peak at 2.4 ppm and the appearance of -N^{+}(CH_3)$_3$ peak at 3.2 ppm (Figure 3.5). Quantitative analysis using the residual peak area at 2.4 ppm showed that approximately 5 % of tertiary amine moieties remained after the reaction, which should not affect the gelation of aqueous dispersions of hairy NPs because of the highly charged hydrophilic inner block.

3.3.3. Reversible Sol-Gel Transitions of a 6.0 wt% Dispersion of Q-100 in Water

Quaternized diblock copolymer brush-grafted silica NPs were relatively easily dispersed in water by ultrasonication in an ice water bath, and the dispersions were transparent; Q-100 showed a yellow coloration while Q-195 was essentially colorless. At moderate concentrations, aqueous dispersions of Q-100 underwent sol-gel transitions upon heating. For example, a 6.0 wt % dispersion of Q-100 was a flowing liquid at 20 °C (Figure 3.6A) and a self-supporting gel at 50 °C (Figure 3.6B); this gelation was fully reversible. The sol-gel transition temperature was determined visually by heating the dispersion to selected temperatures, equilibrating at those temperatures for several minutes, and inverting the vial to assess the state of the sample; the lowest temperature at which a free-standing gel was observed for a 6.0 wt % Q-100 aqueous dispersion was 43.5 °C. Further heating the gel did not noticeably alter the appearance of the dispersion.

To obtain a more quantitative picture of this thermally-induced gelation, oscillatory shear experiments were performed using a 6.0 wt % aqueous dispersion of Q-100 (Figure 3.7). A temperature ramp was performed at a frequency of 1.0 Hz at a heating rate of 3 °C min^{-1}. The strain amplitude was set at 0.2 %, which was well within the linear viscoelastic regime. Dynamic storage modulus (G′) and loss modulus (G″) were measured throughout the temperature range of

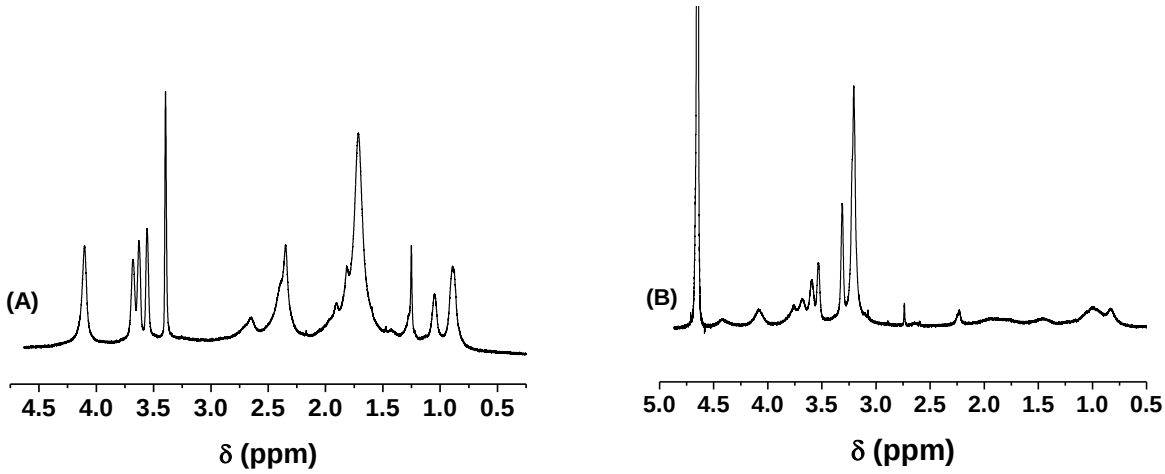

Figure 3.5. ^{1}H NMR spectrum of (A) PDMAEMA-*b*-DEGMMA brush-grafted silica NPs (DB-100) in $CDCl_3$ and (B) P(TMAEMA-I)-*b*-PDEGMMA brush-grafted NPs (Q-100) in D_2O after quaternization with CH_3I.

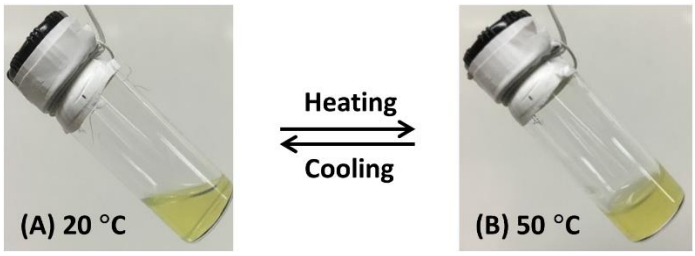

Figure 3.6. Digital optical pictures of a 6.0 wt % aqueous dispersion of P(TMAEMA-I)-*b*-PDEGMMA brush-grafted silica NPs (Q-100) at 20 °C and 50 °C.

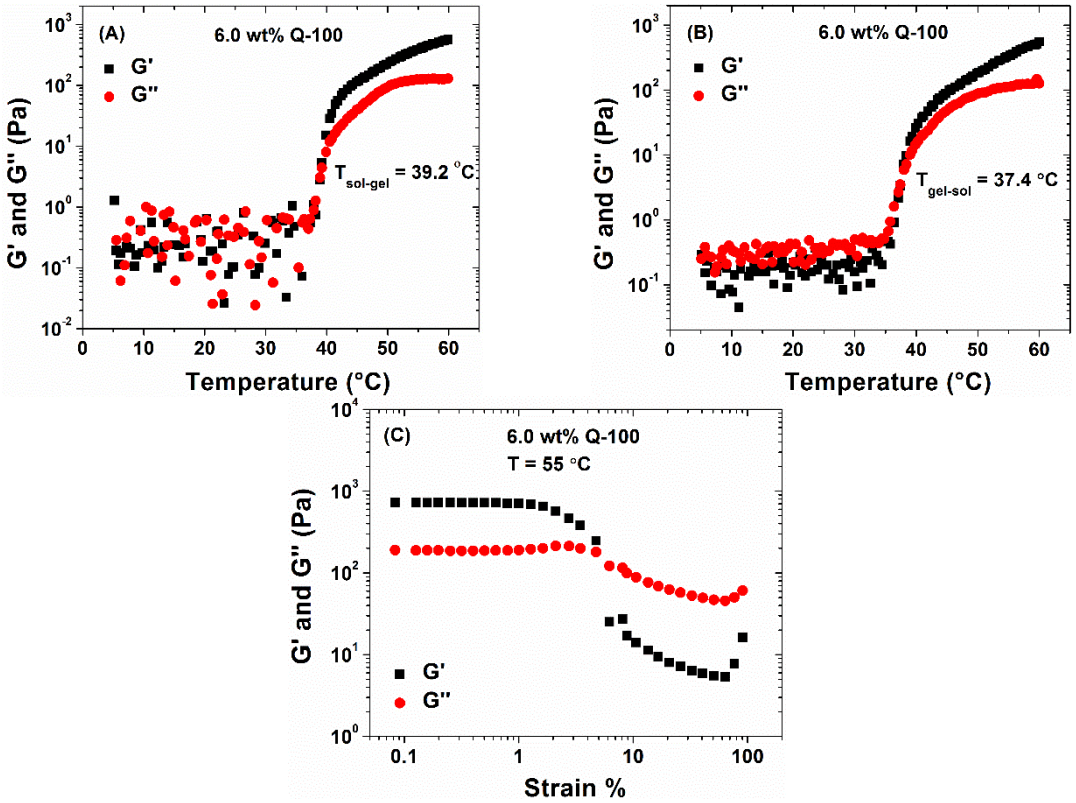

Figure 3.7. Plots of dynamic storage modulus G′ and loss modulus G″ of a 6.0 wt % aqueous dispersion of P(TMAEMA-I)-*b*-PDEGMMA brush-grafted silica nanoparticles (Q-100) obtained from oscillatory shear experiments performed in a temperature ramp at a frequency of 1 Hz, a strain amplitude of 0.2 %, and (A) a heating rate of 3 °C/min or (B) a cooling rate of -3 °C/min. (C) Strain sweep at a frequency of 1 Hz and 55 °C.

5 to 60 °C, with the magnitude of G″ and G′ being low at low temperatures and G′ surpassing G″ at higher temperatures, indicative of a heating-induced sol-gel transition (Figure 3.7A). The crossover point was shown to be 39.2 °C; this point is often taken as the sol-gel transition temperature and is close to 43.5 °C observed visually. The transition was marked by a relatively sharp increase in both G′ and G″ beginning slightly before the crossover temperature was reached. Shortly after the crossover point at 39.2 °C, a slower increase in both moduli was observed, with the gel strength apparently increasing with temperature. Finally, beginning around 50 °C, G″ reached a plateau while G′ kept increasing. A similar result was obtained from the cooling ramp (Figure 3.7B), with the crossover point differing slightly at 37.4 °C, indicating a small hysteresis.

The initial fast gelation should be similar to that for the thermally induced formation of 3-D network micellar hydrogels of thermosensitive ABA and ABC block copolymers as illustrated in Scheme 3.2. When the concentration is above the critical gelation concentration and the temperature is above the LCST of the thermosensitive outer block, the PDEGMMA collapsed and self-assembled into hydrophobic domains or micellar cores, which served to physically crosslink the polymer brush-grafted NPs to form a three dimensional network. Following the rapid sol-gel transition, the G′ increased gradually, indicating strengthening of the gel with increasing temperature. This suggests an increase in the number of bridging chains. It has been shown previously that the LCST transition of thermosensitive polymers can be modulated strongly by the attached end-groups.[37] In the present case, the inner hydrophilic, charged P(TMAEMA-I) block likely increased the LCST of the thermosensitive block, and the polydispersities of core NP size and block lengths likely played a role.

We note here that the linear viscoelastic regime for the gel of the 6.0 wt% aqueous dispersion of Q-100 at 55 °C was only 2 % strain, much narrower than what would normally be expected of

a three-dimensional network hydrogel of, e.g., an ABA triblock copolymer with thermosensitive outer blocks, which was ~ 15% or above.[28] The main difference between our hairy NP-based hydrogels and ABA triblock copolymer 3-D micellar network gels is the covalent linkage of polymer chains to the inorganic core. For thermosensitive ABA triblock copolymer network hydrogels, upon shearing/deformation, the collapsed A block can be pulled out from a micellar core to relieve local stresses (e.g., due to the stretching of the bridging chains). The outer block of a diblock copolymer brush-grafted NP can also react to deformation in this way, but the inner block would require the scission of the chemical bond to detach from the core. Therefore, hairy NP-based hydrogels likely have fewer modes of relaxation upon deformation, potentially making these gels more brittle than their micellar counterparts of ABA or ABC triblock copolymers.

3.3.4. Reversible Sol-Gel Transitions of Dispersions of Q-195 in Water

P(TMAEMA-I)-*b*-PDEGMMA brush-grafted silica NPs with a longer thermosensitive outer block (Q-195) were also tested in aqueous dispersions for gelation. Like Q-100, aqueous dispersions of Q-195 underwent reversible, thermally-induced sol-gel transitions. The increased length of the outer PDEGMMA block significantly decreased the temperature required to achieve gelation; a 6.0 wt% aqueous dispersion of Q-195 became a free standing gel, by visual inspection, at 32 °C, 11.5 °C lower than Q-100 at the same concentration. Figure 3.8 shows this dispersion as a flowing liquid at 20 °C and a free-standing gel at 40 °C. Similarly, rheological measurements performed during heating and cooling ramps (Figure 3.9A and B) showed a crossover point of 29.3 and 27.0 °C, respectively, which were ~ 10 °C lower than the sol-gel and gel-sol transition temperatures observed in the same analysis of the 6.0 wt % aqueous dispersion of Q-100. The evolution of G′ and G″ with temperature for Q-195 is similar to that of Q-100, with four distinct regions. First, a low magnitude liquid region dominated by G″ is observed at low temperatures.

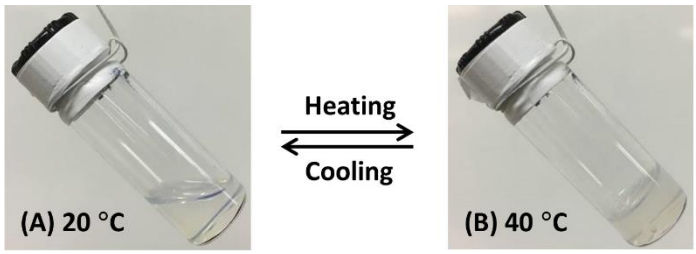

Figure 3.8. Digital optical pictures of a 6.0 wt% aqueous dispersion of P(TMAEMA-I)-*b*-PDEGMMA brush-grafted silica NPs (Q-195) at 20 °C and 40 °C.

0

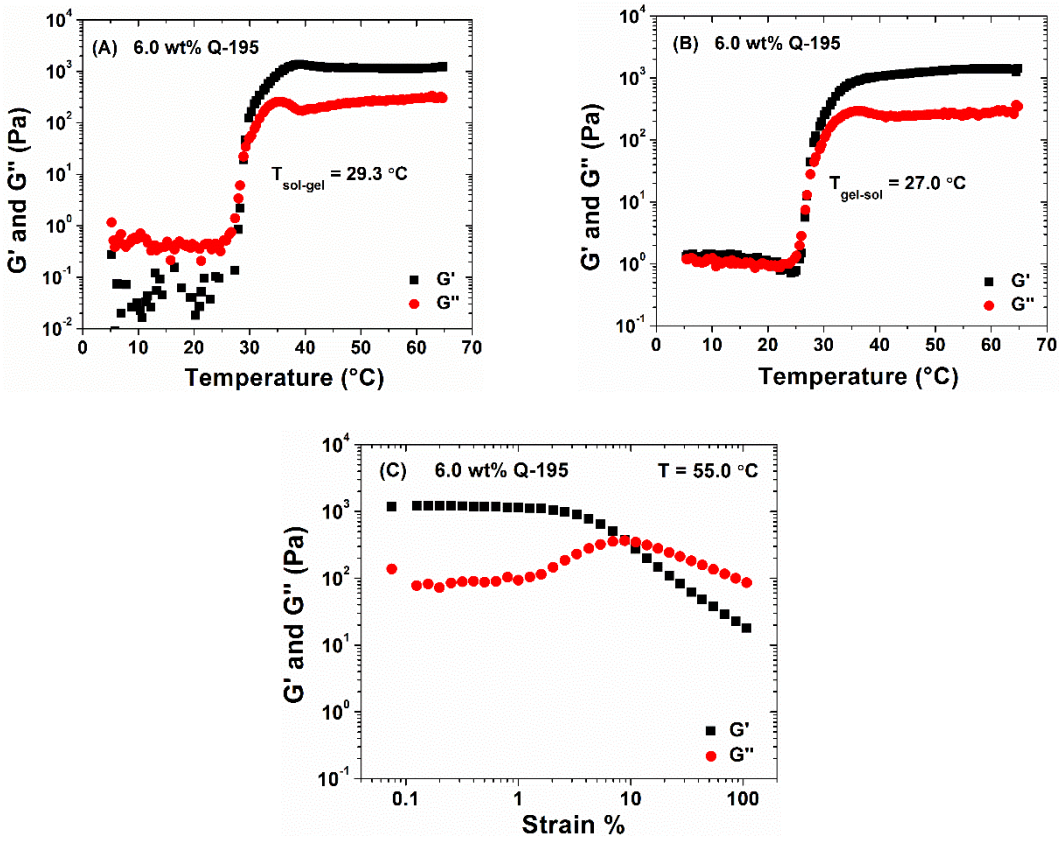

Figure 3.9. Plots of dynamic storage modulus G′ and loss modulus G″ of a 6.0 wt % aqueous dispersion of P(TMAEMA-I)-*b*-PDEGMMA brush-grafted silica nanoparticles (Q-195) obtained from oscillatory shear experiment performed (A) in a heating ramp at a frequency of 1 Hz, a strain amplitude of 0.2 %, and a heating rate of 3 °C/min, and (B) in a cooling ramp using a frequency of 1 Hz, a strain amplitude of 0.2 %, and a cooling rate of -3 °C/min (B). (C) Strain sweep at a frequency of 1 Hz and 55 °C.

Second, a sharp increase in both moduli begins around 26 °C, with G′ overtaking G″ at 29.3 °C, similar to the transition observed for Q-100, albeit shifted to a lower temperature. Third, a region of slower moduli growth with temperature can be seen; this region is much shorter and less pronounced than that exhibited by the Q-100 sample. Finally, a flat, plateau region can be seen where the dynamic moduli were essentially independent of temperature. This region was partiallyobserved for Q-100 (Figure 3.7A), where G″ in particular appeared to cease increasing with temperature, but G′ was not fully realized in the temperature range examined. In general, it appears that the higher molecular weight PDEGMMA block of Q-195 eased the transition from sol to gel and led to a stronger gel, as evidenced by higher values of G′, which reached 1126 Pa at 55 °C. However, the 6.0 wt% Q-195 dispersion still exhibited the same brittleness seen previously, as shown by the breakdown of the gel at even moderate strain amplitudes (Figure 3.9C).

The thermally induced sol-gel transition of the 6.0 wt% aqueous dispersion of Q-195 was also examined by frequency sweep measurements at various temperatures (Figure 3.10). At 10 °C, G″ was consistently greater than G′, indicative of a liquid state. At 27 °C, G′ and G″ essentially overlapped, suggesting that the system was in a transitory state, and at 55 °C, G′ was greater than G″ and nearly independent of frequency, characteristic of a gelled system.

3.3.5. Effect of Concentration on Gelation of Aqueous Dispersions of P(TMAEMA-I)-*b*-PDEGMMA Brush-Grafted Silica NPs

To study the dependencies that the gelation of aqueous dispersions of Q-100 and Q-195 had on the concentration of hairy nanoparticles in the dispersion, heating ramp experiments were performed at various concentrations of hairy NPs. As before, temperature ramps were performed using a heating rate of 3 °C min^{-1}, a frequency of 1 Hz, and a strain amplitude of 0.2 %. The results are summarized in Figure 3.11. In general, increasing the weight fraction of hairy NPs in aqueous

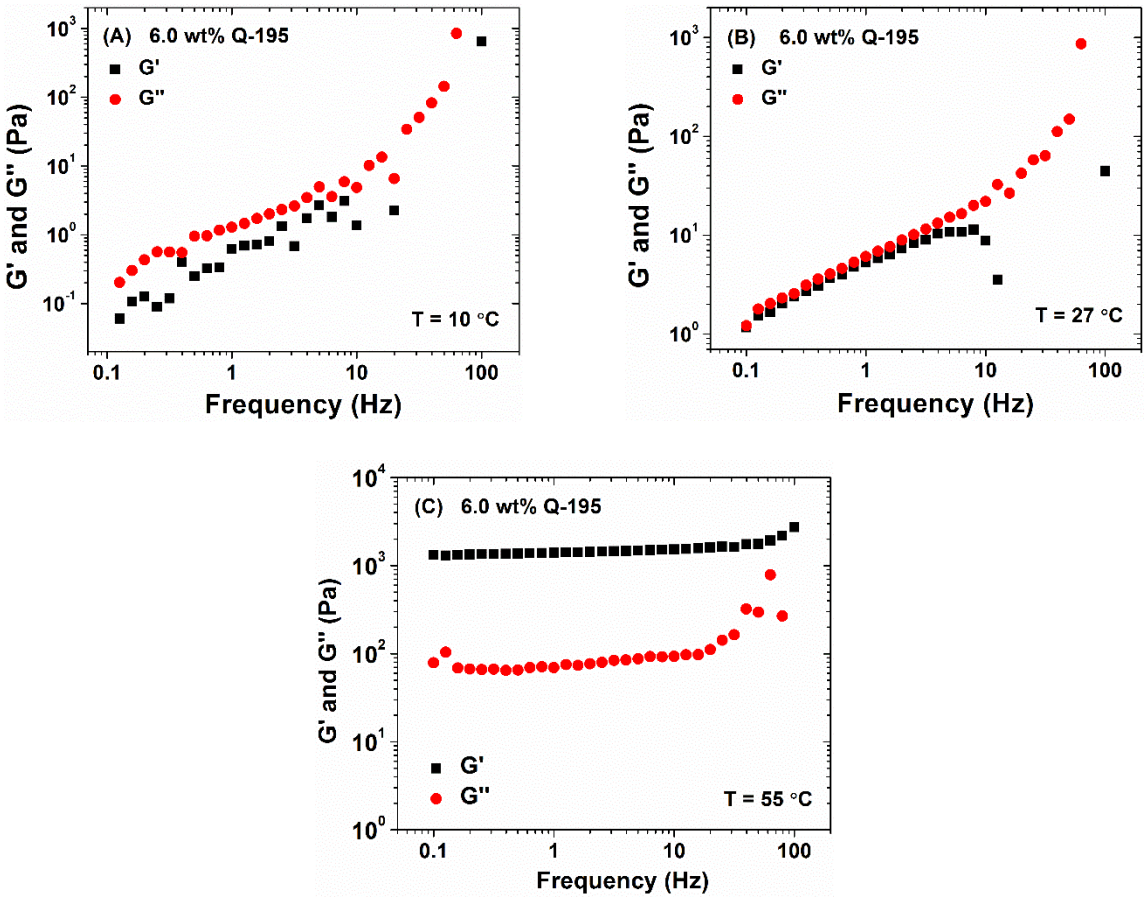

Figure 3.10. Plots of dynamic storage modulus G′ and loss modulus G″ versus frequency for a 6.0 wt% aqueous dispersion of P(TMAEMA-I)-*b*-PDEGMMA brush-grafted silica nanoparticles (Q-195) obtained from oscillatory shear experiments performed at 10 °C (A), 27 °C (B), and 55 °C (C)) at 0.2 % strain amplitude.

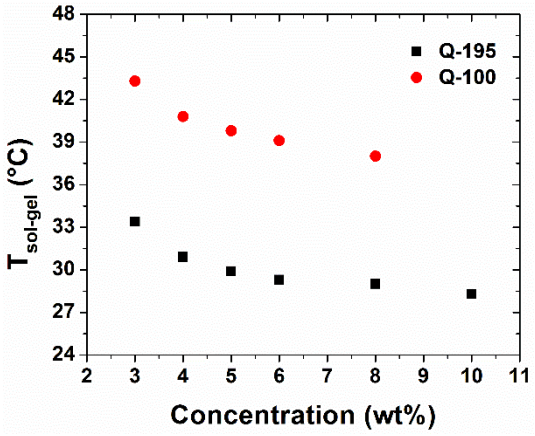

Figure 3.11. Plot of $T_{sol-gel}$ versus concentration for aqueous dispersions of Q-100 (red solid circle) and Q-195 (black solid square), obtained from rheological measurements.

dispersion decreased the sol-gel transition temperature. For Q-100 hairy NPs, $T_{sol\text{-}gel}$ decreased from 43.3 °C at 3 wt % to 38.0 °C at 8 wt %. A similar decrease can be seen for dispersions of Q-195, which exhibited a decrease in $T_{sol\text{-}gel}$ from 33.4 °C at 3 wt % to 29.0 at 8 wt %. This may be a result of increased bridging efficiency; as the number density of hairy NPs increases, the stretching required of the inner block to accommodate the association of the thermosensitive PDEGMMA blocks forming physical "crosslinks" is decreased.

3.3.6. Recovery Test of Physically Crosslinked Hydrogels of Hairy NPs

Given that the proposed mechanism for the gelation of P(TMAEMA-I)-*b*-PDEGMMA brush-grafted silica NPs is the association of collapsed PDEGMMA blocks into hydrophobic domains, forming a network of NPs and PDEGMMA domains bridged by long, polyelectrolyte chains, these hydrogels should reform following disruption of the gel network, e.g., by large amplitude shearing. As discussed above, these gels are somewhat brittle, likely owing to the covalent bonding of the P(TMAEMA-I) block to core NPs, among other factors, and can be broken at relatively low strain amplitudes. To confirm the recoverability of these gels, 6.0 wt% aqueous dispersions of Q-100 and Q-195 at 55 °C, i.e., in the gel state, were subjected to alternating periods of 0.2 % strain amplitude, during which the gels were maintained, and 100 % strain amplitude, during which the gels failed and G″ was larger than G′. Upon return to the lower strain amplitude, the gels were able to reform quickly due to the physical nature of the networks (Figure 3.12).

3.4. Conclusions

Thermosensitive PDMAEMA-*b*-PDEGMMA diblock copolymer brush-grafted 23.5 nm silica NPs were synthesized by sequential SI-ATRP of DMAEMA and DEGMMA from ATRP initiator-functionalized NPs.[38] The DMAEMA monomer units in the brushes were converted to permanently charged TMAEMA-I units through quaternization with methyl iodide. Appropriately

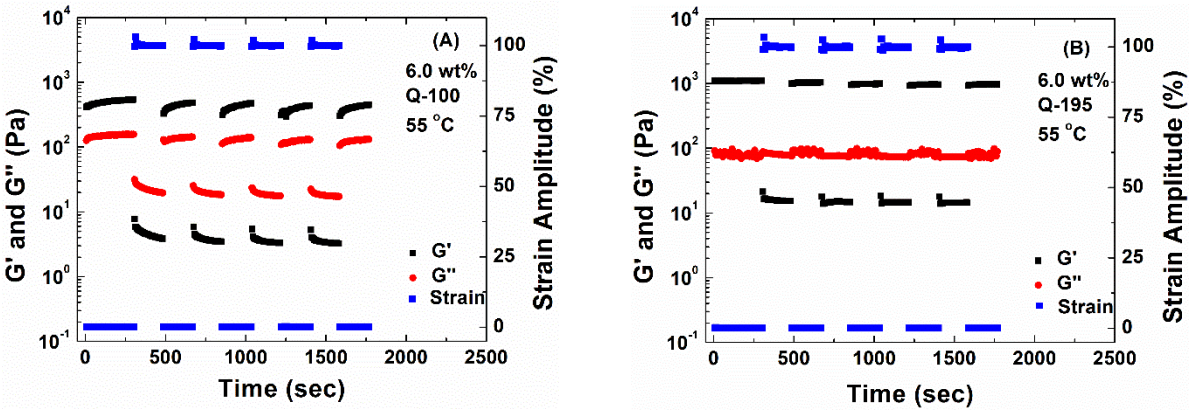

Figure 3.12. Plots of dynamic storage modulus G′ and loss modulus G″ (left axis) of a 6.0 wt % aqueous dispersion of Q-100 (A) and Q-195 (B) obtained from oscillatory shear experiments performed at 55 °C using a frequency of 1 Hz. The strain amplitude was oscillated between 0.2 % and 100 % amplitude (right axis) at given intervals.

concentrated aqueous dispersions of these hairy NPs exhibited a heating-induced transition from a free-flowing liquid to a self-supporting gel; this transition was found to be fully reversible with minimal hysteresis. Similar to 3-D micellar network hydrogels formed by thermosensitive ABA or ABC block copolymers, this gelation was the result of the self-association of collapsed PDEGMMA blocks into hydrophobic domains at temperatures above the LCST. These domains served as physical "crosslinks" and formed a three-dimensional network of hairy NPs in water.

These gels were found to be somewhat more brittle than typical ABA systems, likely due to fewer relaxation modes upon deformation to relieve local strain. It was also observed that by increasing the length of the outer, thermosensitive block, $T_{sol\text{-}gel}$ decreased significantly at the same concentration. The sol-gel transition temperature decreased with increasing NP concentration. We believe that the future utility of these brush-grafted NP-based hydrogels lies in their core NPs, which are as varied and have as much potential as NPs in general and may lead to hydrogels with properties appropriate for a wide array of applications.

References

1. Pyun, J.; Matyjaszewski, K., *Chem. Mater.* **2001,** *13* (10), 3436-3448.
2. Zhao, B.; Zhu, L., *Macromolecules* **2009,** *42* (24), 9369-9383.
3. Wu, T.; Zou, G.; Hu, J.; Liu, S., *Chem. Mater.* **2009,** *21* (16), 3788-3798.
4. von Werne, T.; Patten, T. E., *J. Am. Chem. Soc.* **1999,** *121* (32), 7409-7410.
5. Prucker, O.; Rühe, J., *Macromolecules* **1998,** *31* (3), 592-601.
6. Ohno, K.; Koh, K.; Tsujii, Y.; Fukuda, T., *Angew. Chem. Int. Ed.* **2003,** *42* (24), 2751-2754.
7. Mulvihill, M. J.; Rupert, B. L.; He, R.; Hochbaum, A.; Arnold, J.; Yang, P., *J. Am. Chem. Soc.* **2005,** *127* (46), 16040-16041.
8. Yavuz, M. S.; Cheng, Y.; Chen, J.; Cobley, C. M.; Zhang, Q.; Rycenga, M.; Xie, J.; Kim, C.; Song, K. H.; Schwartz, A. G.; Wang, L. V.; Xia, Y., *Nat. Mater.* **2009,** *8* (12), 935-939.
9. Blomberg, S.; Ostberg, S.; Harth, E.; Bosman, A. W.; Van Horn, B.; Hawker, C. J., *J. Polym. Sci. Part A: Polym. Chem.* **2002,** *40* (9), 1309-1320.
10. Ohno, K.; Morinaga, T.; Takeno, S.; Tsujii, Y.; Fukuda, T., *Macromolecules* **2006,** *39* (3), 1245-1249.
11. Moad, G.; Rizzardo, E.; Thang, S. H., *Aus. J. Chem.* **2005,** *58* (6), 379-410.
12. Bao, C.; Horton, J. M.; Bai, Z.; Li, D.; Lodge, T. P.; Zhao, B., *J. Polym. Sci. Part B: Polym. Phys.* **2014,** *52* (24), 1600-1619.
13. Chen, L.; Klok, H.-A., *Soft Matter* **2013,** *9* (45), 10678-10688.
14. Farmer, S. C.; Patten, T. E., *Chem. Mater.* **2001,** *13* (11), 3920-3926.
15. Vestal, C. R.; Zhang, Z. J., *J. Am. Chem. Soc.* **2002,** *124* (48), 14312-14313.
16. Farrukh, A.; Akram, A.; Ghaffar, A.; Hanif, S.; Hamid, A.; Duran, H.; Yameen, B., *ACS Appl. Mater. Inter.* **2013,** *5* (9), 3784-3793.

17. Liu, G.; Cai, M.; Wang, X.; Zhou, F.; Liu, W., *ACS Appl. Mater. Inter.* **2014,** *6* (14), 11625-11632.

18. Zhu, M.-Q.; Wang, L.-Q.; Exarhos, G. J.; Li, A. D. Q., *J. Am. Chem. Soc.* **2004,** *126* (9), 2656-2657.

19. Horton, J. M.; Bai, Z.; Jiang, X.; Li, D.; Lodge, T. P.; Zhao, B., *Langmuir* **2011,** *27* (5), 2019-2027.

20. Horton, J. M.; Bao, C.; Bai, Z.; Lodge, T. P.; Zhao, B., *Langmuir* **2011,** *27* (21), 13324-13334.

21. Bai, Z.; He, Y.; Lodge, T. P., *Langmuir* **2008,** *24* (10), 5284-5290.

22. He, Y.; Lodge, T. P., *J. Am. Chem. Soc.* **2006,** *128* (39), 12666-12667.

23. Li, D.; Zhao, B., *Langmuir* **2007,** *23* (4), 2208-2217.

24. Hamley, I., Front Matter. In *Block Copolymers in Solution: Fundamentals and Applications*, John Wiley & Sons, Ltd: 2005; pp i-xi.

25. Jeong, B.; Kim, S. W.; Bae, Y. H., *Adv. Drug Delivery Rev.* **2002,** *54* (1), 37-51.

26. Moon, H. J.; Ko, D. Y.; Park, M. H.; Joo, M. K.; Jeong, B., *Chem. Soc. Rev.* **2012,** *41* (14), 4860-4883.

27. Yu, L.; Ding, J., *Chem. Soc. Rev.* **2008,** *37* (8), 1473-1481.

28. Hamley, I. W.; Pople, J. A.; Fairclough, J. P. A.; Ryan, A. J.; Booth, C.; Yang, Y. W., *Macromolecules* **1998,** *31* (12), 3906-3911.

29. Pozzo, D. C.; Walker, L. M., *Macromolecules* **2007,** *40* (16), 5801-5811.

30. Vogt, A. P.; Sumerlin, B. S., *Soft Matter* **2009,** *5* (12), 2347-2351.

31. Li, C.; Buurma, N. J.; Haq, I.; Turner, C.; Armes, S. P.; Castelletto, V.; Hamley, I. W.; Lewis, A. L., *Langmuir* **2005,** *21* (24), 11026-11033.

32. Zhou, C.; Hillmyer, M. A.; Lodge, T. P., *J. Am. Chem. Soc.* **2012,** *134* (25), 10365-10368.

33. Argyo, C.; Weiss, V.; Bräuchle, C.; Bein, T., *Chem. Mater.* **2014,** *26* (1), 435-451.

34. Wright, R. A. E.; Hu, B.; Henn, D. M.; Zhao, B., *Soft Matter* **2015,** *11* (34), 6808-6820.

35. Husseman, M.; Malmström, E. E.; McNamara, M.; Mate, M.; Mecerreyes, D.; Benoit, D. G.; Hedrick, J. L.; Mansky, P.; Huang, E.; Russell, T. P.; Hawker, C. J., *Macromolecules* **1999,** *32* (5), 1424-1431.

36. Li, D.; Sheng, X.; Zhao, B., *J. Am. Chem. Soc.* **2005,** *127* (17), 6248-6256.

37. Jiang, X.; Zhao, B., *J. Polym. Sci. Part A: Polym. Chem.* **2007,** *45* (16), 3707-3721.

38. The work presented in this chapter has been accepted for publication as an article. Wright, R. A. E.; Henn, D. M.; Zhao, B. Thermally Reversible Physically Crosslinked Hybrid Network Hydrogels Formed by Thermoresponsive Hairy Nanoparticles. *J. Phys. Chem. B* **2016.**

Appendix B

for

Chapter 3. Physically Crosslinked Hydrogels Formed Solely by Thermosensitive Hairy Nanoparticles

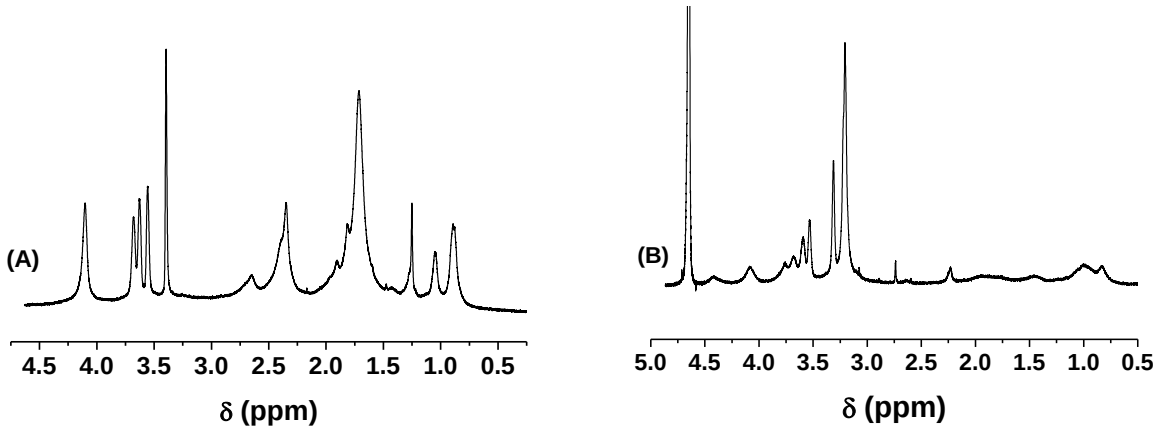

Figure B1. ^{1}H NMR Spectra of free PDMAEMA-*b*-PDEGMMA corresponding to DB-100 (left) and free DB-195 (right). The DP of PDEGMMA was found by comparing the integrations of ethylene glycol protons (3.50 - 3.75 ppm, -$OCH_2CH_2OCH_2CH_2OCH_3$) to the pendant methyl groups of PDMAEMA (2.20 - 2.35 ppm, -$N(CH_3)_2$).

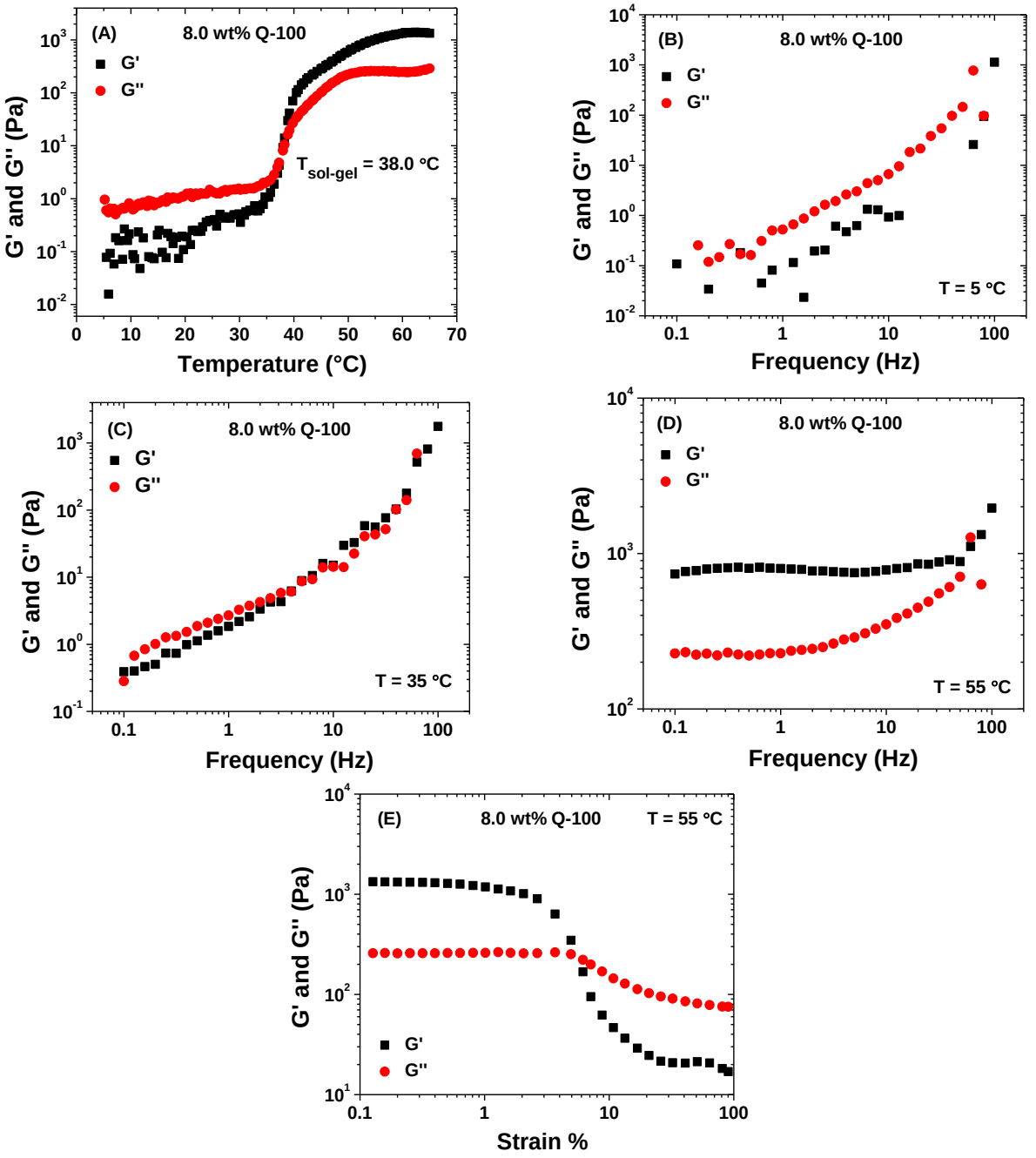

Figure B2. Plots of dynamic storage modulus G′ and loss modulus G″ of a 8.0 wt % aqueous dispersion of P(TMAEMA-I)-*b*-PDEGMMA brush-grafted silica nanoparticles (Q-100) obtained from oscillatory shear experiments performed across a temperature ramp at a frequency of 1 Hz, a strain amplitude of 0.2 %, and a heating rate of 3 °C/min (A). Frequency sweep experiments were performed at 5, 35, and 55 °C (B-D) using a 0.2 % strain amplitude. (E) Strain sweeps performed at 55 °C using a fixed frequency of 1 Hz.

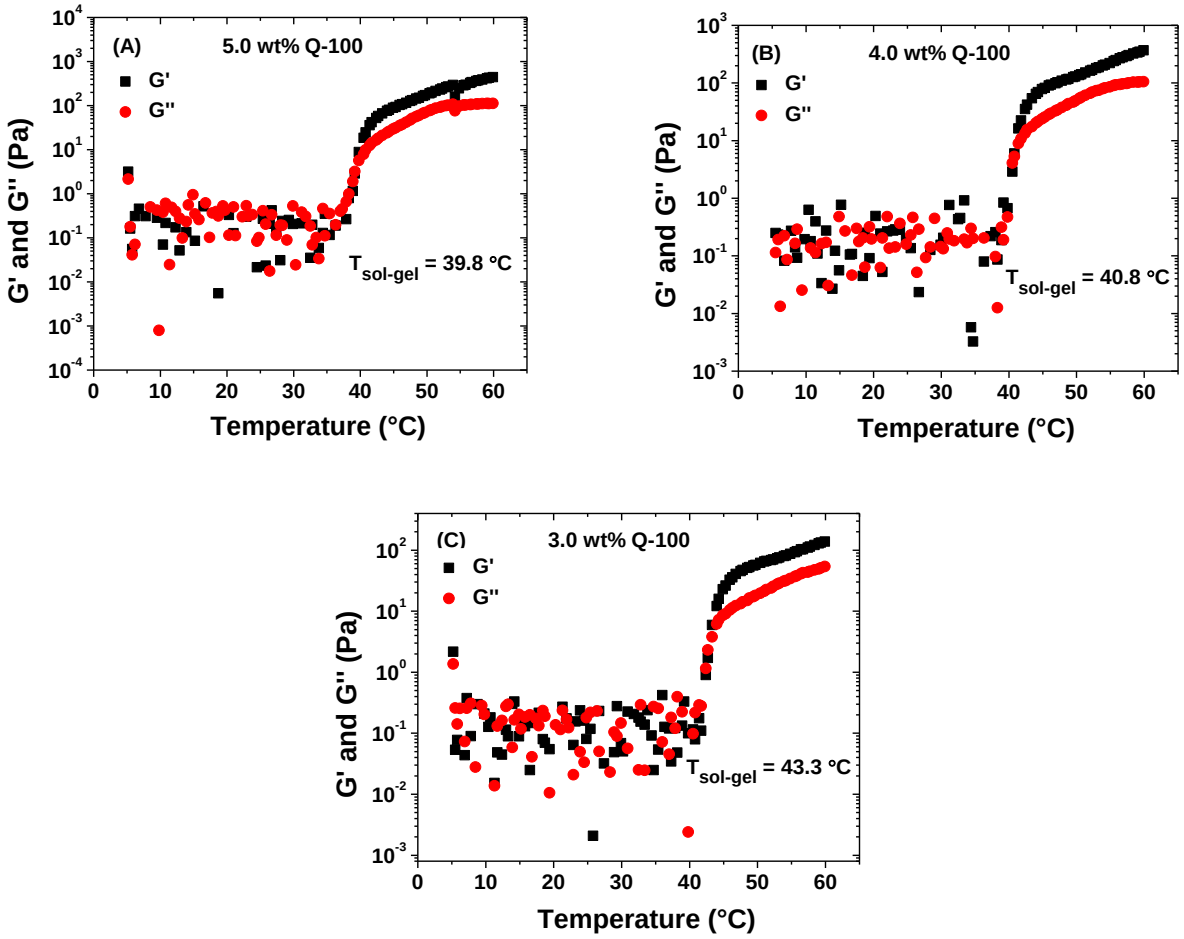

Figure B3. Plots of dynamic storage modulus G′ and loss modulus G″ of aqueous dispersions of P(TMAEMA-I)-*b*-PDEGMMA brush-grafted silica nanoparticles (Q-100) with a concentration of 5.0 wt% (A), 4.0 wt% (B), and 3.0 wt% (C) obtained from oscillatory shear experiments performed across a temperature ramp at a frequency of 1 Hz, a strain amplitude of 0.2 %, and a heating rate of 3 °C/min.

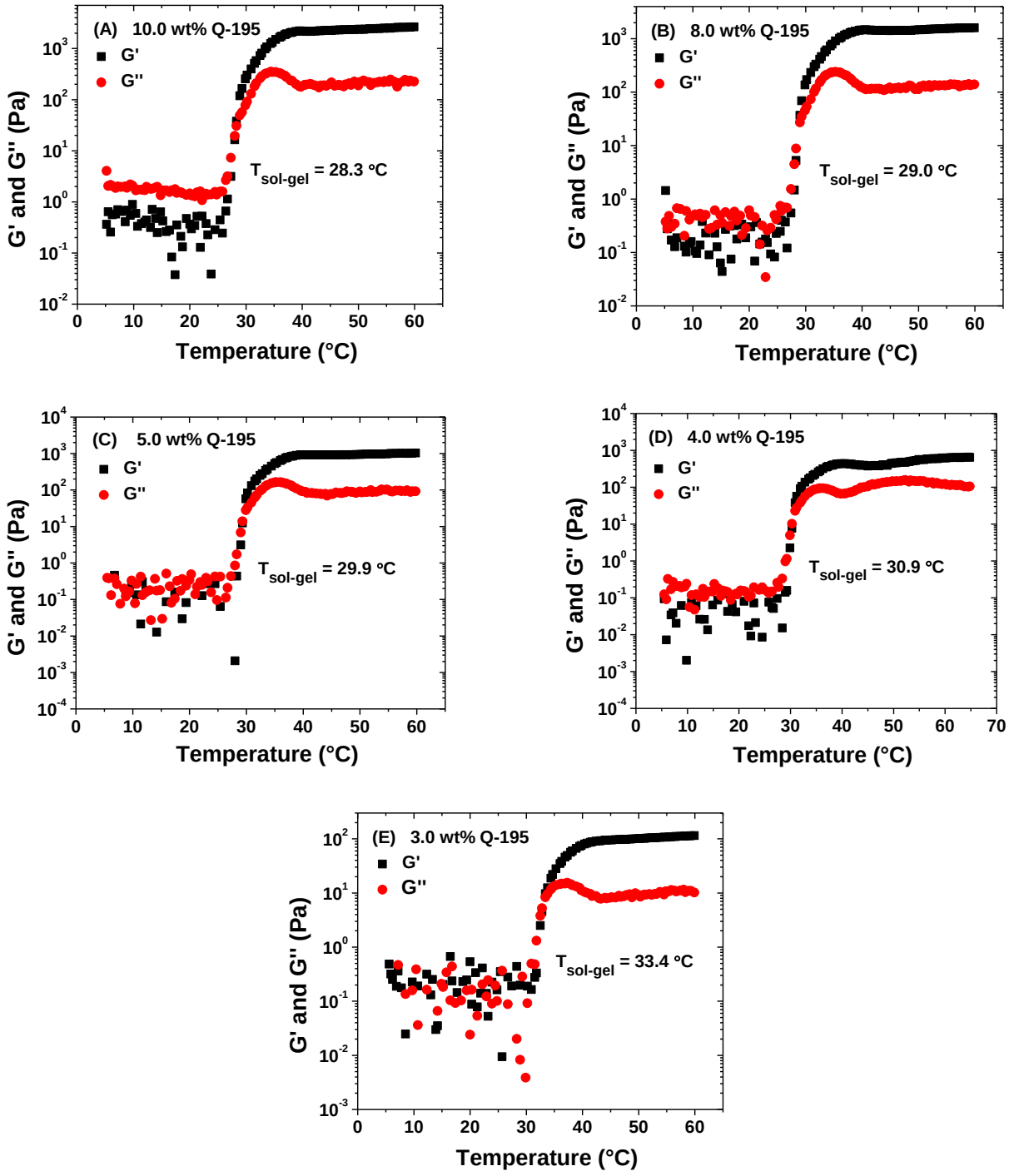

Figure B4. Plots of dynamic storage modulus G′ and loss modulus G″ of an aqueous dispersion of P(TMAEMA-I)-*b*-PDEGMMA brush-grafted silica nanoparticles (Q-195) with a concentration of 10.0 (A), 8.0 (B), 5.0 (C), 4.0 (D), and 3.0 wt % E) obtained from oscillatory shear experiments performed across a temperature ramp at a frequency of 1 Hz, a strain amplitude of 0.2 %, and a heating rate of 3 °C/min.

Chapter 4. Oil-Soluble Polymer Brush-Grafted Silica Nanoparticles as Effective Lubricant Additives

Abstract

Increasingly higher industrial standards and environmental concerns are demanding high performance lubricants. This chapter presents the synthesis of oil-soluble polymer brush-grafted inorganic nanoparticles (hairy NPs) and demonstrates their use as highly effective lubricant additives for friction and wear reduction. A series of oil-miscible poly(lauryl methacrylate) brush-grafted silica NPs were synthesized by surface-initiated atom transfer radical polymerization. These hairy NPs showed exceptional stability in poly(alphaolefin) (PAO) base oil; no change in transparency was observed after being kept at -20, 22, and 100 °C for ≥ 55 days. High contact stress ball-on-flat reciprocating sliding tribological tests at 100 °C showed that the addition of 1 wt% of hairy NPs into PAO resulted in significant reductions in coefficient of friction (up to ~ 30%) and wear volume (up to ~ 90%). The excellent lubricating properties of hairy NPs were further elucidated by the characterization of the tribofilm formed on the flat using the focused ion beam (FIB) technique and transmission electron microscopy. These hairy NPs represent a new type of lubricating oil additives with high efficiency in friction and wear reduction.

4.1. Introduction

Lubricants play an indispensable role in enhancing the durability and efficiency of automotive engines and industrial machinery. They are believed to form stable interfacial films between two rubbing solid materials, decreasing the solid-to-solid contact and improving the load-carrying capabilities. Fully formulated commercial engine lubricants are composed of a base oil (e.g., poly(alphaolefin) (PAO)) and a variety of additives for various functions including anti-wear (AW) agent, friction reducer, antioxidant, detergent, dispersant, viscosity index improver, etc.[1,2] The most commonly used AW and friction reduction agent is zinc dialkyldithiophosphate (ZDDP).[3,4] However, it has been reported that ZDDP may cause damage to the catalysts in the catalytic converters, and the emission of sulfur from ZDDP also raises an environmental concern.[2] While tremendous progress has been made in the lubricant industry, as evidenced by the increasingly longer intervals for engine oil changes for vehicles, the sheer ubiquity of these systems means that even a small increase in lubricant performance could result in a large decrease in energy costs. These potential gains coupled with increased awareness of the need for environmental protection drive the pursuit of more efficient lubrication and environmentally benign additives.

Nanoparticles (NPs) have been suggested to have great potential as effective lubricant additives for reducing friction and wear.[5-19] Various NPs with different chemical compositions and geometries have been evaluated as lubricant additives, including metals (e.g., Cu, Fe, Ni),[5-9] metal oxides (e.g., Fe_2O_3, TiO_2, SiO_2),[10-15] and metal sulfides (MoS_2, WS_2, ZnS).[16-19] While the tribological effects of layered nanomaterials such as MoS_2 and WS_2 mainly derive from progressive delamination under shearing conditions, releasing nanolayers into the interfacial zone,[19] spherical NPs are thought to behave like mini rolling elements at local asperities and to

create, together with the base oil, mechanically strong, uniform load-bearing films between two rubbing solid surfaces, which reduce surface-to-surface contact and decrease interfacial friction. [5-18, 20-22] Moreover, NPs could be physically pressed by the mechanical load onto the contact area or wear track to form a deposition layer (a tribofilm), protecting the rubbing surfaces.[5-25] To realize the tribological benefits of NPs, a critical requirement is that the NPs must be well dispersed in the base oils, forming homogeneous dispersions that exhibit long-term stabilities. While various organic compounds and surface modification methods have been employed to disperse NPs in base oils, achieving the full potential of NPs as lubricant additives and the long-term stability of NPs in lubricating oils remains a great challenge. An example is shown in Figure 4.1., in which the dark additive of a lubricating oil has precipitated onto the vial wall after being stored at ambient conditions for an extended period of time.

Polymer brush-grafted NPs, also called hairy NPs, consist of an inorganic, metallic, or polymeric core and a layer of polymer chains covalently tethered by one end onto the surface of the core NP with a high grafting density.[26-32] Among various interesting properties and behavior exhibited by hairy NPs, their exceptional dispersibility and stability in good solvents are worthy of a special note. The favorable enthalpic interactions between polymer brushes and solvents, which can be clearly "seen" from ^{1}H NMR spectra of hairy NPs in good solvents, and the entropic steric interactions between polymer brushes from different hairy NPs endow hairy NPs with superior solubility and stability in good solvents. Furthermore, polymer brushes have been shown to exhibit excellent lubricating properties.[33] Nevertheless, the tremendous potential of hairy NPs as additives for lubricating oils have not yet been explored. Here we present the synthesis of oil-soluble NPs by surface-initiated atom transfer radical polymerization (SI-ATRP) (Scheme 4.1) and

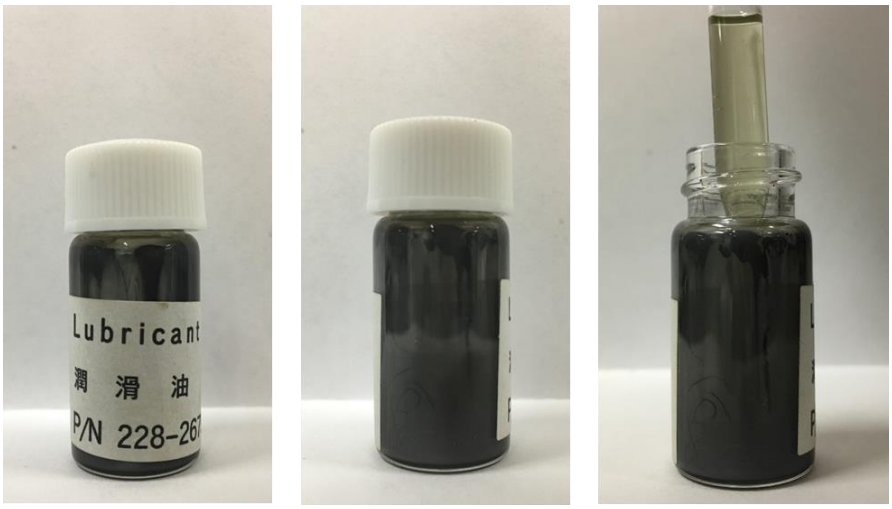

Figure 4.1. Example of an additized lubricant in which the additive is no longer stable in the lubricating oil, as evidenced by the dark vial wall and the clarity of the oil. This lack of stability has likely compromised lubrication performance.

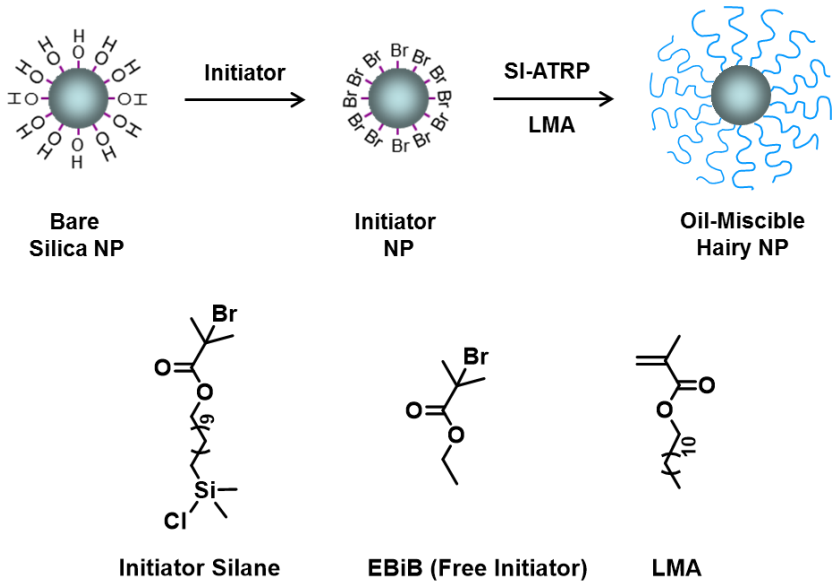

Scheme 4.1. Schematic Illustration for Synthesis of Oil-Miscible Poly(lauryl methacrylate) (PLMA) Brush-Grafted Silica Nanoparticles (NPs) by Surface-Initiated Atom Transfer Radical Polymerization (SI-ATRP).

their use as lubricant additives. High-contact tribological analysis shows that these NPs are highly effective lubricant additives for friction and wear reduction and at the same time exhibit long-term stability in PAO.

4.2. Experimental Section

4.2.1. Materials

MIBK-ST, a dispersion of silica nanoparticles (NPs) with a size of 10–15 nm (according to the manufacturer) in methyl isobutyl ketone (MIBK) (30-31 wt % SiO_2), was obtained from Nissan Chemical. Chlorodimethylsilane (98%) was purchased from Alfa Aesar and stored in a refrigerator. Karstedt's catalyst (Platinum-divinyltetramethyldisiloxane complex in xylene, 2.1~2.4% Pt concentration in xylene) was purchased from Gelest, Inc. CuBr (98%, Aldrich) was stirred in glacial acetic acid overnight, filtered, and washed with absolute ethanol and diethyl ether. After being dried under vacuum, the purified CuBr powder was stored in a desiccator. $CuBr_2$ (anhydrous, 99%) was purchased from Acros and used as received. N, N, N', N', N''-Pentamethyldiethylenetriamine (PMDETA, 99%, Aldrich) and ethyl 2-bromoisobutyrate (EBiB, 98%, Aldrich) were dried with calcium hydride, distilled under reduced pressure, and stored in a desiccator. Lauryl methacrylate (LMA, 97%, Acros) was dissolved in tetrahydrofuran (THF) and passed through a column of silica gel (bottom)/activated basic aluminum oxide (top) (2/1, v/v) to remove the inhibitor; after the removal of THF under high vacuum, the LMA monomer was stored in a refrigerator prior to use. 10-Undecenyl 2-bromoisobutyrate was synthesized from 10-undecenyl-1-ol and 2-bromoisobutryl bromide.[34] Chlorodimethylsilane (98%) was purchased from Alfa Aesar and stored in a refrigerator. The polyalphaolefin (PAO) used in the present work was Spectrasyn^{TM} 4, obtained from Exxon-Mobile. The kinematic viscosities of this PAO at 40 and

100 °C are 19.0 and 4.1 cSt, respectively, and its pour point was – 87 °C. ZDDP was purchased from Lubrizol, containing 5-10 % mineral oil (10 wt% phosphorus). All other chemical reagents were purchased from either Aldrich or Fisher and used without further purification.

4.2.2. General Characterization

Size exclusion chromatography (SEC) of the free polymers formed in the synthesis of oil soluble brush-grafted NPs (Hairy NPs) was carried out at ambient temperature using a PL-GPC 20 (an integrated SEC system from Polymer Laboratories, Inc.) with a refractive index detector, one PLgel 5 μm guard column (50 × 7.5 mm), and two PLgel 5 μm mixed-C columns (each 300 × 7.5 mm, linear range of molecular weight from 200 to 2 000 000 Da). THF was used as the carrier solvent, and the flow rate was 1.0 mL/min. The SEC system was calibrated using narrow-disperse polystyrene standards. The data were processed using Cirrus GPC/SEC software (Polymer Laboratories, Inc.). ^{1}H NMR spectra were recorded on a either a Varian VNMRS 500 MHz or a Mercury 300 MHz spectrometer, and the residual solvent proton signal was used as the internal standard. DLS analysis of hairy NPs was performed using a Malvern Zetasizer (λ = 633 nm) at a scattering angle of 173°. The NP concentrations in THF were 0.2 mg/mL. The samples were filtered using Millipore hydrophilic PTFE filters (0.4 μm pore size). Thermogravimetric analysis (TGA) was carried out in air at a heating rate of 20 °C/min from room temperature to 800 ºC using a TA Discovery TGA-MS or TGA Q-50. Transmission electron microscopy (TEM) was performed using a Zeiss Libra 200 HT FE MC microscope with an accelerating voltage of 200 kV, and bright field images were taken with a bottom-mounted Gatan UltraScan US1000XP CCD camera. TEM samples of hairy NPs were prepared by drop-casting dispersions in chloroform with a concentration of ~ 4 mg/mL onto a carbon-coated, copper TEM grid using a glass pipet and were allowed to dry at ambient conditions. The wear track formed on the cast iron flat that was used in

the tribological test of the PAO containing 1 wt% HNP-SiO_2-4.1k was examined by TEM for studying the tribofilm. The sample for cross-sectional TEM imaging was prepared using a Zeiss Auriga 40 dual beam scanning electron microscope/focused ion beam (SEM/FIB) system. The sample surface was first protected from the electron beam by applying a thin layer (ca. 0.5um) of high resistance, conductive carbon "ink" using a microscopy pen (Ted Pella, Redding, CA). The surface was further protected by electron beam deposition of a thin platinum layer prior to use of the FIB.

4.2.3. Synthesis of ATRP Initiator-Functionalized Silica Nanoparticles

Two batches of ATRP initiator-functionalized silica nanoparticles were made and fractionated using ultracentrifugation: INP-SiO_2-I and INP-SiO_2-II. Below is the detailed procedure for the synthesis of INP-SiO_2-II; INP-SiO_2-I was prepared using a similar process.

10-Undecenyl 2-bromoisobutyrate (6.020 g, 19.14 mmol) was added into a 50 mL two-necked flask and dried under high vacuum, followed by the addition of chlorodimethylsilane (3.041 g, 32.14 mmol) under an N_2 atmosphere and the injection of a solution of Karstedt's catalyst in xylene (75 µL). After the reaction was complete according to ^{1}H NMR spectroscopy, the remaining chlorodimethylsilane was removed under vacuum, and the obtained 11-(chlorodimethylsilyl)undecyl 2-bromoisobutyrate was dissolved in toluene (~ 5 mL).

MIBK-ST (26.670 g, corresponding to 8.001 g bare silica NPs) was added to a 250 mL three-necked flask and diluted with ~25 mL anhydrous toluene. A portion of the mixture (~15 mL) was then distilled off under vacuum in an effort to azeotropically remove any trace amount of water. Dry toluene (~20 mL) was then injected into the flask, and the azeotropic distillation was carried out again. This process was repeated for a total of three times. The resultant dispersion of silica NPs totaled ~ 60 mL. The solution of the freshly synthesized 11-(chlorodimethylsilyl)undecyl 2-

bromoisobutyrate in toluene was added to the dispersion, and the mixture was heated to 90 °C and stirred under a N_2 atmosphere overnight. The initiator-functionalized silica NPs (INP-SiO_2-II) were then diluted in THF and isolated via centrifugation (Beckman Optima L-90K Ultracentrifuge with type 60 Ti rotor, 35,000 rpm, 30 min). The initiator NPs were then dispersed in THF and centrifuged again. This dispersion-centrifugation cycle was repeated for a total of three times. Fractionation of the initiator particles was carried out to achieve a more uniform size distribution. The obtained initiator NPs were dispersed in DMF and the dispersion was centrifuged at 20,000 rpm. The NPs deposited at the bottom of the tube were removed, and the supernatant dispersion was then centrifuged at 30,000 rpm. The nanoparticles collected in this fraction, designated INP-SiO_2-II, were dried to yield a slightly brown powder.

4.2.4. Synthesis of Poly(lauryl methacrylate) (PLMA) Brush-Grafted Silica Nanoparticles

Described below is the synthesis of HNP-SiO_2-38.0k from INP-SiO_2-I *via* surface-initiated ATRP; other PLMA brush-grafted silica NP samples were synthesized using a similar procedure from INP-SiO_2-I except HNP-SiO_2-9.0k, which was made from INP-SiO_2-II. The initiator NPs (INP-SiO_2-I, 1.002 g) were added into a 100 mL three-necked flask, followed by the addition of anisole (35.138 g). The mixture was ultrasonicated until a homogeneous dispersion was obtained. LMA (14.724 g, 0.0579 mol), copper(I) bromide (43.0 mg, 3.00×10^{-4} mol), copper(II) bromide (20.4 mg, 9.13×10^{-5} mol), and ethyl 2-bromoisobutyrate (7.6 mg, 3.9×10^{-5} mol) were added to the dispersion. PMDETA (81.3 mg, 4.69×10^{-4} mol) was injected, and the polymerization mixture was immediately deoxygenated by three freeze–pump–thaw cycles. The flask was then placed in a thermostated oil bath with a pre-set temperature of 50 °C. The polymerization was monitored by ^{1}H NMR spectroscopy analysis. After the reaction proceeded for 445 min, the polymerization was stopped by removing the flask from the oil bath, exposing the mixture to air, and diluting it with

THF. The final monomer conversion was found to be 34.0% from ^{1}H NMR spectroscopy analysis, corresponding to a DP of 117, and the final PLMA hairy silica nanoparticles were designated as HNP-SiO_2-38.0k. The DP was calculated using the monomer conversion, as determined by ^{1}H NMR spectroscopy, and the molar ratio of monomer to the sum of free and surface initiators.[34]

The PLMA brush-grafted silica NPs, HNP-SiO_2-38.0k, were purified by five cycles of dispersion-ultracentrifugation as for the initiator NPs, dried under vacuum, and characterized by TGA and TEM. The free polymer formed from free initiator EBiB was purified by passing through a column of silica gel (bottom)/activated basic aluminum oxide (top) (2:1, v/v) to remove the copper catalyst and subsequent precipitation in methanol three times. SEC analysis showed that the $M_{n,SEC}$ value, relative to polystyrene standards, was 38.0 kDa with a PDI of 1.09.

4.2.5. Preparation of Dispersions of Hairy Silica NPs in PAO and Stability Studies.

PLMA brush-grafted silica NPs were dried under high vacuum and dispersed directly in PAO by ultrasonication to yield a 1 wt % dispersion that was both homogeneous and transparent. To test the stability of dispersions of hairy silica NPs in PAO at different temperatures, HNP-SiO_2-4.1k was selected and dispersed in PAO at a concentration of 1 wt% using the above procedure. Each dispersion was then divided into portions and transferred into three vials, which were kept still at – 20 °C (in a freezer), room temperature (22 °C), and 100 °C (in an oil bath). Digital photographs were taken at given time intervals to record the appearance of the hairy NP dispersions.

4.2.6. Tribological Testing

To investigate the tribological properties of oil-soluble PLMA brush-grafted silica NPs as additives for lubricating base oil PAO, high contact stress ball-on-flat reciprocating sliding tribological tests were performed using a Phoenix Tribology Plint TE 77. PAO Spectrasyn^{TM} 4

base oil was compared with PAO lubricants containing desired concentrations of hairy NP additives, typically 1 wt %. These boundary lubrication tests were conducted at 100 °C for a total sliding distance of 1000 m under a point contact load of 100 N. The AISI 52100 steel balls reciprocated against stationary CL35 cast iron flats submerged in a lubricant at a stroke of 10 mm and an oscillation frequency of 10 Hz. The friction force was captured in situ by a piezoelectric load cell and the friction coefficient was calculated by normalizing by the load. Wear volumes were measured using a Wyko NT9100 optical profilometer after each tribological test.

4.3. Results and Discussion

4.3.1. Synthesis and Characterization of ATRP Initiator-Functionalized Silica Nanoparticles

Bare silica NPs from Nissan Chemical (MIBK-ST) were surface-functionalized with a chlorodimethylsilane-terminated ATRP initiator, 11-(chlorodimethylsilyl)undecyl 2-bromoisobutyrate, for use in the surface-initiated ATRP of LMA to yield oil-soluble polymer brush-grafted silica NPs. As anhydrous conditions are required for the immobilization of the chlorosilane-terminated initiator, the original dispersion of silica NPs in methyl isobutyl ketone was azeotropically distilled with toluene under vacuum three times to remove any trace amount of water in the NP dispersion. The solution of freshly-prepared 11-(chlorodimethylsilyl)undecyl 2-bromoisobutyrate in toluene was added into the silica NP dispersion in toluene. The mass ratio of the chlorodimethylsilane-terminated ATRP initiator to silica NPs was 0.97 : 1.00. After the immobilization reaction was carried out at 90 °C under an N_2 atmosphere for 64 h, the initiator-functionalized NPs were purified by multiple rounds of ultracentrifugation/re-dispersion in THF. The initiator-functionalized NPs were then fractionated using a speed of 20,000 rpm to remove larger nanoparticles and collected at 30,000 rpm to exclude exceedingly small nanoparticles. After drying with a stream of airflow, the initiator NPs were obtained as a slightly brown powder.

Analysis by TEM yielded an average size of 23.8 (± 3.9) nm for INP-SiO_2-I and 23.5 nm (± 5.7 nm) for INP-SiO_2-II.

4.3.2. Synthesis of PLMA Brush-Grafted Silica NPs

Poly(lauryl methacrylate) (PLMA) brushes were synthesized from initiator-functionalized silica NPs (Scheme 4.1) by surface-initiated atom transfer radical polymerization (SI-ATRP). PLMA was chosen for this work as it is known to be soluble in many oils, including PAO, due to the favorable enthalpic interactions between oil and its large, twelve-carbon pendant groups.[1,35] This strong affinity with PAO is necessary to stabilize the otherwise indispersible silica NPs as a long term stability is crucial for the effectiveness of any NP additive. To better control the SI-ATRP and facilitate the characterization of the grafted polymer chains, we added a free initiator, ethyl 2-bromoisobutyrate (EBiB), into the polymerization mixtures. Many researchers have reported that the molecular weights and polydispersities of the grafted polymers on NPs are essentially identical to those of the free polymers formed from the free initiators.[28,34,36] Four PLMA hairy silica NP samples with differing molecular weights were made using INP-SiO_2-I and another one using INP-SiO_2-II. The corresponding free polymers were analyzed by size exclusion chromatography (SEC) relative to polystyrene standards, and unimodal distributions were observed with number average molecular weights ($M_{n,SEC}$) of 38.0, 21.7, 11.8, 4.1, and 9.0 kDa, respectively, and polydispersity indices (PDIs) of < 1.15 (Figure 4.2). The hairy NPs were designated as HNP-SiO_2-38.0k, HNP-SiO_2-21.7k, HNP-SiO_2-11.8k, HNP-SiO_2-4.1k, and HNP-SiO_2-9.0k, respectively, by appending the SEC number average molecular weight to the end of each sample name.

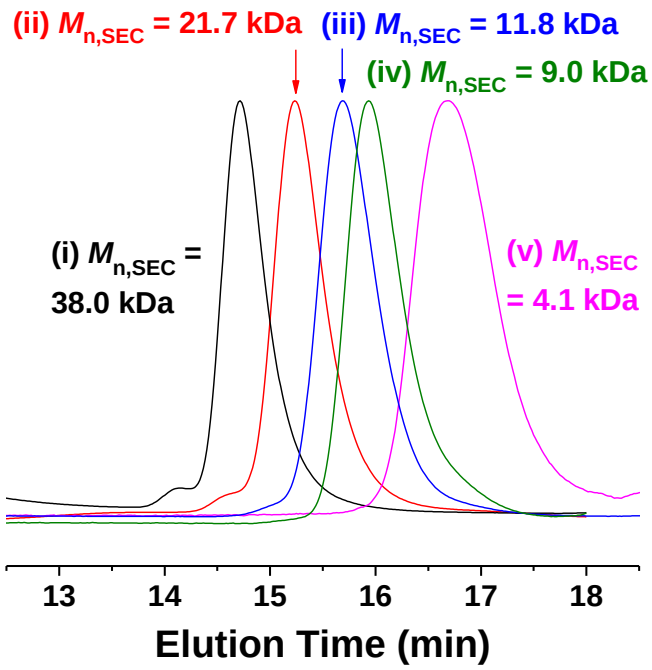

Figure 4.2. Size exclusion chromatography (SEC) traces of free PLMA polymers formed in the synthesis of (i) HNP-SiO_2-38.0k ($M_{n\ SEC}$ = 38.0 kDa, PDI = 1.09), (ii) HNP-SiO_2-21.7k ($M_{n\ SEC}$ = 21.7 kDa, PDI = 1.10), (iii) HNP-SiO_2-11.8k ($M_{n\ SEC}$ = 11.8 kDa, PDI = 1.13), (iv) HNP-SiO_2-9.0k ($M_{n\ SEC}$ = 9.0 kDa, PDI = 1.12 and (v) HNP-SiO_2-4.1k ($M_{n\ SEC}$ = 4.1 kDa, PDI = 1.14).

Thermogravimetric analysis (TGA) showed that the weight retention at 800 °C of hairy NPs decreased with increasing brush molecular weight (Figure 4.3). By using degrees of polymerization (DPs), TGA data, and NP size, the grafting densities of four samples synthesized from INP-SiO2-I were calculated and found to be in the range of 0.67 – 0.72 chains/nm^2 (Table 4.1). HNP-SiO_2-9.0k, made from INP-SiO_2-II, was found to have a similar grafting density of 0.73 chains nm^{-2} (Table 4.1). By assuming that the tethered polymer chains formed a uniform brush layer in the dry state on the surface of a silica core NP, we obtained the volume of the PLMA layer using the TGA data shown in Figure 4.3 and the density of PLMA (0.929 g cm^{-3}) and, through simple geometric relationships, calculated the dry thickness of the polymer brushes. The dry brush thickness was found to be 14.1 nm for HNP-SiO_2-38.0k, 10.2 nm for HNP-SiO_2-21.7k, 7.9 nm for HNP-SiO_2-11.8k, 4.2 nm for HNP-SiO_2-9.0k, and 1.6 nm for HNP-SiO_2-4.1k. Transmission electron microscopy (TEM) analysis of hairy silica NPs cast from their dispersions in $CHCl_3$, a good solvent for PLMA, revealed that the hairy NPs self-assembled into close-packed patterns and the interparticle distance decreased with decreasing brush molecular weight (Figure 4.4)). Dynamic light scattering experiments were performed using dilute (0.2 mg/mL) dispersions of PLMA hairy NPs in THF, showing a progression in size with brush molecular weight (Figure 4.5).

4.3.3. Dispersibility and Stability Study of PLMA Hairy Silica Nanoparticles in PAO

All hairy silica NP samples can be well dispersed from a dry state *via* ultrasonication in a lubricating base oil, PAO Spectrasyn^{TM} 4 (Exxon-Mobile), forming completely transparent dispersions as if no NPs were present at a concentration of 1 wt %. Note that ^{1}H NMR spectrum of PLMA hairy NPs in $CDCl_3$ is essentially identical to that of free PLMA (Figure 4.6), indicating strongly favorable enthalpic interactions between PLMA brushes and good solvents. To examine the stability of hairy silica NPs in PAO, three dispersions of HNP-SiO_2-4.1k were prepared and

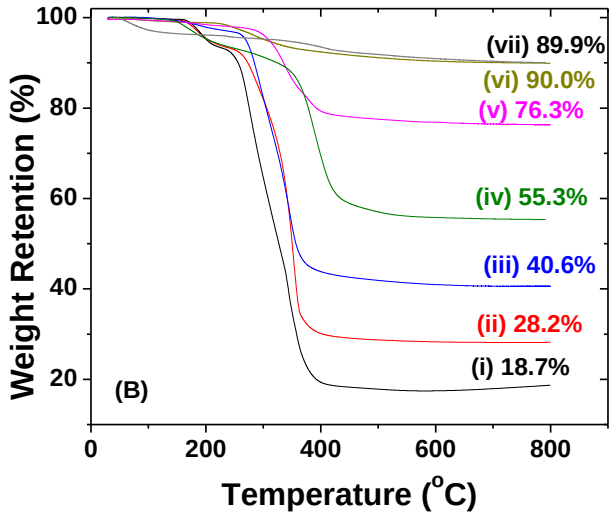

Figure 4.3. Thermogravimetric analysis (TGA) of ATRP initiator-functionalized silica NPs, INP-SiO_2-I (vii) INP-SiO_2-II (vi), with an average size of 23.8 nm and 23.5 nm, respectively, HNP-SiO_2-4.1k (i), HNP-SiO_2-9.0k (ii), HNP-SiO_2-11.8k (iii), HNP-SiO_2-21.7k (iv), and HNP-SiO_2-38.0k (v). HNP-SiO_2-9.0k was synthesized from INP-SiO_2-II; all other PLMA brush-grafted NP samples were synthesized using INP-SiO_2-I. TGA was performed in air at a heating rate of 20 °C/min.

Table 4.1. Characterization Data for PLMA Brush-Grafted Silica Nanoparticles and Corresponding Free PLMA Polymers

Hairy NPs [a]	DP	$M_{n,SEC}$ (kDa) [c]	PDI [c]	Grafting density σ (chains nm^{-2}) [d]
HNP-SiO_2-38.0k	117 [b]	38.0	1.09	0.70
HNP-SiO_2-21.7k	66 [b]	21.7	1.10	0.72
HNP-SiO_2-11.8k	31 [b]	11.8	1.13	0.72
HNP-SiO_2-9.0k [e]	18 [b]	9.0	1.12	0.73
HNP-SiO_2-4.1k	5 [b]	4.1	1.14	0.67

[a] HNP stands for "hairy NPs"; the $M_{n,SEC}$ is appended to the end of the sample name. [b] The degree of polymerization (DP) was calculated using the monomer conversion and the molar ratio of monomer to the sum of free and surface initiators. [c] The $M_{n,SEC}$ and polydispersity index (PDI) were obtained by SEC relative to polystyrene standards. [d] The grafting densities of polymer brushes were calculated by using TGA data, DPs, and the core NP size. [e] HNP-SiO_2-9.0k was synthesized using INP-SiO_2-II; all other PLMA brush-grafted NPs were synthesized from the same initiator NPs, INP-SiO_2-I.

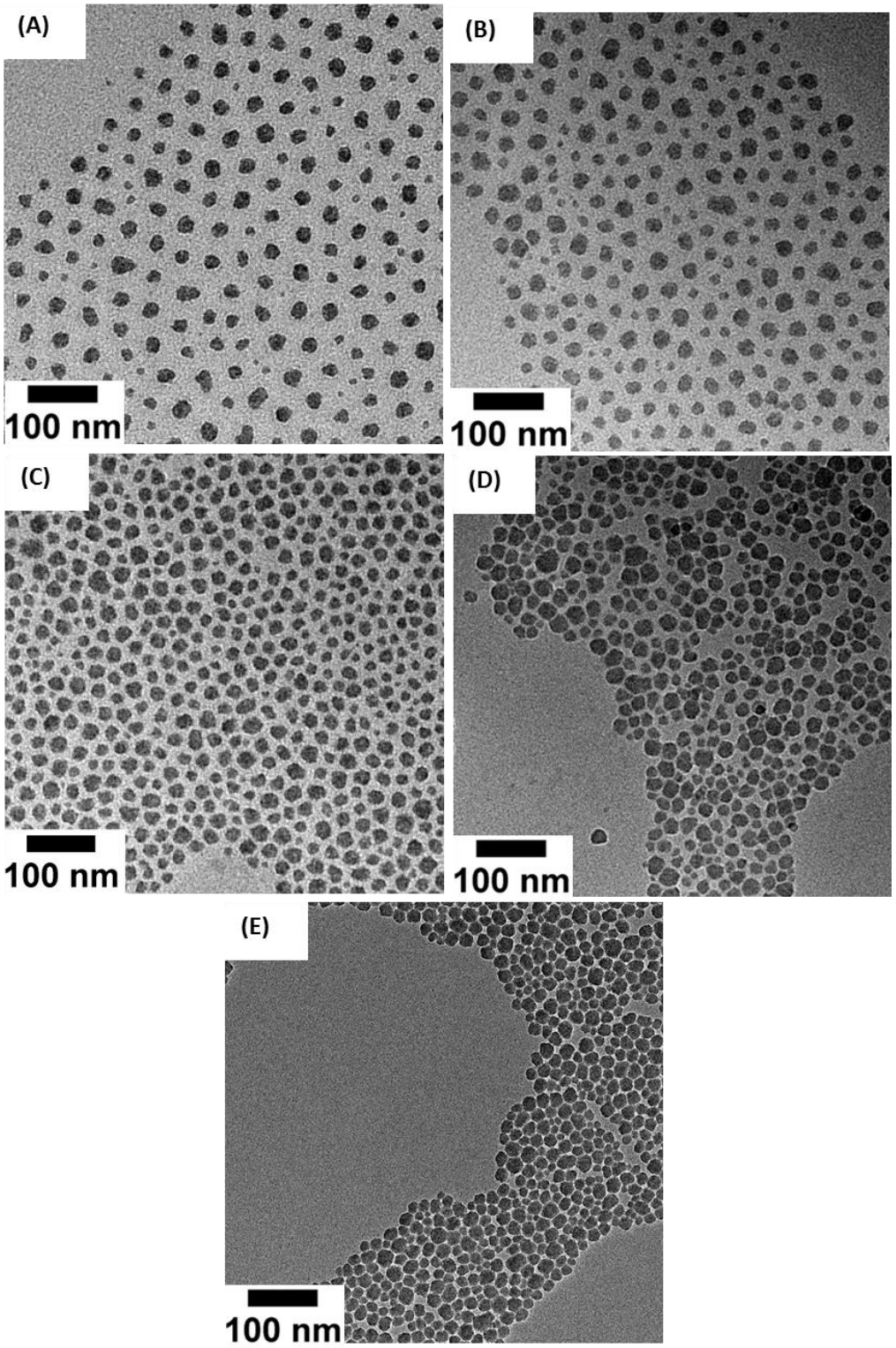

Figure 4.4. Bright field TEM micrographs of PLMA brush-grafted silica NPs with $M_{n,SEC}$ of 38.0 kDa (A), 21.7 kDa (B), 11.8 kDa (C), 9.0 kDa (D), and 4.1 kDa (E). The hairy NPs were cast onto carbon-coated, copper TEM grids from dispersions in $CHCl_3$, a good solvent, with a concentration of 4 mg/mL.

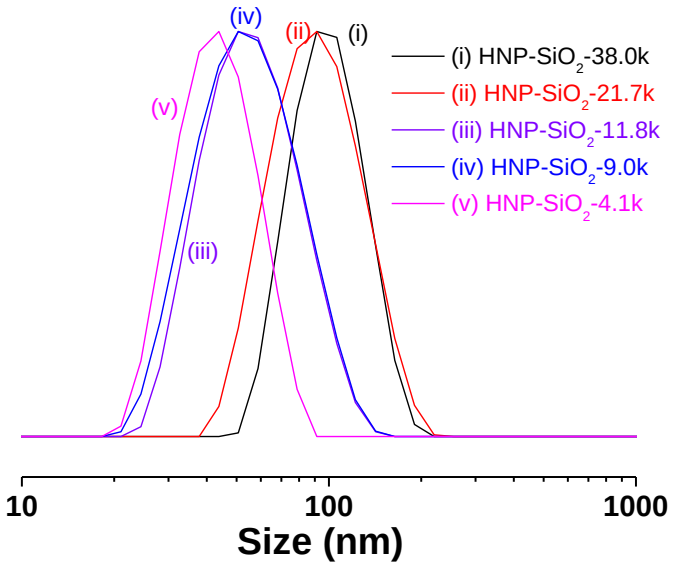

Figure 4.5. Intensity-weighted size distributions obtained by DLS. The average sizes were 102.6 nm for HNP-SiO_2-38k (i), 95.1 nm for HNP-SiO_2-21.7k (ii), 59.2 nm for HNP-SiO_2-11.8k (iii), 56.9 nm for HNP-SiO_2-9.0k (iv), and 44.1 nm for HNP-SiO_2-4.1k (v).

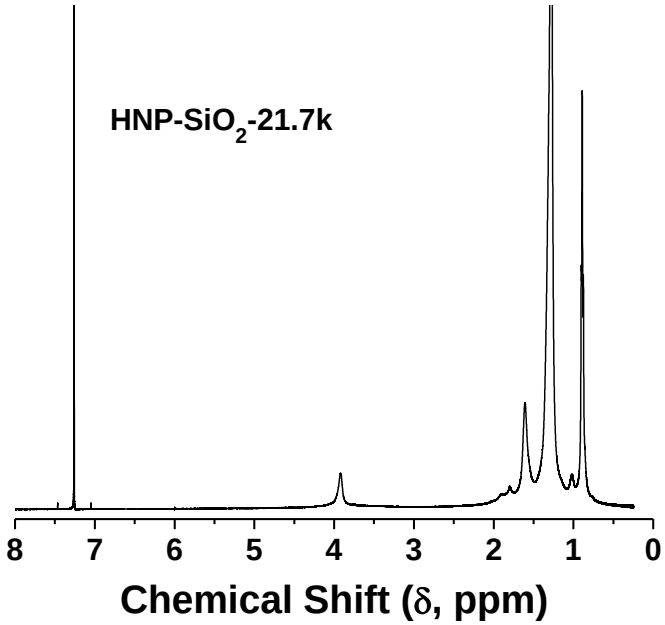

Figure 4.6. ^{1}H NMR spectrum of HNP-SiO_2-21.7k in $CDCl_3$ exhibits all characteristic peaks of PLMA, indicating that the HNPs are well dispersed.

kept at – 20 °C (in a freezer), 22 °C (room temperature), and 100 °C (in a thermostated oil bath), respectively. The dispersions stayed clear and no change in transparency was observed after 55 days (Figure 4.7), demonstrating the superior stability of these hairy NPs in PAO.

4.3.4. Tribological Properties of PLMA Hairy Silica Nanoparticles as Additives for PAO

The lubricating performances of 1 wt% dispersions of hairy silica NP samples in PAO were evaluated using a Plint TE-77 tribo-tester in a ball-on-flat (52100 steel ball against CL35 cast iron flat) reciprocating configuration at 100 °C. The normal load was 100 N, the oscillation frequency was 10 Hz with 10 mm stroke, and the sliding distance was 1000 m. Two repeat tests were carried out for each lubricant and averaged (all individual tribological runs in this work are included in Appendix C). The wear volumes were measured using a Wyko NT9100 optical profilometer after each tribological test. The results are summarized in Figure 4.8 and Table 4.2. For neat PAO, the coefficient of friction (COF) started below 0.08, but rapidly increased to above 0.14, indicating that scuffing occurred.[37,38] The base oil exhibited some recovery from this "wear-in" process, reaching a COF of 0.11 at 115 m, from which a gradual increase to 0.14 was observed over the testing period. The addition of 1 wt% of hairy silica NPs into the PAO greatly improved the lubricating performance; for HNP-SiO_2-38.0k, the COF was noticeably lower than that of neat PAO over the entire sliding experiment, approaching 0.12 at 1000 m. The addition of 1 wt% HNP-SiO_2-21.7k had a similar effect on COF, with a slightly lower value of 0.11 at 1000 m. The use of lower molecular weight samples, HNP-SiO_2-11.8k and -4.1k, showed a marked improvement in COF even over their higher molecular weight analogues, with values lower throughout the testing range and the final COFs around 0.10 at 1000 m; HNP-SiO_2-4.1k performed slightly better in the beginning and at the end of the testing with the COF at 1000 m reduced by ~ 30% compared with neat PAO. Overall, there appears to be a general trend that with decreasing brush molecular weight,

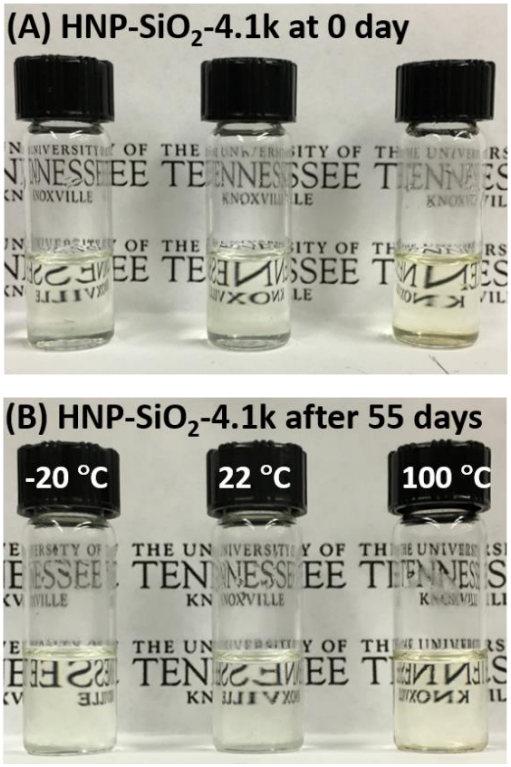

Figure 4.7. Photos of 1 wt% dispersions of HNP-SiO_2-4.1k in PAO in the initial state (A) and after being kept at -20, 22, 100 °C for 55 days (B).

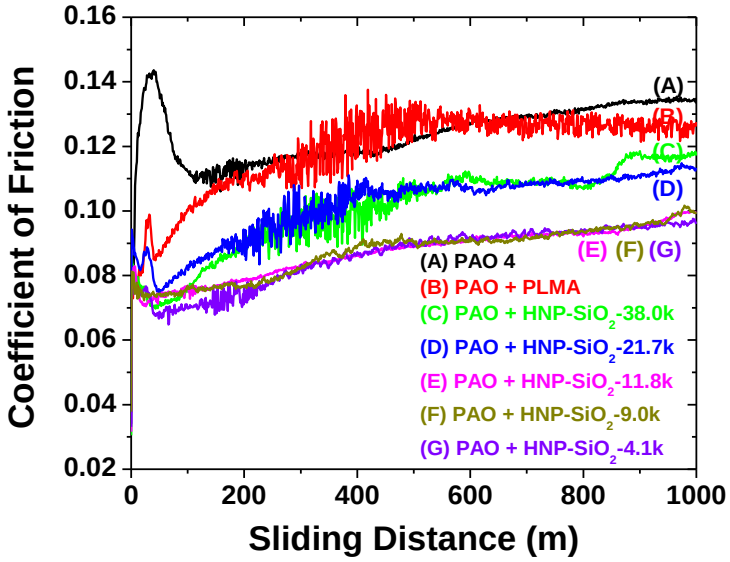

Figure 4.8. Friction curves for PAO SpectraSyn^{TM} 4 (A), PAO containing 1 wt% of free PLMA with a $M_{n,SEC}$ of 38.0 kDa (B), HNP-SiO_2-38.0k (C), HNP-SiO_2-21.7k (D), HNP-SiO_2-11.8k (E), HNP-SiO_2-9.0k (F), and HNP-SiO_2-4.1k (G). The tribological tests were performed using a Plint TE-77 tribo-tester at 100 °C under a point contact load of 100 N for a sliding distance of 1000 m.

Table 4.2. Wear Volumes for Balls and Flats from Tribological Tests

Lubricant Sample	Wear Volume [a]	
	Flat ($\times 10^7$ μm^3)	Ball ($\times 10^7$ μm^3)
PAO	112.99	0.786
PAO + 1 wt% PLMA	19.08	0.059
PAO + 1 wt% HNP-SiO_2-38.0k	15.20	0.091
PAO + 1 wt% HNP-SiO_2-21.7k	16.48	0.157
PAO + 1 wt% HNP-SiO_2-11.8k	17.48	0.035
PAO + 1 wt% HNP-SiO_2-9.0k	17.06	0.085
PAO + 1 wt% HNP-SiO_2-4.1k	8.12	0.052

[a] Volume of material removed during tribological testing. The wear volumes were obtained using optical profilometry.

the friction reduction increases. In addition, all samples showed a marked decrease in wear volume (Table 4.2), partially due to the prevention of scuffing at the beginning of the tribological test. The wear scars formed during tribological analysis were also examined by using an optical microscope, with scar size qualitatively showing a decrease in wear volume using HNP additives relative to neat PAO (Figure 4.9). The 1 wt % HNP-SiO_2-4.1k dispersion showed the least amount of wear.

Free polymer PLMA with a $M_{n,SEC}$ of 38.0 kDa was tested for comparison with hairy silica NPs. As shown in Figure 4.8, the 1 wt% solution of free PLMA in PAO performed similarly to neat PAO for the most part of the sliding though slightly better in the beginning and the end of the experiment, likely a result of interactions between polar ester groups of PLMA and the positively charged metal surface, which help reduce direct metal-metal asperity contact induced adhesion to prevent microwelding or scuffing. Since the 1 wt% solution of free PLMA contained more polymer than any tested hairy NP-additized PAO lubricant, it can be inferred that a substantial portion of the benefit of blending hairy NPs into PAO stems from the inorganic NPs, though it is unclear if the polymer brush lubrication mechanism operates here due to the much harsher conditions used compared with those typical for brush lubrication studies.[33] This is further bolstered by the apparent superiority of lower molecular weight samples in friction reduction, which is likely a result of their high number density of NPs at 1 wt%, a trend somewhat suggested by the lowest wear volume being observed with HNP-SiO_2-4.1k additized oil (Table 4.2).

To investigate the concentration effect of hairy silica NPs on lubrication performance, tribological tests were carried out using three additional dispersions of HNP-SiO_2-21.7k in PAO with concentrations of 0.25, 2.0, and 4.0 wt% (Figure 4.10). The COF was observed to decrease with increasing NP concentration, but there was a limit; the 4.0 wt% lubricant performed only slightly better that the 2.0 wt% sample. It is interesting to note that at 2.0 wt% and 4 wt% HNP-

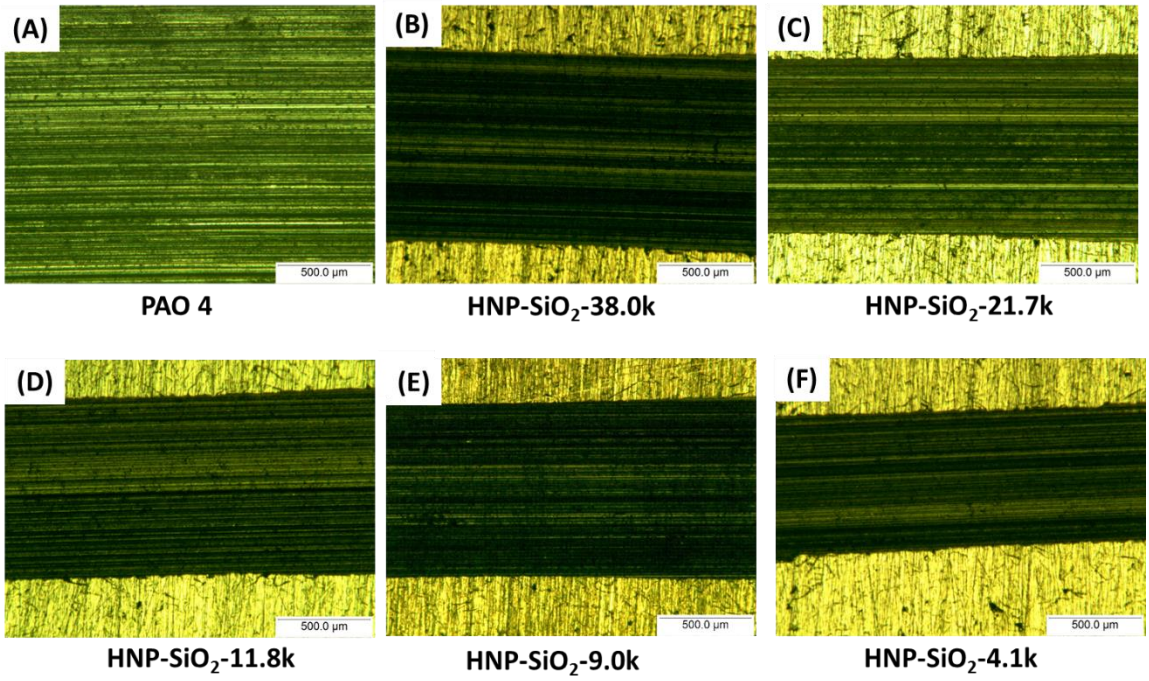

Figure 4.9. Optical micrographs of wear scars on the iron flats following tribological testing of neat PAO (A), and 1 wt% dispersion of HNP-SiO_2-38.0k (B), HNP-SiO_2-21.7 (C), HNP-SiO_2-11.8k (D), HNP-SiO_2-9.0k (E), and HNP-SiO_2-4.1k (F) in PAO. Note the entire width of the wear scar obtained from neat PAO testing was too large to be fully shown in the viewing area, a result of the scuffing observed in the corresponding COF curve.

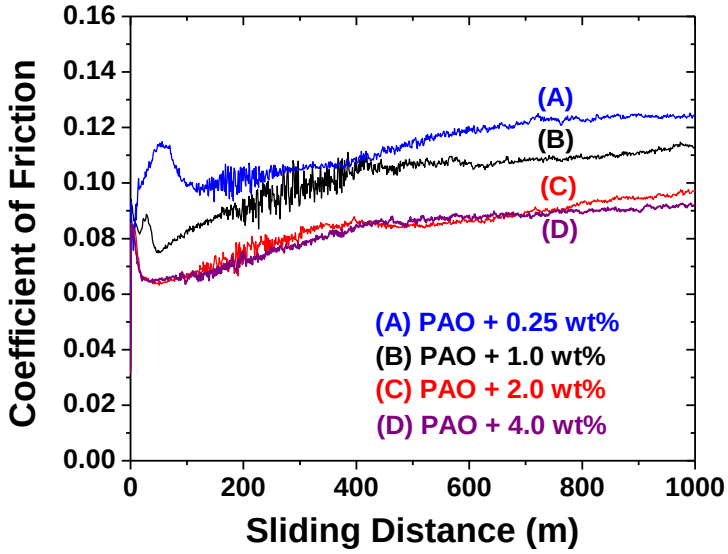

Figure 4.10. Friction curves for PAO dispersion containing (A) 0.25 wt%, (B) 1.0 wt%, (C) 2.0 wt%, and (D) 4.0 wt% of HNP-SiO_2-21.7k performed using a Plint TE-77 tribo-tester at 100 °C under a point contact load of 100 N for a sliding distance of 1000 m.

SiO_2-21.7k performed similarly to HNP-SiO_2-11.8k and -4.1k. A clear trend was also observed in wear reduction, with wear decreasing with increasing concentration (Table 4.3).

Finally, the friction reduction of hairy silica NPs was compared with commercially used friction reduction additives: amine phosphate and ZDDP. The tribological data for amine phosphate were obtained from another work, in which tribological testing and conditions were identical to those described above.[39] This additive was tested at 1.67 wt % at 100 °C and was found to have a comparable COF profile to the 1 wt% dispersion of HNP-SiO_2-4.1k in PAO (Figure 4.11). The COF for 1.67 wt% amine-phosphate was higher at the beginning of the experiment (< ~ 400m). At longer sliding distance, it was lower than the 1 wt% HNP-SiO_2-4.1k dispersion, eventually reaching a value of ~0.09 at 1000 m. The performance of PAO additized with 1 wt % ZDDP was comparable to the 1 wt% dispersion of HNP-SiO_2-4.1k; COFs are virtually the same for the two lubricants at the beginning and end of the experiments, while the 1 wt% HNP-SiO_2-4.1k dispersion exhibited slightly higher COFs in the middle of the friction curve. Overall, HNP-SiO_2-4.1k performed similarly to the commercial additives in terms of friction reduction. It should be noted here that our lab has also synthesized PLMA brush-grafted TiO_2 nanoparticles with a brush molecular weight of 8.1k. The size of the TiO_2 NPs was 15 nm according to the manufacturer. At 1 wt%, this sample exhibited better friction properties than both of the commercial additives (Figure 4.11). This bodes well for the future of hairy NPs as lubricant additives.[40]

4.3.5. Characterization of the Tribofilm Formed from Tribological Testing

The observed friction and wear reductions for hairy SiO_2 NP-additized PAO lubricants are believed to result from the function of NPs at the interfacial zone between the two rubbing surfaces and the formation of a tribofilm. To confirm the existence of the tribofilm and to further its

Table 4.3. Wear Volumes for Balls and Flats from Tribological Testing

Lubricant Sample	Wear Volume [a]	
	Flat ($\times 10^7$ μm^3)	Ball ($\times 10^7$ μm^3)
PAO + 0.25 wt% HNP-SiO_2-21.7k	85.20	0.572
PAO + 1.0 wt% HNP-SiO_2-21.7k	16.48	0.157
PAO + 2.0 wt% HNP-SiO_2-21.7k	14.55	0.080
PAO + 4.0 wt% HNP-SiO_2-21.7k	12.55	0.037

[a] Volume of material removed during tribological testing. Wear volumes were obtained using optical profilometry

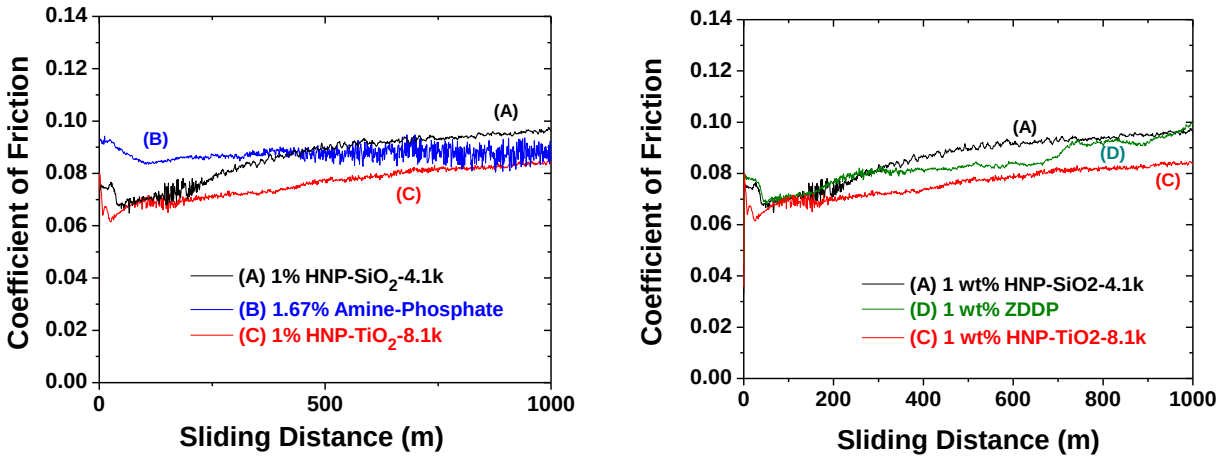

Figure 4.11. Friction curves for PAO additized with (A) 1 wt% HNP-SiO_2-4.1k, (B) 1.67 wt % amine phosphate,[39] (C), 1 wt% HNP-TiO_2-8.1k,[40] and (D) 1 wt% ZDDP. Measurements were performed using a Plint TE-77 tribo-tester at 100 °C under a point contact load of 100 N for a sliding distance of 1000 m.

characterization, we used the focused ion beam (FIB) technique to extract a thin, cross-sectional lamella from the wear scar formed on the cast iron flat during the tribological testing of PAO lubricant containing 1 wt% HNP-SiO_2-4.1k. The interfacial zone was analyzed using TEM. As shown in Figures 4.12 and 4.13, a 200-400 nm thick tribofilm can be clearly seen between the cast iron substrate and the carbon layer (for protecting the surface during the FIB process). A closer examination reveals that the tribofilm is an amorphous matrix embedded with small nanocrystals (Figures 4.12 and 4.13). Interestingly, both the thickness and morphology of the NP-formed tribofilm are similar to the tribofilms formed by organic AW additives such as ZDDP[3,4] or ionic liquids[41,42]. Energy-dispersive X-ray spectroscopy (EDS) analysis showed that the tribofilm contains high concentrations of silicon, iron, and oxygen. We believe that under the rather harsh tribological testing conditions (a point contact load of 100 N at 100 °C), complex mechano-chemical reactions, which involved hairy NPs, occurred, producing a nanostructured tribofilm on the wear track. Such a dynamic, self-healing tribofilm provided a protective boundary for the underneath material, thereby preventing scuffing and reducing friction and wear.[39,43,44]

4.4. Conclusions

A series of oil-soluble polymer brush-grafted SiO_2 NPs were synthesized through the SI-ATRP of LMA from initiator-functonalized NPs. These hairy NPs were shown to be a promising class of friction and wear reduction additives for lubricating oils. Unlike bare or even initiator-functionalized silica NPs, the PLMA hairy NPs can be well dispersed in PAO, exhibiting exceptional stability at both low and high temperatures; no changes in transparency were observed over a period of 55 days. Significant reductions in both COF and wear were observed with the addition of 1 wt% hairy silica NPs in PAO; the lubrication performance increased with decreasing

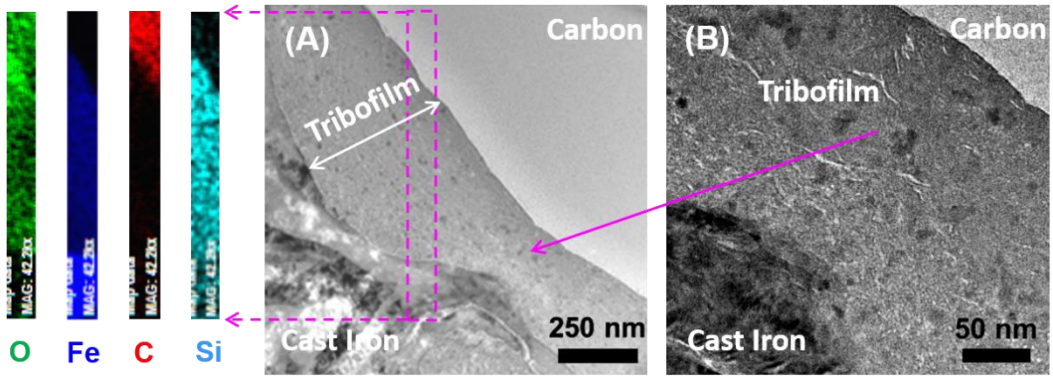

Figure 4.12. (A) Transmission electron micropscopy (TEM) micrograph of the cross-section of the wear scar on the cast iron flat tested with 1 wt% HNP-SiO_2-4.1k-additized PAO. The element mapping data of Si, C, Fe, and O of the selected area are shown on the left. The cross-section TEM sample was prepared using the focused ion beam (FIB) technique. (B) Higher magnification TEM micrograph of the area of the tribofilm pointed to by the arrow.

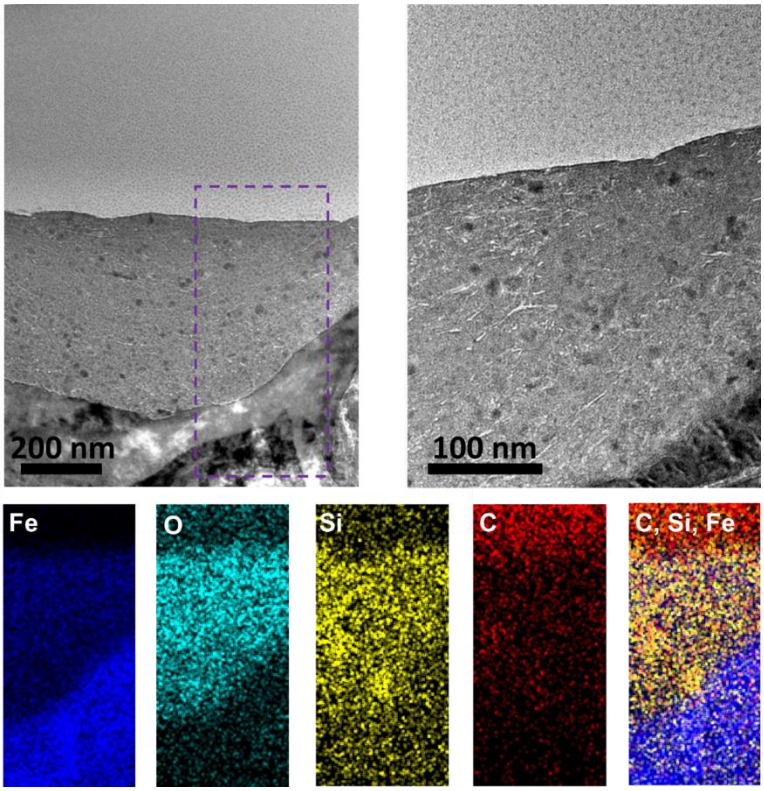

Figure 4.13. Transmission electron micropscopy (TEM) micrographs of the cross-section of the wear scar on the cast iron flat tested with 1 wt% HNP-SiO_2-4.1k-additized PAO. The element mapping data of Fe, O, Si, C, and a combined overlay of the selected area are shown on the bottom row. The cross-section TEM sample was prepared using the focused ion beam (FIB) technique.

brush molecular weight and increasing concentration of Hairy NPs in PAO. The friction reduction of the lowest molecular weight PLMA hairy silica NPs was found to compare well with commercial additives, specifically amine phosphate and ZDDP. Cross-sectional TEM analysis revealed a protective tribofilm formed at the rubbing interface during the tribological test. In light of these positive results, we believe that the use of oil-soluble polymer brushes to functionalize inorganic NPs makes it possible to realize the full potential of NPs as lubricant additives for friction and wear reduction, opening up new opportunities to further improve durability and efficiency in mechanical systems.

References

1. Rudnick, L. R. *Lubricant Additives: Chemistry and Applications, 2nd ed*. CRC Press: 2009.
2. Erickson, L. E.; Koodali, R. T.; Richards, R. M., Ed. *Nanoscale Materials in Chemistry: Environmental Applications, ACS Symposium Series, Vol. 1045*, **2010**, Chapter 8, 137-163.
3. Spikes, H. *Tribol. Lett.* **2004**, *17*, 469-489.
4. Nicholls, M. A.; Do, T.; Norton, P. R.; Kasrai, M.; Bancroft, G. M. *Tribol. Int.* **2005**, *38*, 15-39.
5. Choi, Y.; Lee, C.; Hwang, Y.; Park, M.; Lee, J.; Choi, C.; Jung, M. *Curr. Appl. Phys.* **2009,** *9*, e124-e127.
6. Padgurskas, J.; Rukuiza, R.; Prosyčevas, I.; Kreivaitis, R. *Tribol. Int.* **2013,** *60*, 224-232.
7. Qiu, S.; Zhou, Z.; Dong, J.; Chen, G. *J. Tribol.* **1999,** *123*, 441-443.
8. Tarasov, S.; Kolubaev, A.; Belyaev, S.; Lerner, M.; Tepper, F. *Wear* **2002,** *252*, 63-69.
9. Zhou, J.; Yang, J.; Zhang, Z.; Liu, W.; Xue, Q. *Mater. Res. Bull.* **1999,** *34*, 1361-1367.
10. Hernandez Battez, A.; Fernandez Rico, J. E.; Navas Arias, A.; Viesca Rodriguez, J. L.; Chou Rodriguez, R.; Diaz Fernandez, J. M. *Wear* **2006,** *261*, 256-263.
11. Hernández Battez, A.; González, R.; Felgueroso, D.; Fernández, J. E.; del Rocío Fernández, M.; García, M. A.; Peñuelas, I. *Wear* **2007,** *263*, 1568-1574.
12. Hernández Battez, A.; González, R.; Viesca, J. L.; Fernández, J. E.; Díaz Fernández, J. M.; Machado, A.; Chou, R.; Riba, J. *Wear* **2008,** *265*, 422-428.
13. Kim, D.; Archer, L. A. *Langmuir* **2011,** *27*, 3083-3094.
14. Xue, Q.; Liu, W.; Zhang, Z., *Wear* **1997,** *213*, 29-32.
15. Ye, W.; Cheng, T.; Ye, Q.; Guo, X.; Zhang, Z.; Dang, H., *Mater. Sci. Eng. A* **2003,** *359*, 82-85.

16. Chen, S.; Liu, W. *Mater. Res. Bull.* **2001,** *36,* 137-143.

17. Chen, S.; Liu, W.; Yu, L. *Wear* **1998,** *218,* 153-158.

18. Liu, W.; Chen, S. *Wear* **2000,** *238,* 120-124.

19. Rapoport, L.; Lvovsky, M.; Lapsker, I.; Leshchinsky, V.; Volovik, Y.; Feldman, Y.; Margolin, A.; Rosentsveig, R.; Tenne, R. *Nano Lett.* **2001,** *1,* 137-140.

20. Bakunin, V. N.; Suslov, A. Y.; Kuzmina, G. N.; Parenago, O. P.; Topchiev, A. V. *J. Nanoparticle Res.* **2004,** *6,* 273-284.

21. Demydov, D.; Adhvaryu, A.; McCluskey, P.; Malshe, A. P. In *Nanoscale Materials in Chemistry: Environmental Applications,* American Chemical Society: 2010; Vol. 1045, pp 137-163.

22. Li, B.; Wang, X.; Liu, W.; Xue, Q. *Tribol. Lett.* **2006,** *22,* 79-84.

23. Dong, J. X.; Hu, Z. S. *Tribol. Inter.* **1998,** *31,* 219-223.

24. Wu, Y. Y.; Tsui, W. C.; Liu, T. C. *Wear* **2007,** *262,* 819-825.

25. Zhang, M.; Wang, X.; Fu, X.; Xia, Y. *Tribol. Inter.* **2009,** *42,* 1029-1039.

26. Chen, L.; Klok, H.-A. *Soft Matter* **2013,** *9,* 10678-10688.

27. (a) Hui, C. M.; Pietrasik, J.; Schmitt, M.; Mahoney, C.; Choi, J.; Bockstaller, M. R.; Matyjaszewski, K. *Chem. Mater.* **2014,** *26,* 745-762; (b) Pyun, J.; Matyjaszewski, K., *Chem. Mater.* **2001,** *13,* 3436-3448.

28. Husseman, M.; Malmström, E. E.; McNamara, M.; Mate, M.; Mecerreyes, D.; Benoit, D. G.; Hedrick, J. L.; Mansky, P.; Huang, E.; Russell, T. P.; Hawker, C. J. *Macromolecules* **1999,** *32,* 1424-1431.

29. Ohno, K.; Koh, K.; Tsujii, Y.; Fukuda, T. *Angew. Chem. Inter. Ed.* **2003,** *42,* 2751-2754.

30. Prucker, O.; Rühe, J. *Macromolecules* **1998,** *31,* 592-601.

31. Wang, L.; Benicewicz, B. C. *ACS Macro Lett.* **2013,** *2*, 173-176.

32. Zhao, B.; Zhu, L. *Macromolecules* **2009,** *42*, 9369-9383.

33. (a) Briscoe, W. H.; Titmuss, S.; Tiberg, F.; Thomas, R. K.; McGillivray, D. J.; Klein, J. *Nature* **2006**, *444*, 191-194; (b) Nomura, A.; Okayasu, K.; Ohno, K.; Fukuda, T.; Tsujii, Y. *Macromolecules* **2011**, *44*, 5013-5019; (c) Banquy, X.; Burdyńska, J.; Lee, D. W.; Matykaszewski, K.; Israelachvili, J. *J. Am. Chem. Soc.* **2014**, *136*, 6199-6202; (d) Mocney, P.; Klok, H.-A. *Mol. Syst. Des. Syn.* **2016**, DOI: 10.1039/c5me00010f

34. Wright, R. A. E.; Hu, B.; Henn, D. M.; Zhao, B. *Soft Matter* **2015,** *11*, 6808-6820.

35. Bielecki, R. M.; Benetti, E. M.; Kumar, D.; Spencer, N. D., *Tribol. Lett.* **2012,** *45*, 477-487.

36. Li, D.; Sheng, X.; Zhao, B. *J. Amer. Chem. Soc.* **2005,** *127*, 6248-6256.

37. Qu, J.; Truhan, J. J.; Blau, P. J.; Meyer III, H. M. *Wear* **2005**, *259*, 1031-1040.

38. Qu, J.; Truhan, J. J.; Blau, P. J. *Int. J. Engine Res.* **2005**, *6* 1-9.

39. Zhou, Y.; Dyck, J.; Graham, T. W.; Luo, H.; Leonard, D. N.; Qu, J. *Langmuir* **2014,** *30*, 13301-13311.

40. The work presented in this chapter has been published online an early view article. Wright, R. A. E.; Wang, K.; Qu, J.; Zhao, B. *Angew. Chem. Int. Ed.* **2016**, *55*, 8656-8660.

41. Qu, J.; Chi, M.; Meyer, H. M.; Blau, P. J.; Dai, S.; Luo, H. *Tribol. Lett.* **2011,** *43*, 205-211.

42. Qu, J.; Barnhill, W. C.; Luo, H.; Meyer, H. M.; Leonard, D. N.; Landauer, A. K.; Kheireddin, B.; Gao, H.; Papke, B. L.; Dai, S. *Adv. Mater.* **2015,** *27*, 4767-4774.

43. Martin, J. M. *Tribol. Lett.* **1999,** *6*, 1-8.

44. Qu, J.; Bansal, D. G.; Yu, B.; Howe, J. Y.; Luo, H.; Dai, S.; Li, H.; Blau, P. J.; Bunting, B. G.; Mordukhovich, G.; Smolenski, D. J., *ACS Appl. Mater. & Interfaces* **2012,** *4*, 997-1002.

Appendix C

for

Chapter 4. Oil-Miscible Polymer Brush-Grafted Silica Nanoparticles as Effective Lubricant Additives

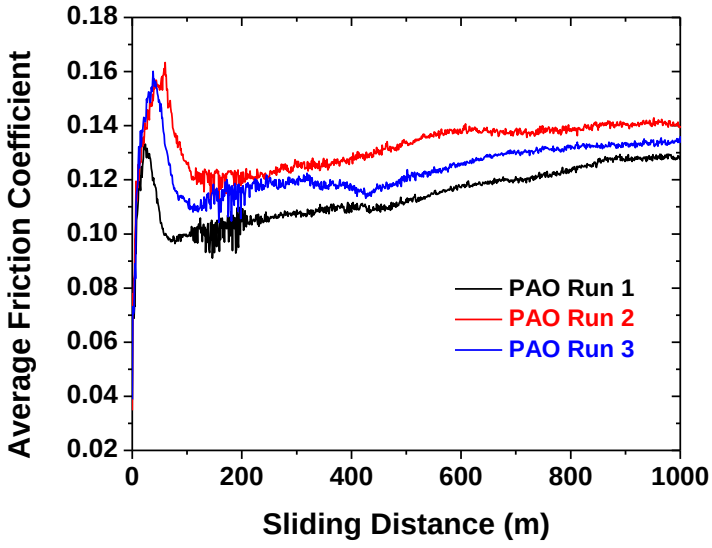

Figure C1. Individual friction curves for neat PAO obtained using a Plint TE-77 tribo-tester at 100 °C under a point contact load of 100 N for a sliding distance of 1000 m.

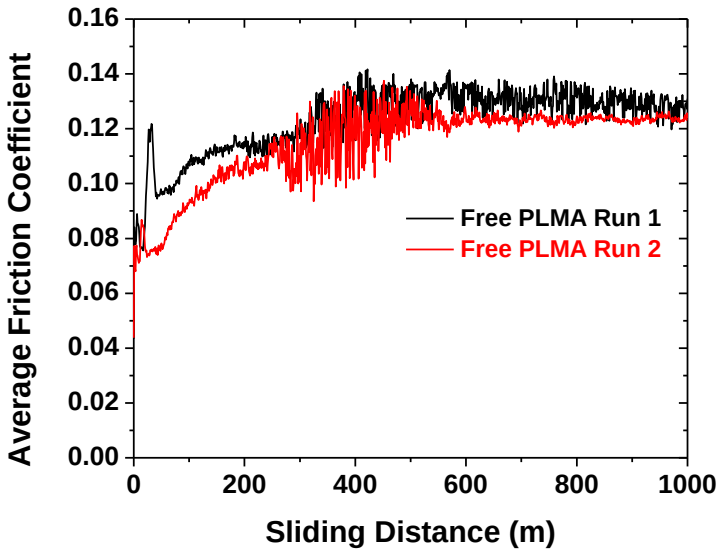

Figure C2. Individual friction curves for 1 wt% free PLMA-38.0k PAO solution obtained using a Plint TE-77 tribo-tester at 100 °C under a point contact load of 100 N for a sliding distance of 1000 m.

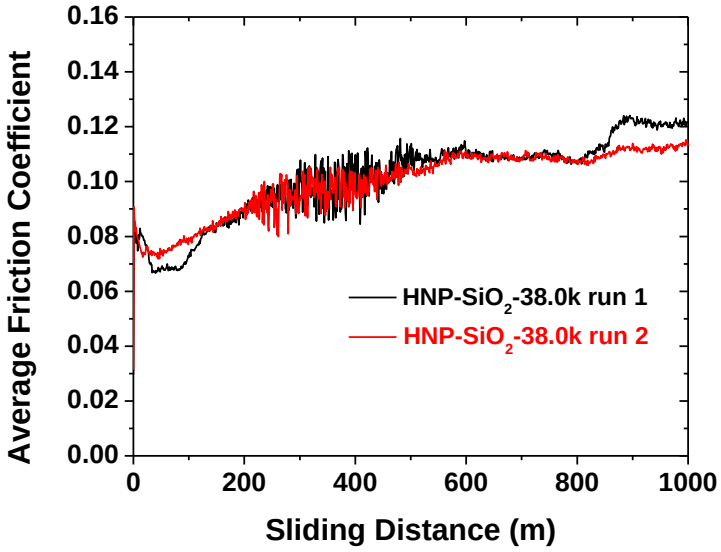

Figure C3. Individual friction curves for 1 wt% HNP-SiO_2-38.0k PAO dispersion obtained using a Plint TE-77 tribo-tester at 100 °C under a point contact load of 100 N for a sliding distance of 1000 m.

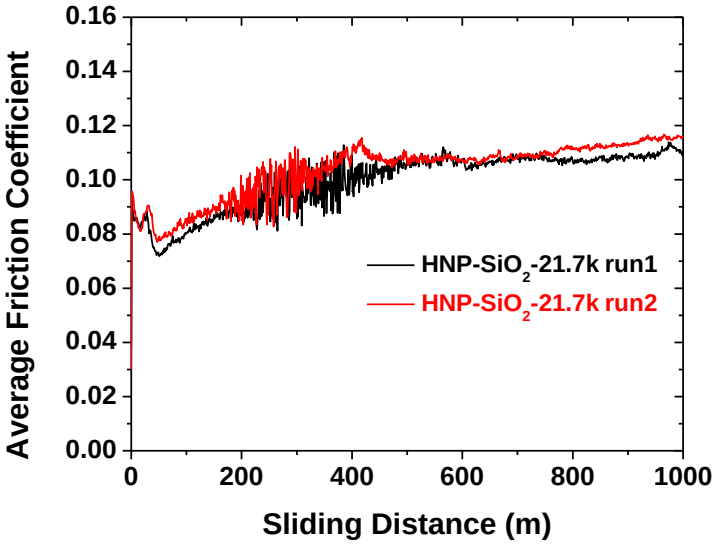

Figure C4. Individual friction curves for 1 wt% HNP-SiO_2-22.7k PAO dispersion obtained using a Plint TE-77 tribo-tester at 100 °C under a point contact load of 100 N for a sliding distance of 1000 m.

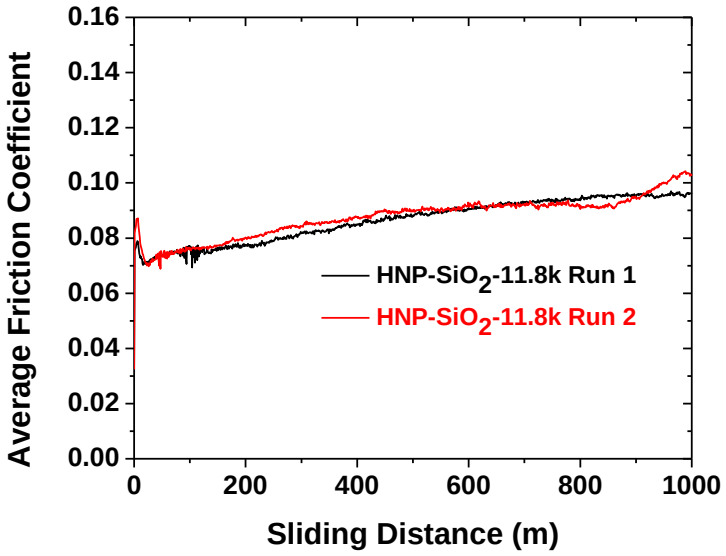

Figure C5. Individual friction curves for 1 wt% HNP-SiO_2-11.8k PAO dispersion obtained using a Plint TE-77 tribo-tester at 100 °C under a point contact load of 100 N for a sliding distance of 1000 m.

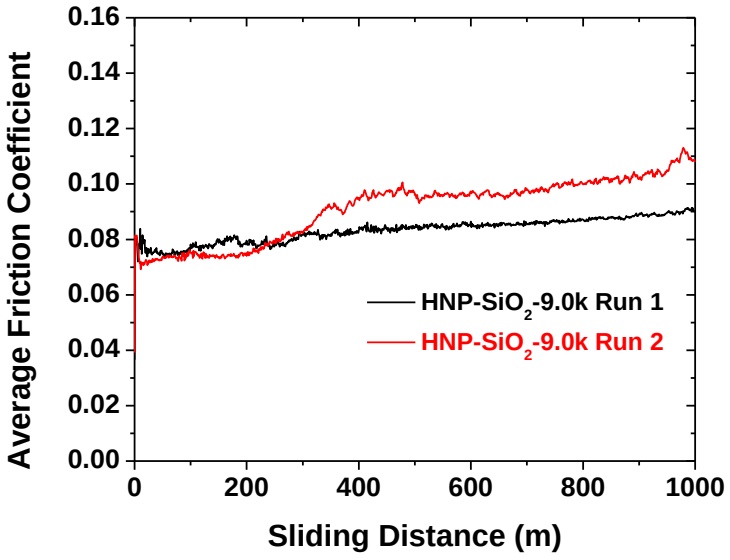

Figure C6. Individual friction curves for 1 wt% HNP-SiO_2-9.0k PAO dispersion obtained using a Plint TE-77 tribo-tester at 100 °C under a point contact load of 100 N for a sliding distance of 1000 m.

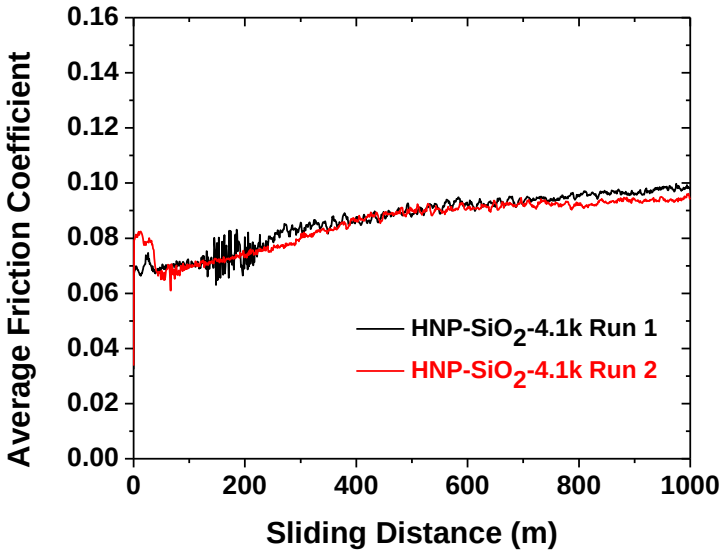

Figure C7. Individual friction curves for 1 wt% HNP-SiO_2-4.1k PAO dispersion obtained using a Plint TE-77 tribo-tester at 100 °C under a point contact load of 100 N for a sliding distance of 1000 m.

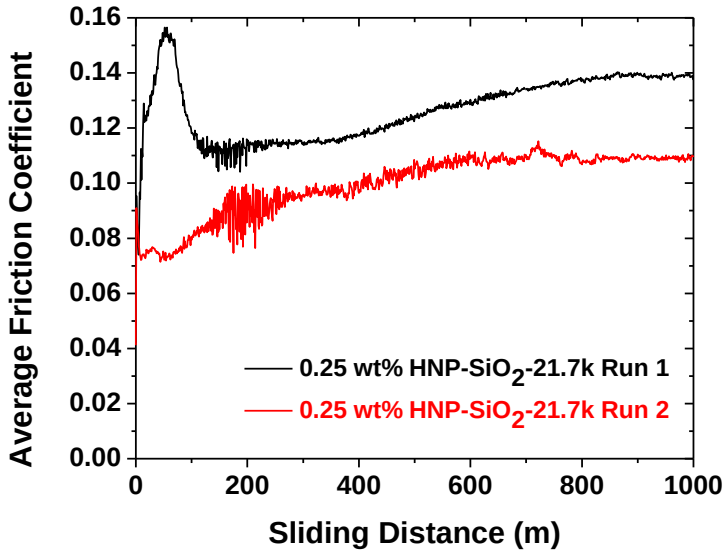

Figure C8. Individual friction curves for 0.25 wt% HNP-SiO_2-21.7k PAO dispersion obtained using a Plint TE-77 tribo-tester at 100 °C under a point contact load of 100 N for a sliding distance of 1000 m.

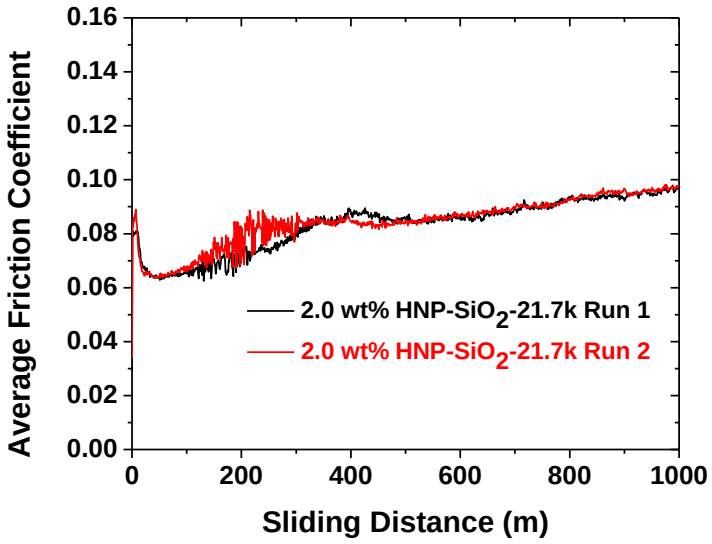

Figure C9. Individual friction curves for 2 wt% HNP-SiO_2-21.7k PAO dispersion obtained using a Plint TE-77 tribo-tester at 100 °C under a point contact load of 100 N for a sliding distance of 1000 m.

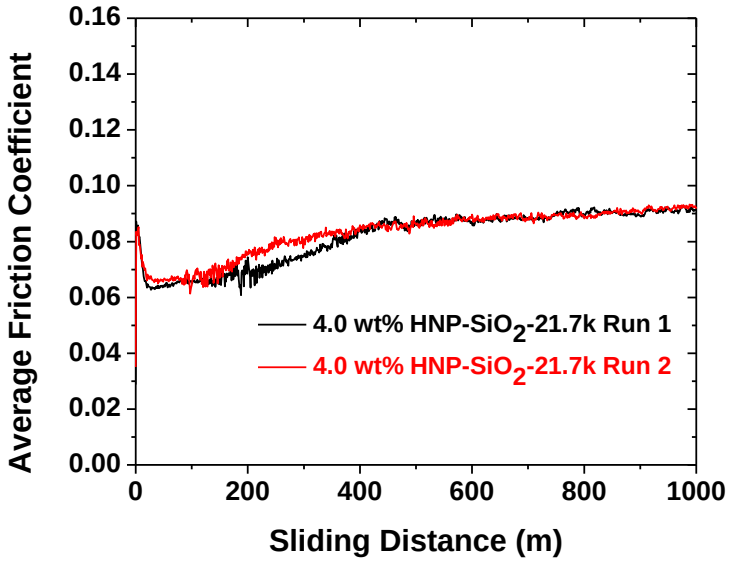

Figure C10. Individual Friction curves for 4 wt% HNP-SiO_2-21.7k PAO dispersion obtained using a Plint TE-77 tribo-tester at 100 °C under a point contact load of 100 N for a sliding distance of 1000 m.

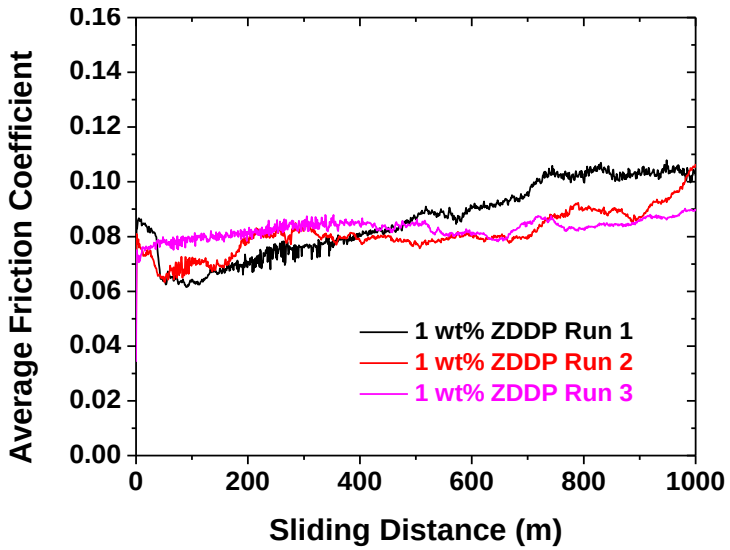

Figure C11. Individual friction curves for 1 wt% ZDDP PAO solution obtained using a Plint TE-77 tribo-tester at 100 °C under a point contact load of 100 N for a sliding distance of 1000 m.

Chapter 5. Synthesis, Characterization, and Microphase Separation of Poly(*n*-butyl acrylate)-*b*-Polystyrene Diblock Copolymer Brushes Grafted on Silica Particles

Abstract

Inspired by the theoretically predicted phase morphologies of diblock copolymer brushes grafted on spherical nanoparticles, this chapter presents the synthesis of a series of poly(*n*-butyl acrylate)-*b*-polystyrene (P*n*BA-*b*-PS) brush-grafted silica particle samples and a preliminary TEM study of their morphologies. The brushes were synthesized by sequential surface-initiated atom transfer radical polymerizations of *n*-butyl acrylate and styrene from initiator-functionalized silica particles with the addition of a sacrificial initiator in each step. A cleavage experiment using HF to etch the silica core confirmed the targeted diblock copolymer architecture. Differential scanning colarimetry analysis of a free P*n*BA-*b*-PS diblock copolymer, formed in the synthesis of a diblock copolymer brush sample, revealed two distinct glass transitions, indicating the microphase separation of two blocks. For TEM studies, the P*n*BA-*b*-PS brush-grafted particles were drop cast onto carbon-coated, copper grids and stained with RuO_4. A preliminary investigation showed that there appeared to be an evolution from a stripe-like nanostructure to a more uniform layered structure with the increase of the outer PS block molecular weight. The results were qualitatively in line with theoretical predictions, and will likely serve as a starting point for further investigation.

5.1 Introduction

Block copolymers are composed of two or more chemically distinct polymers covalently linked to each other. These polymers are usually incompatible due to the low mixing entropy of macromolecules, causing microphase separation into block rich domains.[1] These domains typically have dimensions on the nanoscale and can have a long range order on the mesoscale or even larger. The two-component, AB diblock copolymers are the best understood in terms of the phase morphology. The primary parameter governing microphase separation is the Flory-Huggins interaction parameter, χ, which is a measure of the energetic cost of AB contact per monomer unit.[2] Other factors include the total degree of polymerization, N, the increase in which further lowers mixing entropy of unlike blocks and thus increases incompatibility, and the volume fraction of A-type monomer units, f_A, which determines the morphology of the microphase-separated domains. As f_A is increased, an evolution of A-rich domains can be observed from spherical microdomains at low f_A, to cylinders, bicontinuous gyroid, to lamellar structures when f_A approaches 0.5; when f_A exceeds the volume fraction of the B-block, inverse morphologies are formed.[2-5] The most favorable phase morphology for a given block copolymer system is determined by two opposing forces: the minimization of unfavorable segment-segment interactions and maximizing the conformational entropy of polymer chains. Decreasing A-B contact is achieved in the AB system by forming block-rich nanodomains, but can only be brought about by the stretching of polymer chains. This stretching decreases the number of conformations available to the polymer chains and results in an entropy-driven force attempting to restore the random coil.[4]

Diblock copolymers end-tethered to a substrate, i.e., block copolymer brushes, also exhibit microphase separation dependent on the chemical nature of constituent blocks, block size, and DP as well as grafting density of polymer chains on the surface of the substrate.[6] For the diblock

copolymer brushes on a flat surface with the B block grafted on the substrate and the A block being the outer block, four equilibrium phases have been predicted to form with increasing f_A: hexagonal, stripe, inverse hexagonal, and a laterally uniform phase. The uniform layered state is the most entropically favorable morphology. The driving force for diblock copolymer brushes to form periodic structures is the reduction of interfacial A-B contact. As was the case in the bulk state, this force is balanced by the entropic penalty of chains stretching to form unique domains. These morphologies can be shifted to lower or higher f_A by increasing B-block or A-block affinity for the environment: increased grafted B block surface tension decreases the appearance of nonuniform phases, and increased outer A block surface tension encourages the formation of B-rich domains at the brush-air interface.[6,7] This is a unique facet of grafted diblock copolymer brush films, as non-tethered diblocks will simply rearrange to place the higher surface tension block in contact with the generally more hydrophilic substrate. Other more complex morphologies like the pinned micellar "garlic" and "onion" nanostructures, as well as metastable structures, may be observed in the presence of selective solvents.[8-10]

Experimentally, O'Driscol et al. used linear diblock copolymers terminated with thiol and hydroxyl groups to form brushes on gold-coated silicon and silica wafers, respectively. Using atomic force microscopy, morphologies were observed that agree qualitatively with simulations.[7,10] Recently, considerable work has been done to predict the phase behavior of diblock copolymer brushes on a sphere. Predicted morphologies consisted of dots, stripes, and holes as f_A was increased, as shown in Figure 5.1.[11-13] The phase morphology of linear AB diblock brushes on spherical substrates have not yet been studied experimentally, and the direct observation of the evolution of morphology as a function of f_A using TEM is likely to be enlightening. We note here

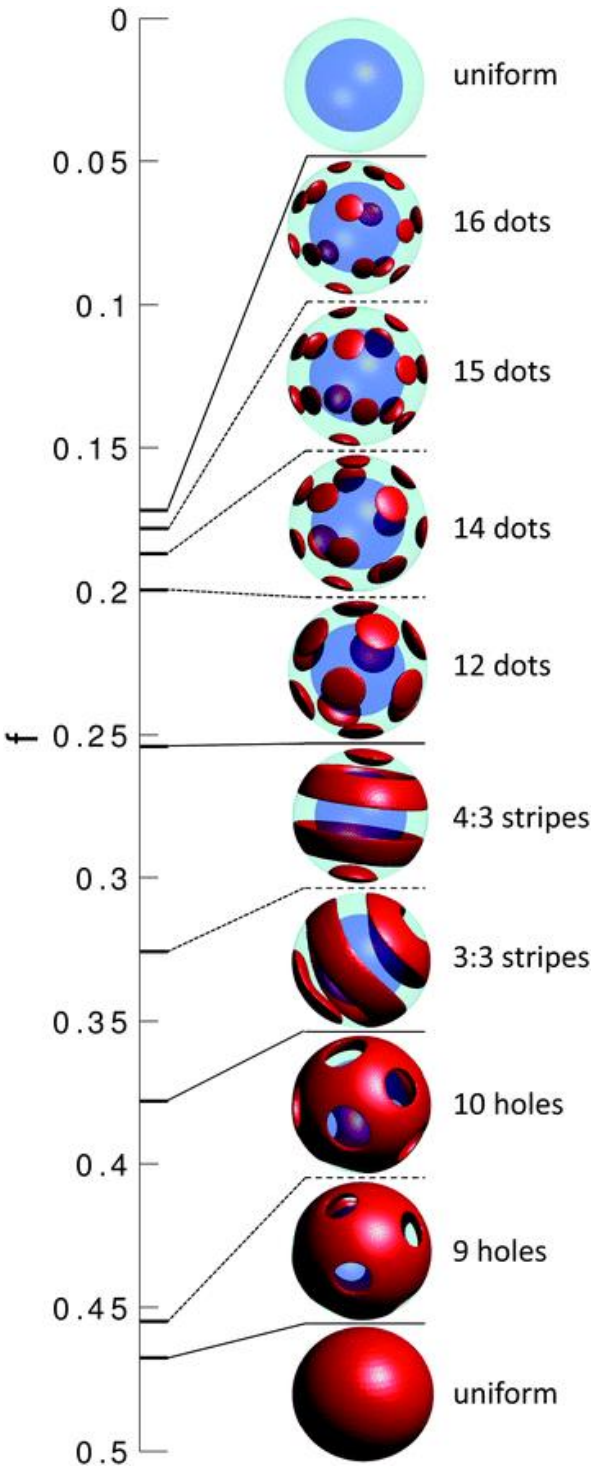

Figure 5.1. Evolution of phase morphologies of diblock copolymer brushes grafted by the B block to a spherical substrate. B-rich domains are transparent, while A-rich domains are red.[13] (Reprinted from Ref. 13 with permission from the Royal Society of Chemistry)

that the majority of the nanostructures predicted for diblock copolymer brushes grafted on spheres are of great interest to explore patchy particles, a topic that is being intensively studied.

The work presented in this chapter represents our first step toward the synthesis of well-defined diblock copolymer brushes on silica particles and the study of their phase morphology, especially with respect to block volume fraction. In this work, we first functionalized silica particles with a chlorosilane-terminated ATRP-initiator. Poly(*n*-butyl acrylate)-*b*-polystyrene (P*n*BA-*b*-PS) brushes with various molecular weights for the two blocks were then grown from the surface of initiator-modified silica particles by means of sequential surface initiated ATRP of *n*BA and styrene (Scheme 5.1).

5.2 Experimental

5.2.1 Materials

CuBr (98%) was purchased from Aldrich and was purified prior to use by stirring in glacial acetic acid overnight. It was then filtered, washed with absolute ethanol and diethyl ether, dried in vacuum, and stored in a desiccator. *N*, *N*, *N'*, *N'*, *N''*-Pentamethyldiethylenetriamine (PMDETA, 99%, Aldrich), ethyl 2-bromoisobutyrate (98%, Aldrich), styrene (99%, Aldrich), and *n*-butyl acrylate (99%, Aldrich) were dried with calcium hydride and distilled under reduced pressure. Chlorodimethylsilane (98%) was purchased from Alfa Aesar and stored in a refrigerator. Platinum-divinyltetramethyldisiloxane complex in xylene (2.1~2.4% Pt concentration in xylene) was purchased from Gelest, Inc. and stored in a desiccator. 10-Undecen-1-yl 2-bromo-2-methylpropionate was synthesized according to the literature procedure.[14] All other chemical reagents were purchased from either Aldrich or Fisher and used without further purification.

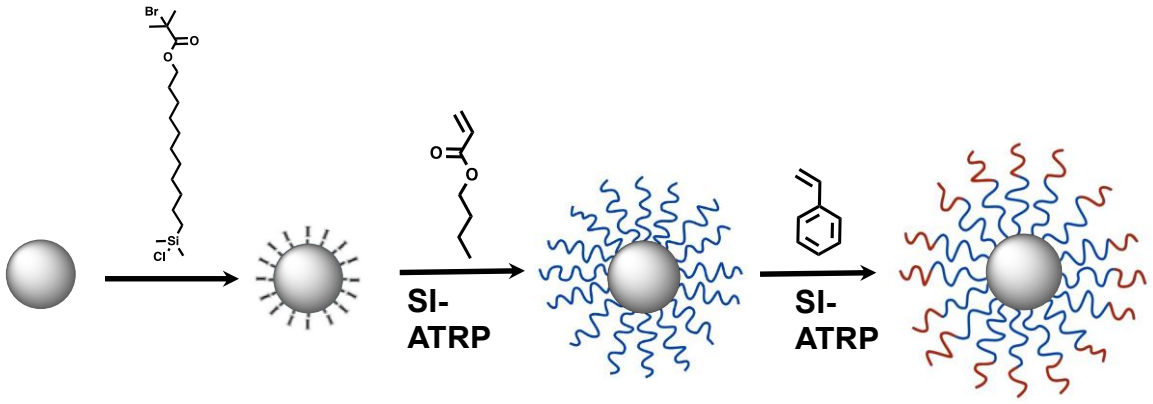

Scheme 5.1. Synthesis of P*n*BA-*b*-PS brush-grafted silica particles from ATRP initiator-functionalized silica particles through sequential SI-ATRP of *n*BA and styrene.

5.2.2 Characterization

Size exclusion chromatography (SEC) was carried out at ambient temperature using PL-GPC 20 (an integrated SEC system from Polymer Laboratories, Inc.) with a refractive index detector, one PLgel 5 μm guard column (50 × 7.5 mm), and two PLgel 5 μm mixed-C columns (each 300 × 7.5 mm, linear range of molecular weight from 200 to 2,000,000 according to Polymer Laboratories, Inc.). The data were processed using Cirrus^{TM} GPC/SEC software (Polymer Laboratories, Inc.). THF was used as the carrier solvent at a flow rate of 1.0 mL/min. Polystyrene standards (Polymer Laboratories, Inc.) were used for calibration. ^{1}H NMR spectra were recorded by means of a Varian Mercury 300 NMR spectrometer or Varian VNMRS 500 MHz spectrometer. Thermogravimetric analysis was performed in air at a heating rate of 20 °C/min from 30 °C to 800 °C using a TA Discovery TGA-MS. Transmission electron microscopy (TEM) was performed using a Zeiss Libra 200 HT FE MC microscope with an accelerating voltage of 200 kV, and bright field images were taken with a bottom-mounted Gatan UltraScan US1000XP CCD camera.

5.2.3 Synthesis of Bare Silica Particles

The bare silica particles was synthesized by means of the Stöber process. Ammonium hydroxide (25% in water, 19.932 g) and tetraethoxysilane (TEOS, 10.504 g) were each dissolved in ethanol (each 10 mL). The two solutions were added into a 500 mL flask that contained 280 mL ethanol under vigorous stirring. The mixture was stirred vigorously at room temperature for 5 h. The particles were then isolated by centrifugation (Eppendorf 5804 centrifuge, 6000 rpm, 15 min), re-dispersed in ethanol, and centrifuged again. This washing process was repeated with ethanol one more time, water four times, and ethanol again. The silica particles were then dried with a stream of air. The average size of the particles was 171 nm, as determined by TEM.

5.2.4 Synthesis of ATRP Initiator-Functionalized Silica Particles (IP)

10-Undecen-1-yl 2-bromo-2-methylpropionate (342 mg, 1.08 mmol) was added into a 25 mL two-necked round bottom flask and mixed with chlorodimethylsilane (4.00 mL, 37.9 mmol) under a nitrogen atmosphere, followed by the injection of Pt complex in xylenes (40 μL). The mixture was stirred at 45 °C and was monitored by ^{1}H NMR spectroscopy. Once the reaction proceeded to completion, excess chlorodimethylsilane was removed by vacuum, and the product was dissolved in anhydrous THF (3.0 mL). This solution was then added dropwise to the dispersion of bare silica particles (900 mg) in anhydrous THF (10 mL) prepared by ultrasonication. The resultant mixture was then placed in a 70 °C oil bath and stirred overnight. The particles were isolated by centrifugation, re-dispersed in THF, and isolated again. This washing process was repeated an additional four times. The initiator-functionalized particles, designated as IP, were dried with a stream of air flow.

5.2.5 Synthesis of P*n*BA Brush-Grafted Silica Particles

Copper(I) bromide (16.4 mg, 0.114 mmol), copper(II) bromide (3.5 mg, 1.6×10^{-5} mol), and initiator particles (137.3 mg) were placed into a 50 mL two-necked flask and dried under high vacuum at 35 °C for 150 min. The mixture was then placed under an N_2 atmosphere, and a solution of *n*-butyl acrylate (10.072 g, 78.560 mmol) and anisole (664 mg) was added into the flask. The particles were then dispersed by means of sonication. A solution of ethyl 2-bromoisobutyrate (EBiB, 17.8 mg, 9.12×10^{-5} moles), PMDETA (20.3 mg, 1.17×10^{-4} moles), and anisole (1.306 g) was then injected. An initial ^{1}H NMR sample was taken, and the solution was degassed by three freeze–pump–thaw cycles before being placed in a thermostated oil bath at 95 °C. The polymerization continued for 185 min, until a monomer conversion of 22.5 % was reached, calculated by ^{1}H NMR using the integrals of peaks located at 4.25 and 4.04 ppm, corresponding

to the COOCH_2 signals of *n*BA and P*n*BA, respectively. This monomer conversion and the monomer-to-free initiator molar ratio were used to find a degree of polymerization of 193.

The flask was removed from the oil bath, opened to air, and diluted with THF. The P*n*BA brush-grafted particles were then isolated by centrifugation (Eppendorf 5804, 11000 rpm, 15 min). The copper catalyst was removed from the free polymer supernatant solution by passing it through a neutral aluminum oxide/silica gel column using THF as an eluent. The free polymer was then dried under high vacuum to remove monomer. The free polymer was characterized by SEC and found to have an M_n of 23.0 kDa and a PDI of 1.15. The P*n*BA hairy particles were re-dispersed in THF and isolated by centrifugation. This purification process was repeated an additional four times. The P*n*BA brush-grafted silica particles were open to air and allowed to dry naturally. The particles were then transferred into a 25 mL two-necked flask and dried under high vacuum overnight. A small portion of the particles was examined using thermogravimetric analysis (TGA).

5.2.6 Synthesis of P*n*BA-*b*-PS Brush-Grafted Silica Particles

A subsequent ATRP polymerization of styrene was then carried out at 95 °C using the P*n*BA brushes as surface-tethered macroinitiator and the free P*n*BA polymer formed in the synthesis of P*n*BA brush-grafted particles as sacrificial initiator. P*n*BA brush-grafted particles (136.3 mg) were dried under high vacuum and dispersed in anisole (10.107 g) before being added into a 50 mL two-necked flask, along with copper(I) bromide (17.6 mg, 0.123 mmol), copper(II) bromide (3.4 mg, 1.5×10^{-5} mol), and styrene (4.732 g, 0.0454 mol). A solution of P*n*BA (458.6 mg, 1.951×10^{-5} mol) in anisole (3.257 g) was also added to the flask. Immediately after adding PMDETA (24.5 mg, 0.141 mmol), the mixture was degassed by three freeze–pump–thaw cycles, and the flask was placed in a thermostated oil bath with a temperature of 95 °C. The polymerization was monitored by SEC. Large samples (~ 3.5 mL) were taken at 120, 155, 180, and 215 minutes. Each sample

was exposed to air, diluted with THF, and purified in a manner similar to that of the P*n*BA brush-grafted particles described above. These diblock copolymer brush-grafted particles were referred to according to their time in the reaction mixture: DBP-120, DBP-155, DBP-180, and DBP-215, respectively. The free block copolymers, designated correspondingly as BC-120, BC-155, BC-180, and BC-215, were characterized by SEC and ^{1}H NMR.

5.2.7 Cleavage of P*n*BA-*b*-PS Brushes from Silica Particles

The P*n*BA-*b*-PS brushes from the sample taken at 180 min (DBP-180) were cleaved from silica particles by HF and analyzed by SEC. DBP-180 (9.98 mg) was dispersed in 5.00 mL toluene in a 60 mL plastic bottle. Hydrofluoric acid (HF, 48~51% aq., 0.3 mL) was added, and the mixture was stirred at room temperature for ~ 4 h. A saturated aqueous solution of calcium hydroxide (4 mL) was then added, along with 4 mL of water. The toluene layer was removed and concentrated, and the polymer dried under high vacuum. The cleaved polymer was characterized by SEC and found to have an $M_{n,SEC}$ of 55.9 kDa and a PDI of 1.09. Note that the $M_{n,SEC}$ and PDI of the corresponding free polymer were 54.9 kDa, and 1.15, respectively.

5.2.8 Differential Scanning Calorimetry of Free P*n*BA-*b*-PS

The free diblock copolymer BC-155 (taken from the reaction mixture at reaction time of 155 min) was used for DSC analysis. BC-155 (9.017 mg) was heated to 140 °C, cooled to -80 °C, and subjected to a second heating ramp at 20 °C/min. DSC analysis was performed on a TA Q-1000 DSC instrument calibrated with a sapphire standard.

5.2.9. Transmission Electron Microscopy Study of P*n*BA-*b*-PS Brush-Grafted Particles

P*n*BA-*b*-PS diblock copolymer brush-grafted particles were dispersed in chloroform, a nonselective good solvent for P*n*BA and PS, by ultrasonication at a concentration of 1 mg mL^{-1}. The particle dispersion was drop cast onto a carbon-coated, copper TEM grid and dried at ambient

conditions. The TEM samples were annealed with $CHCl_3$ vapor at room temperature for several hours and were then allowed to air dry for ~ 30 min. The samples were then stained with RuO_4 vapor at room temperature for 20 min.

5.3 Results and Discussion

5.3.1 Synthesis of P*n*BA Brush-Grafted Silica Particles

P*n*BA brush-grafted silica particles were synthesized by surface-initiated ATRP as shown in Scheme 5.1. The bare silica particles were prepared by the Stöber process, which is known to produce spherical particles with a relatively narrow size distribution. The bare particles were surface-functionalized with 11-(2-bromo-2-methyl)propionyloxyundecyldimethylchlorosilane. The initiator particles, designated as IP, were then used to make polymer brush-grafted particles by surface-initiated ATRP. A free initiator, ethyl 2-bromoisobutyrate (EBiB), was added into the reaction mixture to facilitate the control of surface-initiated polymerization. It also allowed the progress of polymerization to be monitored by ^{1}H NMR spectroscopy for monomer conversion and size exclusion chromatography (SEC) analysis of the molecular weight of the free polymer grown from the sacrificial initiator. The resultant free P*n*BA was found to have a DP of 193, calculated by monomer conversion as determined by ^{1}H NMR. SEC analysis showed a unimodal distribution with an M_n of 23.0 kDa with a PDI of 1.15 (Figure 5.2), indicating a well-controlled polymerization. TGA was used to confirm the presence of P*n*BA grown from the surface of the ATRP initiator-functionalized silica particles, with a weight retention of 68.9 % at 800 °C, as compared to 86.4 % for IP at the same temperature (Figure 5.3). By using the size of silica particles, DP of P*n*BA, and the TGA data, the grafting density of P*n*BA was calculated to be 0.46 chains nm^{-2}.

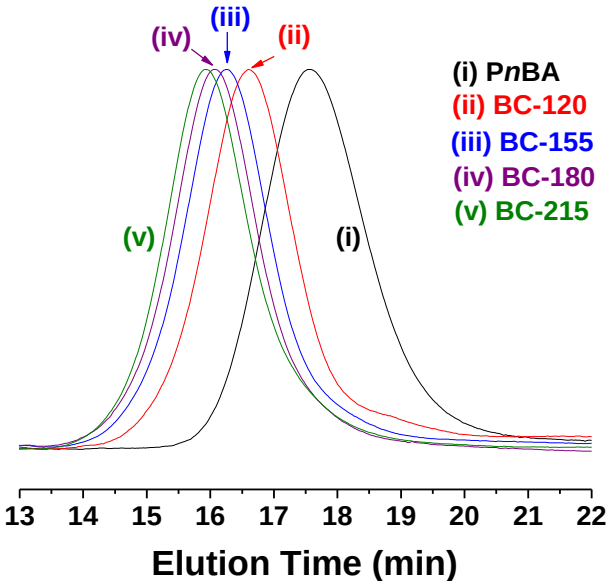

Figure 5.2. SEC traces of free P*n*BA (i), P*n*BA-*b*-PS diblock copolymer withdrawn from the polymerization mixture at 120 min (ii, BC-120), 155 min (iii, BC-155), 180 min (iv, BC-180), and 215 min (v, BC-215).

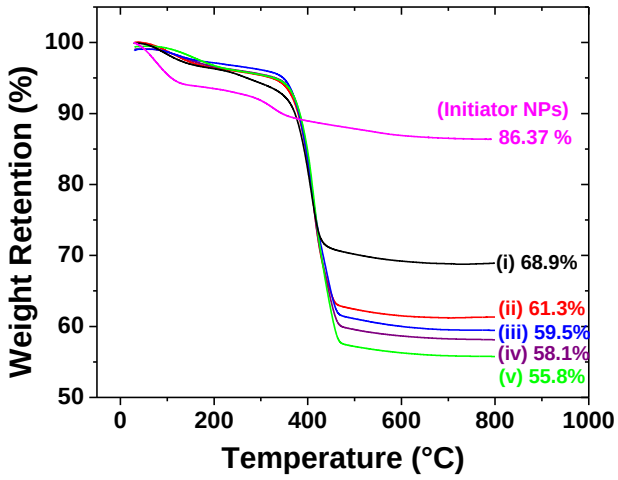

Figure 5.3. Thermogravimetric analysis of initiator particles, P*n*BA brush-grafted particles (i), DBP-120 (ii), DBP-155 (iii), DBP-180 (iv), and DBP-215 (v).

5.3.2 Synthesis of P*n*BA-*b*-PS Diblock Copolymer Brush-Grafted Silica Particles

Using P*n*BA brush-grafted particles as macroinitiator, four samples of diblock copolymer brushes with differing PS molecular weights were obtained by removing large portions of the reaction mixture during the polymerization of styrene. Like EBiB in the SI-ATRP of *n*BA, free P*n*BA was used as a sacrificial macroinitiator, allowing for the regulation of the surface polymerization, monitoring of the reaction by SEC, and convenient characterization of the tethered diblocks. The diblock copolymer brush-grafted particles were purified by repeated centrifugation-redispersion cycles in THF. The P*n*BA-*b*-PS brush-grafted silica particles are designated as DBP-120, DBP-155, DBP-180, and DBP-215, according to their reaction time in the polymerization mixture.

Each sample was analyzed by TGA, and the weight retention at 800 °C were found to decrease with increasing PS molecular weight (Figure 5.2). All diblock copolymer brush particles had lower weight retentions than that of the P*n*BA brush-grafted particles and much lower than that of initiator particles, as shown in Figure 5.2. From SEC analysis, the $M_{n,SEC}$ was shown to increase relatively smoothly from the initial macroinitiator to diblocks with increasing reaction time (Figure 5.1). The polydispersity indices of the free diblock copolymers were consistently between 1.15 and 1.17, indicating that the polymerization was well controlled and that the removal of large portions of the reaction mixture did not adversely impact the polymerization. The DP of PS in each sample was determined from ^{1}H NMR spectra of purified free diblock samples by comparing the aromatic peaks of PS at 6.3 ppm to 7.2 ppm (5H) to the peaks corresponding to the ester moieties of P*n*BA at 4.1 ppm (2H), using the known DP of P*n*BA as a reference. By using the size of bare silica particles, TGA data, and the DPs of both blocks of the free block copolymers,

the grafting densities of the P*n*BA-*b*-PS brush-grafted particles were calculated to be in the range of 0.42-0.47 chains nm^{-2}. A summary of all characterization data can be found in Table 5.1.

It has been reported that the molecular weight and molecular weight distribution of polymer brushes on silica particles synthesized by surface-initiated "living"/controlled radical polymerization are essentially identical to those of the free polymer formed from free initiator. While there was no mechanistic reason that this should not also be the case for ATRP from tethered and free macroinitiators, we took advantage of the silica substrate's ability to be etched away by hydrofluoric acid to confirm that the control was maintained both on the surface and in solution. DB-180 was selected as an example and was etched with HF. After neutralization with $Ca(OH)_2$ and extraction with toluene, the cleaved polymer was found to have a molecular weight distribution essentially identical to that of the corresponding free polymer BC-180 by SEC (Figure 5.4), with an $M_{n,SEC}$ of 55.9 kDa and a PDI of 1.09. This molecular weight was very close to that of the free diblock BC-180 ($M_{n,SEC}$ = 54.9 kDa), and, interestingly, the PDI was lower than that of free polymer BC-180 (1.15). This result confirmed the validity of the use of free polymers grown from the sacrificial macroinitiator to mirror their surface-tethered counterparts.

To ensure that the molecular weights of P*n*BA-*b*-PS diblock copolymers were sufficiently large to enable microphase separation, BC-155 was examined by differential scanning calorimetry (DSC). The polymer was first heated to 140 °C to erase the thermal history, then cooled to -80 °C, and heated again to 140 °C at a heating rate of 20 °C per minute. Two distinct glass transition temperatures were observed (Figure 5.5): one at -44 °C corresponding to P*n*BA and another one at 84 °C corresponding to PS. The existence of two glass transition temperatures suggests that the diblock copolymer microphase separated into nearly pure microdomains.

Table 5.1. Characterization Data for P*n*BA and P*n*BA-*b*-PS Brush-Grafted Silica Particles and Their Corresponding Free Polymers

Brush-Grafted Particle Sample	**$M_{n,SEC}$ (kDa)** [a]	**PDI** [a]	**DP_{PnBA}** [b]	**DP_{PS}** [c]	**f_{PS}** [d]	**Grafting Density** [e]
P*n*BA Particle [e]	23.0	1.15	193	0	0	0.46 chains nm^{-2}
DBP-120 [e]	41.6	1.17	193	153	0.40	0.45 chains nm^{-2}
DBP-155 [e]	50.1	1.16	193	207	0.47	0.43 chains nm^{-2}
DBP-180 [e]	54.8	1.15	193	247	0.52	0.42 chains nm^{-2}
DBP-215 [e]	56.5	1.16	193	261	0.53	0.47 chains nm^{-2}

[a] As determined by size exclusion chromatography (SEC) calibrated with polystyrene standards. [b] The degree of polymerization (DP) of the inner, P*n*BA block was calculated using monomer conversion. [c] The DP of the outer, PS block was calculated using the ^{1}H NMR analysis of the free block copolymers. [d] f_{PS} , the volume fraction of PS in P*n*BA-*b*-PS, was calculated using the molecular weights of both blocks and the densities of 1.050 g cm^{-3} for PS and 1.087 g cm^{-3} for P*n*BA. [e] The grafting densities of polymer brushes were calculated using TGA data, the DPs of both blocks, and the core silica nanoparticle size of 171 nm. [e] P*n*BA Particle and DBP are designations for P*n*BA brush-grafted particles and P*n*BA-*b*-PS brush-grafted silica NPs. Their corresponding free polymers are P*n*BA, BC-120, -155, -180, and -215 respectively.

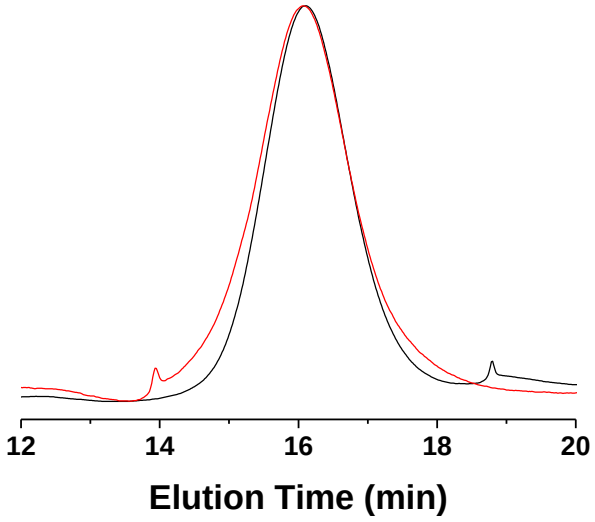

Figure 5.4. SEC traces of the diblock copolymer cleaved from DBP-155 and free BC-155 P*n*BA-*b*-PS (red).

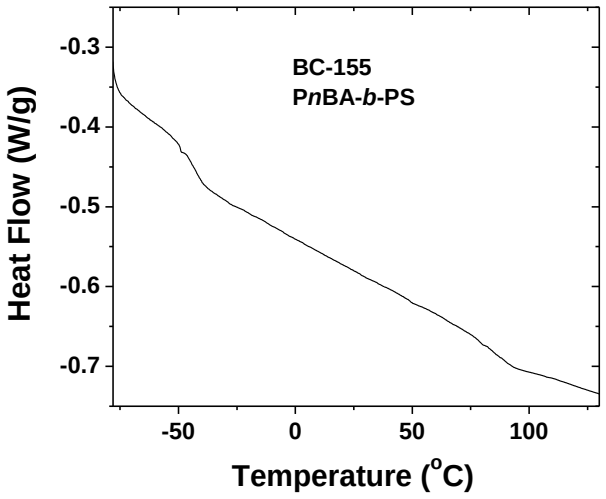

Figure 5.5. DSC trace of P*n*BA-*b*-PS with $M_{n,SEC}$ = 50.1 kDa and PDI = 1.16, showing two distinct glass transition temperatures: one at -44 °C corresponding to P*n*BA and another one at 84 °C corresponding to PS.

5.3.3 TEM Study of Microphase Separation of P*n*BA-*b*-PS Brushes Grafted on Particles

Microphase separation of P*n*BA-*b*-PS brushes was primarily studied by transmission electron microscopy (TEM). The TEM samples were prepared by drop-casting from a 1 mg/mL dispersion in chloroform onto carbon film coated copper grids; chloroform was chosen as it is a good solvent for both P*n*BA and PS and is essentially nonselective between the two polymers. After the solvent was evaporated, the samples were annealed at room temperature using chloroform vapor for several hours, aiding in the equilibration of microphase separated domains. The brushes were then stained with RuO_4 vapor, which is known to selectively stain aromatic moieties, such as those of PS, causing PS domains to appear darker under bright-field TEM.

DBP-120, the sample with the lowest f_{PS}, appears to exhibit clear microphase separation (Figure 5.6). The particles were arrayed hexagonally, and microphase separation was particularly evident on the top of the particles, where dark stripe-like nanostructures can be seen. According to the theoretical prediction by Matsen and coworkers, a f_{PS} of 0.40 would fall in the window of the hole morphology.[6,12] It should be noted, however, that theoretical predictions were made by considering only one hairy particle, and the assembly of the particles shown in the TEM micrographs certainly influenced the morphology through interparticle interactions. In addition, the non-uniform collapse of brushes on particles during the solvent evaporation process also affected the morphology. These effects were investigated in a recent work for mixed P*t*BA/PS brushes grafted on silica particles.[15] With the increase of PS block length from DB-120 to DB-155, DB-180, and DB-215, the dark stripe-like nanodomains became more connected (Figure 5.6 – 5.9), indicating the progression toward the uniform layered morphology. In particular, for DB-215, the bright P*n*BA layer was more visible at the particle edge, possibly signaling the advent of full PS coverage and the increased segregation strength between two blocks. In fact, increasing f_{PS}

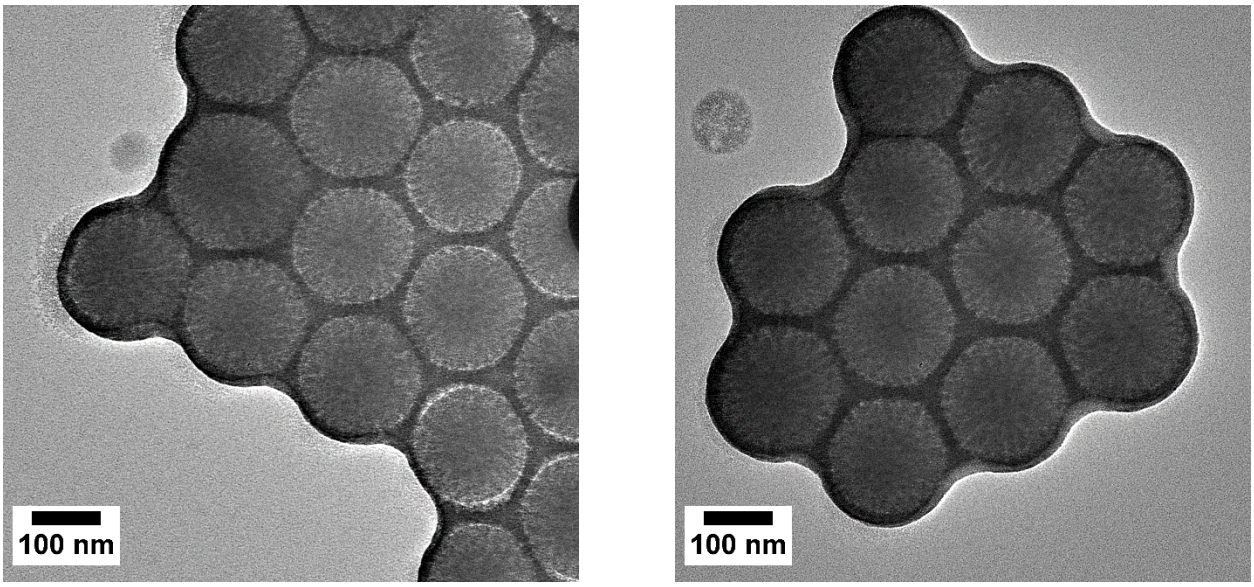

Figure 5.6. Bright field TEM micrographs of P*n*BA-*b*-PS brush-grafted silica particles with DP_{PnBA} of 193 and DP_{PS} of 153 (DBP-120). The hairy NPs were cast onto carbon-coated, copper TEM grids from $CHCl_3$, a nonselective good solvent, at a concentration of 1 mg mL^{-1}.

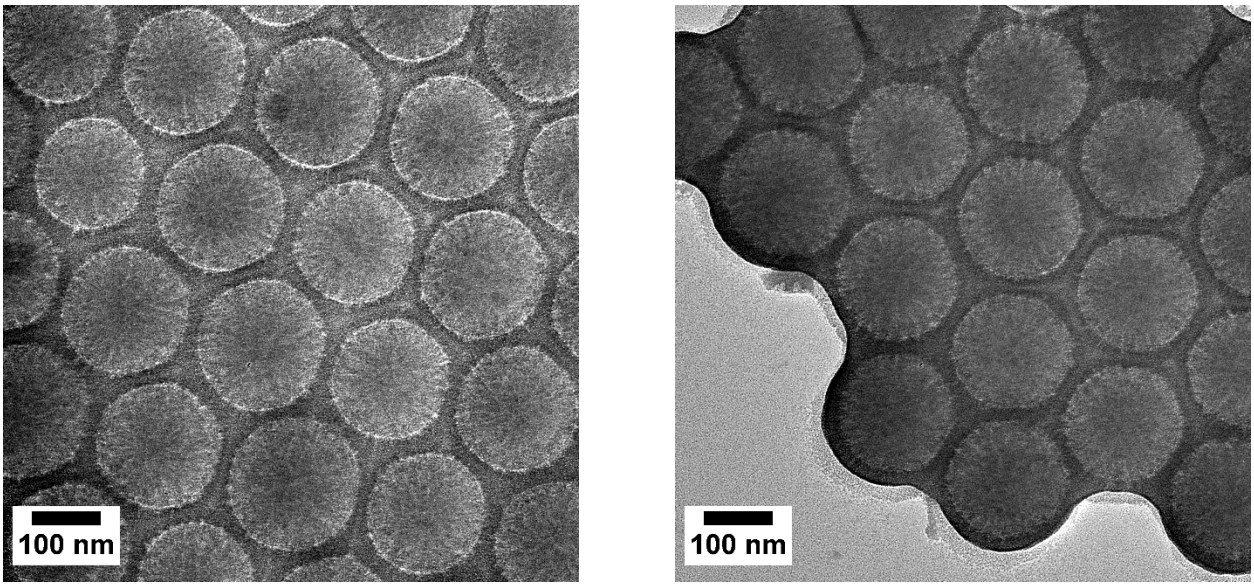

Figure 5.7. Bright field TEM micrographs of P*n*BA-*b*-PS brush-grafted silica particles with DP_{PnBA} of 193 and DP_{PS} of 207 (DBP-155). The hairy NPs were cast onto carbon-coated, copper TEM grids from $CHCl_3$, a nonselective good solvent, at a concentration of 1 mg mL^{-1}.

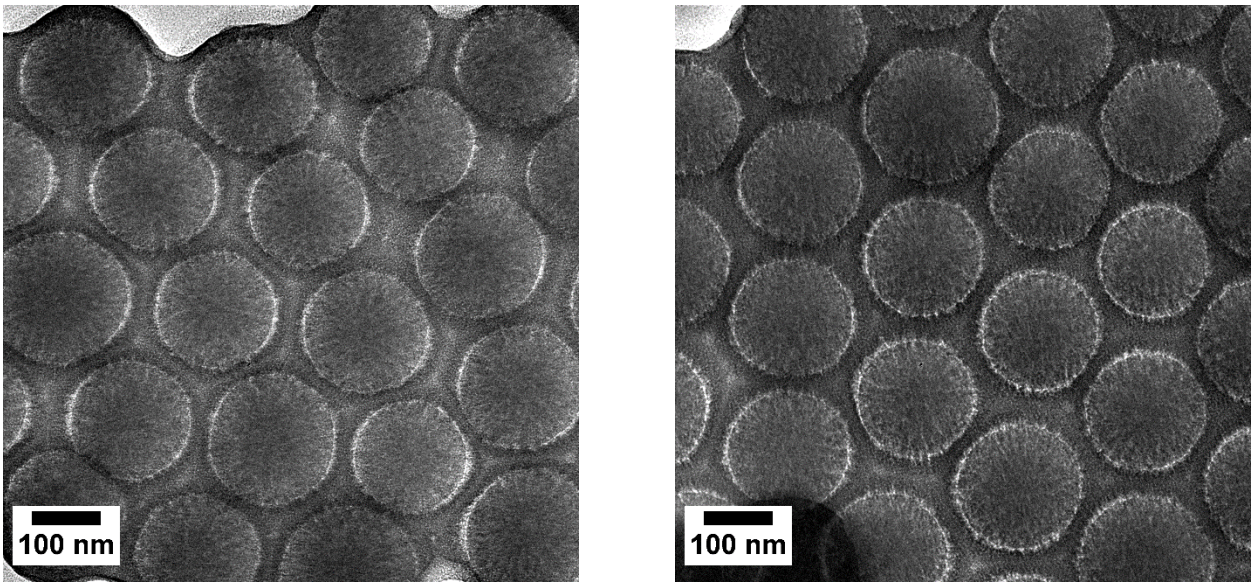

Figure 5.8. Bright field TEM micrographs of P*n*BA-*b*-PS brush-grafted silica particles with DP_{PnBA} of 193 and DP_{PS} of 247 (DBP-180). The hairy NPs were cast onto carbon-coated, copper TEM grids from $CHCl_3$, a nonselective good solvent, at a concentration of 1 mg mL^{-1}.

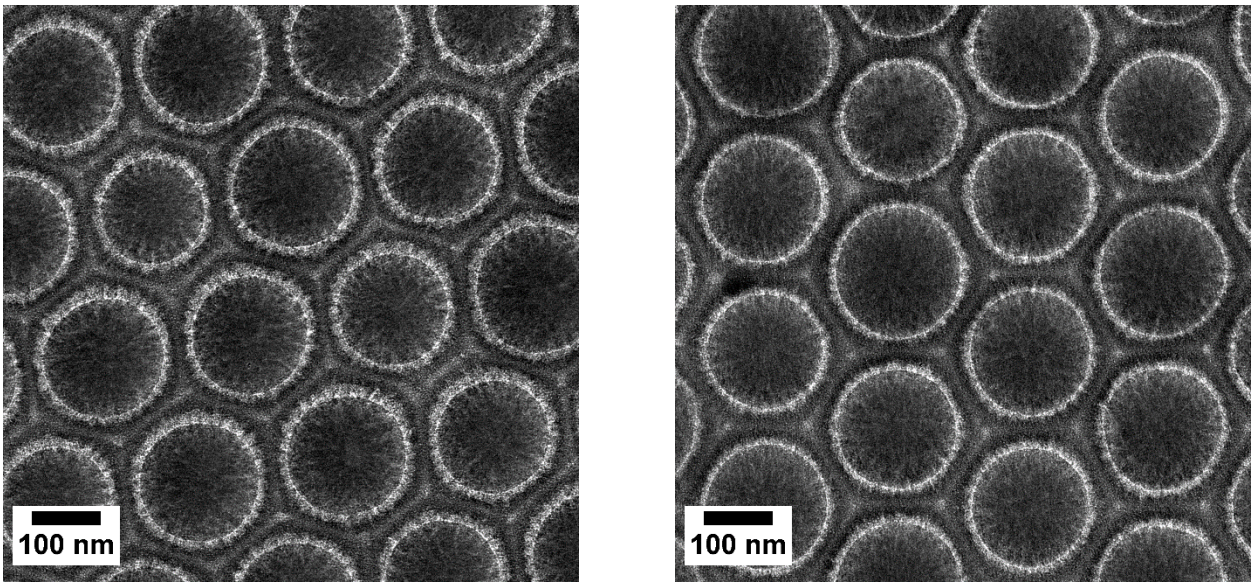

Figure 5.9. Bright field TEM micrographs of P*n*BA-*b*-PS brush-grafted silica particles with DP_{PnBA} of 193 and DP_{PS} of 261 (DBP-215). The hairy NPs were cast onto carbon-coated, copper TEM grids from $CHCl_3$, a nonselective good solvent, at a concentration of 1 mg mL^{-1}.

to 0.58, the PS volume fraction of DBP-215, seems to have tipped the system fully into the uniform layered phase morphology. The PS phase appears clearly for DBP-215 (Figure 5.9), with relatively sharp distinction between the light P*n*BA grafted on the particle and the dark PS domain surrounding it. Nevertheless, more detailed TEM study is needed for both individual, uniformly collapsed hairy particles and the assemblies of particles.

5.4 Conclusion

A series of well-defined diblock copolymer brush-grafted, 171 nm silica particles were synthesized by sequential SI-ATRPs of *n*BA and styrene, yielding hairy particles with a grafted P*n*BA block with a DP of 193 and PS outer blocks with varying DPs. Using TGA and ^{1}H NMR data, the grafting densities of P*n*BA-*b*-PS brushes were found to be in the range between 0.42 and 0.47 chains/nm^2, comparing well with the grafting density of P*n*BA brush-grafted particles (0.46 chains/nm^2). TEM studies were carried out by using RuO_4 to stain PS domains, which appeared dark under TEM. With the increase of PS block length, there seems to be an evolution from stripe-like nanostructure to a more uniform layered structure. More detailed TEM study is needed to fully elucidate the phase morphologies of these diblock copolymer brushes on silica particles.

References

1. Leibler, L., *Macromolecules* **1980,** *13* (6), 1602-1617.
2. Bates, F. S.; Fredrickson, G. H., *Annu. Rev. Phys. Chem.* **1990,** *41* (1), 525-557.
3. Matsen, M. W.; Schick, M., *Phys. Rev. Lett.* **1994,** *72* (16), 2660-2663.
4. Bates, F. S.; Fredrickson, G. H., *Physics Today* **1999,** *52* (2), 32-38.
5. Khandpur, A. K.; Foerster, S.; Bates, F. S.; Hamley, I. W.; Ryan, A. J.; Bras, W.; Almdal, K.; Mortensen, K., *Macromolecules* **1995,** *28* (26), 8796-8806.
6. Matsen, M. W.; Griffiths, G. H., *The European Physics Journal E* **2009,** *29*, 219-227.
7. O'Driscoll, B. M. D.; Griffiths, G. H.; Matsen, M. W.; Perrier, S. b.; Ladmiral, V.; Hamley, I. W., *Macromolecules* **2010,** *43* (19), 8177-8184.
8. Zhulina, E. B.; Singh, C.; Balazs, A. C., *Macromolecules* **1996,** *29* (19), 6338-6348.
9. Yin, Y.; Sun, P.; Li, B.; Chen, T.; Jin, Q.; Ding, D.; Shi, A.-C., *Macromolecules* **2007,** *40* (14), 5161-5170.
10. O'Driscoll, B. M. D.; Griffiths, G. H.; Matsen, M. W.; Hamley, I. W., *Macromolecules* **2011,** *44* (21), 8527-8536.
11. Chantawansri, T. L.; Bosse, A. W.; Hexemer, A.; Ceniceros, H. D.; García-Cervera, C. J.; Kramer, E. J.; Fredrickson, G. H., *Physical Review E* **2007,** *75* (3), 031802.
12. Griffiths, G. H.; Vorselaars, B.; Matsen, M. W., *Macromolecules* **2011,** *44* (9), 3649-3655.
13. Vorselaars, B.; Kim, J. U.; Chantawansri, T. L.; Fredrickson, G. H.; Matsen, M. W., *Soft Matter* **2011,** *7* (11), 5128-5137.
14. Horton, J. M.; Bai, Z.; Jiang, X.; Li, D.; Lodge, T. P.; Zhao, B., *Langmuir* **2011,** *27* (5), 2019-2027.

15. Tang, S.; Lo, T.-Y.; Horton, J. M.; Bao, C.; Tang, P.; Qiu, F.; Ho, R.-M.; Zhao, B.; Zhu, L., *Macromolecules* **2013,** *46* (16), 6575-6584.

Appendix D

for

Chapter 5. Synthesis, Characterization, and Microphase Separation of Poly(*n*-butyl acrylate)-*b*-Polystyrene Diblock Copolymer Brushes Grafted on Silica Particles

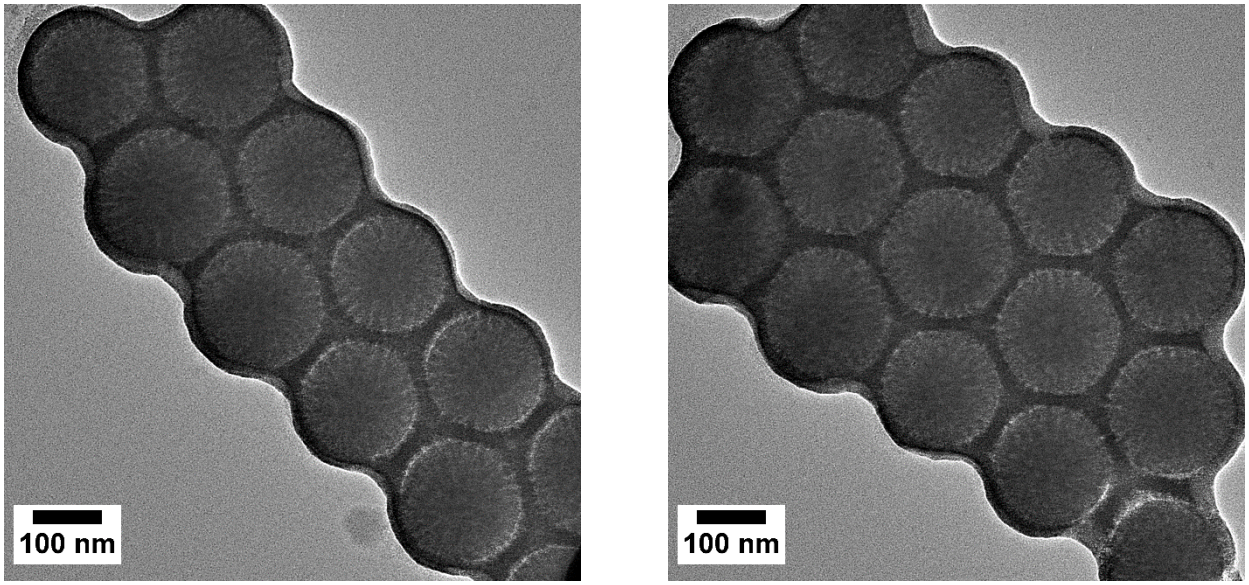

Figure D1. Bright field TEM micrographs of P*n*BA-*b*-PS brush-grafted silica particles with DP_{PnBA} of 193 and DP_{PS} of 153 (DBP-120). The hairy NPs were cast onto carbon-coated, copper TEM grids from $CHCl_3$, a nonselective good solvent, at a concentration of 1 mg mL^{-1}.

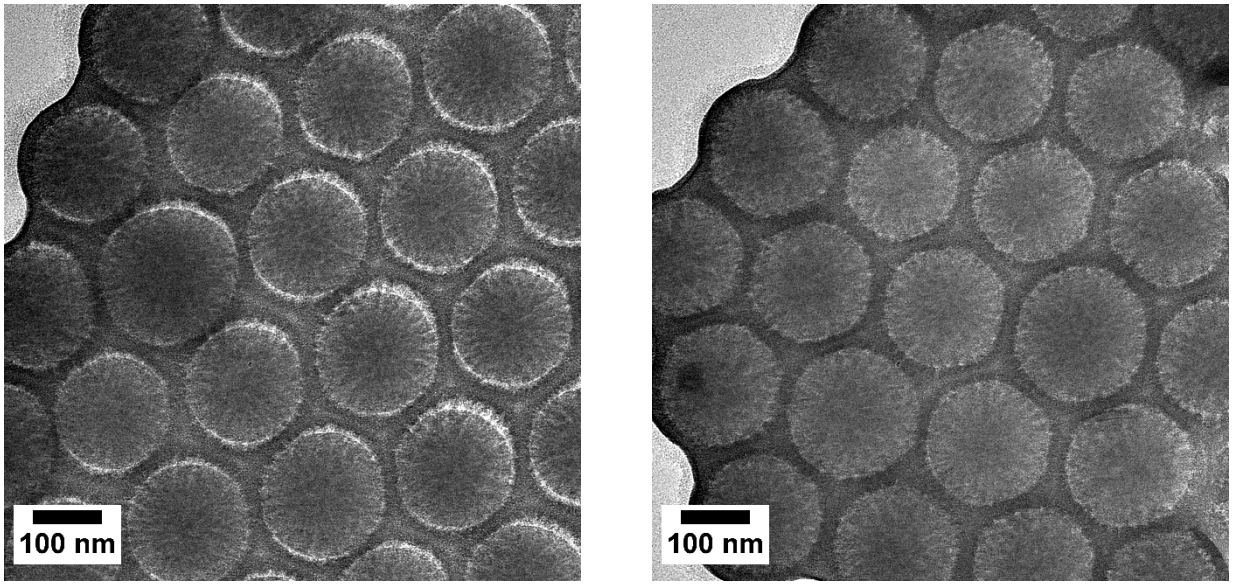

Figure D2. Bright field TEM micrographs of P*n*BA-*b*-PS brush-grafted silica particles with DP_{PnBA} of 193 and DP_{PS} of 207 (DBP-155). The hairy NPs were cast onto carbon-coated, copper TEM grids from $CHCl_3$, a nonselective good solvent, at a concentration of 1 mg mL^{-1}.

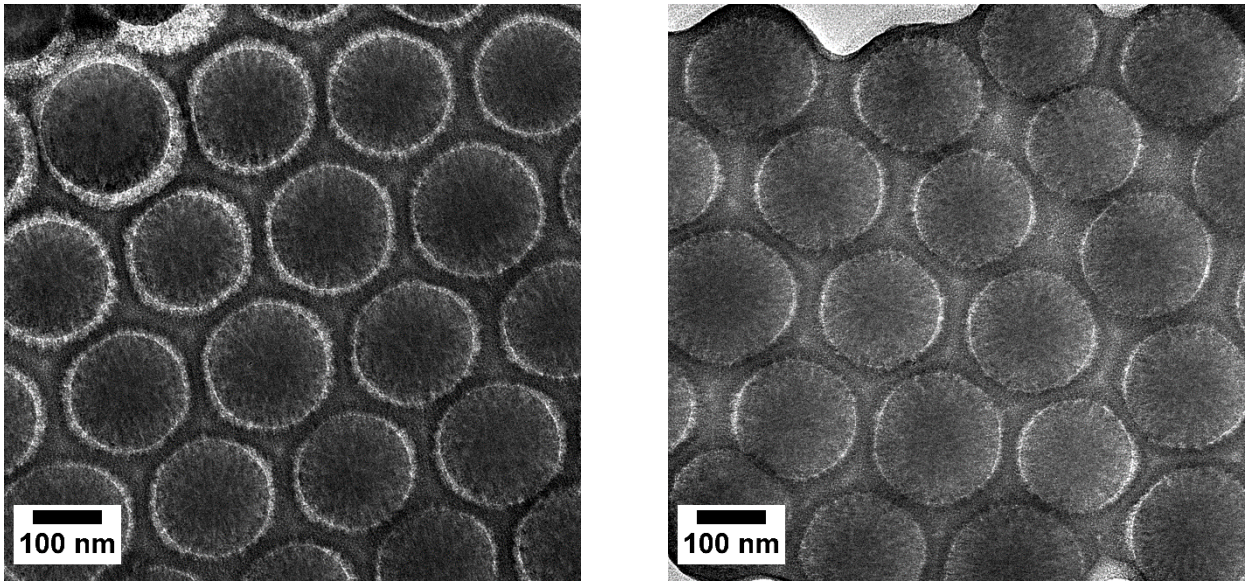

Figure D3. Bright field TEM micrographs of P*n*BA-*b*-PS brush-grafted silica particles with DP_{PnBA} of 193 and DP_{PS} of 247 (DBP-180). The hairy NPs were cast onto carbon-coated, copper TEM grids from $CHCl_3$, a nonselective good solvent, at a concentration of 1 mg mL^{-1}.

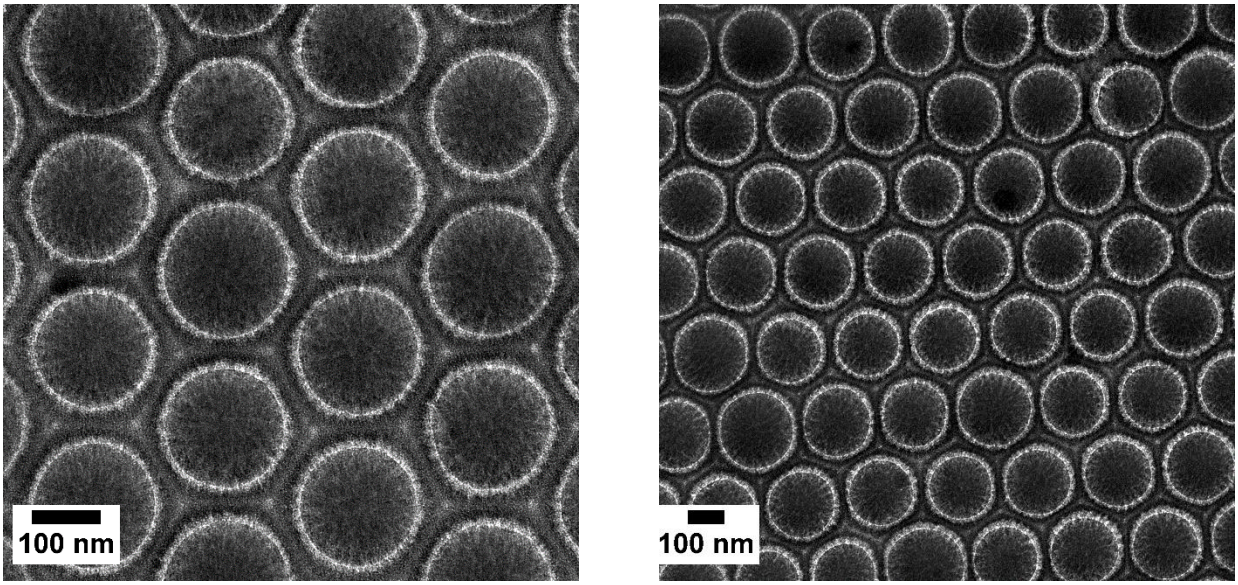

Figure D4. Bright field TEM micrographs of P*n*BA-*b*-PS brush-grafted silica particles with DP_{PnBA} of 193 and DP_{PS} of 261 (DBP-215). The hairy NPs were cast onto carbon-coated, copper TEM grids from $CHCl_3$, a nonselective good solvent, at a concentration of 1 mg mL^{-1}.

Chapter 6. Conclusions and Future Work

Homopolymer and diblock brush-grafted silica (nano)particles were synthesized by surface-initiated atom transfer radical polymerization (SI-ATRP) in the presence of a sacrificial, free initiator, which allowed for the synthesis of free analogues to the polymer brushes. These free polymers have been demonstrated on multiple occasions to be representative of their grafted counterparts, and allowed for convenient molecular characterization and analysis of these hairy particles. The polymer brush-grafted nanoparticles themselves were studied as dispersions in water (Chapters 2-3) and lubricating base oil poly(alphaolefin) (Chapter 4) by rheological and tribological measurements, respectively. Variations in molecular weight and composition were shown to have a significant effect on the physical properties of these nanoparticle dispersions.

Chapters 2 and 3 report the use of stimuli-sponsive hydrophilic hairy nanoparticles for the formation of physical hydrogels and their subsequent characterization by rheological experiments. Thermosensitive block copolymers are capable of forming micelles in water under appropriate conditions, and, depending on the molecular architecture and chemical nature of these polymers, are capable of undergoing reversible gelation as well. As thermosensitive hairy particles are conceptually similar to micelles with a thermosensitive corona, the use of hairy particles in place of these micelles for the formation of physical hydrogels was explored. Such hydrogels could be made to incorporate the unique properties of various nanoparticles (NPs) into systems with which they would otherwise have been incompatible. Classic block copolymer micellar hydrogels comprises two types: packing-based gels and network-based gels.[1] Chapter 2 presents the synthesis of thermosensitive diblock copolymer brush-grafted 17 nm silica NPs for use in packing-based hydrogels. The brushes consisted of a thermosensitive poly(methoxydi(ethylene glycol) methacrylate) (PDEGMMA) grafted block and a poly(methoxydi(ethylene glycol) methacrylate-*co*-*N*,*N*-dimethylaminoethyl methacrylate) (P(DEGMMA-*co*-DMAEMA)) outer block; the

tertiary amine moieties in the outer block were quaternized with methyl iodide to yield a permanently charged, poly(DEGMMA-*co*-2-(methacryloyloxy)ethyltrimethylammonium iodide) (P(DEGMMA-*co*-TMAEMA-I) block.[2] This charged block aided in the dispersion of the hairy nanoparticles in water and prevented aggregation at temperatures above the lower critical solution temperature (LCST) of the grafted thermosensitive block. These hairy NPs were found to exhibit cooling-induced, reversible sol-gel transitions at concentrations as low as 5.3 wt % in water. The gel-sol transition temperature ($T_{gel\text{-}sol}$) was measured rheologically and found to increase with increasing NP concentration and with length of the charged outer block. The sol-gel transition was found to be a result of the swelling of the thermosensitive inner block at lower temperature, as confirmed by dynamic light scattering experiments. This swelling resulted in an increase in brush volume fraction and, below the $T_{gel\text{-}sol}$, this volume fraction was sufficient to prevent flow; this mechanism of gelation is analogous to the packing of micelles of thermosensitive diblock copolymers.[3]

Chapter 3 presents a complementary work to Chapter 2, in that thermosensitive hairy nanoparticles were used to make hydrogels analogous to the other classic type of micellar gel: 3D network physical gels.[4] Brush-grafted silica NPs were synthesized with a P(TMAEMA-I) grafted block and a thermosensitive PDEGMMA outer block by sequential SI-ATRP of DMAEMA and DEGMMA and quaternization with methyl iodide. Aqueous dispersions of these hairy NPs were observed to undergo gelation at concentrations as low as 3 wt % upon heating to temperatures sufficiently above the LCST of the outer block; upon cooling, the liquid sol state was restored. This reversible sol-gel transition resulted from the association of the PDEGMMA blocks into hydrophobic domains above the LCST. These PDEGMMA domains acted as physical crosslinks connected to the silica NPs by the grafted polyelectrolyte block, resulting in a gel network like

those observed for thermosensitive ABA or ABC systems.[5] This gelation was studied rheologically, and $T_{sol\text{-}gel}$ was found to decrease with increasing NP concentration.

Chapter 4 reports the synthesis of oil-soluble polymer brush-grafted silica NPs and their use as effective lubricant additives.[6] Through the SI-ATRP of lauryl methacrylate (LMA), a series of oil-miscible hairy nanoparticles were synthesized. These hybrid nanoparticles were found to form transparent dispersions in poly(alpha olefin) (PAO) base oil and exhibited superb stability; no sedimentation or change in appearance was observed after being kept for more than 55 days at -20, 22, and 100 °C. Tribological characterization of additized PAO was performed using high contact stress reciprocating ball-on-flat experiments at 100 °C. The addition of 1 wt % hairy NPs was found to significantly reduce the coefficient of friction (COF) and material wear, with reductions as high as ~30 % and ~90 %, respectively. Cross-sectional TEM analysis of an iron flat used in tribological experiments revealed the formation of a tribofilm, a load bearing film that served to reduce contact at the rubbing interface and minimize scuffing and micro-welding.

Chapter 5 describes a preliminary exploration of the phase morphology of grafted diblock copolymers on silica particles. It has been shown theoretically that diblock copolymers tethered to a spherical substrate exhibit interesting phase morphologies. At sufficiently high segregation strength and grafting density, an evolution of dot, stripe, hole, and uniform nanostructures are expected to arise with increasing volume fraction of the outer block.[5] Sequential SI-ATRP of *n*-butyl acrylate and styrene with initiator-functionalized 171 nm silica particles was employed to synthesize a series of P*n*BA-*b*-PS brushes with the same inner block length and increasing PS block length; in this way, the effect of the outer PS block volume fraction was investigated. Microphase separation was observed between the two blocks on the surface of the silica particles by TEM, using RuO_4 as a selective staining agent, and an evolution was observed from a stripe-

like morphology to full PS coverage. A more thorough investigation of block volume fraction and other parameters, however, is warranted to more fully understand the rich phase behavior of this system. Nevertheless, insights gleaned from this work may prove useful in fabrication of nanostructured particles for use in various technologies.

Hairy NPs are a unique class of materials with a varied set of properties and potential applications.[8] Possible future work in the exploration of brush-grafted NP-based hydrogels would include the use of functional NPs as substrates. These functions could include magnetic properties for the syntheses of unique magneto-rheological fluids and gels. Another area of exploration could be the use of mesoporous or hollow NP substrates. Where micellar hydrogels are typically limited to hydrophobic cores, these particles could be functionalized as desired for the loading and delivery of a variety of drugs and other payloads. Release profiles could be further modulated both by physical gel properties and the use of a grafted thermosensitive or other stimuli-responsive block on the NP surface to impede or even prevent flow in and out of the pores under the desired conditions.

References

1. Hamley, I. W. *Block Copolymers in Solution: Fundamentals and Applications*, John Wiley & Sons, Chicester, 2005
2. Wright, R. A. E.; Hu, B.; Henn, D. M.; Zhao, B. *Soft Matter* **2015,** *11* (34), 6808-6820.
3. (a) Jin, N.; Zhang, H.; Jin, S.; Dadmun, M. D.; Zhao, B. *J. Phys. Chem. B* **2012,** *116* (10), 3125-3137; (b) Jin, N.; Zhang, H.; Jin, S.; Dadmun, M. D.; Zhao, B. *Macromolecules* **2012,** *45* (11), 4790-4800.
4. Wright, R. A. E.; Henn, D. M.; Zhao, B. Thermally Reversible Physically Crosslinked Hybrid Network Hydrogels Formed by Thermoresponsive Hairy Nanoparticles, Manucript accepted for publication as an article in *J. Phys. Chem. B* **2016.**
5. (a) Woodcock, J. W.; Jiang, X.; Wright, R. A. E.; Zhao, B. *Macromolecules* **2011,** *44* (14), 5764-5775; (b) Woodcock, J. W.; Wright, R. A. E.; Jiang, X.; O'Lenick, T. G.; Zhao, B. *Soft Matter* **2010,** *6* (14), 3325-3336; (c) Henn, D. M.; Wright, R. A. E.; Woodcock, J. W.; Hu, B.; Zhao, B. *Langmuir* **2014**, *30*, 2541–2550 (d) Hu, B.; Henn, D. M.; Wright, R. A. E.; Zhao, B. *Langmuir* **2014**, *30*, 11212-11224. (e) Hu, B.; Wright, R. A. E.; Jiang, S. S.; Henn, D. M.; Zhao, B. *Polymer*, **2016**, *82*, 206-216. (f) Zhou, C.; Hillmyer, M. A.; Lodge, T. P. *J. Am. Chem. Soc.* **2012,** *134* (25), 10365-10368.
6. Wright, R. A. E.; Wang, K.; Qu, J.; Zhao, B. Oil-Soluble Polymer Brush-Grafted Nanoparticles as Effective Lubricant Additives for Friction and Wear Reduction, *Angew. Chem. Int. Ed.* **2016**, *55*, 8656-8660
7. Vorselaars, B.; Kim, J. U.; Chantawansri, T. L.; Fredrickson, G. H.; Matsen, M. W. *Soft Matter* **2011,** *7* (11), 5128-5137.

8. (a) Li, J.; Shiraki, T.; Hu, B.; Wright, R. A. E.; Zhao, B.; Moore, J. S. *J. Am. Chem. Soc.* **2014**, *136*, 15925–15928. (b) Bao, C. H.; Tang, S. D.; Wright, R. A. E.; Tang, P.; Qiu, F.; Zhu, L.; Zhao, B. *Macromolecules* **2014**, *47*, 6824–6835. (c) Li, W.; Bao, C. H.; Wright, R. A. E.; Zhao, B. *RSC Advances* **2014**, *4*, 18772-18781.

Vita

Roger Anthony Emory Wright was born in Knoxville, TN. In 2011, he received his B. S. degree in Chemistry from the University of Tennessee, Knoxville. Later that year, he enrolled as graduate student and joined Professor Bin Zhao's research group. His research focused on the synthesis and application of polymer brush-grafted nanoparticles. He went on to receive a Doctor of Philosophy Degree in Chemistry from the University of Tennessee, Knoxville in August, 2016.